FP I ZS 2022

Drift
Diffusion
Ambipolar diffusion

Cosmic flux versus particle energy

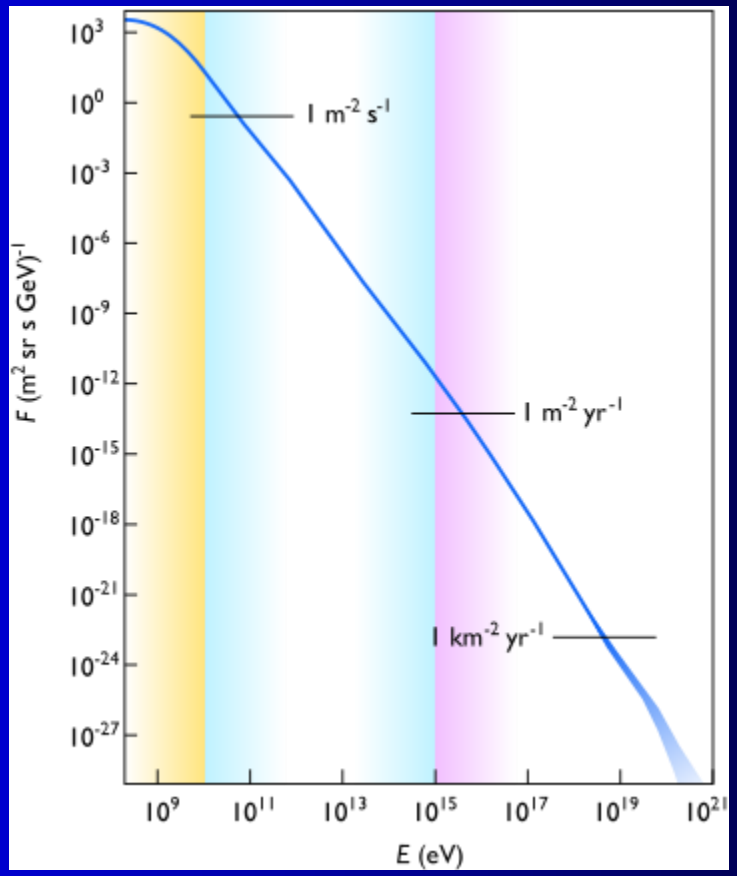

about 90% are simple protons (i.e., hydrogen nuclei); 9% are alpha particles, identical to helium nuclei; and 1% are the nuclei of heavier elements

Interactions of electron
Rotational and vibrational excitation

Rutherford atom

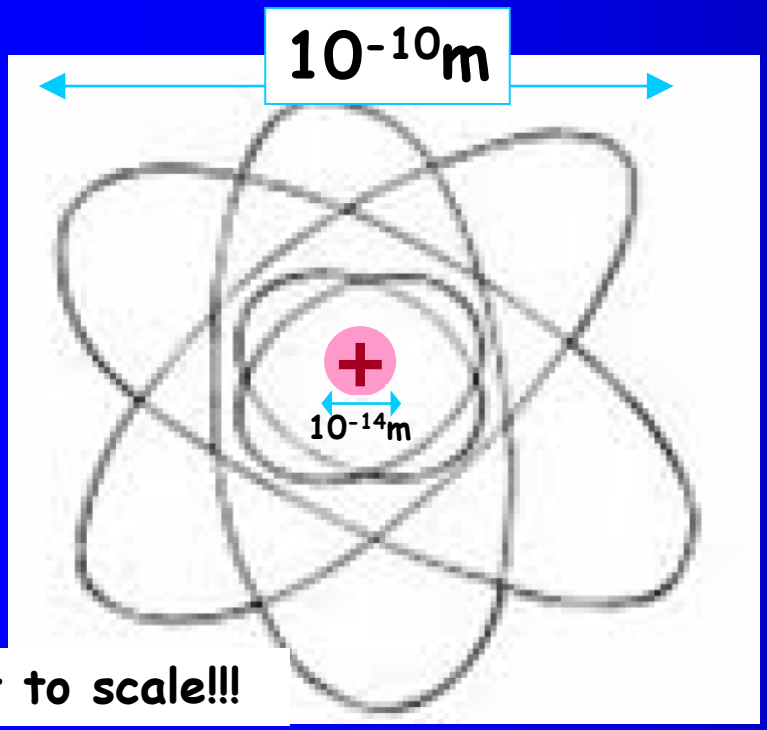

Excitation energies

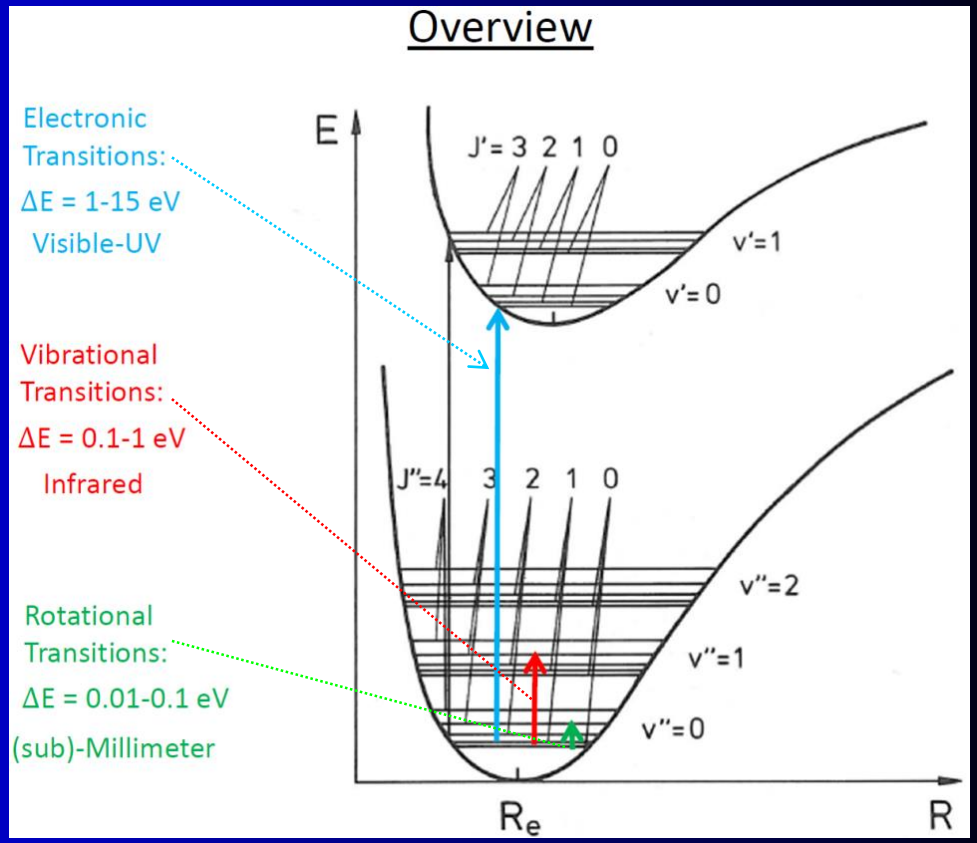

Electron: 1eV → v=5.9x10^{7}cm s^{-1}

$\tau \sim a_0/v \sim 10^{-8}/ 5.9x10^7 = 2x10^{-16}$s

$P \sim \langle \psi_{initial}. \psi_{final} \rangle^{2.}$

Franck Condon principle

James Franck
1882-1964
1925 Nobel prize

Edward Condon
1902-1974

The probability (or amplitude) of a simultaneous electronic and vibrational transition to a new "vibronic" state depends on the overlap between the wavefunctions of the ground and excited states.

Or:
Electrons move much faster than nuclei. For an electronic excitation to occur, the nucleic configuration should be optimal (the same).

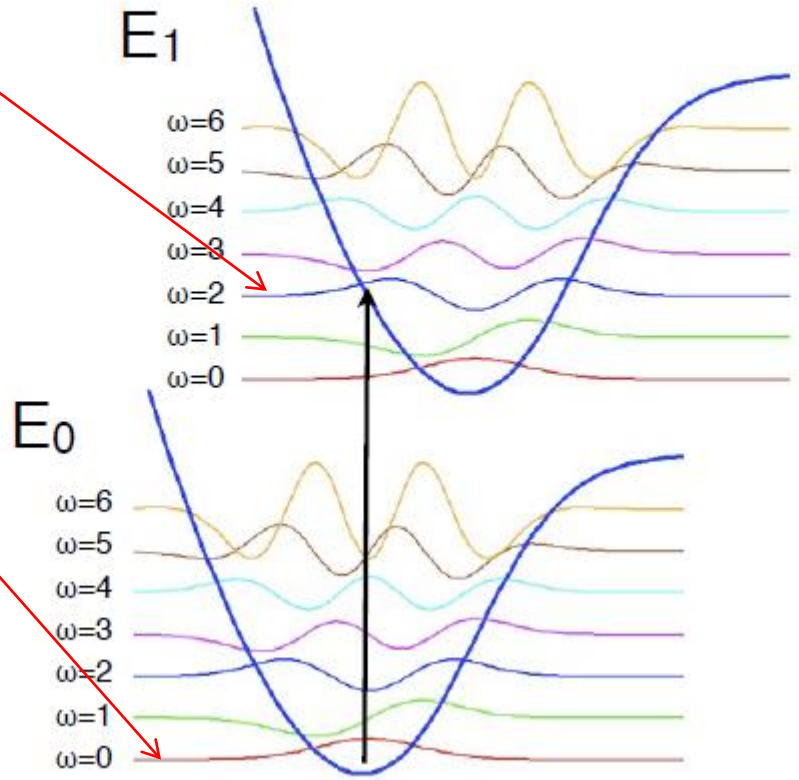

Transitions between molecular potential energy surfaces

During an electronic transition

the complex absorbs energy

electrons change orbital

the complex changes energy state

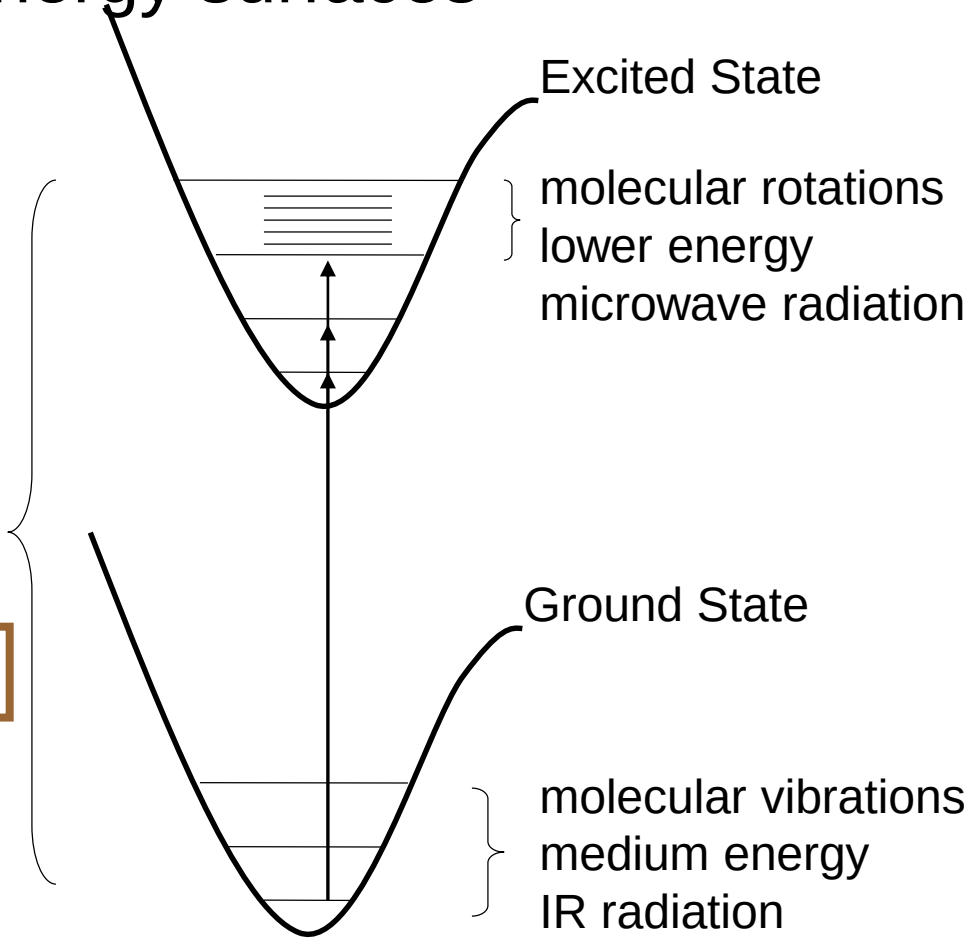

Electron: 1eV → $v=5.9\times10^{7}$ cm s^{-1}

$\tau \sim a_0/v \sim 10^{-8}/\ 5.9\times10^{7} = 2\times10^{-16}$ s

Timescale : ≈10^{-15} sec

Timescale of geometry changes (vibrations): ≈10^{-12} sec

As a result, observe vertical (Franck-Condon) transitions

In other words, we assume that we only have to consider the electronic portion of the ground- and excited-state wavefunctions to understand these transitions: Born-Oppenheimer approximation

Potential Energy Surface Description of the Ionization of Dihydrogen

PES of H2

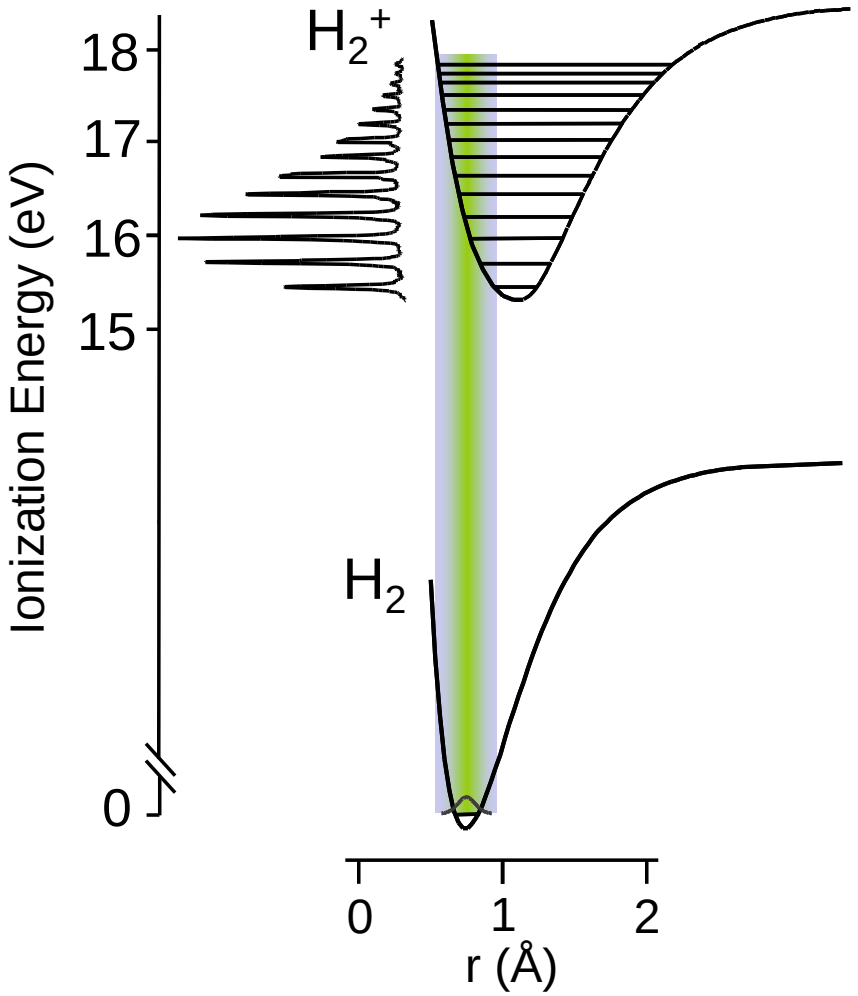

PES of H2

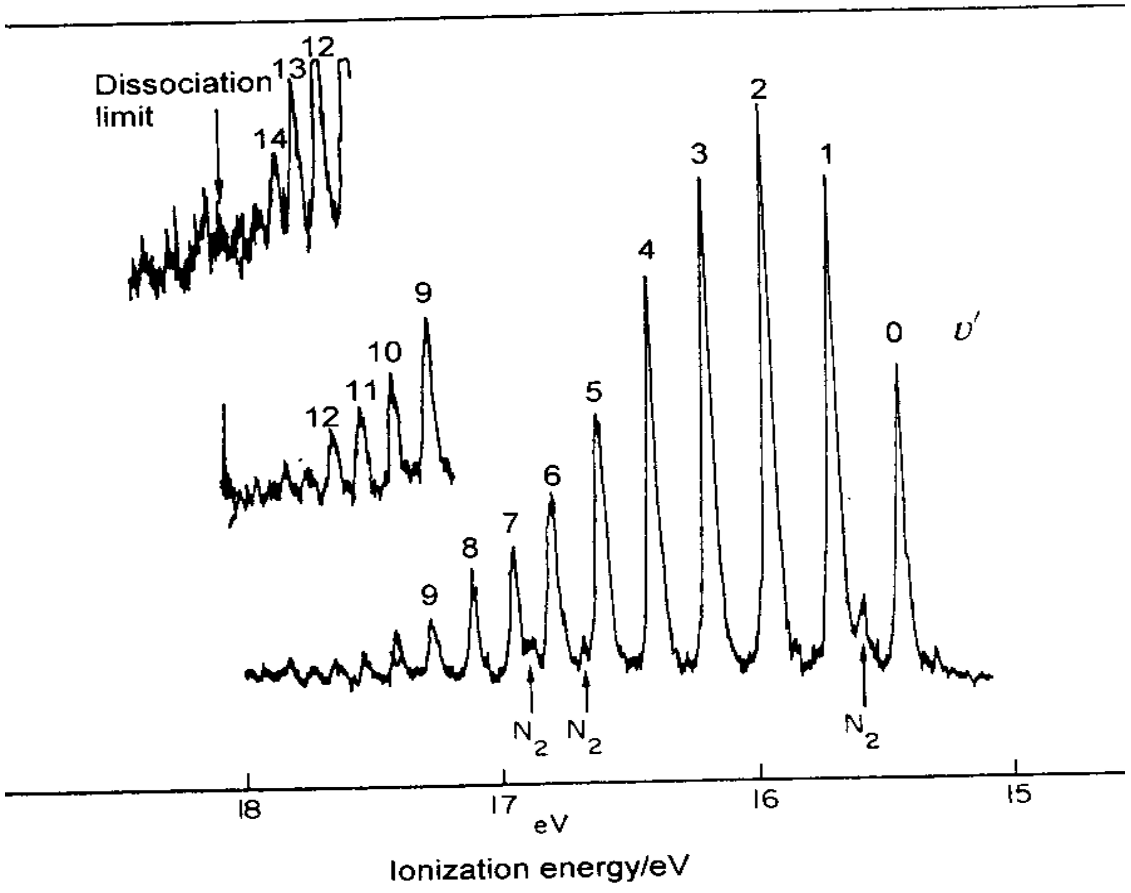
Dissociation limit
13
12
14
9
10
11
12
9
8
7
6
5
4
3
2
1
0
υ′
N2
N2
N2
18
17
eV
16
15
Ionization energy/eV

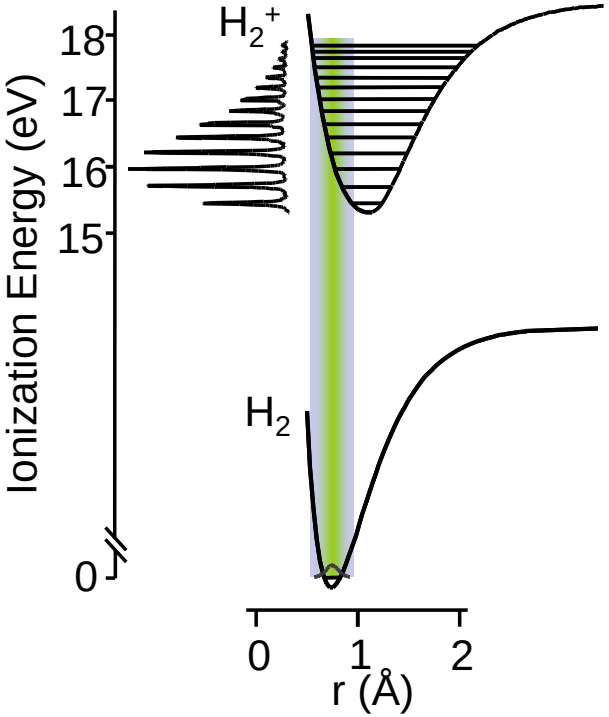
H2+
18
17
16
15
Ionization Energy (eV)
0
H2
0
1
2
r (Å)

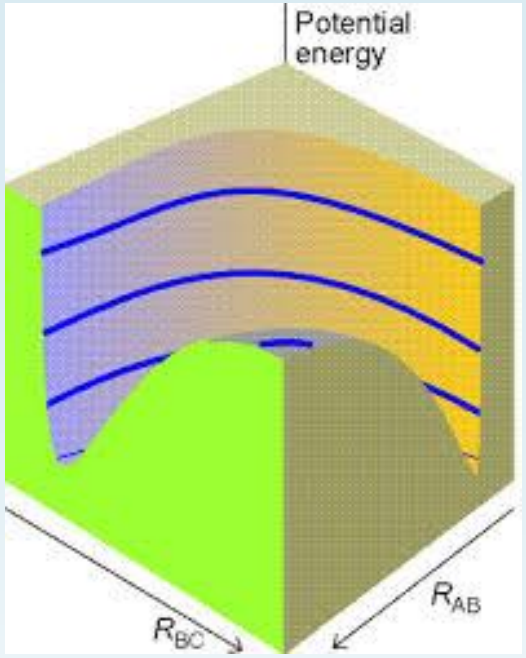
Potential
energy
R_{BC}
R_{AB}

H-C + D ➔ H C D ➔ H + C-D
H + C
H⇔C
Energy Surface for H-C + D ⟺ H + C-D 1 < x < 10 A, 1 < y < 8 A
H⇔C
Press
N New Start
S Repeat Start
<CR> End Program
8.0
R(DC)
1.0
1.0
R(CH)
10.0
D + C
D
H
C⇔D

THE JOURNAL OF PHYSICAL CHEMISTRY A
Article
pubs.acs.org/JPCA
2015

Accurate Time-Dependent Wave Packet Calculations for the $O^+ + H_2 \rightarrow OH^+ + H$ Ion–Molecule Reaction

N. Bulut,[†] J.F. Castillo,[‡] P. G. Jambrina,[‡] J. Klos,[§] O. Roncero,[∥] F. J. Aoiz,[‡] and L. Bañares*[,‡]

J. Phys. Chem. A 2015, 119, 11951–11962

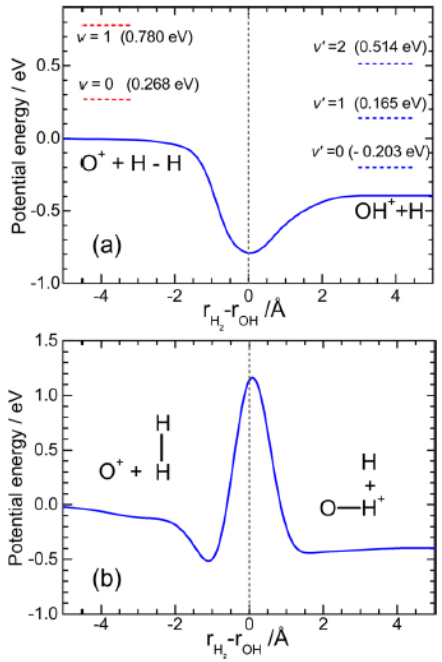

Figure 1. Minimum energy path for the $O^+ + H_2 \rightarrow OH^+ + H$ reaction calculated on the MMG PES[10] as a function of $r_{H_2} - r_{OH}$. (a) Collinear configuration, $\widehat{OHH}$ angle $\alpha = 180°$. The dashed horizontal lines indicate the energy of the initial H_2 $v = 0$ and $v = 1$, and final OH^+ $v' = 0$, $v' = 1$, and $v' = 2$ vibrational states. (b) Perpendicular configuration $\widehat{OHH}$ angle $\alpha = 90°$.

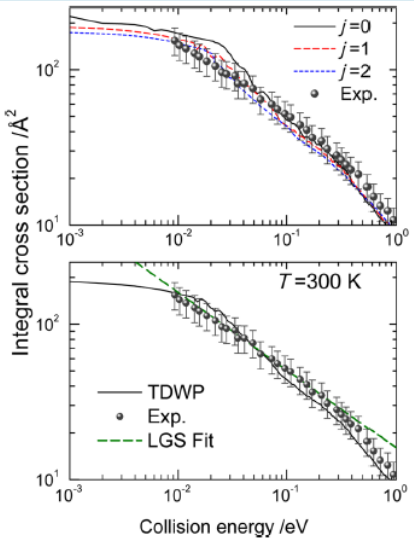

Figure 8. Top: total reaction cross section as a function of collision energy for the $O^+ + H_2(v=0,j)$ reactions. Solid black line: $j = 0$. Red dashed line: $j = 1$. Blue short-dashed line: $j = 2$. Solid circles: experimental results from ref 7. Bottom: Total reaction cross section as a function of collision energy for the $O^+ + H_2(v=0,\langle j \rangle)$ reaction averaged over the thermal rotational population at 300 K. Black solid line: TDWP. Solid circles: experimental results from ref 7. Green dashed line: Langevin model, $\sigma_r(E_c) = AE_c^{-1/2}$; $A = 16$ Å^2 eV$^{1/2}$.

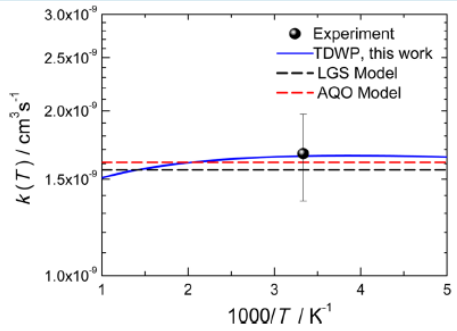

Figure 9. Thermal rate constants for the $O^+ + H_2$ reaction. Blue solid line: TDWP. Solid circle: experimental result from ref 7. Black dashed line: Langevin model. Red dashed line: AQO model.

Reaction Coordinate Diagrams

" ……We can follow the progress of a reaction on its way from reactants to products by graphing the energy of the species versus the reaction coordinate. We will be vague in describing the reaction coordinate because its definition is a mess of other variables composed to best make sense of the progress of the reaction. The value of the reaction coordinate is between zero and one. Understanding the meaning of the reaction coordinate is not important, just know that small values of reaction coordinate (0-0.2) mean little reaction has taken place and large values (0.8-1.0) mean that the reaction is almost over. It is a kind of scale of the progress of a reaction. A typical reaction coordinate diagram for a mechanism with a single step is shown below: ….."

Dynamics studies of $O^+ + D_2$ reaction using the time-dependent wave packet method

2019

Ziliang Zhu[a,b], Li Li[b], Qiju Li[b] and Bing Teng[a]

[a]College of Physics, Qing dao University, Qing dao, People's Republic of China; [b]Shandong Peninsula Engineering Research Center of Comprehensive Brine Utilization, Weifang University of Science and Technology, Shouguang, People's Republic of China

ABSTRACT

Based on the potential energy surface (PES) reported by Li *et al.* (Phys. Chem. Chem. Phys. **20**, 1039 (2018)), the initial state dynamics calculation of $O^+ + D_2$ ($v = 0, j = 0$) reaction was conducted using the time-dependent wave packet method with a second order split operator. Dynamics properties such as reaction probability, integral cross section, differential cross section, and distribution of products were calculated and compared with available experimental and theoretical results. The present integral cross section values were in good agreement with experimental results. In addition, the differential cross section indicates that the mechanism of the complex-formation reaction plays a dominant role during the reaction.

ARTICLE HISTORY
Received 15 November 2018
Accepted 7 May 2019

KEYWORDS
Reaction probability; $O^+ + D_2$ reaction; integral cross section; time-dependent wave packet

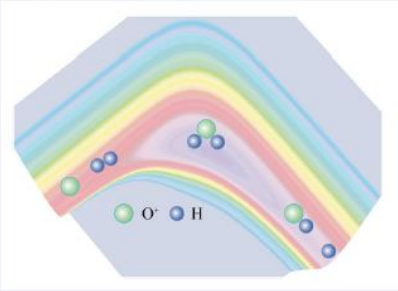

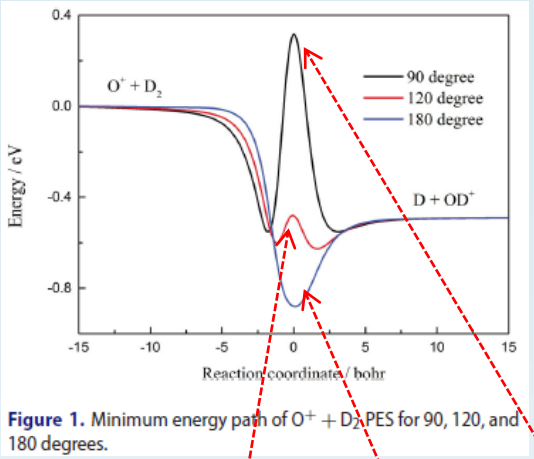

Figure 1. Minimum energy path of $O^+ + D_2$ PES for 90, 120, and 180 degrees.

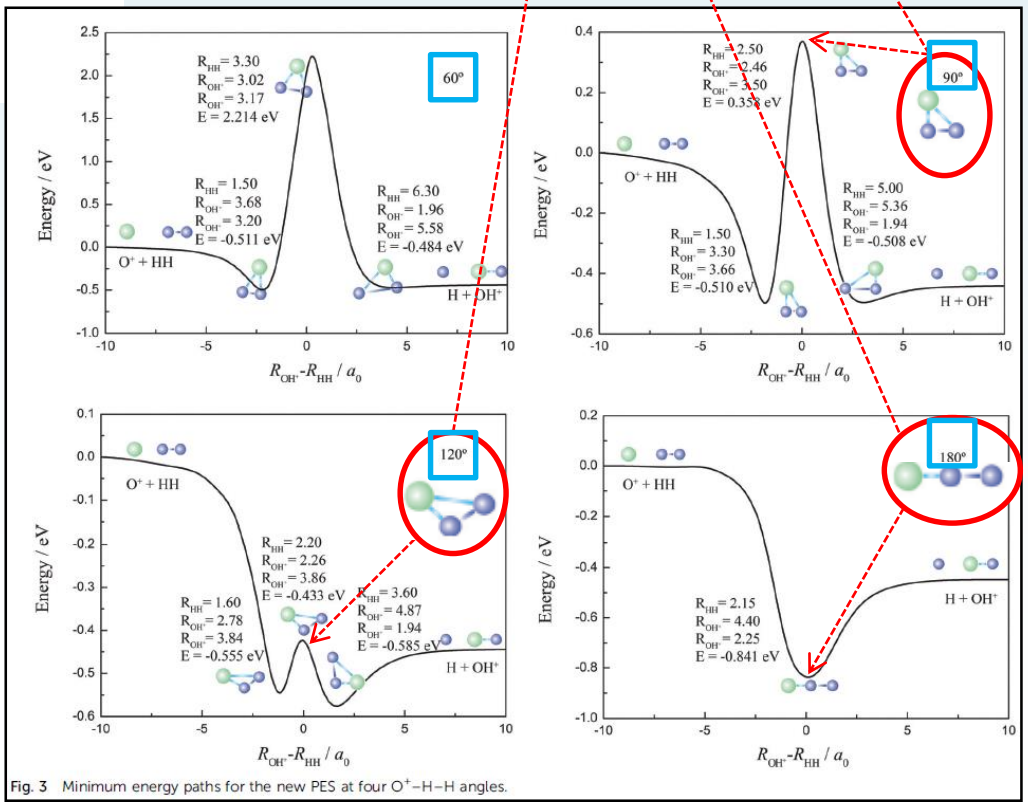

Fig. 3 Minimum energy paths for the new PES at four O^+–H–H angles.

"…..In chemistry, a **reaction coordinate**[1] is an abstract one-dimensional coordinate which represents progress along a reaction pathway. It is usually a geometric parameter that changes during the conversion of one or more molecular entities. In molecular dynamics simulations, a reaction coordinate is called **collective variable**.[2] ….."

Reaction Coordinate

PCCP

PAPER

View Article Online
View Journal | View Issue

Check for updates

Cite this: Phys. Chem. Chem. Phys., 2018, 20, 1039

A new potential energy surface of the OH_2^+ system and state-to-state quantum dynamics studies of the $O^+ + H_2$ reaction†

Wentao Li,[a] Jiuchuang Yuan,[b] Meiling Yuan,[c] Yong Zhang,[d] Minghai Yao[a] and Zhigang Sun*[b]

2018

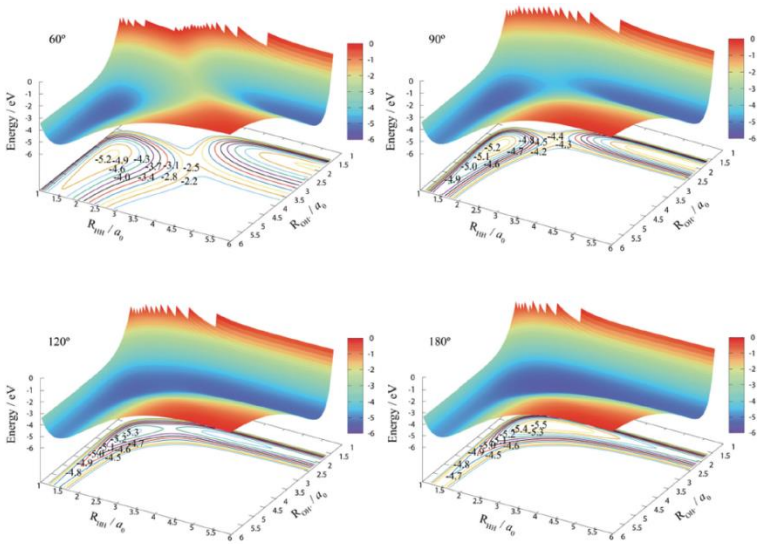

Fig. 2 Potential energy surfaces for O^+–H–H angles of 60°, 90°, 120°, and 180°.

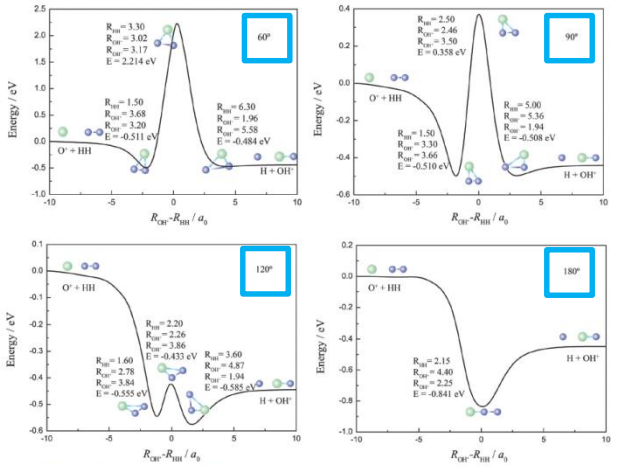

Fig. 3 Minimum energy paths for the new PES at four O^+–H–H angles.

Minimum energy paths

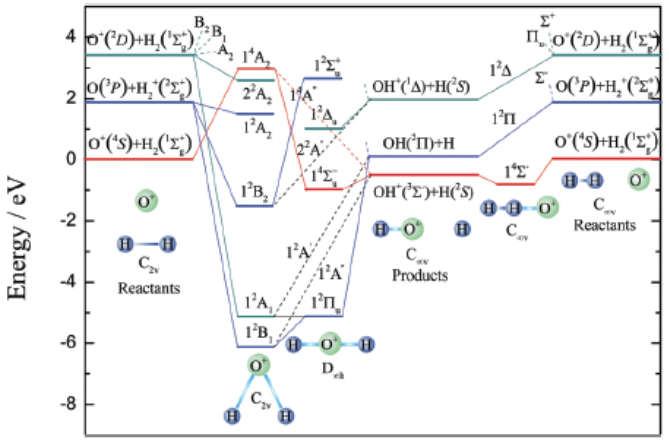

Fig. 1 Electronic correlation diagram for reactant, intermediate, and product arrangements of the H_2O^+ system under C_{2v}, $C_{\infty v}$, and $D_{\infty h}$ symmetries. The PESs of the title reaction are plotted by the red lines. This diagram is an adaptation of that reported in ref. 24.

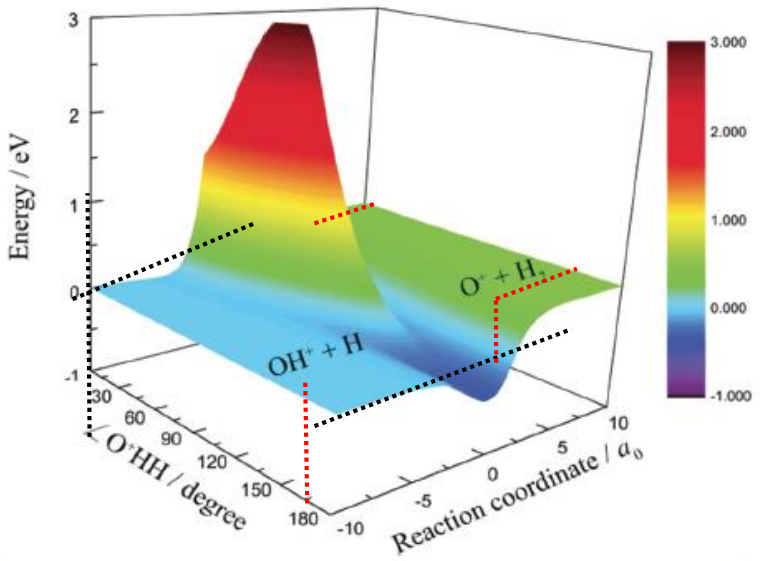

Fig. 4 Minimum energy paths of the new PES as a function of the bond–bond angle.

Reaction Coordinate

Reaction Coordinate

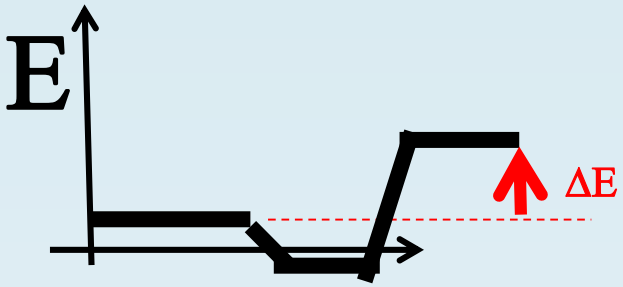

Reaction coordinate

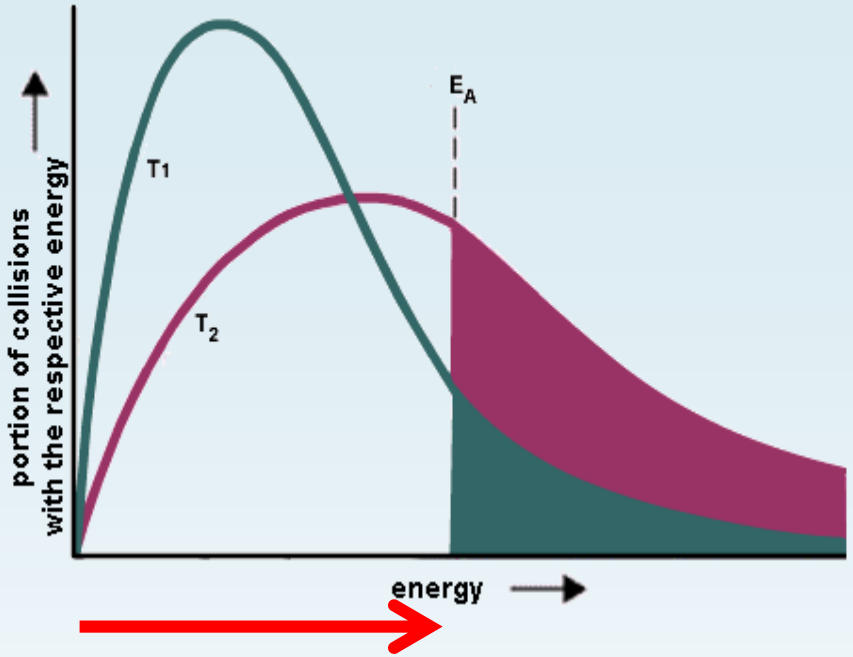

ΔE ……. E_A

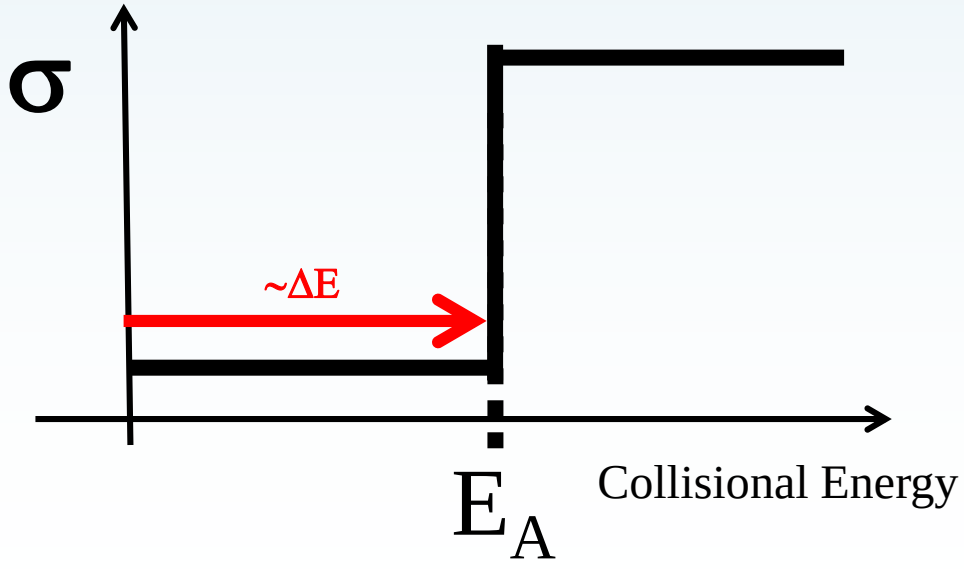

Kinetics of elementary process

$\mathbf{k(T)=<v\sigma>}$ →

$$k = \int_{Max(T)} f(v).v.\sigma(v)dv = k(T)$$

$$\nu \sim N v \sigma$$

$$\tau \sim 1/Nk$$

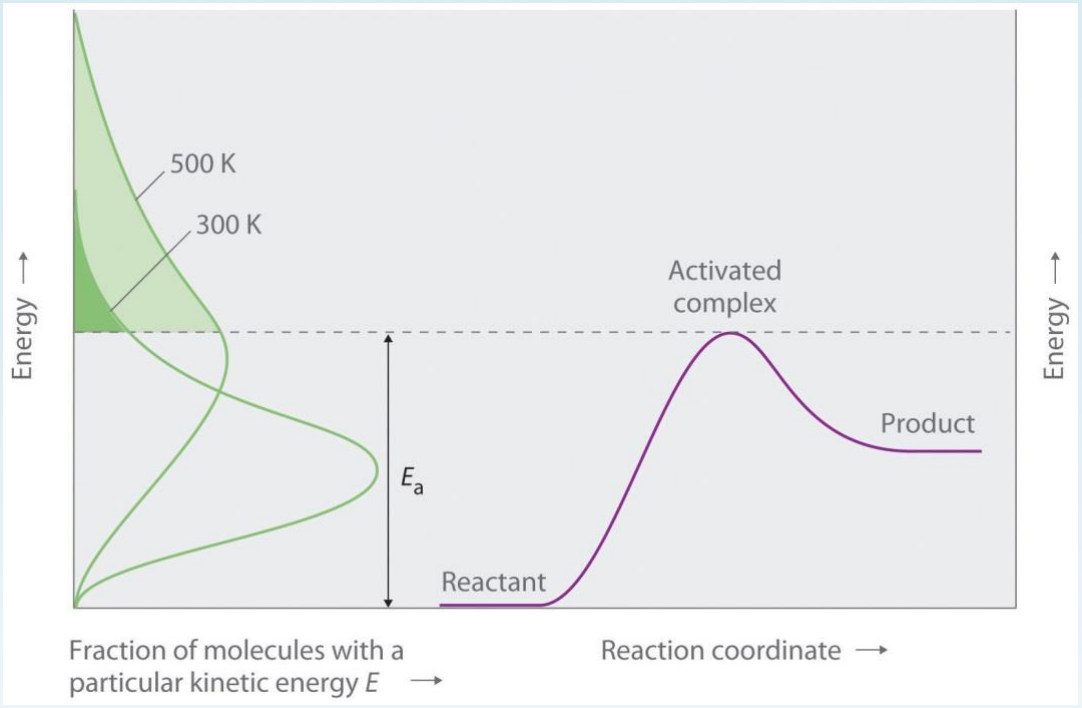

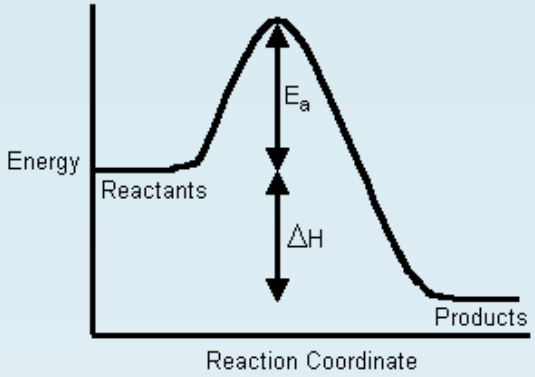

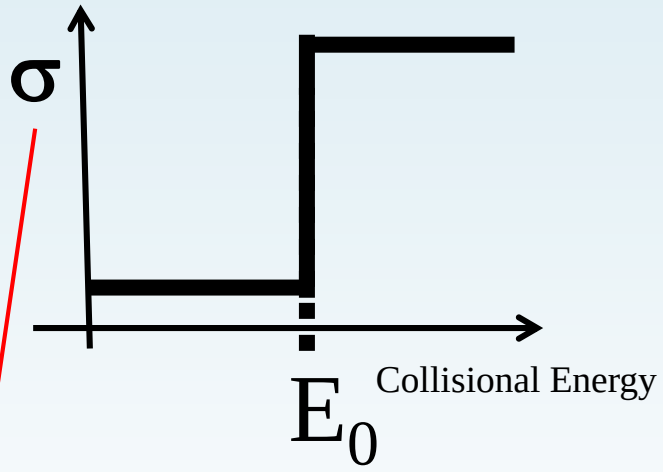

k(T)=<vσ>

$$k = \int_{Max(T)} f(v).v.\sigma(v)dv = k(T)$$

k(T)=

The thermally averaged rate constant $\alpha_{th}(T)$ (in a.u.) is obtained from the energy-dependent cross-section $\sigma(E)$ as

$$\alpha_{th}(T) = \frac{8\pi}{(2\pi kT)^{3/2}} \int_0^\infty \sigma(E_{el}) e^{-\frac{E_{el}}{kT}} E_{el} dE_{el}, \qquad (4)$$

where T is the temperature. Temperature dependencies $\alpha_{th}(T)$ for different rovibrational transitions $v \rightarrow v'$ obtained using equation (4) are shown in Fig. 3 as solid lines.

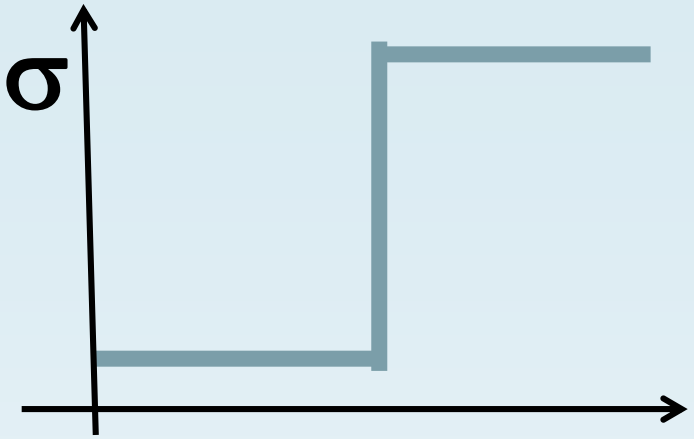

Electron impact rotational excitation of CH^+

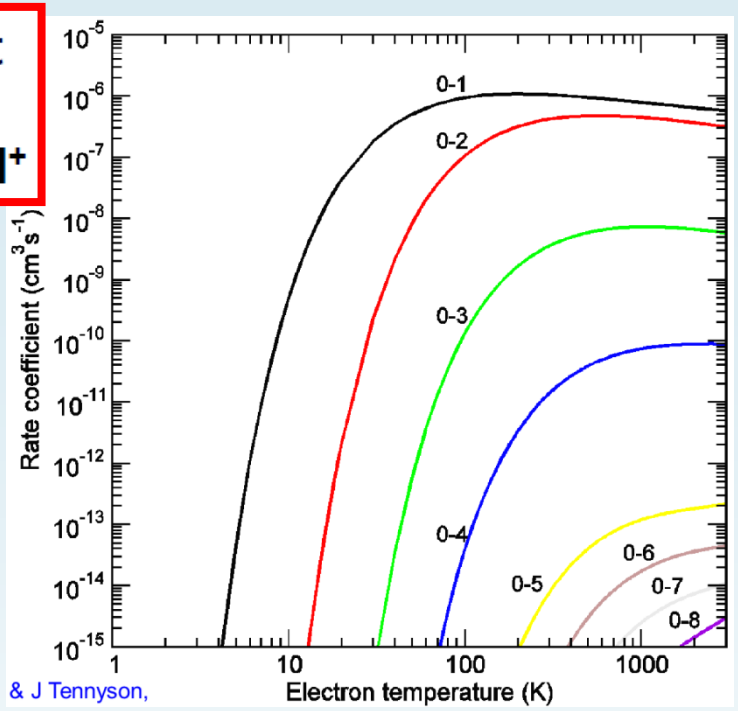

ΔE ..... E_A

The thermally averaged rate constant $\alpha_{th}(T)$ (in a.u.) is obtained from the energy-dependent cross-section $\sigma(E)$ as

k(T)=

$$\alpha_{th}(T) = \frac{8\pi}{(2\pi kT)^{3/2}} \int_0^\infty \sigma(E_{el}) e^{-\frac{E_{el}}{kT}} E_{el} dE_{el}\,, \qquad (4)$$

where T is the temperature. Temperature dependencies $\alpha_{th}(T)$ for different rovibrational transitions $v \rightarrow v'$ obtained using equation (4) are shown in Fig. 3 as solid lines.

For further discussion, it is convenient to represent the cross-section $\sigma(E_{el})$ in the form

$$\sigma(E_{el}) = \frac{\pi}{k^2} P(E_{el})\,, \qquad (5)$$

where k is the wave vector of the incident electron, $P(E_{el})$ is the probability for vibrational (de-)excitation at collision energy E_{el}.

$$k = A\, e^{-\frac{E_a}{RT}}$$

activation energy

pre-exponential factor

average kinetic energy

$$\ln k = \ln A - \frac{E_a}{RT}$$

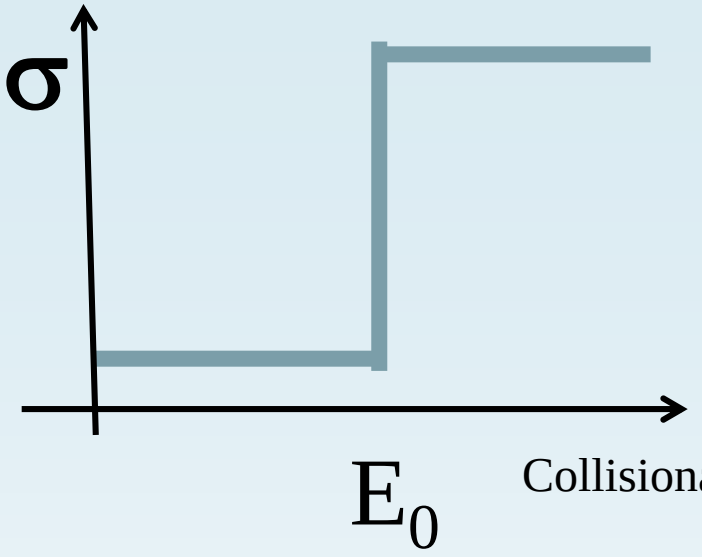

Electron impact rotational excitation of CH^+

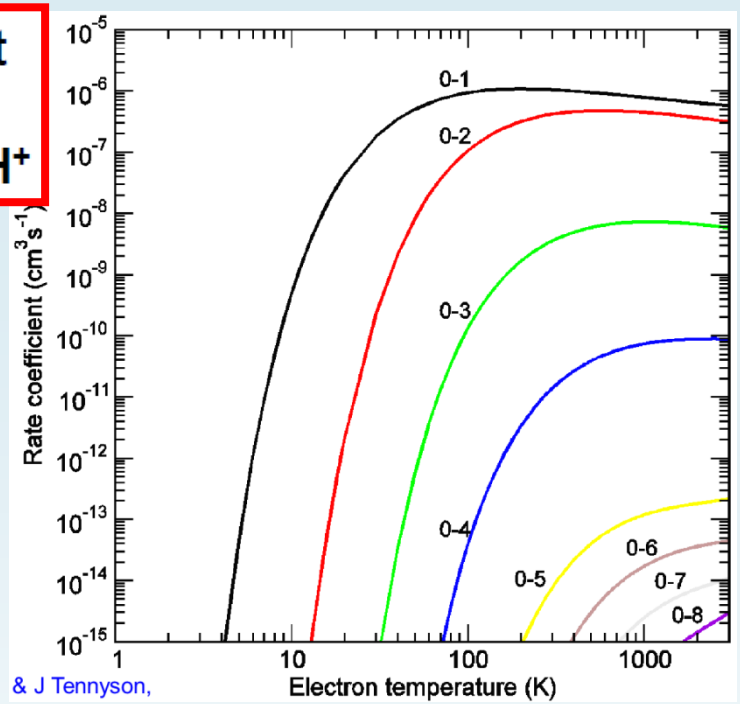

Arrhenius plot

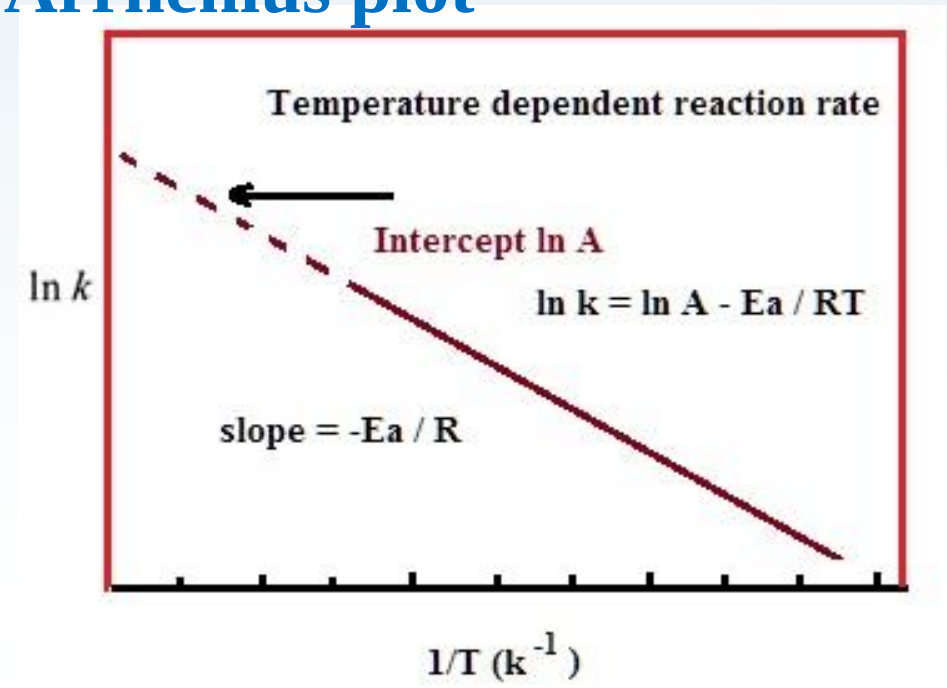

$$k = A\, e^{-\frac{E_a}{RT}}$$

activation energy

pre-exponential factor

average kinetic energy

$$\ln k = \ln A - \frac{E_a}{RT}$$

$$OD^- + H_2 \rightarrow OH^- + HD, \quad \Delta H = 24.0 \text{ meV}. \qquad (2)$$

1eV corresponds to ~ 11604K

$$k = A\, e^{-\frac{E_a}{RT}}$$

activation energy

pre-exponential factor

average kinetic energy

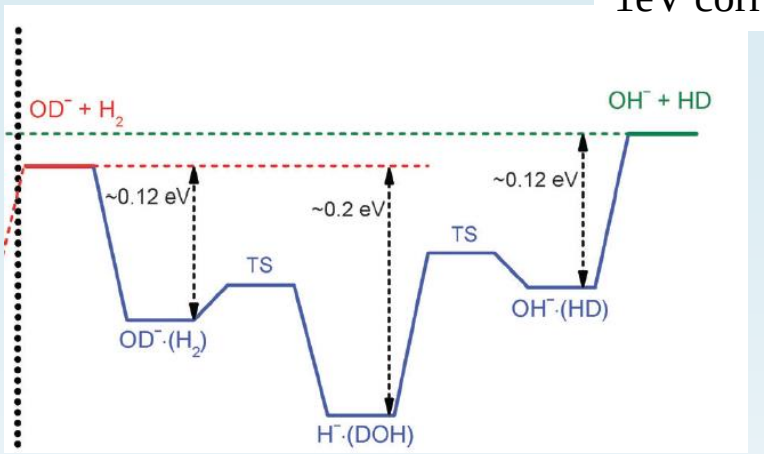

$$\ln k = \ln A - \frac{E_a}{RT}$$

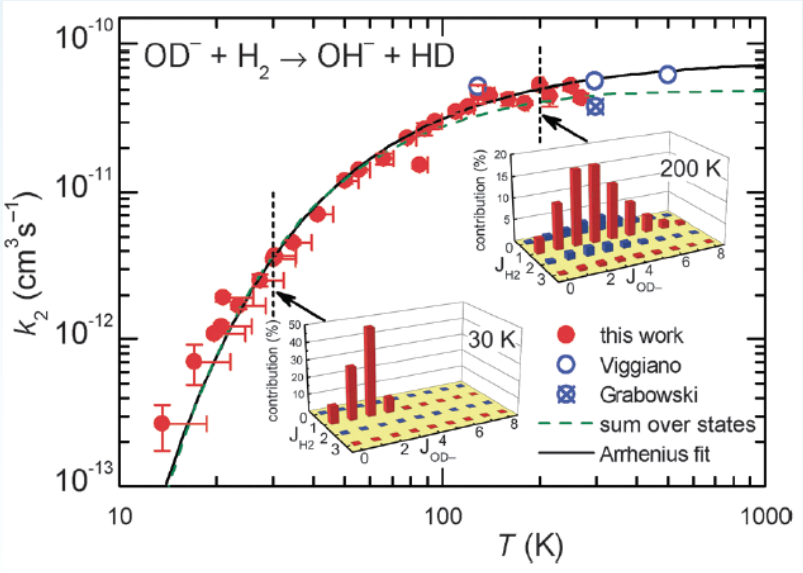

Temperature dependence of the rate coefficient k_2

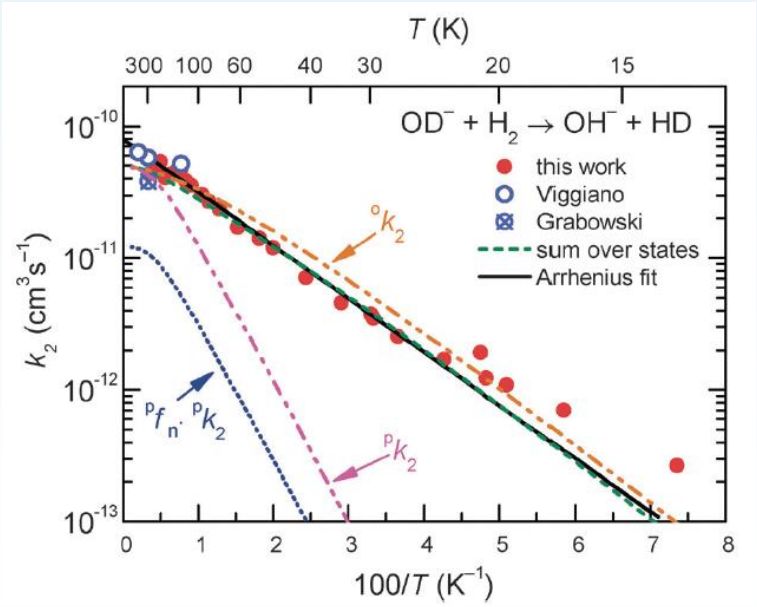

Arrhenius plot of rate coefficient k_2 for reaction (2)

2018

$$\ln k = \ln A - \frac{E_a}{RT}$$

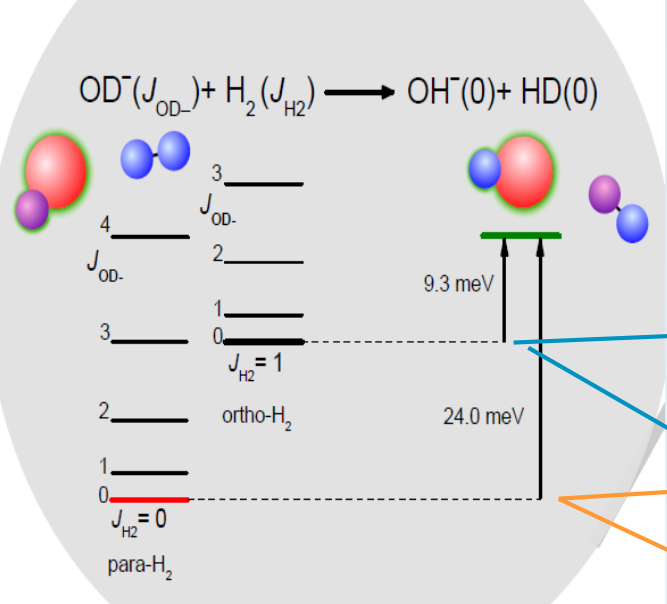

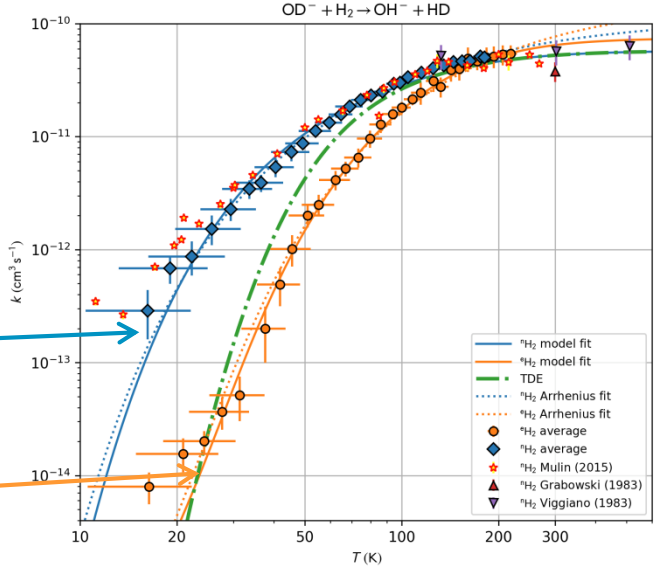

$$^{o/p}k_2 = \frac{1}{^{o/p}f} k_{20} \sum_{JOD-} \sum_{JH2}^{o/p} \left(P_{JH2} P_{JOD-} e^{\frac{-Max\{(\Delta H - E_{JH2} - E_{JOD-});0\}}{k_B T}} \right)$$

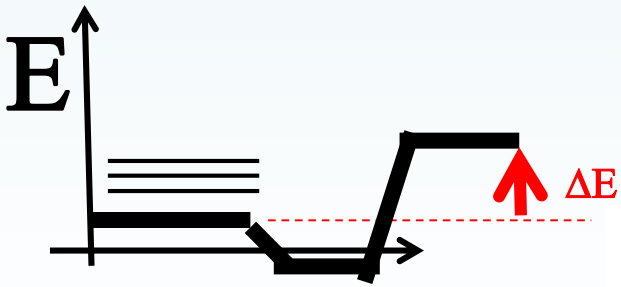

Reaction coordinate

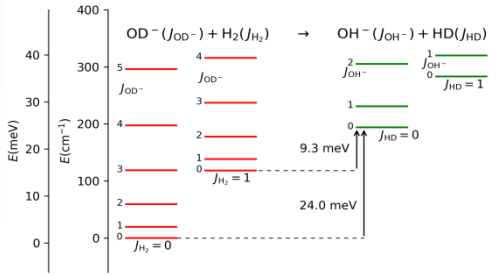

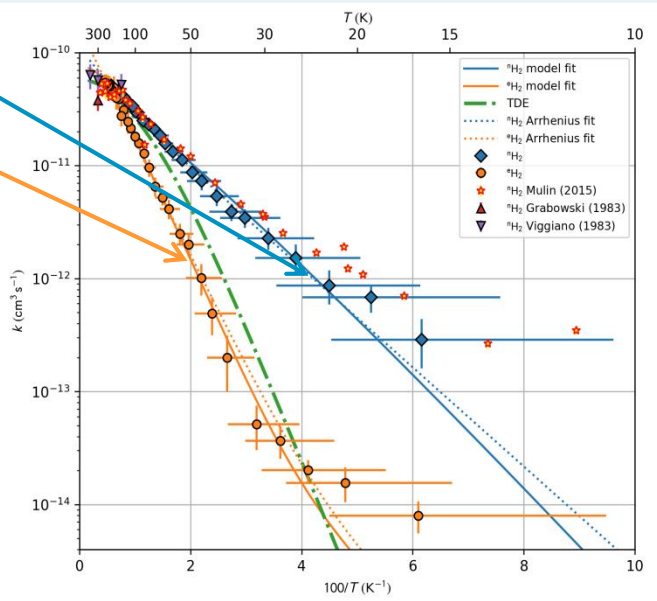

Arrhenius plot

ELSEVIER

1994

International Journal of Mass Spectrometry and Ion Processes 134 (1994) 67–71

Mass Spectrometry and Ion Processes

Short communication

Observations of Arrhenius behaviour over 56 decades: dissociation of N_4^+ ions

J. Glosík[a,b], V. Skalský[a,b], W. Lindinger[a]

$$\ln k = \ln A - \frac{E_a}{RT}$$

The equilibrium constant K_c for the formation and destruction of N_4^+, described by Eqs. (4) and (8)

$$K_c = \frac{k_{forward}}{k_{reverse}} = \frac{k_3}{k_2} \qquad (11)$$

is expressed in the van't Hoff formula,

$$RT \ln K_p = -\Delta G_p = -\Delta H_p + T\Delta S_p \qquad (12)$$

where ΔG_p, ΔH_p and ΔS_p (subscript p means constant pressure) is the free energy, enthalpy and entropy change, respectively, $K_p = K_c(R'T)^{\Delta n}$ and Δn is the mole change in the reaction. In reaction (10), $\Delta n = -1$. For more details see Ref. 22.

$$N_4^+ + He \underset{k_3}{\overset{k_2}{\rightleftharpoons}} N_2^+ + N_2 + He$$

$$k_2 = A \exp\left(-\frac{3E_a}{2E_b}\right) = A \exp\left(-\frac{E_a}{kT_b}\right)$$

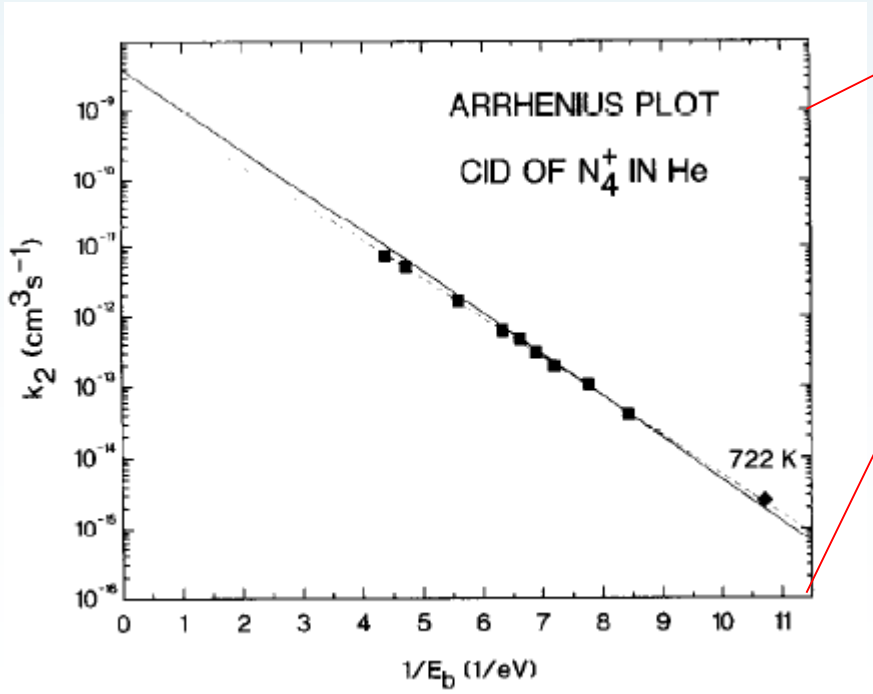

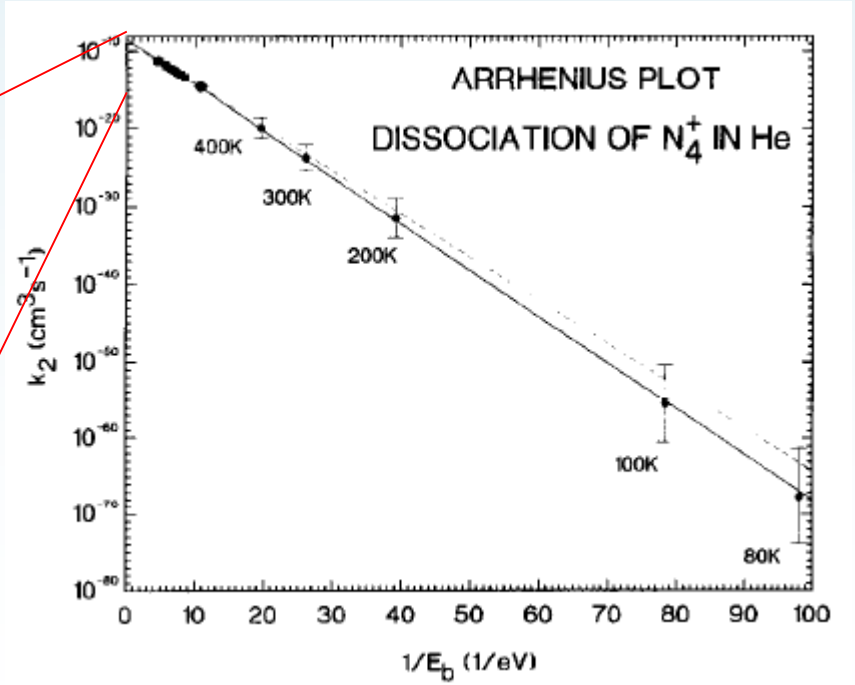

exo

$$OH^- + HD \rightarrow OH_2D^- \rightarrow OD^- + H_2$$

OH_2D^-

endo

$$OD^- + HD \rightarrow OD_2H^- \rightarrow OH^- + D_2$$

OD_2H^-

Quantum State-Resolved Study of the Four-Atom Reaction OH^- ($X^1\Sigma^+$) + D_2 ($X^1\Sigma_g^+$, $v = 0$) → HOD (X^1A', v') + D^- (^1S)

Yue Li, Li Liu, and James M. Farrar*

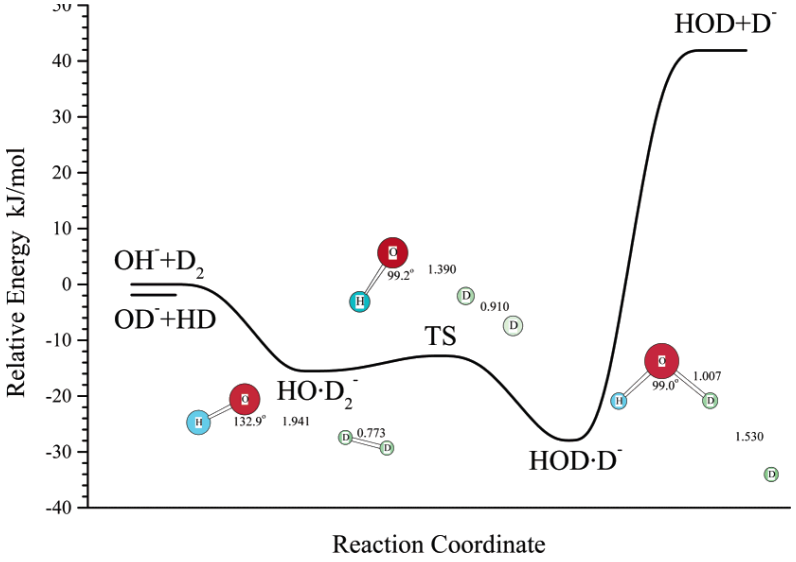

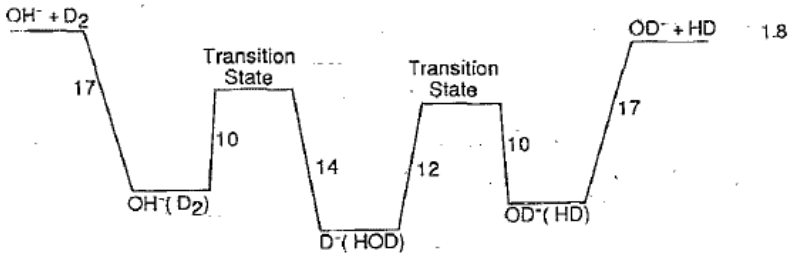

FIG. 4. Schematic of the potential energy diagram. Values refer to approximate energies relative to that of $OH^- + D_2$ in kJ/mol and are taken from Chalasinski *et al.* (Ref. 27). These values are not known with high certainty and are somewhat different than those found in Ortiz (Ref. 28).

Viggiano

Miller *et al.*: Formation and destruction of H_3O^-

J. Chem. Phys., Vol. 100, No. 8, 15 April 1994

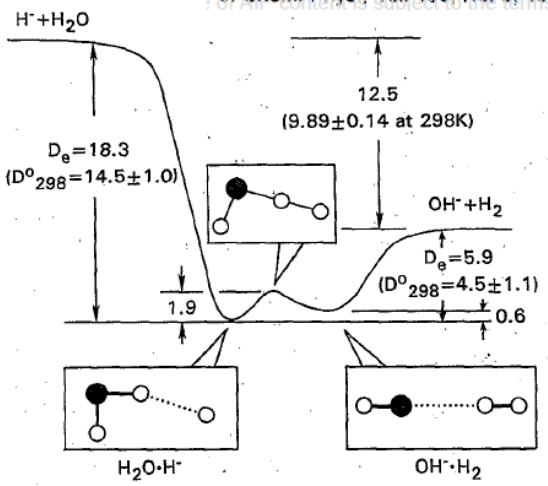

FIG. 1. Sketch of the potential surface for $H^- + H_2O \rightarrow OH^- + H_2$. Energies are theoretical values from Ref. 9 and are given in kcal mol^{-1}. Experimental energies are given in parentheses; the D^0_{298} values are from the present paper, and the asymptotic energy difference is from Ref. 5. Adapted from Dunning *et al.*, Ref. 9.

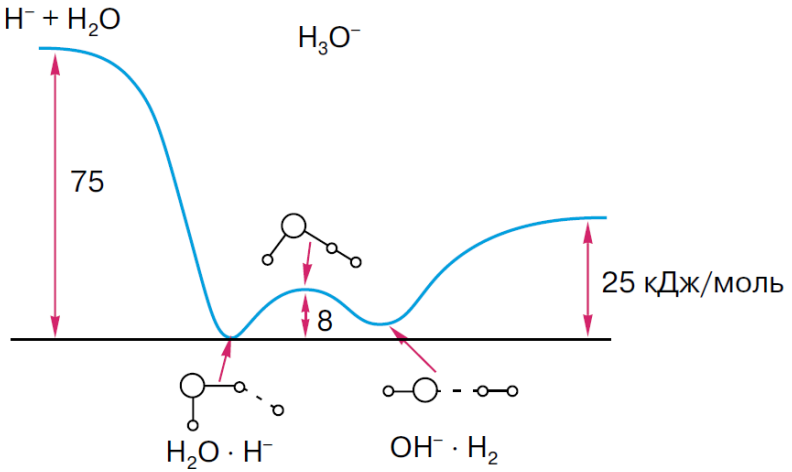

Рис. 4. Сечение потенциальной поверхности вдоль пути реакции для молекулы H_3O^- (по данным [3]).

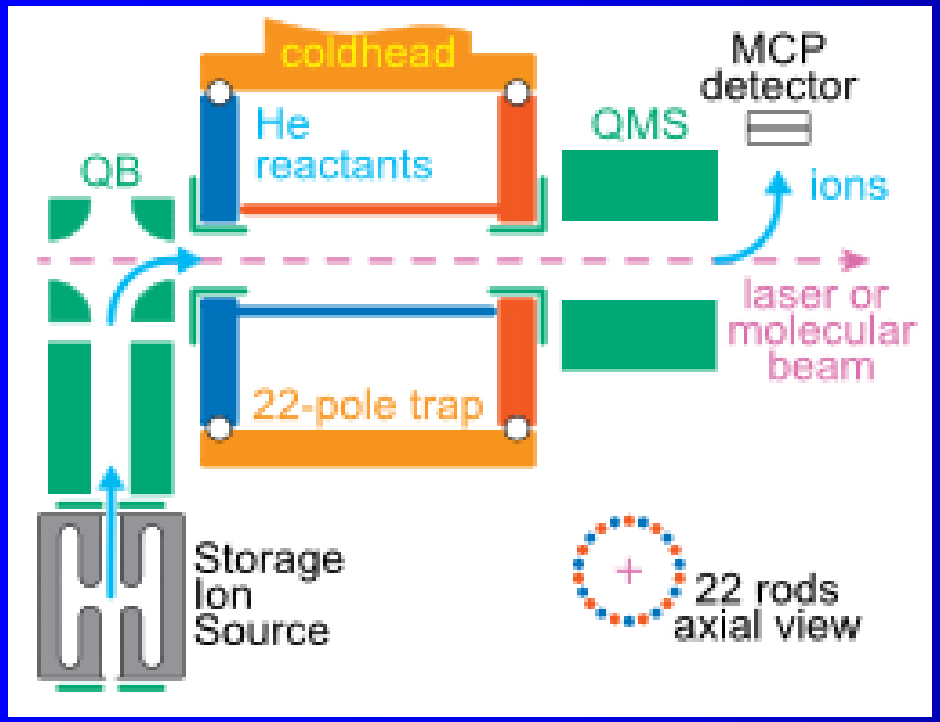

$OD^- + HD \rightarrow OH^- + D_2$ endothermic $\Delta H_0 = 17.2$ meV, (1)

$OH^- + D_2 \rightarrow OD^- + HD$ exothermic $\Delta H_0 = -17.2$ meV. (2)

$OD^- + HD \rightarrow OH^- + D_2$ endothermic $\Delta H_0 = 17.2$ meV, (1)

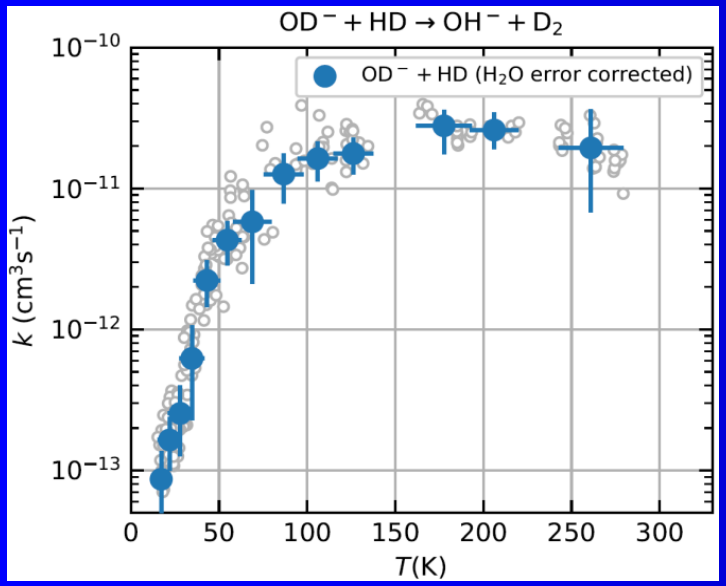

$OH^- + D_2 \rightarrow OD^- + HD$ exothermic $\Delta H_0 = -17.2$ meV. (2)

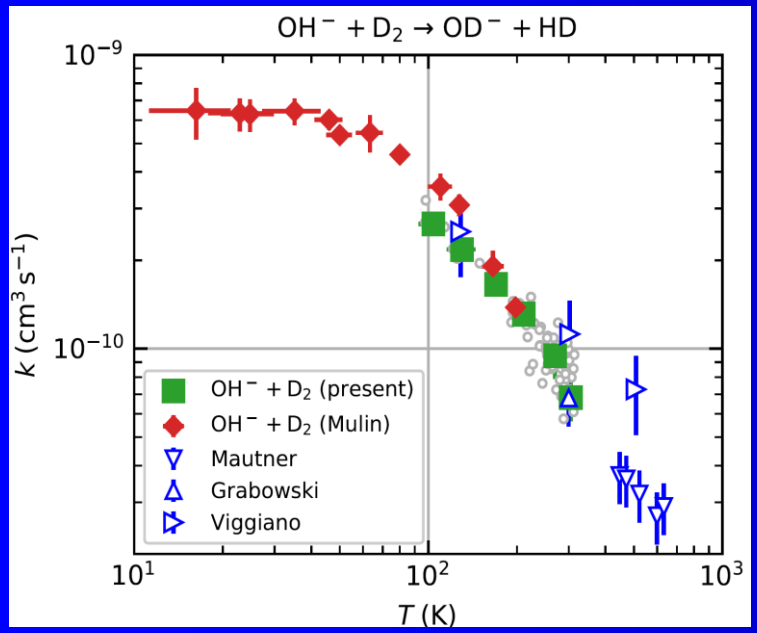

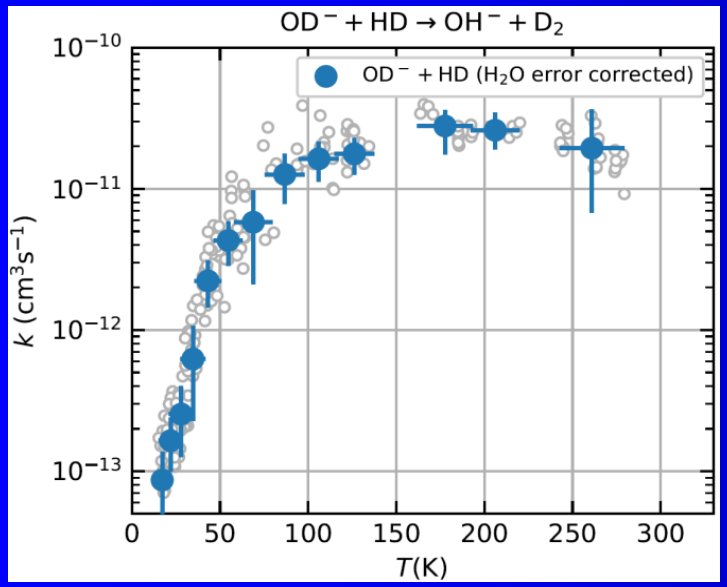
$OD^- + HD \rightarrow OH^- + D_2$
$OD^- + HD$ (H_2O error corrected)
k ($cm^3 s^{-1}$)
T(K)

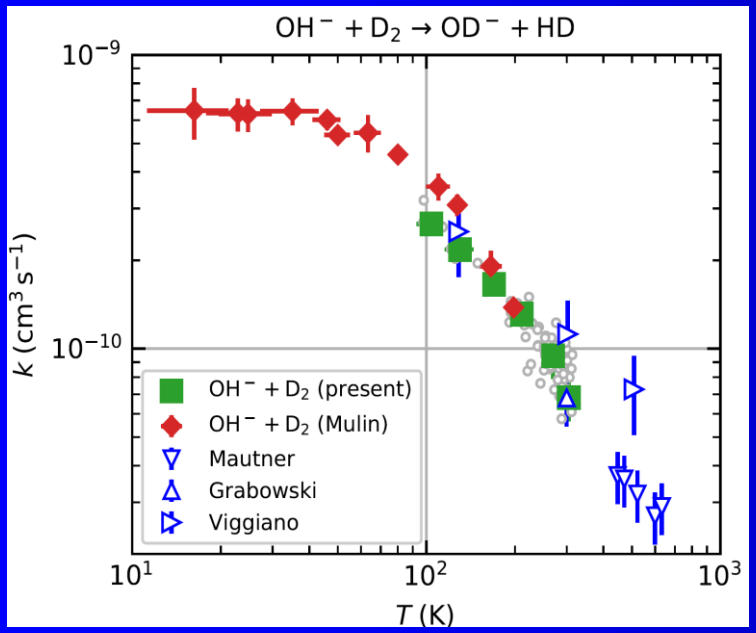
$OH^- + D_2 \rightarrow OD^- + HD$
$OH^- + D_2$ (present)
$OH^- + D_2$ (Mulin)
Mautner
Grabowski
Viggiano
k ($cm^3 s^{-1}$)
T (K)

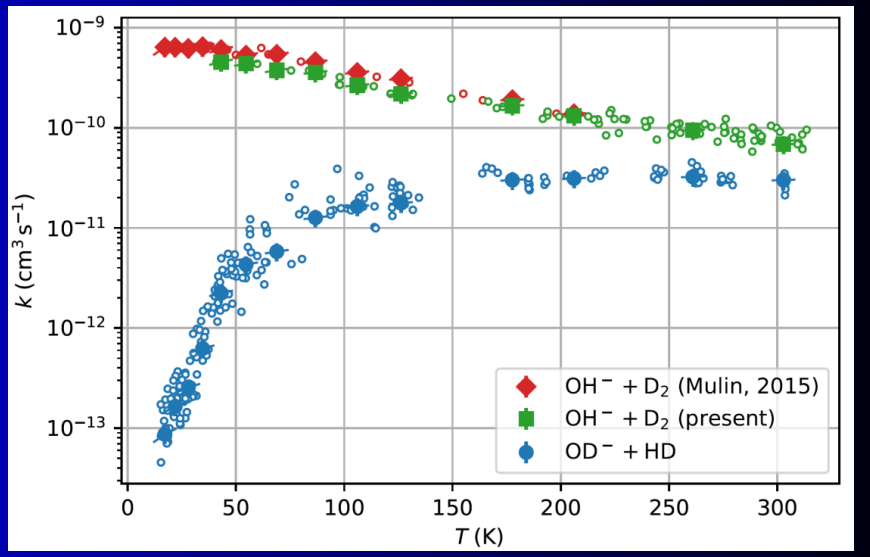
$OH^- + D_2$ (Mulin, 2015)
$OH^- + D_2$ (present)
$OD^- + HD$
k ($cm^3 s^{-1}$)
T (K)

$OD^- + HD \rightarrow OH^- + D_2$ endothermic $\Delta H_0 = 17.2$ meV,

$OH^- + D_2 \rightarrow OD^- + HD$ exothermic $\Delta H_0 = -17.2$ meV.

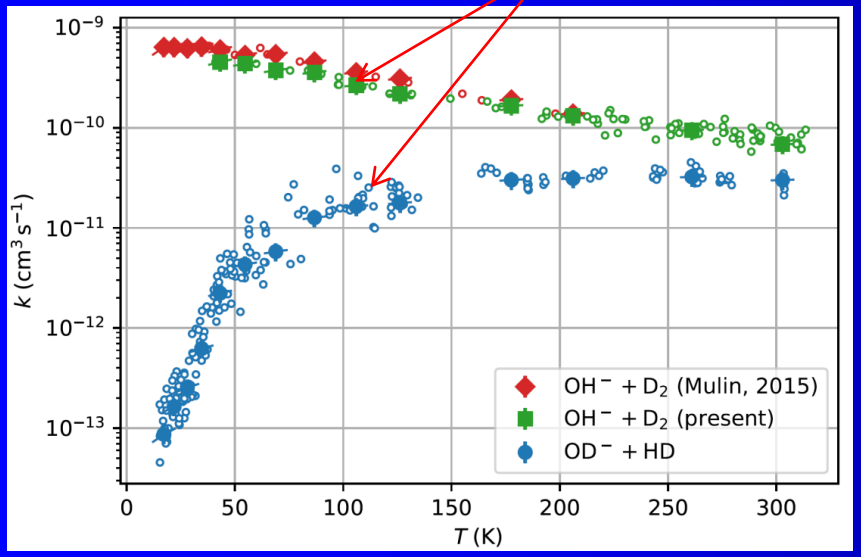

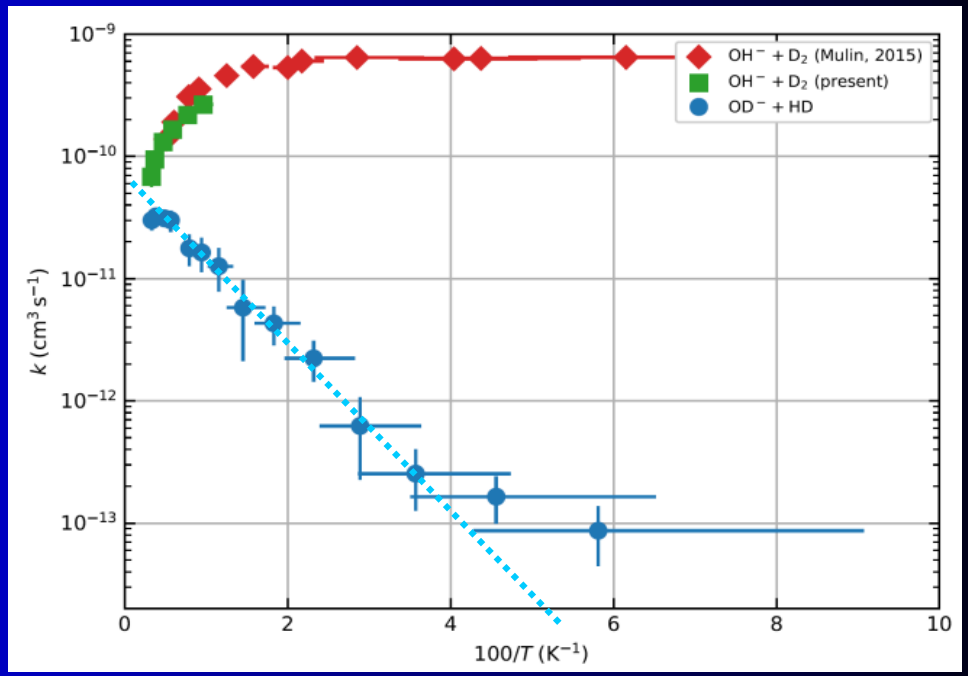

OD- + HD → k_{f1} → OH- + D_2.

OD- + HD ← k_{r2} ← OH- + D_2.

$$K_{eq12}(T) = k_{f1}/k_{r2}$$

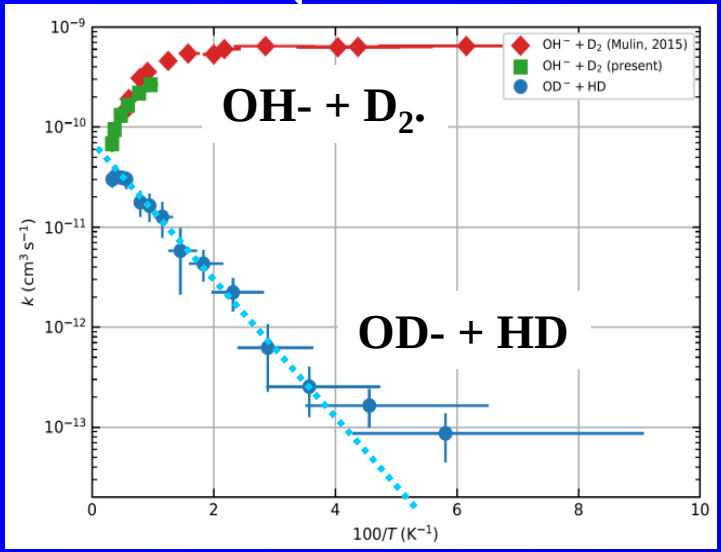

Combining the well-known formula for the Gibbs free energy of reaction

$$\Delta_r G^\ominus = \Delta_r H^\ominus - T\Delta_r S^\ominus,$$

where S is the entropy of the system, with the Gibbs free energy isotherm equation:[5]

$$\Delta_r G^\ominus = -RT \ln K_{\mathrm{eq}},$$

we obtain

$$\ln K_{\mathrm{eq}} = -\frac{\Delta_r H^\ominus}{RT} + \frac{\Delta_r S^\ominus}{R}.$$

Van 't Hoff equation

Van 't Hoff plot for an endothermic reaction

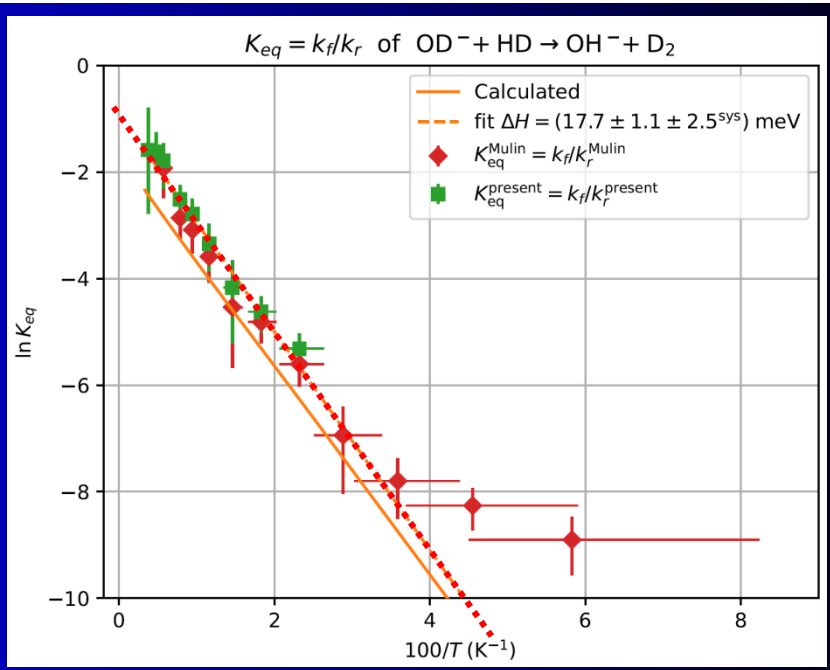

Arrhenius plots of the rate coefficient k_{f1} and k_{r2}

Arrhenius function $k_{f1} = k_{f1A}\exp(-E_{f1A}/k_BT)$

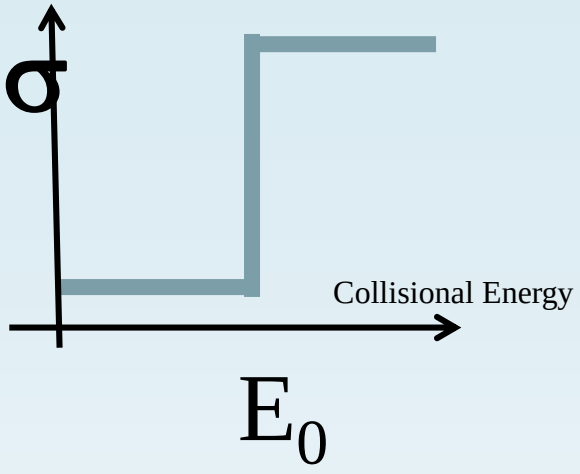

$H_3^+ + e$

Figure 2. Probabilities of vibrational excitation from the ground vibrational level $\{00^0\}$ to several excited vibrational levels calculated using the vibrational frame transformation only. Energies of vibrational thresholds are labelled with arrows and the corresponding vibrational quantum numbers.

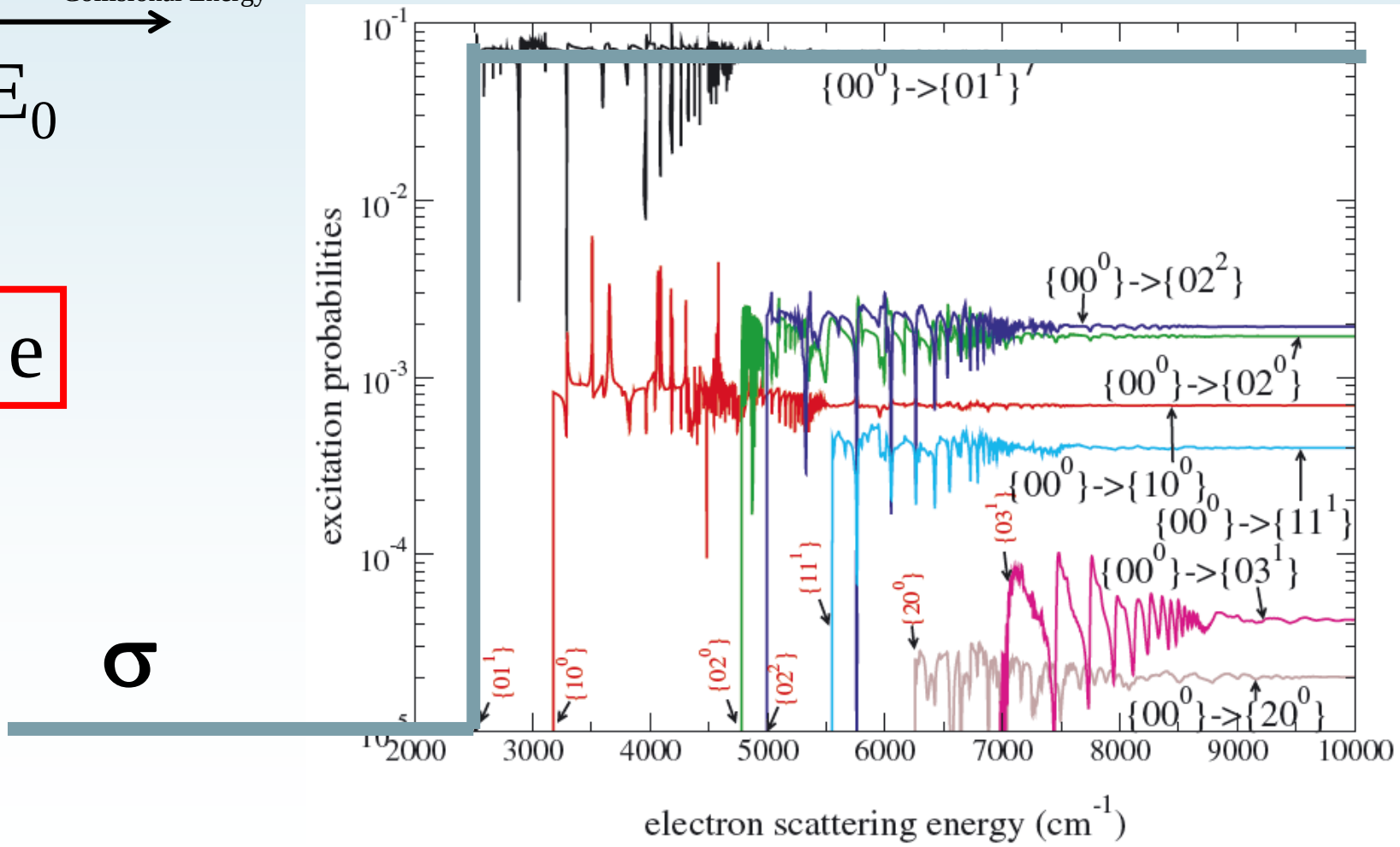

Rovibrational excitation

$H_3^+ + e$

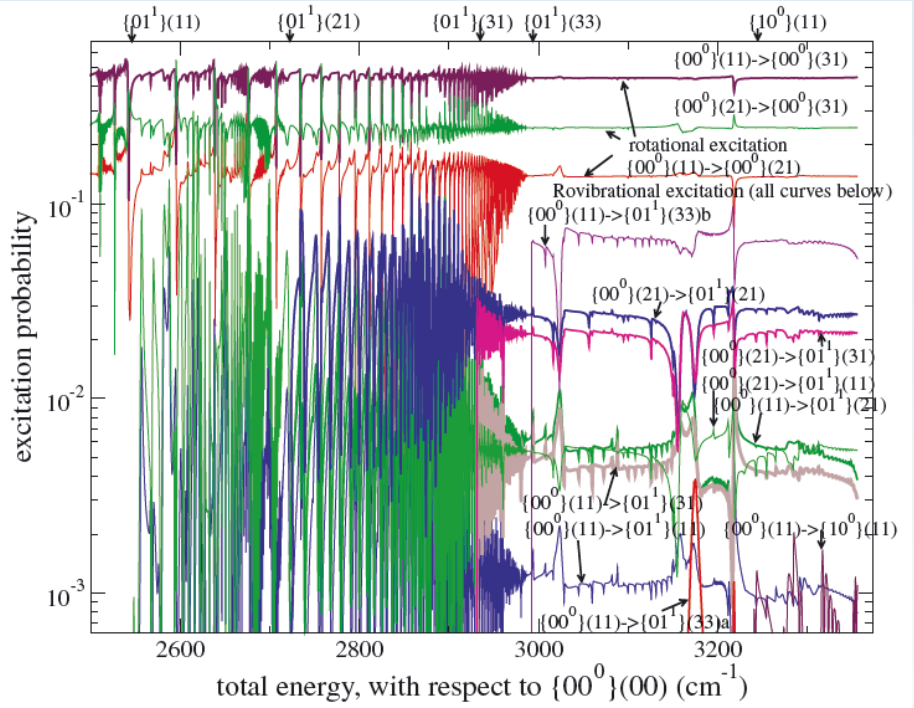

Figure 1. Probabilities of rovibrational excitation of the H_3^+ ion calculated using the full rovibrational frame transformation. Only transitions from the ground vibrational level $\{00^0\}$ are shown. The $\{00^0\} \rightarrow \{01^1\}$ probabilities oscillate a lot below 3000 cm^{-1} and become less energy-dependent above. The oscillations are due to the strong rotational coupling between individual rotational levels of the initial and final states of the ion. When averaged over the initial and summed over the final rotational states and averaged over the appropriate energy distribution, the resulting probabilities are similar in magnitude to the probabilities shown in Fig. 2. The labels on top of the figure indicate different rovibrational ionization limits. Note that the zero of energy in the figure is set to the energy of the forbidden rovibrational level $\{00^0\}(00)$.

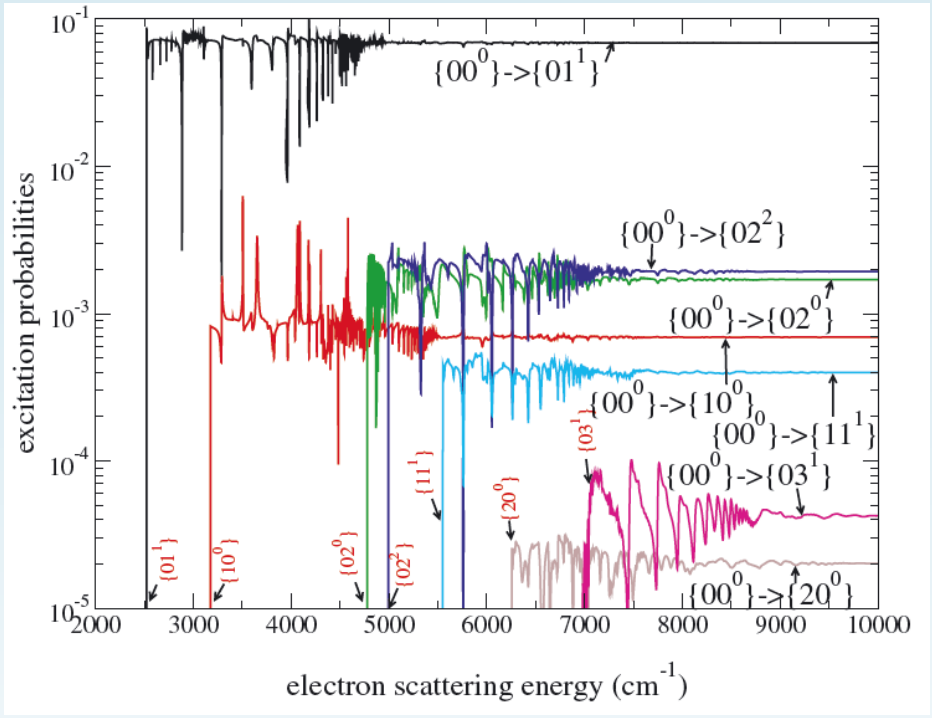

Figure 2. Probabilities of vibrational excitation from the ground vibrational level $\{00^0\}$ to several excited vibrational levels calculated using the vibrational frame transformation only. Energies of vibrational thresholds are labelled with arrows and the corresponding vibrational quantum numbers.

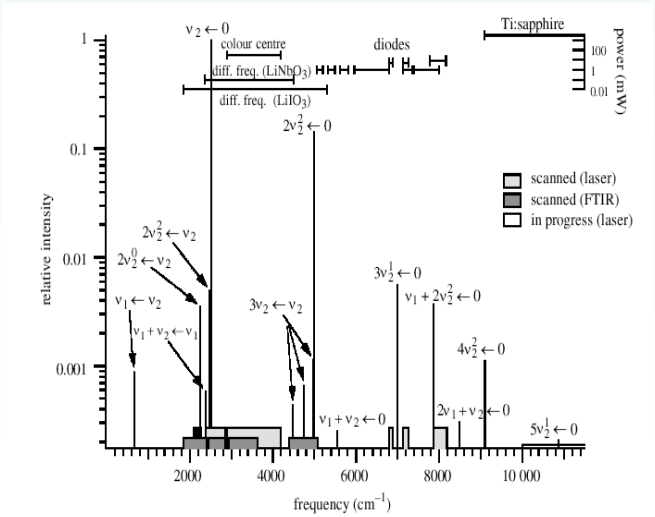

Chlazení elektronů v plazmatu

- A

Available online at www.sciencedirect.com
SCIENCE DIRECT®
ELSEVIER
Chemical Physics Letters 372 (2003) 728–732
2003
CHEMICAL PHYSICS LETTERS
www.elsevier.com/locate/cplett

The influence of electron–electron collisions on electron thermalization in He and Ar afterglow plasmas

D. Trunec [a,*], P. Španěl [b], D. Smith [c]

[a] *Department of Physical Electronics, Faculty of Science, Masaryk University, Kotlářská 2, 611 37 Brno, Czech Republic*
[b] *J. Heyrovsky Institute of Physical Chemistry, Academy of Sciences of the Czech Republic, Dolejškova 3, 182 23 Prague 8, Czech Republic*
[c] *Centre for Science and Technology in Medicine, School of Postgraduate Medicine, Keele University, Thornburrow Drive, Hartshill, Stoke-on-Trent ST4 7QB, UK*

Received 6 January 2003; in final form 18 March 2003

Abstract

The electron energy distribution functions for electron thermalization in helium and argon afterglow plasmas have been calculated taking into account electron–neutral and electron–electron collisions. This work shows that electron–electron collisions can lead to the Maxwellization of the electron energy distribution function and thus to different rates of electron thermalization.

Boltzmann equation

2. Boltzmann equation

The time rate of change of the electron distribution function, $f(v,t)$, is described by the Boltzmann equation [16]

$$\frac{\partial f(v,t)}{\partial t} = C_{en} + C_{ee}, \tag{1}$$

where C_{en} is the collision term for electron–neutral collisions

$$C_{en} = n_n \frac{m_e}{m_n} \frac{1}{v^2} \frac{\partial}{\partial v} \left(v^4 \sigma_T(v) \left(f + \frac{kT_n}{m_e} \frac{1}{v} \frac{\partial f}{\partial v} \right) \right) \tag{2}$$

and C_{ee} is the collision term for electron–electron collisions

$$C_{ee} = \Gamma_{ee} \frac{1}{v^2} \frac{\partial}{\partial v} \left(I_0^0 f + (I_2^0 + J_{-1}^0) \frac{v}{3} \frac{\partial f}{\partial v} \right), \tag{3}$$

$$I_p^0 = \frac{4\pi}{v^p} \int_0^v v^{2+p} f \, dv,$$

$$J_p^0 = \frac{4\pi}{v^p} \int_v^\infty v^{2+p} f \, dv,$$

$$\Gamma_{ee} = 4\pi \left(\frac{e^2}{4\pi\epsilon_0 m_e} \right)^2 \ln \Lambda,$$

where n_n is the number density of neutral gas, T_n is the gas temperature, m_n is the mass of neutral gas atoms and σ_T is the momentum transfer cross-section for electron–neutral collisions. $\Lambda = \lambda_D / b_0$ (λ_D is the Debye length, b_0 is the impact parameter for a 90° scattering). For our conditions (see below) $\ln \Lambda = 10$. As can be seen from Eq. (2), only elastic collisions are taken into account. The distribution function has the normalization

$$n_e = 4\pi \int_0^\infty v^2 f(v) \, dv, \tag{4}$$

so that the function

$$F(v) = \frac{4\pi v^2}{n_e} f(v)$$

is a velocity distribution function.

The initial distribution for the calculation was chosen as

$$f(v,0) = \frac{n_e}{4\pi k T_n \sqrt{\pi}} \frac{1}{v^2} \exp\left(- \left(\frac{v - v_0}{kT_n} \right)^2 \right) \tag{5}$$

with $v_0 = 1.19 \times 10^6$ ms^{-1}. This v_0 corresponds to electrons with energies in a narrow peak round 4 eV. The peak width is $2kT_n$.

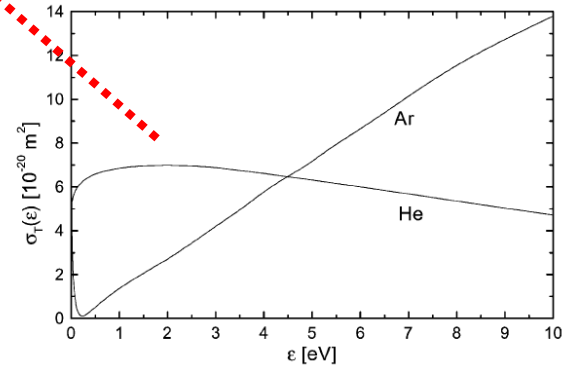

Fig. 2. The momentum transfer cross-sections for electron–argon [20] and electron–helium elastic collisions [21].

El.-neutral He collisions only

3.2. Electron–neutral collisions

Let us study first the energy relaxation due to electron–neutral collision only. For simplicity let us consider that the molecules of neutral gas are at rest ($T_n = 0$ K) and that the momentum transfer cross-section does not depend on the velocity, which is good approximation for helium.

Thus we obtain the equation

$$\frac{\partial f(v,t)}{\partial t} = n_n \frac{m_e}{m_n} \sigma_T \frac{1}{v^2} \frac{\partial}{\partial v}\left(v^4 f\right). \quad (6)$$

This equation can be solved analytically; the solution is

$$f(v,t) = \frac{1}{v^4} g\left(at - \frac{1}{v}\right), \quad (7)$$

where $a = n_n \frac{m_e}{m_n} \sigma_T$ and g is an arbitrary function, which must be determined from initial condition. For our initial condition (5) we obtain

$$f(v,t) = \frac{n_e}{4\pi k T_n \sqrt{\pi}} \frac{1}{v^2 (atv-1)^2} \times \exp\left(-\left(\frac{\frac{v}{atv-1} + v_0}{kT_n}\right)^2\right). \quad (8)$$

The time development of this distribution function is shown in Fig. 1.

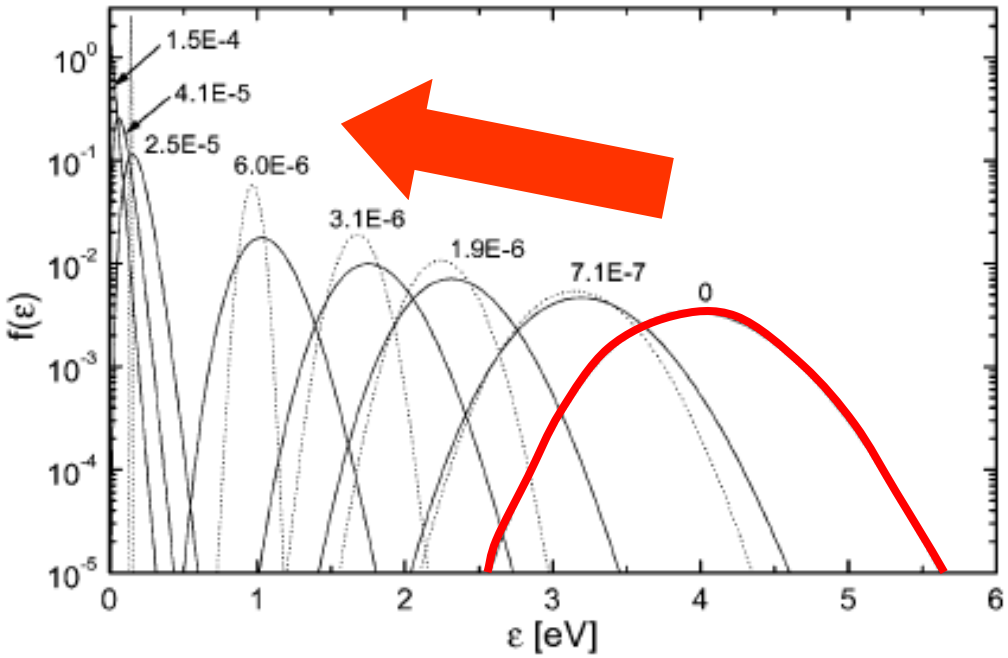

Fig. 1. The time dependence of the electron distribution function in helium afterglow plasma. The neutral gas number density is $n_n = 1.65 \times 10^{16}$ cm^{-3}, the neutral gas temperature: dotted line, $T_n = 0$ K; full line, $T_n = 293$ K. The time in seconds is given by the numbers near each curve. Electron–electron collisions are not taken in the account.

Collision frequency is ~10^9 s^{-1}

Time scale of relaxation of EEDF

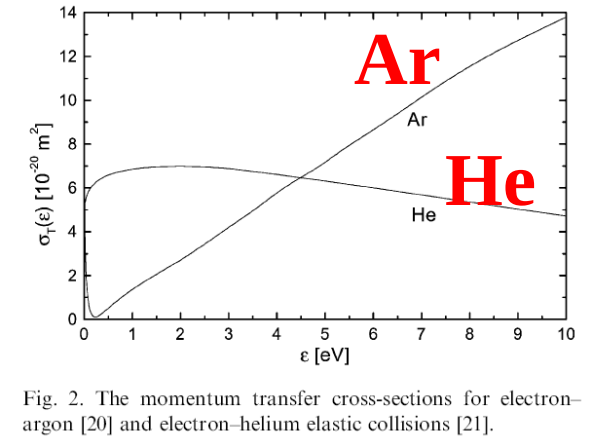

Fig. 2. The momentum transfer cross-sections for electron–argon [20] and electron–helium elastic collisions [21].

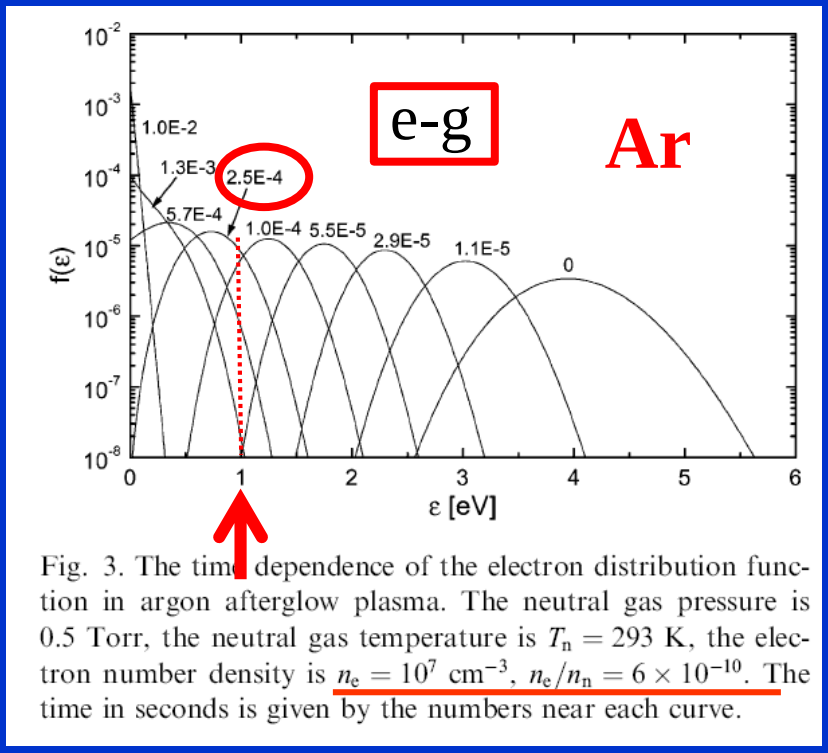

Fig. 3. The time dependence of the electron distribution function in argon afterglow plasma. The neutral gas pressure is 0.5 Torr, the neutral gas temperature is $T_n = 293$ K, the electron number density is $n_e = 10^7$ cm^{-3}, $n_e/n_n = 6 \times 10^{-10}$. The time in seconds is given by the numbers near each curve.

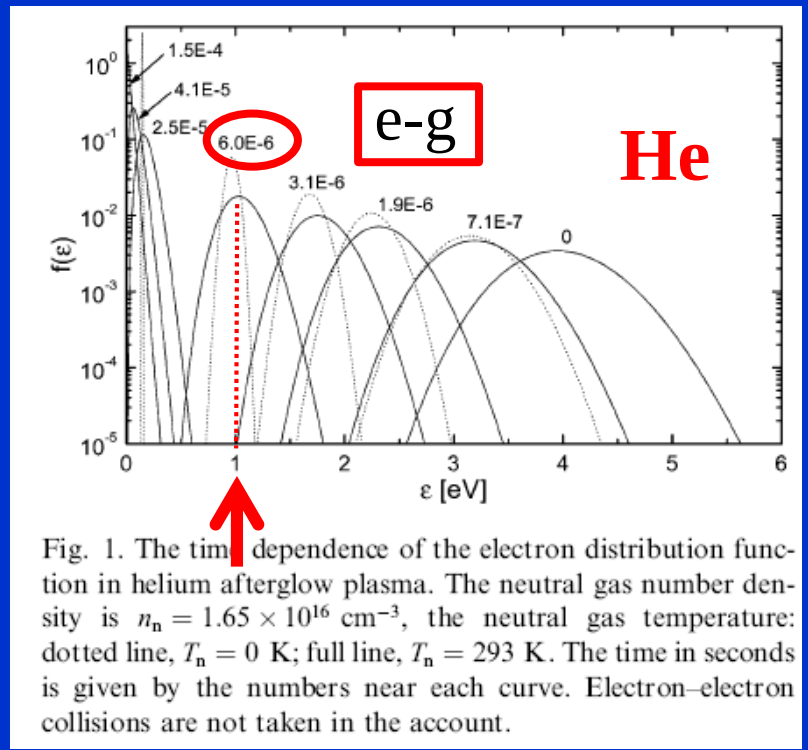

Fig. 1. The time dependence of the electron distribution function in helium afterglow plasma. The neutral gas number density is $n_n = 1.65 \times 10^{16}$ cm^{-3}, the neutral gas temperature: dotted line, $T_n = 0$ K; full line, $T_n = 293$ K. The time in seconds is given by the numbers near each curve. Electron–electron collisions are not taken in the account.

Time scale of relaxation of EEDF

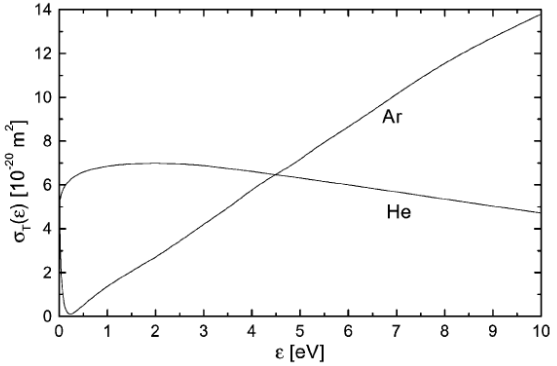

Fig. 2. The momentum transfer cross-sections for electron–argon [20] and electron–helium elastic collisions [21].

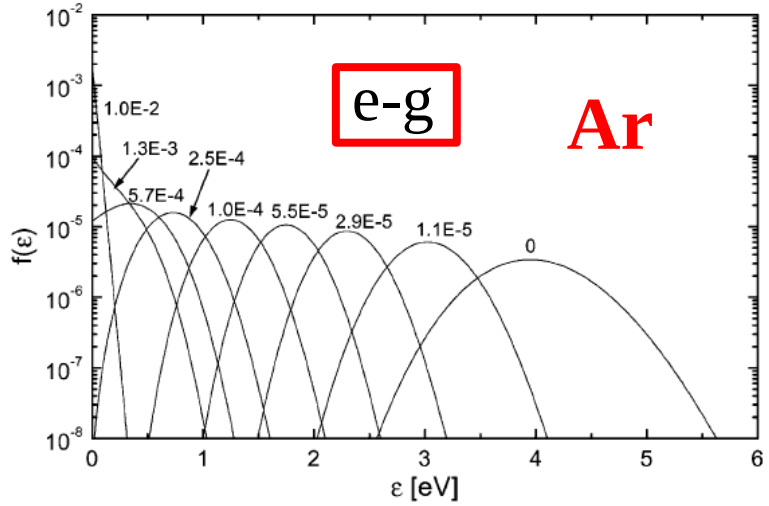

Fig. 3. The time dependence of the electron distribution function in argon afterglow plasma. The neutral gas pressure is 0.5 Torr, the neutral gas temperature is $T_n = 293$ K, the electron number density is $n_e = 10^7$ cm^{-3}, $n_e/n_n = 6 \times 10^{-10}$. The time in seconds is given by the numbers near each curve.

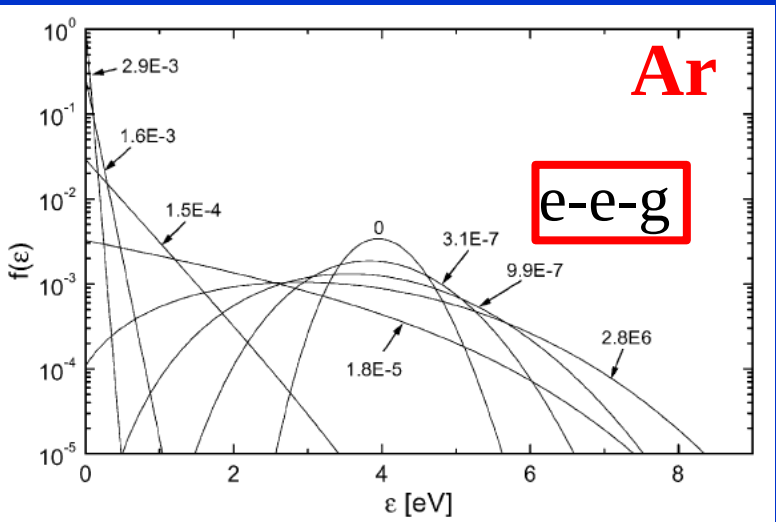

Fig. 4. The time dependence of the electron distribution function in argon afterglow plasma. The neutral gas pressure is 0.5 Torr, the neutral gas temperature is $T_n = 293$ K, the electron number density is $n_e = 10^{10}$ cm^{-3}, $n_e/n_n = 6 \times 10^{-7}$. The time in seconds is given by the numbers near each curve.

Time scale of relaxation of EEDF

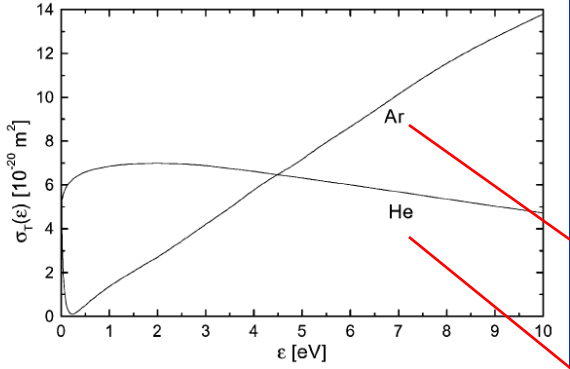

Fig. 2. The momentum transfer cross-sections for electron–argon [20] and electron–helium elastic collisions [21].

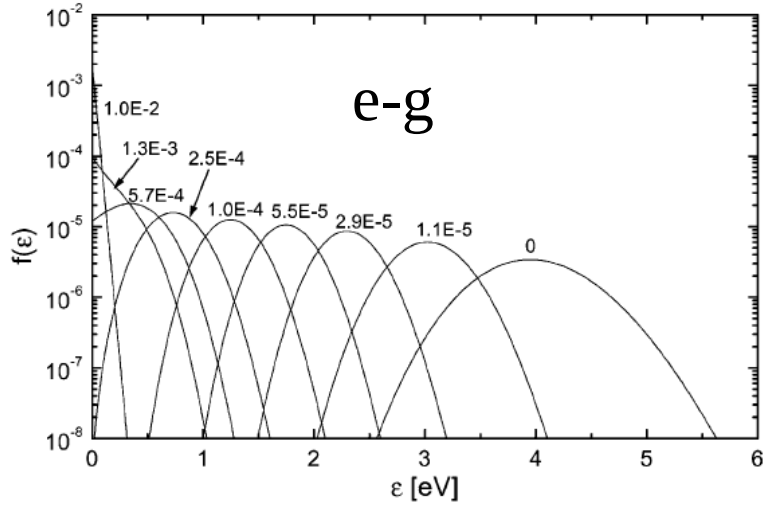

Fig. 3. The time dependence of the electron distribution function in argon afterglow plasma. The neutral gas pressure is 0.5 Torr, the neutral gas temperature is $T_n = 293$ K, the electron number density is $n_e = 10^7$ cm^{-3}, $n_e/n_n = 6 \times 10^{-10}$. The time in seconds is given by the numbers near each curve.

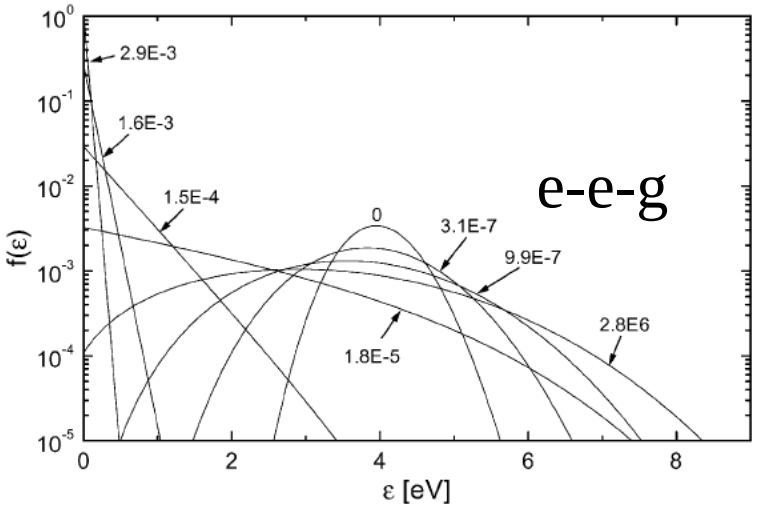

Fig. 4. The time dependence of the electron distribution function in argon afterglow plasma. The neutral gas pressure is 0.5 Torr, the neutral gas temperature is $T_n = 293$ K, the electron number density is $n_e = 10^{10}$ cm^{-3}, $n_e/n_n = 6 \times 10^{-7}$. The time in seconds is given by the numbers near each curve.

energy relaxation

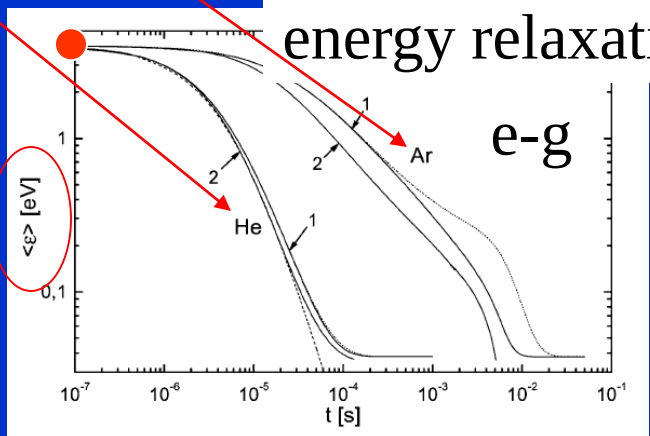

Fig. 5. The time dependence of the mean electron energy in helium and argon afterglow plasmas. The neutral gas pressure is 0.5 Torr, the neutral gas temperature is $T_n = 293$ K. Electron number densities: 1 – $n_e = 10^7$ cm^{-3} ($n_e/n_n = 6 \times 10^{-10}$), 2 – $n_e = 10^{10}$ cm^{-3} ($n_e/n_n = 6 \times 10^{-7}$). Dotted lines, calculations without electron–electron collisions; dashed line, calculation without electron–electron collisions and $T_n = 0$ K.

- Cross sections and plasma parameters

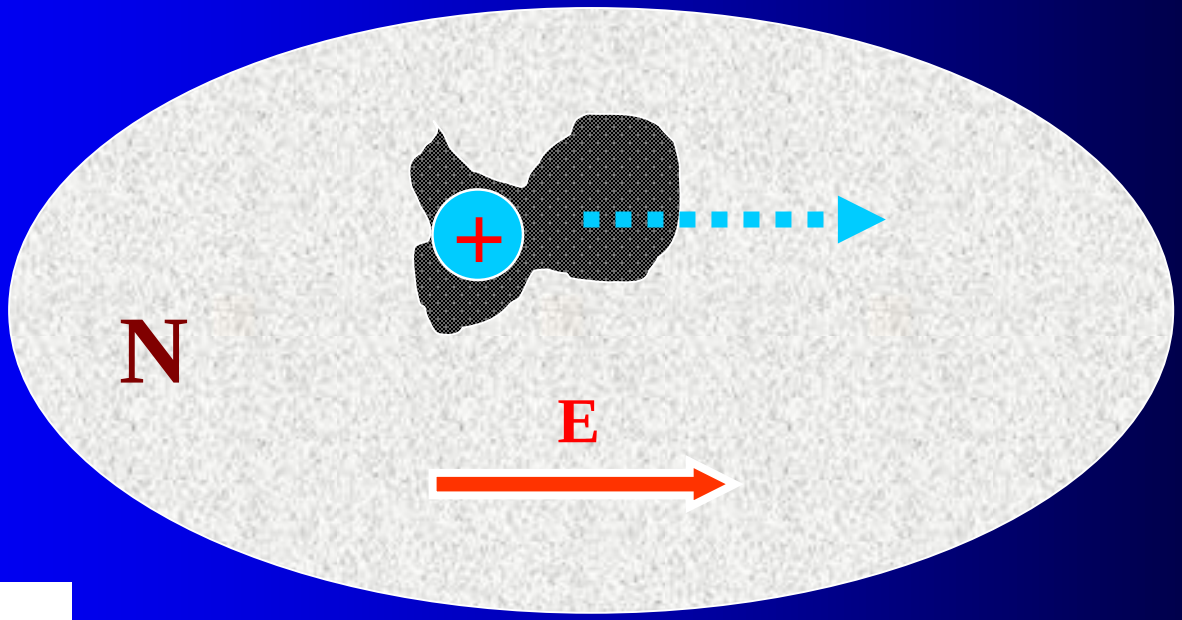

$\nu \sim N v \sigma$

DIFÚZE , DRIFT

$$\nu_1 \sim N v \sigma$$

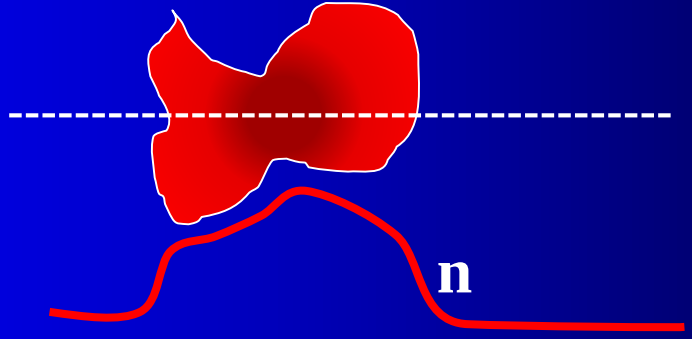

N

n

grad(**n**)

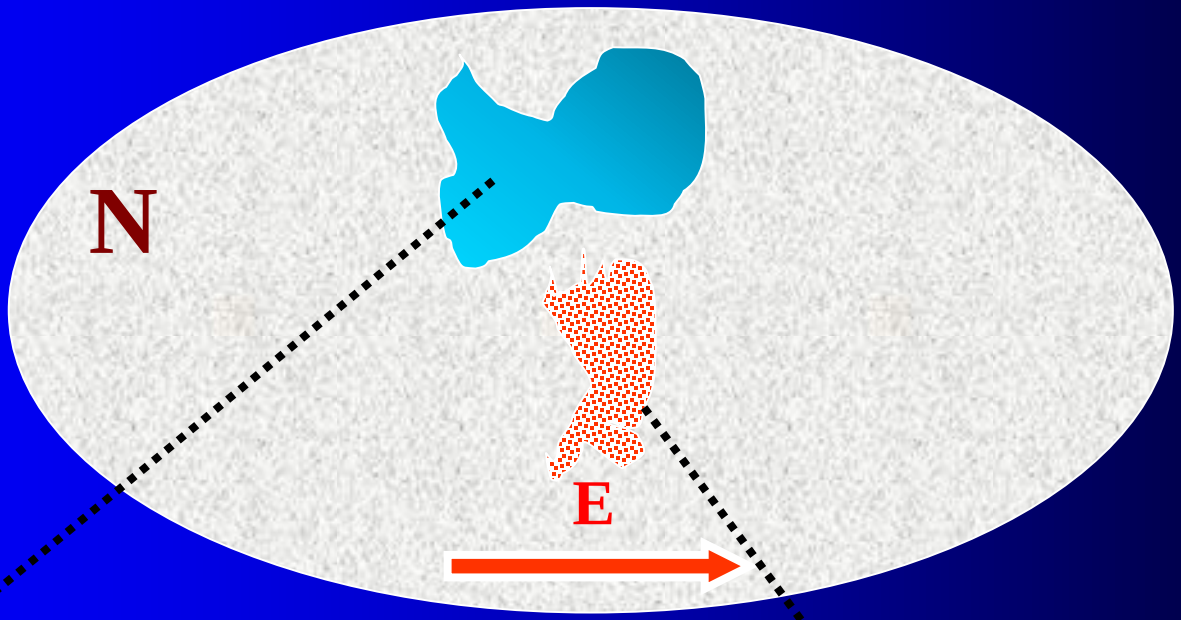

Difúze

$$\vec{\nu} = -D\frac{\nabla_r n}{n}$$

Drift

$$\vec{\nu} = \pm\mu\vec{E}$$

DIFÚZE , DRIFT

$\nu_1 \sim N v \sigma$

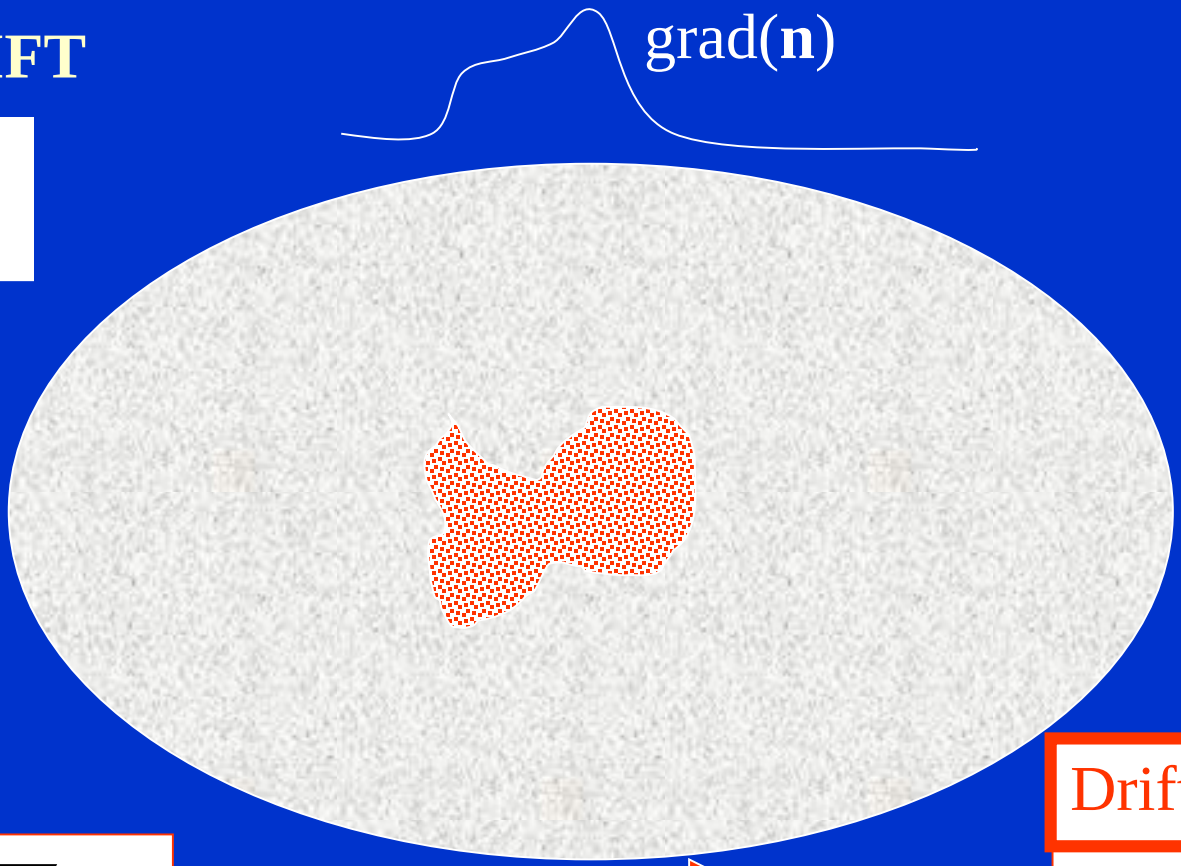

Difúze

$$\vec{v} = -D\frac{\nabla_r n}{n}$$

$\vec{E}$

Drift

$$\vec{v} = \pm\mu\vec{E}$$

$$D = \frac{kT}{m\nu_1}$$

$$\mu = \frac{e}{m\nu_1}$$

Ambipolar diffusion

Adolf Eugen Fick (1829-1901)

Fick's first law

$$J = -D\frac{\partial \phi}{\partial x} \qquad J = -D\nabla\phi$$

Fick's second law

$$\frac{\partial \phi}{\partial t} = D\frac{\partial^2 \phi}{\partial x^2} \qquad \frac{\partial \phi}{\partial t} = D\nabla^2\phi$$

Where

- ϕ • is the concentration in dimensions of [(amount of substance) length^{-3}],
- t • is time [s]
- D • is the diffusion coefficient in dimensions of [length^2 time^{-1}], example $\left(\frac{m^2}{s}\right)$
- x • is the position [length]

approximation $n(x,t) = n(0)\left[1 - 2\left(\frac{x}{2\sqrt{Dt\pi}}\right)\right]$ $2\sqrt{Dt}$

Drift of ions

$$\mu = \frac{e}{m\nu_1}$$

$$D = \frac{kT}{m\nu_1}$$

Drift iontů - experiment

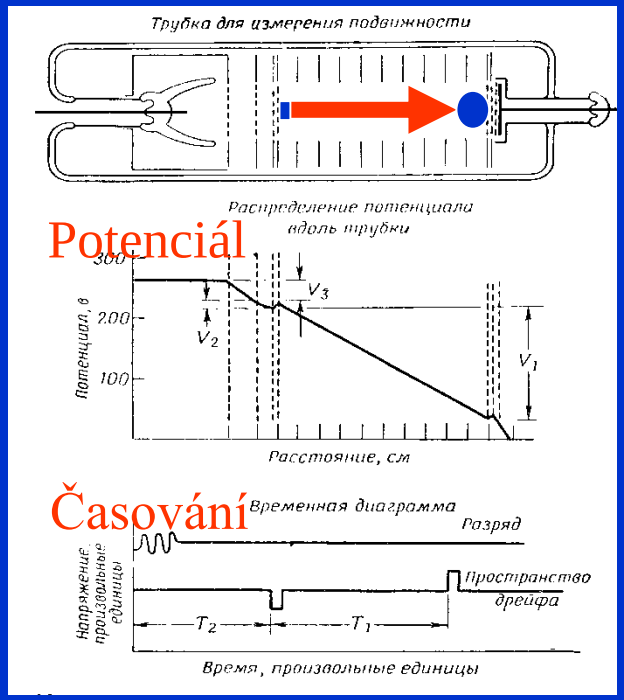

Potenciál

Časování

$$v_d' = \mu \cdot E$$

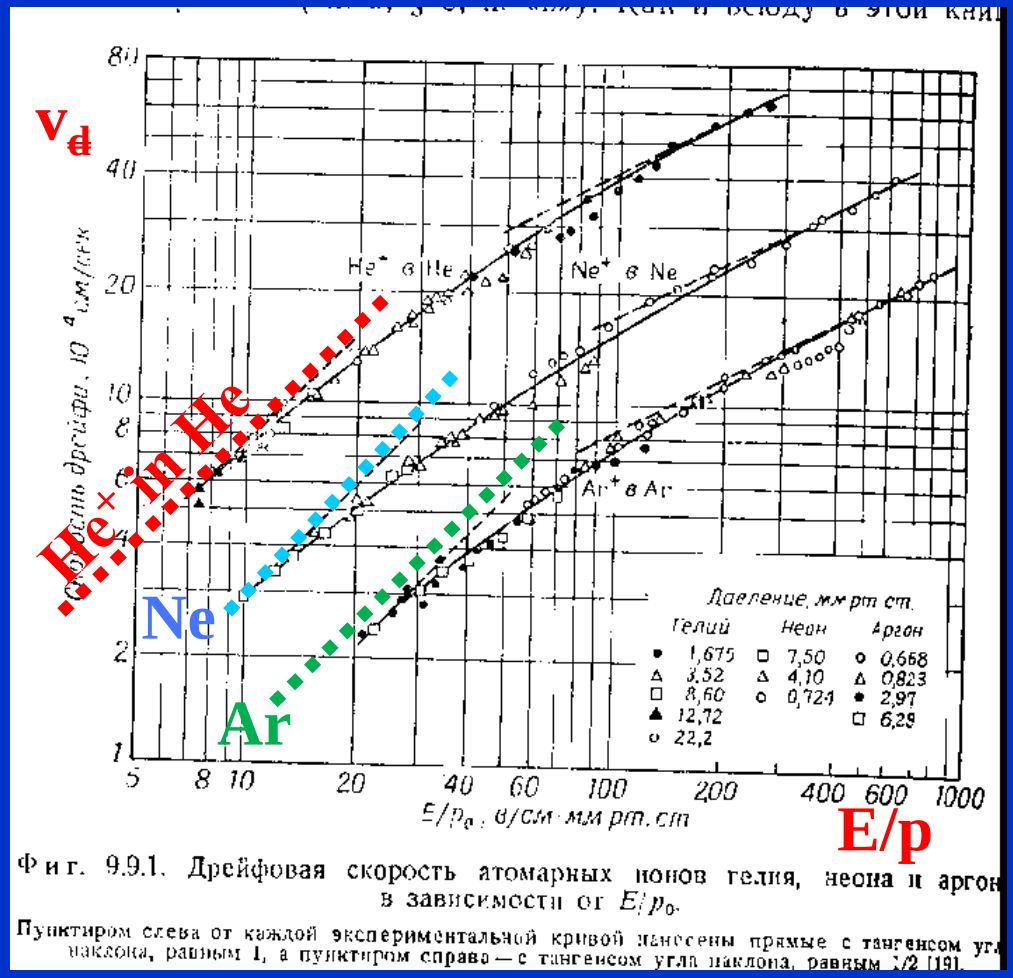

Фиг. 9.9.1. Дрейфовая скорость атомарных ионов гелия, неона и аргона в зависимости от E/p_0.

Пунктиром слева от каждой экспериментальной кривой нанесены прямые с тангенсом угла наклона, равным 1, а пунктиром справа — с тангенсом угла наклона, равным 1/2 [191].

Drift of charged particles

Drift tube

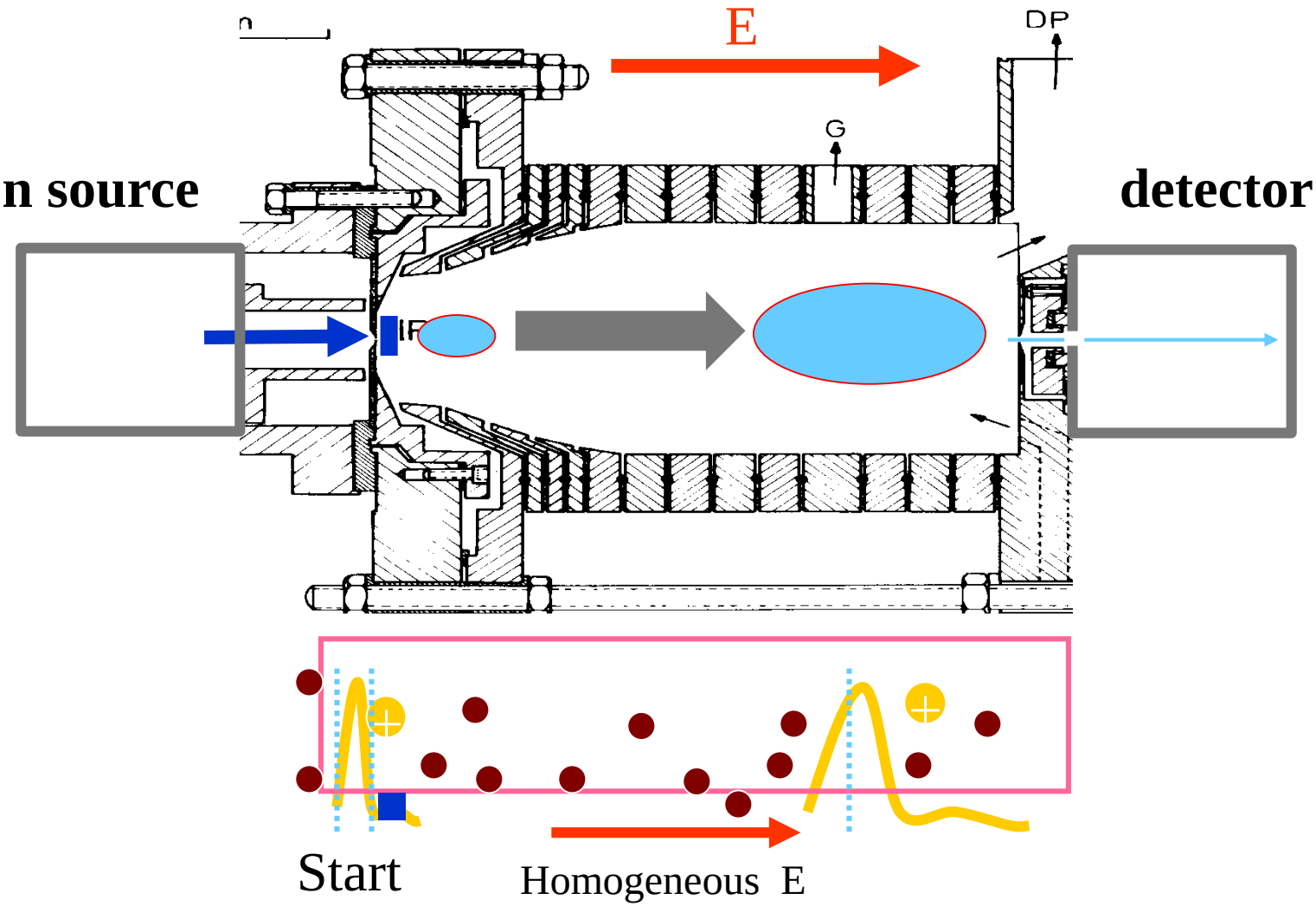

Drift iontů - experiment

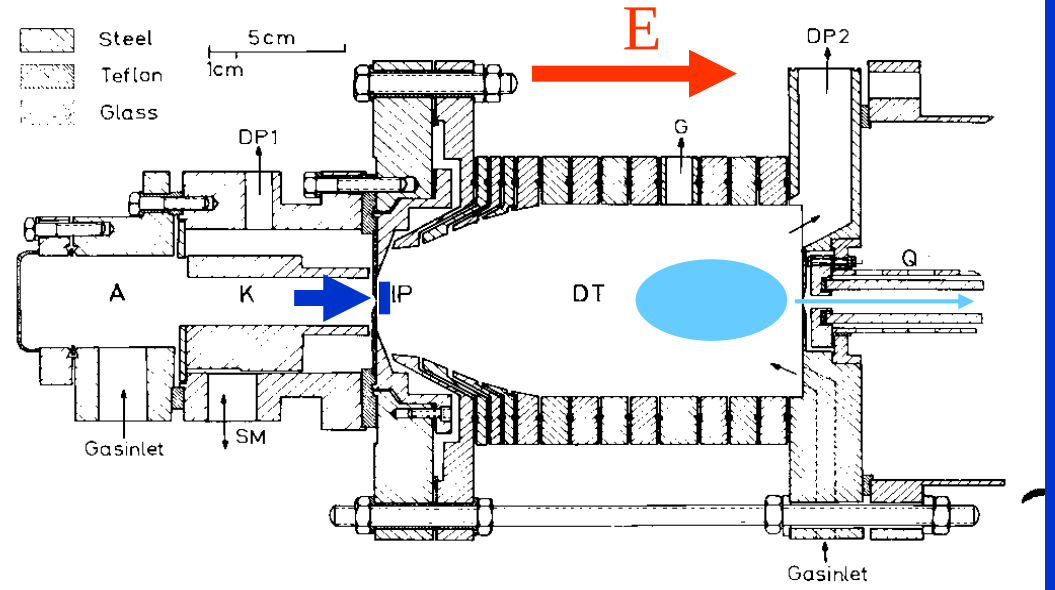

Fig. 1. Section through the main part of the apparatus. A, anode; K, cathode; DP, diffusion pump; SM, shift mechanism (not used in this work); HP, hole probe; DT, drift tube; G, pressure gauge; Q, quadrupole.

Drift iontů $CO.N_2^+$ a N_4^+ v N_2

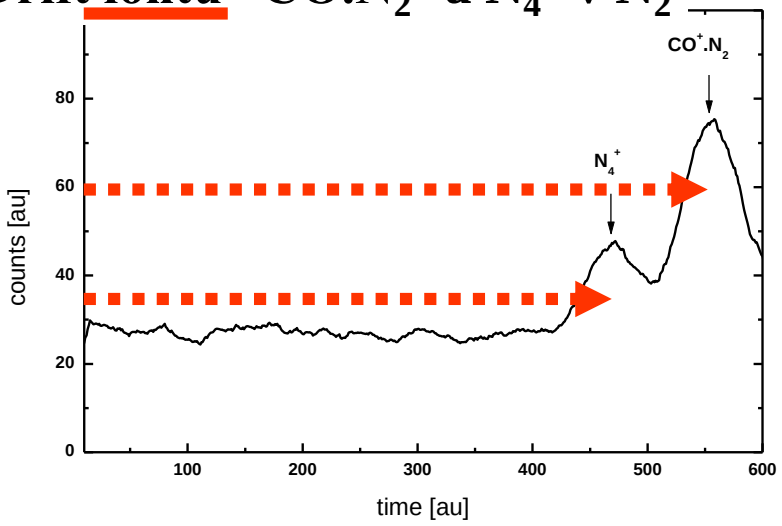

$$v_d' = \mu \cdot E$$

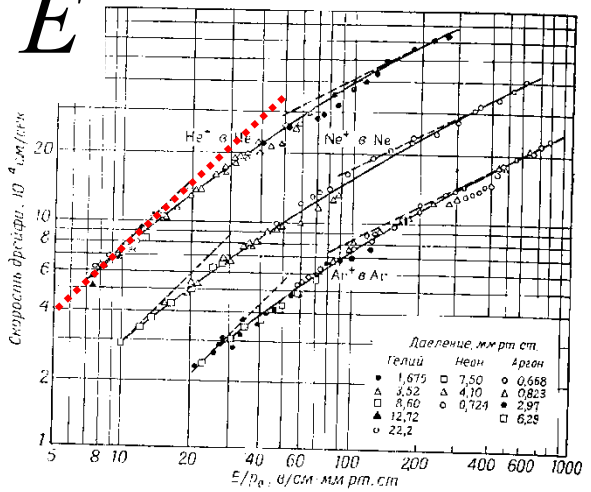

Фиг. 9.9.1. Дрейфовая скорость атомарных ионов гелия, неона и аргона в зависимости от E/p_0.

Пунктиром слева от каждой экспериментальной кривой нанесены прямые с тангенсом угла наклона, равным 1, а пунктиром справа — с тангенсом угла наклона, равным 1/2 [15].

Drift of ions- time of flight

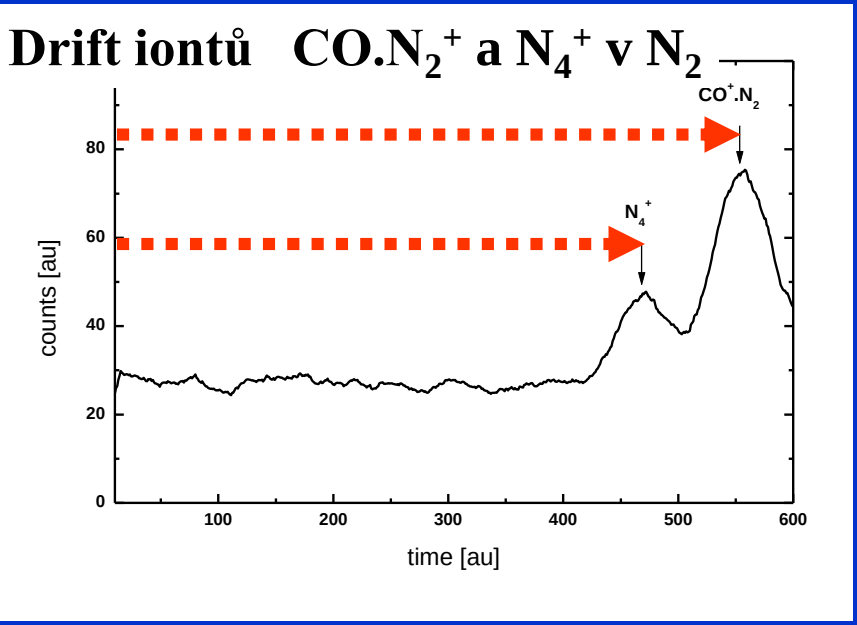

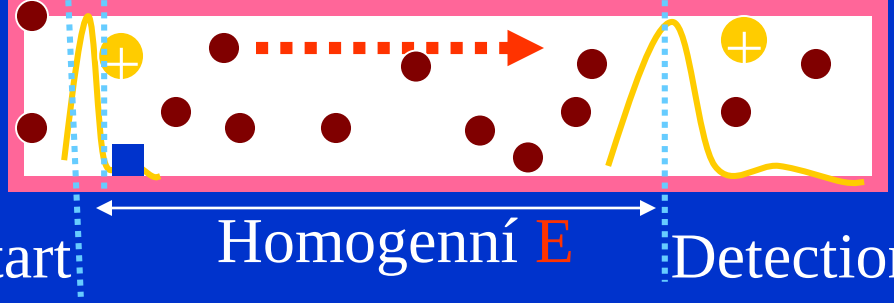

"Time of flight“ spektrum iontů N_4^+ a $CO^+.N_2$ v dusíku a průběhy odpovídajících pohyblivostí.

Drift of ions CO^+ , N_2^+ , $CO.N_2^+$ a N_4^+ v N_2

$$v_d' = \mu \cdot E$$

$$\mu_0 = \mu \cdot \frac{p}{760} \cdot \frac{273}{T}$$

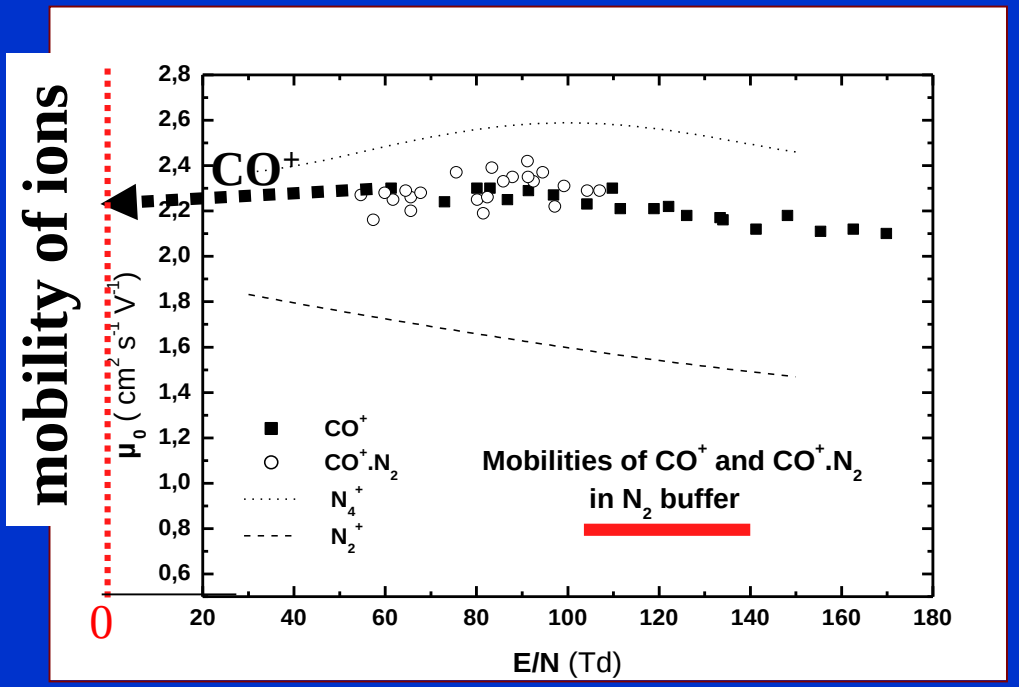

$$1\,\mathrm{Td} = 10^{-21}\,\mathrm{V}\cdot\mathrm{m}^2 = 10^{-17}\,\mathrm{V}\cdot\mathrm{cm}^2.$$

Drift of electrons

Drift elektronů v He, Ne, Ar…

$$\mu = function \quad of\left(\frac{E}{p}\right)$$

- e in He, Ar, Xe

Pro daný plyn

$$v = function \quad of\left(\frac{E}{p}\right)$$

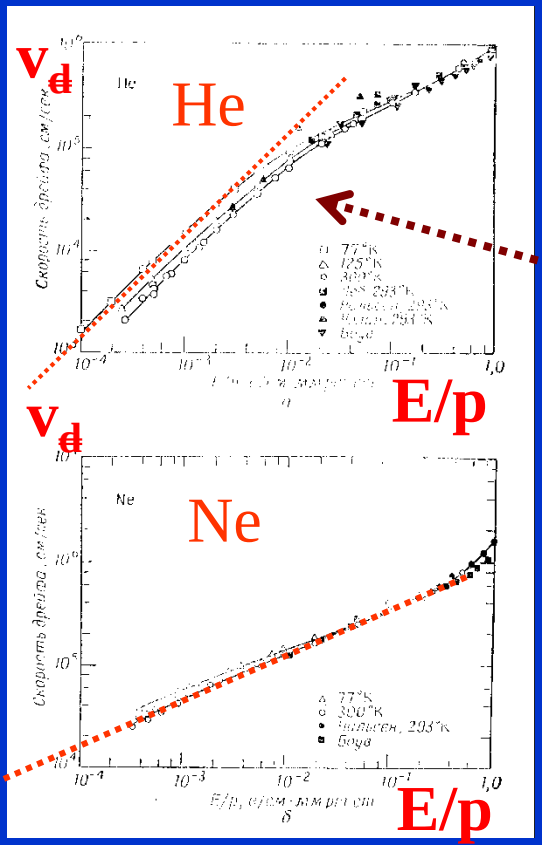

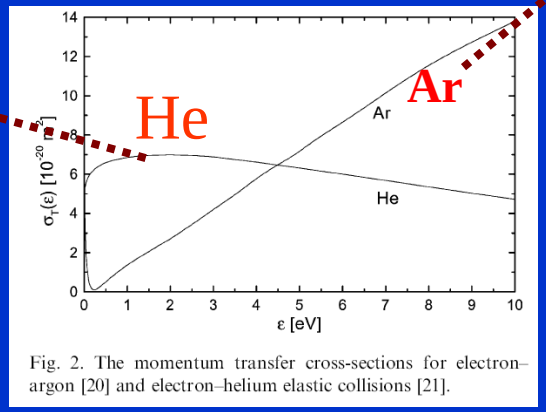

Fig. 2. The momentum transfer cross-sections for electron–argon [20] and electron–helium elastic collisions [21].

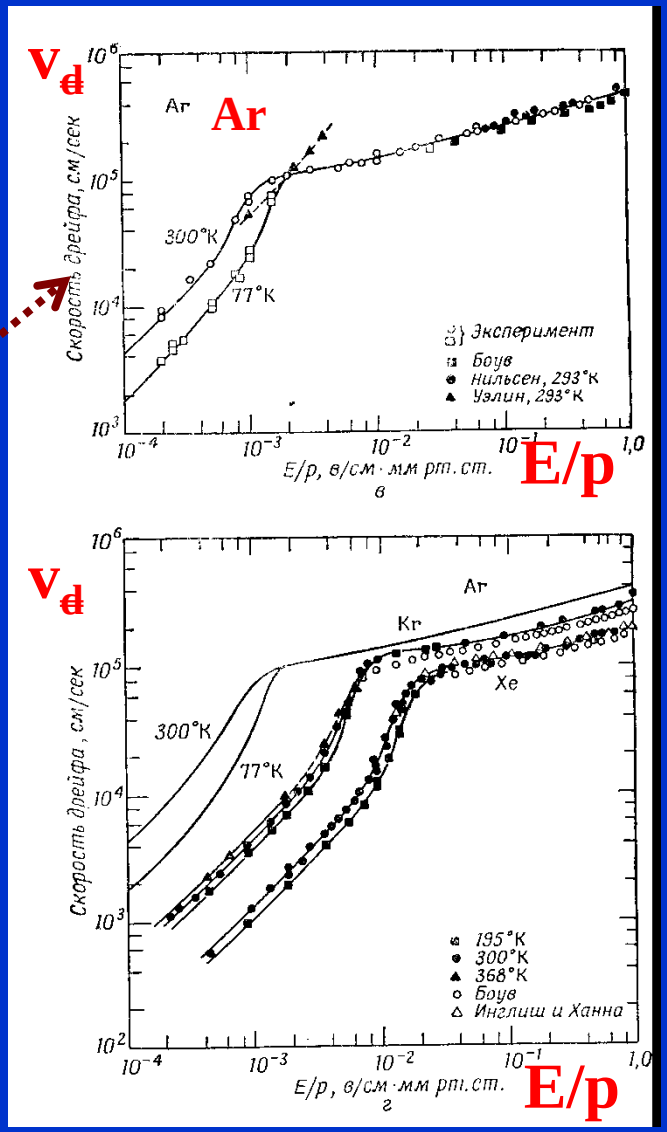

Energie elektronů

- Energia, rychlost,
- Einsteinův vztah

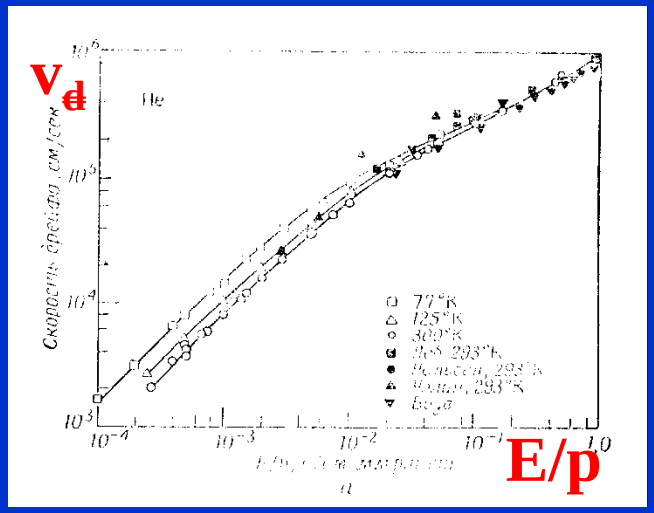

$$\frac{\mu}{D} = \frac{e}{kT}; \qquad \frac{D}{\mu} = \frac{kT}{e}$$

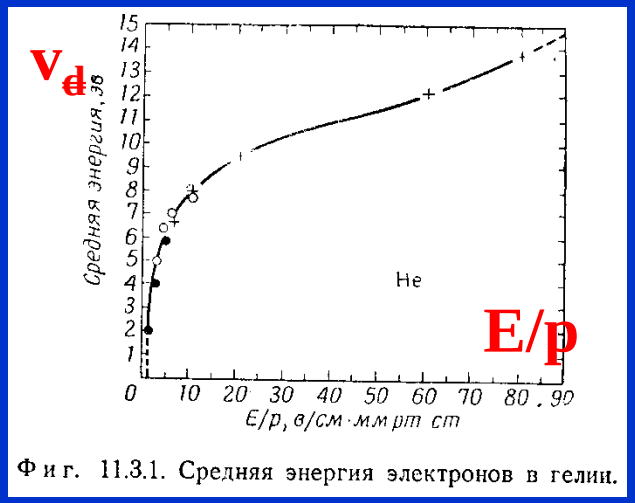

Фиг. 11.3.1. Средняя энергия электронов в гелии.

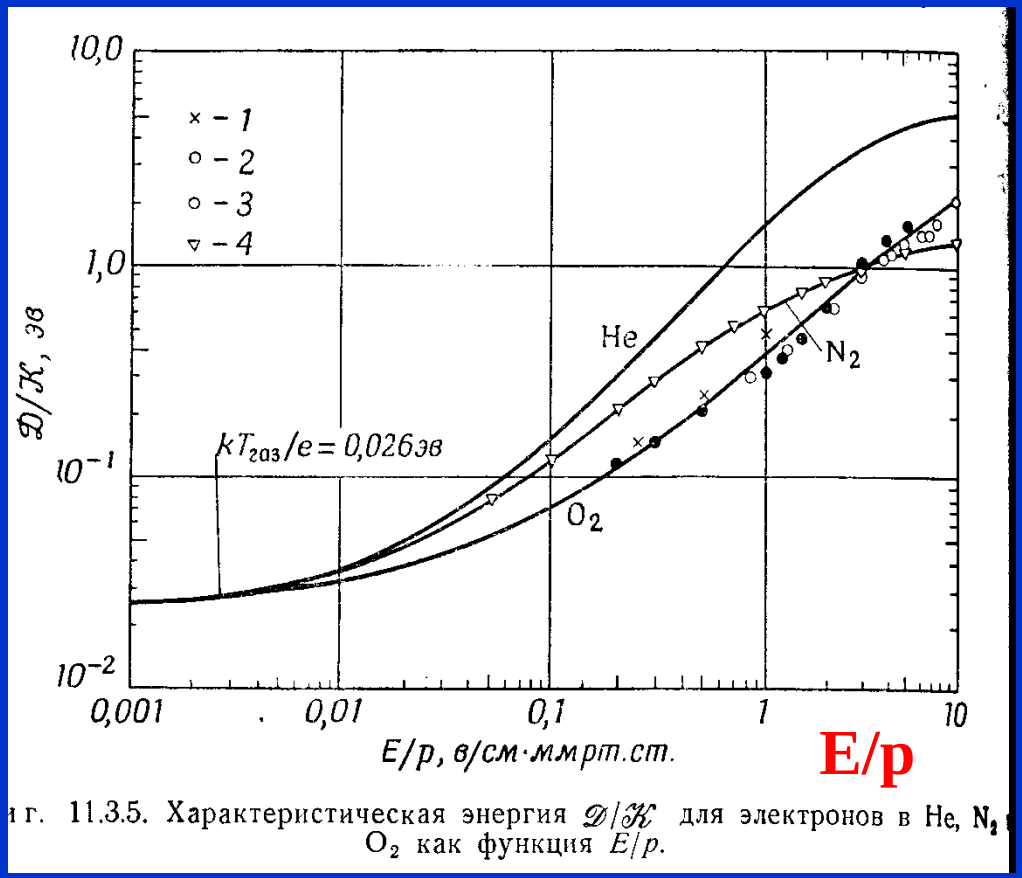

ı г. 11.3.5. Характеристическая энергия $\mathcal{D}/\mathcal{K}$ для электронов в He, N_2 и O_2 как функция E/p.

Energie elektronů === odtržení teploty elektronů…

Drift of ions and electrons – comparison of experimental data

e^- in Ar

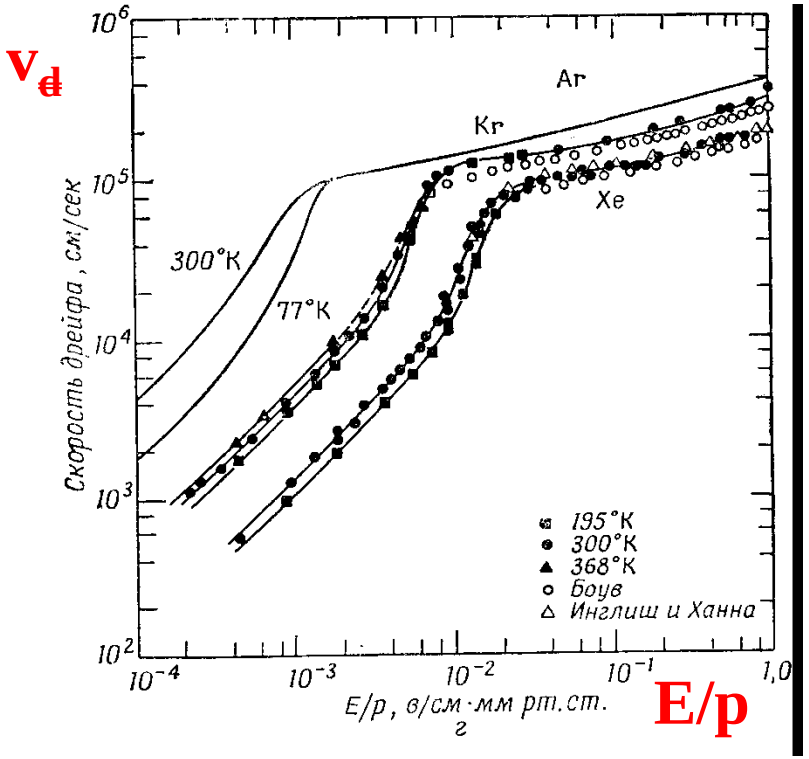

Drift of ions and electrons – comparison of experimental data

e^- in Ar

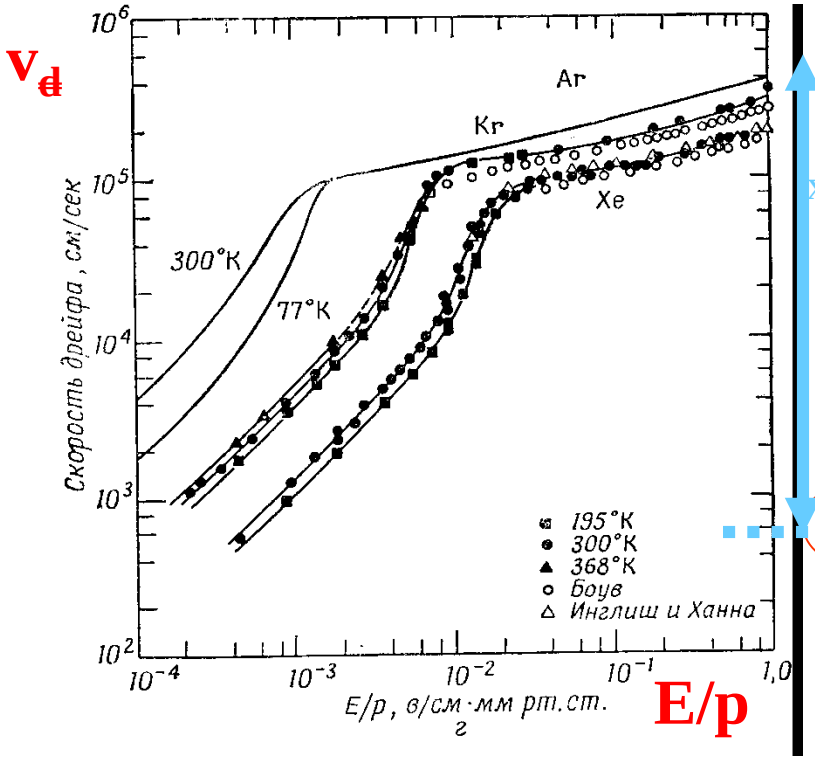

x300

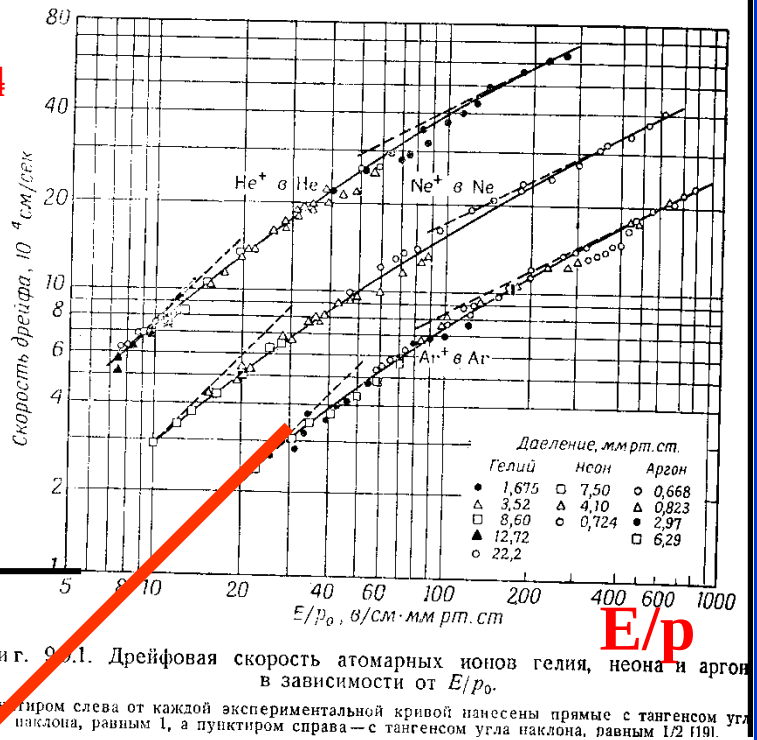

~10^3cm/s

Ar^+ in Ar

1V/cm Torr

The Townsend (symbol Td) is a physical unit of the reduced electric field (ratio E/N), where E is electric field and N is concentration of neutral particles. It is defined by the relation

$$1\,\mathrm{Td} = 10^{-21}\,\mathrm{V}\cdot\mathrm{m}^2 = 10^{-17}\,\mathrm{V}\cdot\mathrm{cm}^2.$$

Drift iontů

mobility of ions

$$v_d = \mu \cdot E$$

$$\mu_0 = \mu \cdot \frac{p}{760} \cdot \frac{273}{T}$$

$$\mu = \mu_0 \cdot \frac{760}{p} \cdot \frac{T}{273}$$

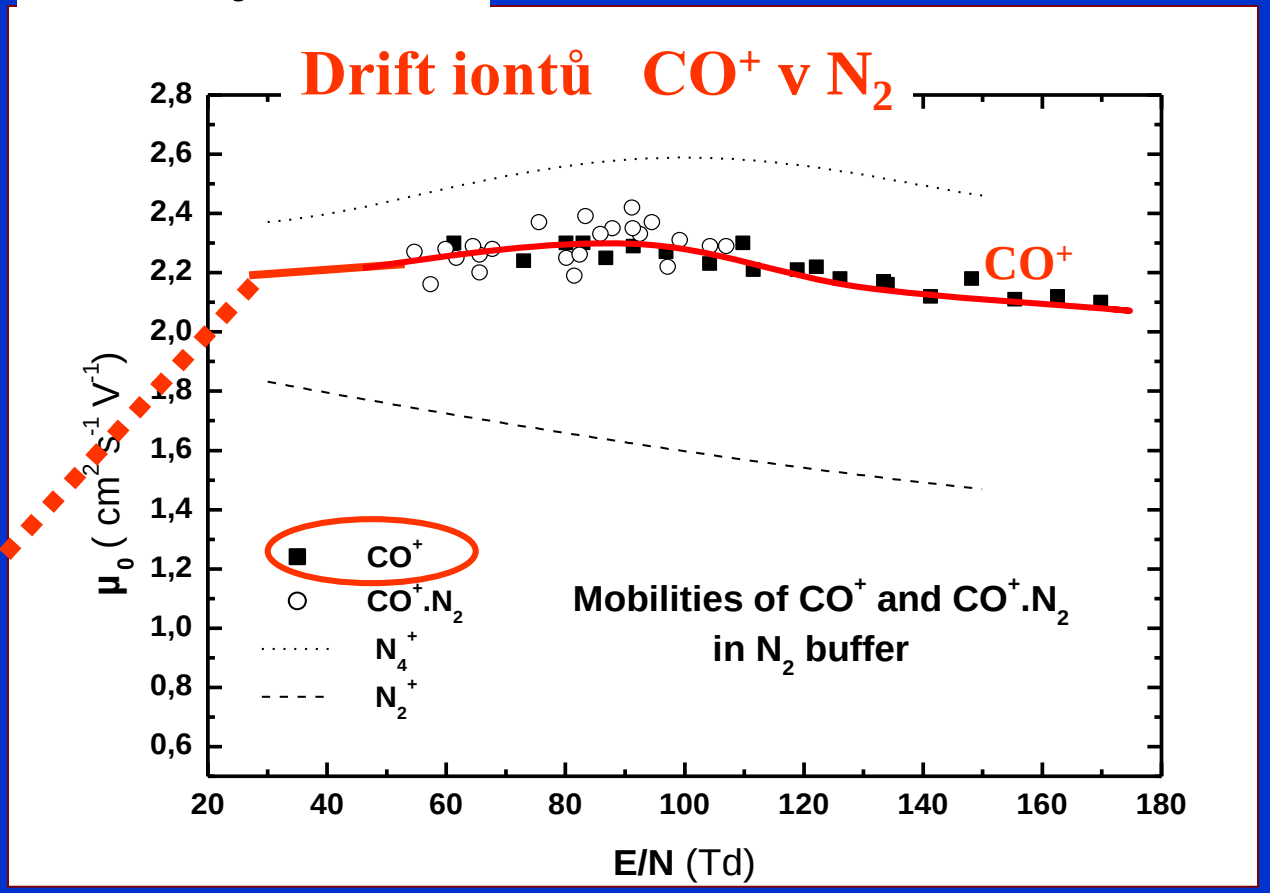

$$\mu = 2.2 \cdot \frac{760}{1} \cdot 1 \sim 1700 cm^2 s^{-1} V^{-1}$$

$$v_d = \mu \cdot E = 1700 cm/s = 17 m/s$$

CO^+ v N_2

$$E = 1V/cm = 100V/1m$$

Dependence on mass of buffer gas and ions

$$\mu = \frac{e}{m\nu_1}$$

$$\sigma_0 = \pi\rho_0^2 = \frac{2\pi e}{\nu_0(4\pi\varepsilon_0)}\sqrt{\frac{\alpha}{\mu}}$$

$$\sigma_{coll} = \sigma_L = const\,\frac{1}{v}\sqrt{\frac{\alpha}{\mu}} \sim \sigma_0\frac{v_0}{v}cm^2$$

$\mu \sim (m)^{-0.5}$

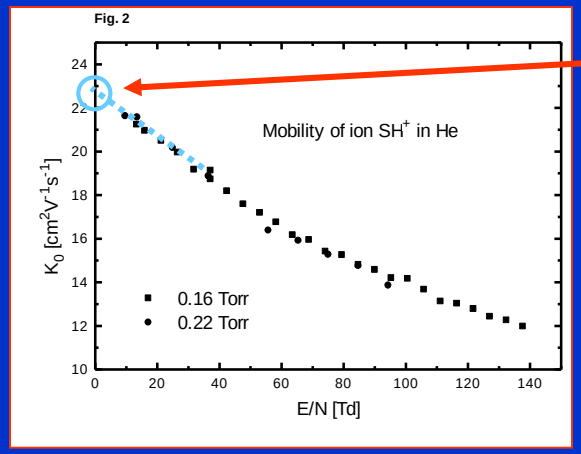

Low E region

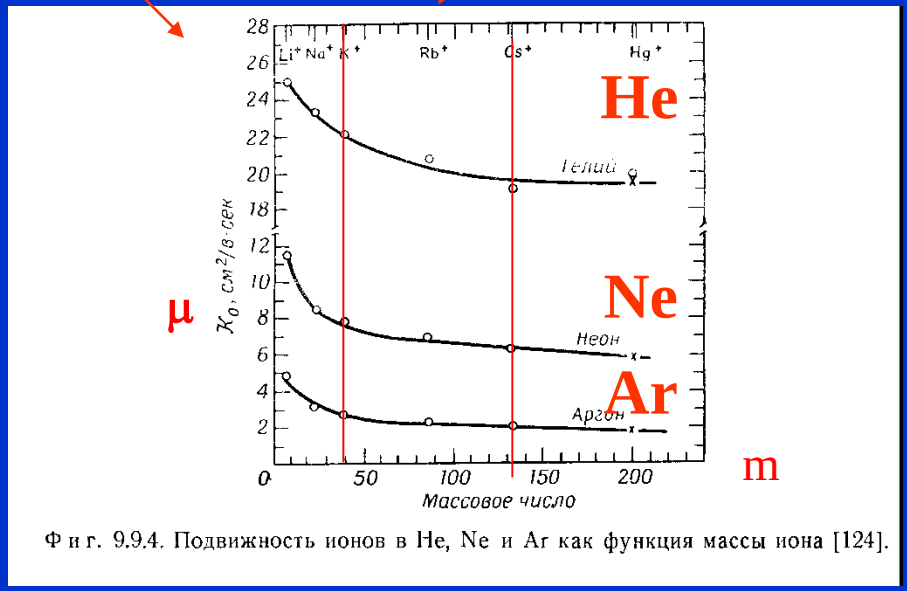

Фиг. 9.9.4. Подвижность ионов в He, Ne и Ar как функция массы иона [124].

Theory

Boltzmann equation

$$\frac{\partial f_i}{\partial t} + \vec{v}_i \cdot \nabla_r f_i + \frac{\vec{F}_i}{m_i} \cdot \nabla_{v_i} f_i = \frac{\delta f_i}{\delta t}$$

$$f(\vec{v}, \vec{r}, t)$$

$$f(\vec{v}, \vec{r}, t) = f_0(v, \vec{r}, t) + \frac{\vec{v}}{v} \cdot \vec{f}_1(v, \vec{r}, t)$$

Řešení B. rovnice

Lorentzovské přiblížení pro dvousložkový systém tvořený jednak neutrálními částicemi a jednak částicemi, které mají elektrický náboj….

$$\frac{\partial f_i}{\partial t} + \vec{v}_i \cdot \nabla_r f_i + \frac{\vec{F}_i}{m_i} \cdot \nabla_{v_i} f_i = \frac{\delta f_i}{\delta t}$$

Závislost na rychlosti

Hledáme řešení ve tvaru

$$f(\vec{v},\vec{r},t) = f_0(v,\vec{r},t) + \frac{\vec{v}}{v} \cdot \vec{f}_1(v,\vec{r},t)$$

aby jsme vyjádřili toky částic

$$\frac{\partial\left(f_0(v,\vec{r},t) + \frac{\vec{v}}{v} \cdot \vec{f}_1(v,\vec{r},t)_i\right)}{\partial t} + \vec{v}_i \cdot \nabla_r \left(f_0(v,\vec{r},t) + \frac{\vec{v}}{v} \cdot \vec{f}_1(v,\vec{r},t)\right) + \frac{\vec{F}_i}{m_i} \cdot \nabla_{v_i} \left(f_0(v,\vec{r},t) + \frac{\vec{v}}{v} \cdot \vec{f}_1(v,\vec{r},t)\right) = \frac{\delta f_i}{\delta t}$$

Řešení B. rozklad do dvou rovnic

- Velký Kracík
- Rovnice (A) a (B)

(5.14) $$\nu_1 = 2\pi N v \int_0^\pi (1 - \cos\chi)\,\sigma(\chi, v)\sin\chi\,d\chi$$

Držíme se Velkého Kracíka proto:

$$f(\vec{v},\vec{r},t) = f_0(v,\vec{r},t) + \vec{v}\cdot\vec{f}_1(v,\vec{r},t)$$

Veličinu $\nu_l(v)$ definovanou rovnicí (5.11) resp. (5.12) můžeme interpretovat jako relaxační frekvenci l-tého řádu pro různé anisotropie plynu lehkých částic. Speciálně

(5.14) $$\nu_1 = 2\pi N v \int_0^\pi (1 - \cos\chi)\,\sigma(\chi, v)\sin\chi\,d\chi$$

N

$$\Gamma = \frac{Ze}{m}E, \quad \omega_c = -\frac{Ze}{m}B,$$

(5.95) $$\mathbf{f}_{(k)} = 0 \quad \text{pro} \quad k \geqq 2,$$

redukuje se rozklad (5.55) resp. (5.55′) na

(5.96) $$f(v, r, t) = f_0(v, r, t) + v\,.\,f_1(v, r, t)$$

a rovnice pro funkce f_0 a f_1 mají tvar

(5.97′) $$\frac{\partial f_0}{\partial t} + \frac{v^2}{3}\nabla_r\,.\,f_1 + \frac{1}{3v^2}\frac{\partial}{\partial v}(v^3\Gamma\,.\,f_1) = J_{\text{I.L.}}(f_0),$$

nebo rozepíšeme-li pravou stranu podle (5.40)

(5.97) $$\frac{\partial f_0}{\partial t} + \frac{v^2}{3}\nabla_r\,.\,f_1 + \frac{1}{3v^2}\frac{\partial}{\partial v}(v^3\Gamma\,.\,f_1) = \frac{1}{2v^2}\frac{\partial}{\partial v}\left[\frac{2m}{M}\nu_1 v^3\left(f_0 + \frac{2kT}{m}\frac{\partial f_0}{\partial(v^2)}\right)\right]$$

A

a

(5.98) $$\frac{\partial f_1}{\partial t} + \nabla_r f_0 + \frac{\Gamma}{v}\frac{\partial f_0}{\partial v} - (\omega_c \times f_1) = -\nu_1 f_1\,.$$

B

interpretace

(5.131) $$f_0 = C \exp\left\{ - \int \frac{v\,dv}{\frac{kT}{m} + \frac{\mathscr{G}(v_1)}{3\gamma v_1^2}} \right\},$$

a) Nechť vnější elektrické pole je nulové, tj. $\Gamma = 0$. Potom

(5.133) $$\mathscr{G}(v_1) = 0$$

B může byt nenulové

a pro $f_0(v)$ máme Maxwellovu rozdělovací funkci

(5.134) $$f_0 = C \exp\left(- \frac{mv^2}{2kT} \right),$$

kde

(5.135) $$C = n \left(\frac{m}{2\pi kT} \right)^{3/2}.$$

b) Nechť vnější magnetické pole je nulové, tj. $\omega_c = 0$. Potom

(5.136) $$\mathscr{G}(v_1) = \Gamma^2$$

a (5.131) můžeme upravit na tvar

(5.137) $$f_0 = C \exp\left\{ - \int \frac{m}{kT} \left(\frac{v v_1^2}{v_1^2 + \left(\frac{\Gamma^2 m}{3\gamma kT} \right)} \right) dv \right\}.$$

Bude-li nyní srážková frekvence v_1 nezávislá na rychlosti, tj.

(5.138) $$v_1 = v = \text{konst},$$

pak f_0 bude opět maxwellovské rozdělení

(5.139) $$f_0 = C \exp\left[- \frac{mv^2}{2k\left(T + \frac{\Gamma^2 m}{3\gamma k} v^{-2} \right)} \right] = C \exp\left(- \frac{mv^2}{2kT^*} \right)$$

ale s teplotou

(5.140) $$T^* = T + \frac{m}{3\gamma k} \left(\frac{\Gamma}{v} \right)^2 = T + \frac{M}{3k} \left(\frac{ZeE}{mv} \right)^2.$$

To ale znamená, že při $v_1 = \text{konst}$ je kinetická teplota lehkých nabitých částic (elektronů) vyšší ve srovnání s teplotou neutrálních částic.

Předpoklad, že srážková frekvence elektronů s neutrálními částicemi je konstantní, nezávislá na rychlosti, je příliš ostrý. V obecném případě totiž platí, že v_1 na rychlosti elektronů závisí. Předpokládejme, že

(5.141) $$v_1(v) = Av^l,$$

kde l je libovolné číslo*) a A je konstanta (pro $l = 1$ máme

(5.141′) $$v_1 = Av$$

a tedy $A^{-1} = \lambda$, kde λ je střední volná dráha elektronů).

Rovnice pro f_0 (5.137) má nyní tvar

(5.142) $$f_0 = C \exp\left\{ - \int \frac{m}{kT} \frac{v^{2l+1}}{v^{2l} + \frac{\Gamma^2 m}{3\gamma A^2 kT}} dv \right\}.$$

Pro $l = 1$, tj. případ modelu dokonale pružných koulí (viz kapitolu 2), kdy

(5.143) $$v_1 = Av,$$

je integrál v (5.142) snadno spočitatelný a f_0 má tvar

(5.144′) $$f_0 = C \left[1 + \frac{3A^2}{\Gamma^2} \frac{kT}{m} v^2 \right]^{(m\Gamma/AkT)^2 \cdot (1/6\gamma)} \cdot \exp\left(- \frac{mv^2}{2kT} \right).$$

Po kratších úpravách pak dostaneme

(5.144) $$f_0 = C \left[v^2 + \frac{M}{3} \left(\frac{ZeE}{mA} \right)^2 \frac{1}{kT} \right]^{(mM/6k^2T^2) \cdot (ZeE/mA)^2} \cdot \exp\left(- \frac{mv^2}{2kT} \right),$$

což je rozdělovací funkce, kterou jako první odvodil Davydov.**) Pro silné elektrické pole, kdy

(5.145) $$\frac{\Gamma^2 m}{3\gamma AkT} = \frac{M}{3kT} \left(\frac{ZeE}{mA} \right)^2 \gg v^2,$$

přechází Davydovova rozdělovací funkce na známou rozdělovací funkci Druyvesteyna (o tom je možno se přesvědčit z (5.142), kde položíme $l = 1$ a provedeme příslušné zanedbání), která má tvar

(5.146) $$f_0 = C \exp\left(- \frac{3}{4} \gamma \left(\frac{A}{\Gamma} \right)^2 v^4 \right) = C \exp\left[- \frac{3}{4} \frac{m}{M} \left(\frac{mA}{ZeE} \right)^2 v^4 \right].$$

*) Závislost (5.141) pro $l = 0$ vystihuje s dobrou přesností srážky elektronů s atomy He a H_2, pro $l = 1$ pak srážky v Ne a dále pro $l = 3$, 3,5 a 4 pak srážky pomalých elektronů v Ar, Kr a Xe; viz D. Darbiere: Phys. Rev. *84* (1951), 653; S. C. Brown: Handbuch der Physik, ed. S. Flüge, Vol. 22 (Berlin 1956), 531; G. L. Braglia: Phys. Lett. *17* (1965), 260.

**) B. Davydov, ŽETF *6* (5) (1936), 463; viz též B. Davydov, Uspěchi fiz. nauk *93* (1967), 401.

Odvození difúzní rovnice z B. rovnice

Rovnice (A)

$$f(\vec{v},\vec{r},t) = f_0(v,\vec{r},t) + \vec{v}\cdot\vec{f}_1(v,\vec{r},t)$$

$$\frac{\partial f_1}{\partial t} + \nabla_r f_0 + \frac{\boldsymbol{\Gamma}}{v}\frac{\partial f_0}{\partial v} - (\omega_c \times f_1) = -\nu_1 f_1$$

Rovnice B

$$\nabla_r f_0 = -\nu_1 \vec{f}_1$$

$$\varphi = v\varphi'(v, \boldsymbol{r}, t)$$

$$\bar{\varphi} = \frac{1}{n}\int (f_0 + \boldsymbol{v}\,.\boldsymbol{f}_1)\, v\varphi'\, \mathrm{d}\boldsymbol{v} = \frac{1}{n}\int (\boldsymbol{v}\,.\boldsymbol{f}_1)\, v\varphi'\, \mathrm{d}\boldsymbol{v} = \frac{4\pi}{3}\frac{1}{n}\int_0^\infty v^4 f_1 \varphi'\, \mathrm{d}v$$

$$\bar{\varphi} = \frac{4\pi}{n}\int_0^\infty v^2 f_0 \varphi\, \mathrm{d}v$$

$$\vec{\varphi} = \vec{v}.1$$

$$\bar{\vec{v}} = \frac{4\pi}{3}\frac{1}{n}\int v^4 f_1 dv = -\frac{4\pi}{3}\frac{1}{n}\int v^4 \frac{\nabla f_0}{\nu_1} dv = \ldots \sim \ldots = -\frac{1}{3}\frac{4\pi}{n}\int \frac{v^2}{\nu_1} v^2 \nabla f_0 dv = \ldots = -\frac{1}{3}\nabla\left(\left(\frac{\overline{v^2}}{\nu_1}\right).n\right)$$

$$\bar{\vec{v}} = -\frac{1}{3}\frac{1}{n}\nabla\left(\left(\frac{\overline{v^2}}{\nu_1}\right).n\right) \Rightarrow \bar{\vec{v}} = -\frac{1}{3}\frac{1}{n}\nabla\left(\left(\frac{\overline{v^2}}{\nu_1}\right).n\right) = -D\frac{\nabla n}{n} \Rightarrow D = \frac{1}{3}\left(\frac{\overline{v^2}}{\nu_1}\right)$$

Odvození rovnice pro drift z B. rovnice

Rovnice B

$$\frac{\partial f_1}{\partial t} + \nabla_r f_0 + \frac{\Gamma}{v}\frac{\partial f_0}{\partial v} - (\omega_c \times f_1) = -\nu_1 f_1$$

$\frac{\partial}{\partial t} = 0$ $\quad \nabla_r = 0$ $\quad \vec{E} \neq 0$ $\quad B = 0$

$$\frac{\Gamma}{v}\frac{\partial f_0}{\partial v} = -\nu_1 \vec{f}_1$$

$$\vec{\Gamma} = \frac{e\vec{E}}{m}$$

$$\vec{f}_1 = -\frac{1}{\nu_1}\frac{\Gamma}{v}\frac{\partial f_0}{\partial v}$$

Per-partes
+ conditions of limits for *f*

$$\vec{\bar{v}} = \frac{4\pi}{3}\frac{1}{n}\int v^4 \vec{f}_1 dv = -\frac{4\pi}{3}\frac{1}{n}\int v^4 \frac{1}{\nu_1}\frac{\Gamma}{v}\frac{\partial f_0}{\partial v} dv = \ldots = -\frac{4\pi}{3}\frac{1}{nm\nu_1} e\vec{E}\int v^3 \frac{\partial f_0}{\partial v} dv = -\frac{4\pi}{3}\frac{3}{nm\nu_1} e\vec{E}\int v^2 f_0 dv$$

ν_1~const

$\nu_1 \sim N v \sigma$

$$\mu_1 = f\left(\frac{E}{\nu_1}\right) = f\left(\frac{E}{N}\right)$$

$$\bar{\varphi} = \frac{4\pi}{n}\int_0^\infty v^2 f_0 \varphi \, dv$$

ν_1~const

$$\vec{\bar{v}} = -\frac{4\pi}{3}\frac{3}{nm\nu_1} e\vec{E}\int v^2 f_0 dv = -\frac{e}{m\nu_1}\vec{E}\frac{4\pi}{n}\int v^2 f_0 dv = -\frac{e}{m\nu_1}\vec{E}.1$$

$$\varphi = 1$$

ν_1~function of v

$$\vec{\bar{v}} = -\frac{4\pi}{3}\frac{e}{nm}\vec{E}\int \frac{v^3}{\nu_1}\frac{\partial f_0}{\partial v} dv = \vec{E}\left(-\frac{4\pi}{3}\frac{e}{nm}\int \frac{v^3}{\nu_1}\frac{\partial f_0}{\partial v} dv\right)$$

$$\vec{\bar{v}} = -\frac{e}{m\nu_1}\vec{E} = \mu\vec{E}$$

Runaway mobility of ions

- H^+ and D^+ in He

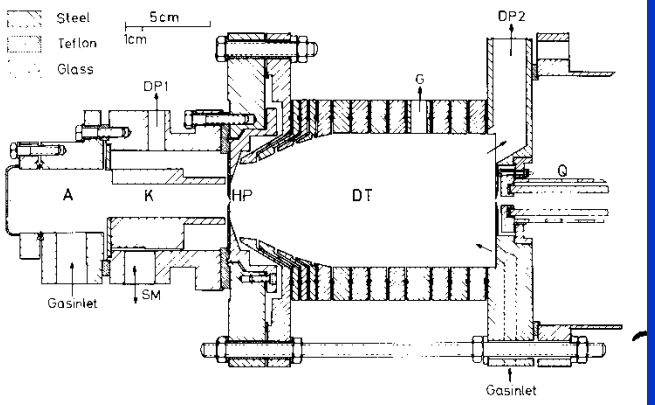

Fig. 1. Section through the main part of the apparatus. A, anode; K, cathode; DP, diffusion pump; SM, shift mechanism (not used in this work); HP, hole probe; DT, drift tube; G, pressure gauge; Q, quadrupole.

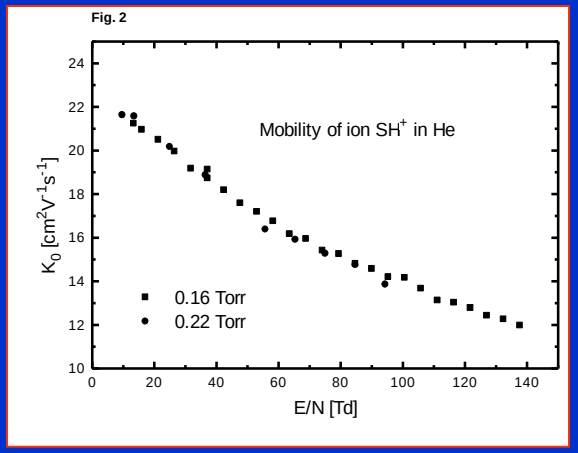

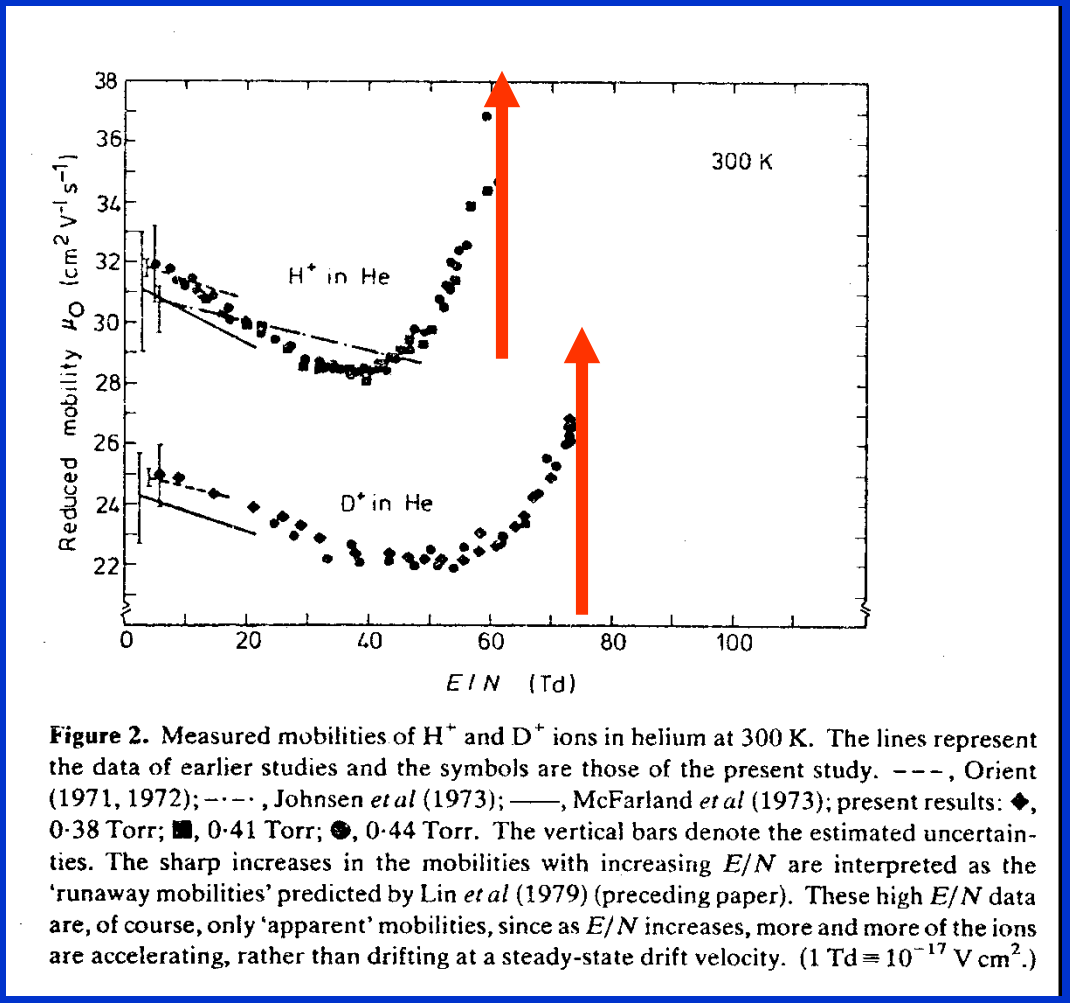

Figure 2. Measured mobilities of H^+ and D^+ ions in helium at 300 K. The lines represent the data of earlier studies and the symbols are those of the present study. – – –, Orient (1971, 1972); –·–·–, Johnsen *et al* (1973); ——, McFarland *et al* (1973); present results: ◆, 0·38 Torr; ■, 0·41 Torr; ●, 0·44 Torr. The vertical bars denote the estimated uncertainties. The sharp increases in the mobilities with increasing E/N are interpreted as the 'runaway mobilities' predicted by Lin *et al* (1979) (preceding paper). These high E/N data are, of course, only 'apparent' mobilities, since as E/N increases, more and more of the ions are accelerating, rather than drifting at a steady-state drift velocity. (1 Td = 10^{-17} V cm^2.)

J. Phys. B: Atom. Molec. Phys., Vol. 12, No. 24, 1979. Printed in Great Britain

1979

H^+ and D^+ ions in He: observations of a runaway mobility

F Howorka†, F C Fehsenfeld and D L Albritton

$$\bar{\vec{v}} = -\frac{4\pi}{3}\frac{e}{nm}\vec{E}\int\frac{v^3}{\nu_1}\frac{\partial f_0}{\partial v}dv = \vec{E}\left(-\frac{4\pi}{3}\frac{e}{nm}\int\frac{v^3}{\nu_1}\frac{\partial f_0}{\partial v}dv\right)$$

$\nu_1 \sim N v \sigma$

Srovnaní driftů iontů a elektronů

- Drift iontů
- Drift elektronů

$$E = 1V/cm = 100V/1m$$

$$p = 1Torr$$

CO^+ v N_2

$$v_d = \mu \cdot E = 1700cm/s = 17m/s$$

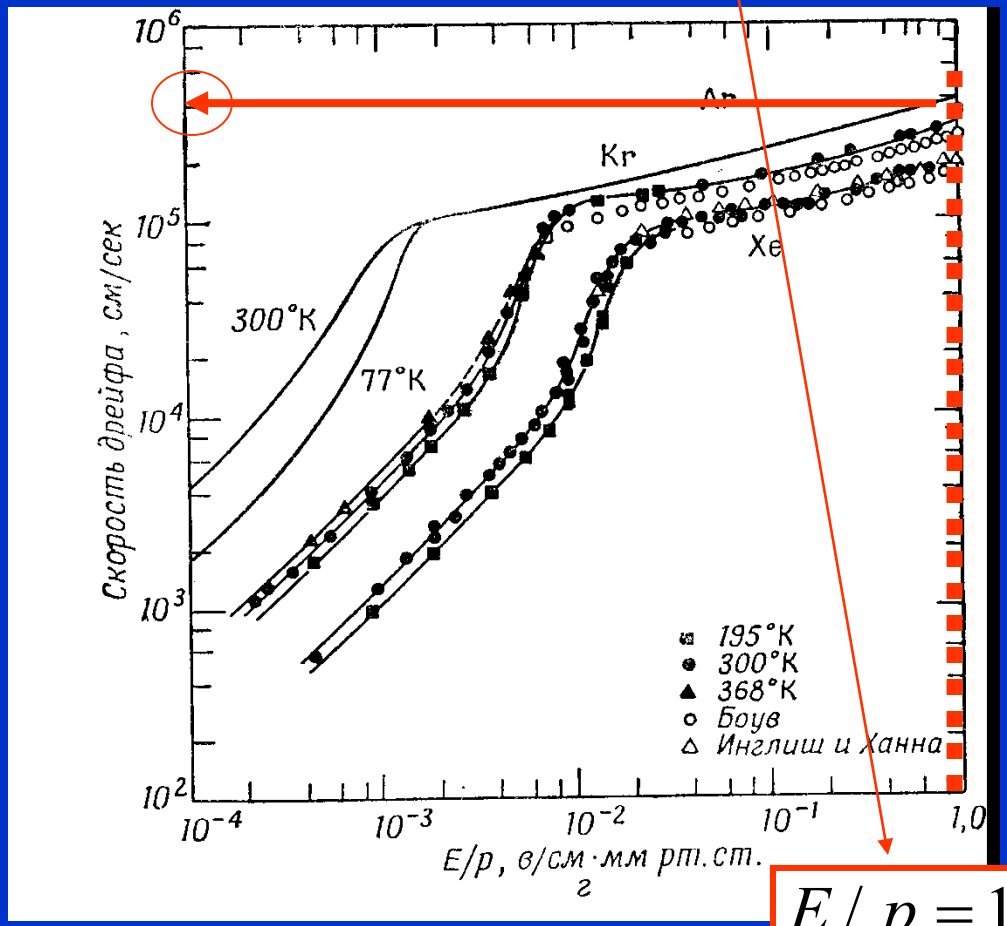

Drift elektronů

e^- v Ar

235x

$$v_{dELECTRON} = 4000m/s$$

$$\mu_e >> \mu_i$$

A co bude dělat plazma v E ??!!

$$E/p = 1V/cmTorr$$

DIFÚZE , DRIFT

Difúze

$$\vec{\bar{v}} = -D\frac{\nabla_r n}{n}$$

Drift

$$\vec{\bar{v}} = \pm\mu\vec{E}$$

$$\vec{\bar{v}} = \pm\mu\vec{E} - D\frac{\nabla_r n}{n}$$

Koeficient difúze

$$D = \frac{kT}{m\nu_1}$$

POHYBLIVOST

$$\mu = \frac{e}{m\nu_1}$$

$$\nu_1 \sim N v \sigma$$

DIFÚZE , DRIFT

$$\vec{\bar{v}} = \pm \frac{e}{m\nu_1}\vec{E} - \frac{kT}{m\nu_1}\frac{\nabla_r n}{n} = \pm\mu\vec{E} - D\frac{\nabla_r n}{n}$$

POHYBLIVOST $\mu = \frac{e}{m\nu_1}$

Koeficient difúze $D = \frac{kT}{m\nu_1}$

pozor na závislost na v

$$\nu_1 = 2\pi N v \int_0^{\pi} (1 - \cos\chi)\,\sigma(\chi, v)\sin\chi\,d\chi$$

$\nu_1 \sim N v \sigma$

$$\vec{\bar{v}} = \pm\mu\vec{E} - D\frac{\nabla_r n}{n}$$

Difúze

$$\vec{\bar{v}} = -D\frac{\nabla_r n}{n}$$

Drift

$$\vec{\bar{v}} = \pm\mu\vec{E}$$

Einsteinův vztah

$$\mu = \frac{e}{m\nu_1} \qquad D = \frac{kT}{m\nu_1}$$

$$\nu_1 = 2\pi N v \int_0^{\pi} (1 - \cos\chi)\,\sigma(\chi, v)\sin\chi\,d\chi$$

$$\nu_1 \sim N v \sigma$$

$$\frac{\mu}{D} = \frac{e}{kT}$$

Einsteinův vztah

$$Dp = D_0 p_0$$

The reduced mobility μ_0 m^2 s^{-1} V^{-1} is the value at a gas number density of 2.69×10^{25} m^{-3}.

$$\mu p = \mu_0 p_0$$

Difúze

$$\vec{\bar{v}} = -D\frac{\nabla_r n}{n}$$

Fickův zákon

$$\vec{\Gamma} = -D\nabla_r n$$

Tok částic

Drift

$$\vec{\bar{v}} = \pm\mu\vec{E}$$

Závislost difúze na tlaku a na teplotě

$$\nu_1 \sim N v \sigma$$

$$D = \frac{kT}{m\nu_1}$$

$$D = \frac{kT}{m\nu_1} \sim \frac{kT}{mNv\sigma} \sim \frac{(kT)^2}{mkTN\sqrt{T}\sigma} \sim \frac{1}{p}$$

$$D \sim \frac{1}{p}$$

$$Dp \sim const. \Rightarrow Dp = D_0 p_0$$

Drift nabitých částic v elektrickém poli

$$\vec{v} = \pm \mu \vec{E}$$

$$\mu = \frac{e}{m \nu_1}$$

$$\nu_1 \sim N v \sigma$$

$$D \sim \frac{1}{p} \qquad \frac{\mu}{D} = \frac{e}{kT}$$

$$\mu \sim \frac{1}{p}$$

$$\mu = \text{function} \quad \text{of} \left(\frac{E}{p}\right)$$

Low E

$$\mu_0 = \mu \cdot \frac{p}{760} \cdot \frac{273}{T}$$

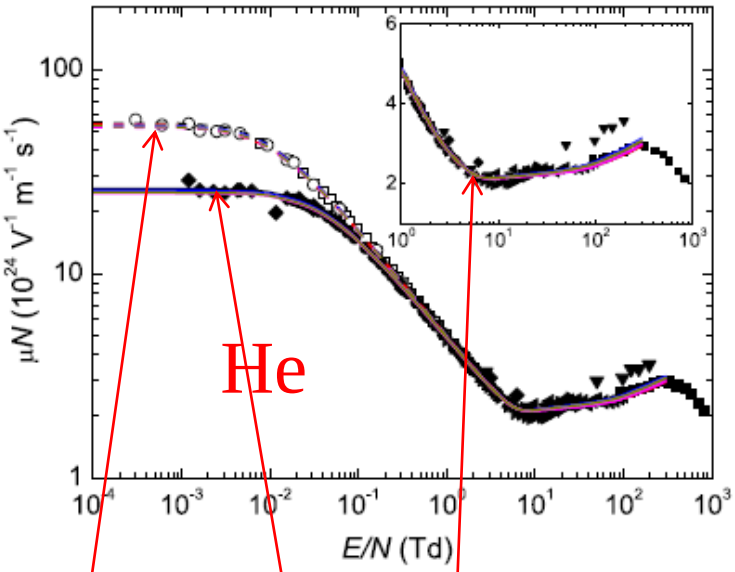

Figure 9. Reduced mobility in helium, as a function of the reduced electric field. The lines are calculations at $T_g = 300$ K (solid) and 77 K (dashed), obtained using a two-term Boltzmann solver with the cross sections from the following databases: BIAGI-v8.9 (——), BIAGI-v7.1 (——), IST-LISBON (——), MORGAN (——), PHELPS (——). The points are measurements from the following authors: Stern (1963) (■), Crompton *et al* (1967) (293 K, ●), Milloy and Crompton (1977) (293 K, ▲), Kücükarpaci *et al* (1981) (▼), Pack *et al* (1992) (300 K, ♦), Dall'Armi *et al* (1992) (◄), Šašić *et al* (2005) (►), Crompton *et al* (1970) (77 K, □), Pack *et al* (1992) (77 K, ⊖). The inset is a zoom in the 1–1000 Td region.

$$\mu p = \mu_0 p_0$$

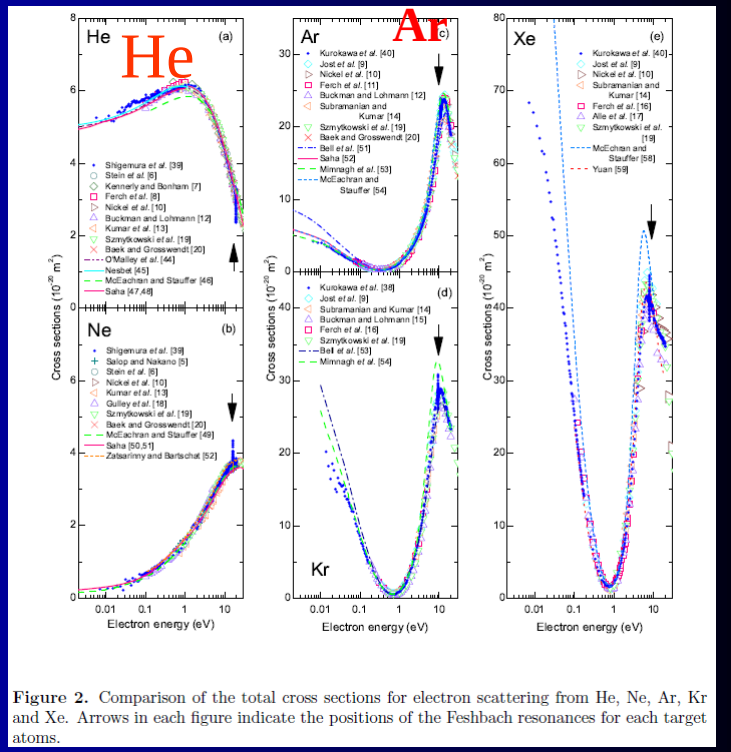

Figure 2. Comparison of the total cross sections for electron scattering from He, Ne, Ar, Kr and Xe. Arrows in each figure indicate the positions of the Feshbach resonances for each target atoms.

The reduced mobility μ_0 m^2 s^{-1} V^{-1} is the value at a gas number density of 2.69×10^{25} m^{-3}.

Loschmidovo číslo ~2,687x10^{19}cm^{-3}

$$1\,\mathrm{Td} = 10^{-21}\,\mathrm{V}\cdot\mathrm{m}^2 = 10^{-17}\,\mathrm{V}\cdot\mathrm{cm}^2.$$

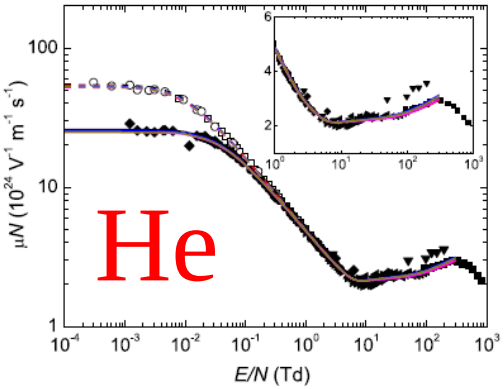

Figure 9. Reduced mobility in helium, as a function of the reduced electric field. The lines are calculations at $T_g = 300$ K (solid) and 77 K (dashed), obtained using a two-term Boltzmann solver with the cross sections from the following databases: BIAGI-v8.9 (——), BIAGI-v7.1 (——), IST-LISBON (——), MORGAN (——), PHELPS (——). The points are measurements from the following authors: Stern (1963) (■), Crompton *et al* (1967) (293 K, ●), Milloy and Crompton (1977) (293 K, ▲), Kücükarpaci *et al* (1981) (▼), Pack *et al* (1992) (300 K, ♦), Dall'Armi *et al* (1992) (◄), Šašić *et al* (2005) (►), Crompton *et al* (1970) (77 K, □), Pack *et al* (1992) (77 K, ○). The inset is a zoom in the 1–1000 Td region.

$$\vec{\bar{v}} = \pm \mu \vec{E}$$

$$\vec{\bar{v}} = -\frac{e}{m\nu_1}\vec{E} = \mu \vec{E}$$

$$\nu_1 = 2\pi N v \int_0^{\pi} (1 - \cos\chi)\,\sigma(\chi, v)\sin\chi\, d\chi$$

$$\vec{\bar{v}} = -\frac{4\pi}{3}\frac{e}{nm}\vec{E}\int \frac{v^3}{\nu_1}\frac{\partial f_0}{\partial v}dv = \vec{E}\left(-\frac{4\pi}{3}\frac{e}{nm}\int \frac{v^3}{\nu_1}\frac{\partial f_0}{\partial v}dv\right)$$

$$\mu_1 = f\left(\frac{E}{\nu_1}\right) = f\left(\frac{E}{N}\right)$$

$$\nu_1 \sim N v \sigma$$

Vodivost

- Pohyb elektronů v elektrickém poli

$$\vec{v} = \pm \mu \vec{E}$$

$$\mu = \frac{e}{m \nu_1}$$

$$\mathbf{J_e} = e n_e \underline{\mathbf{v_e}} = (e^2 n_e / \nu_1 m_e) \cdot \mathbf{E} = \sigma_{COND} E$$

vodivost

$$\nu_1 \sim N v \sigma$$

$$\sigma_{cond.} = \frac{e^2 n_e}{m_e \nu_{1e}}$$

$$\mu p = \mu_0 p_0$$

The reduced mobility μ_0 $m^2\ s^{-1}\ V^{-1}$ is the value at a gas number density of $2.69 \times 10^{25}\ m^{-3}$.

vodivost

Energia elektronů

- Energia, rychlost, Einsteinův vztah

$$1\,\mathrm{Td} = 10^{-21}\,\mathrm{V}\cdot\mathrm{m}^2 = 10^{-17}\,\mathrm{V}\cdot\mathrm{cm}^2.$$

$$D = \frac{1}{3}\left(\frac{\overline{\nu^2}}{\nu_1}\right)$$

$$\mu = \frac{e}{m\nu_1}$$

$$\frac{D}{\mu} = \frac{m}{3}\left(\frac{\overline{\nu^2}}{e}\right) = \frac{2\bar{\varepsilon}}{3e} \sim \frac{kT}{e}$$

$$\frac{D}{\mu} = \frac{kT}{e}$$

která je to T

limita

At 300K ➔kT~.025eV

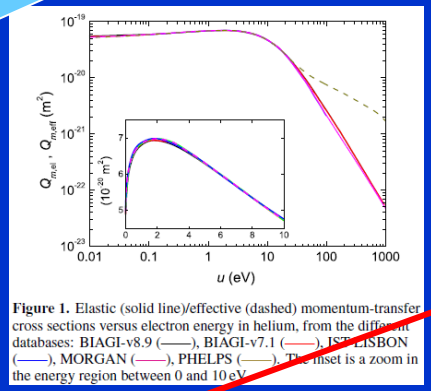

Figure 1. Elastic (solid line)/effective (dashed) momentum-transfer cross sections versus electron energy in helium, from the different databases: BIAGI-v8.9 (——), BIAGI-v7.1 (——), IST-LISBON (——), MORGAN (——), PHELPS (——). The inset is a zoom in the energy region between 0 and 10 eV.

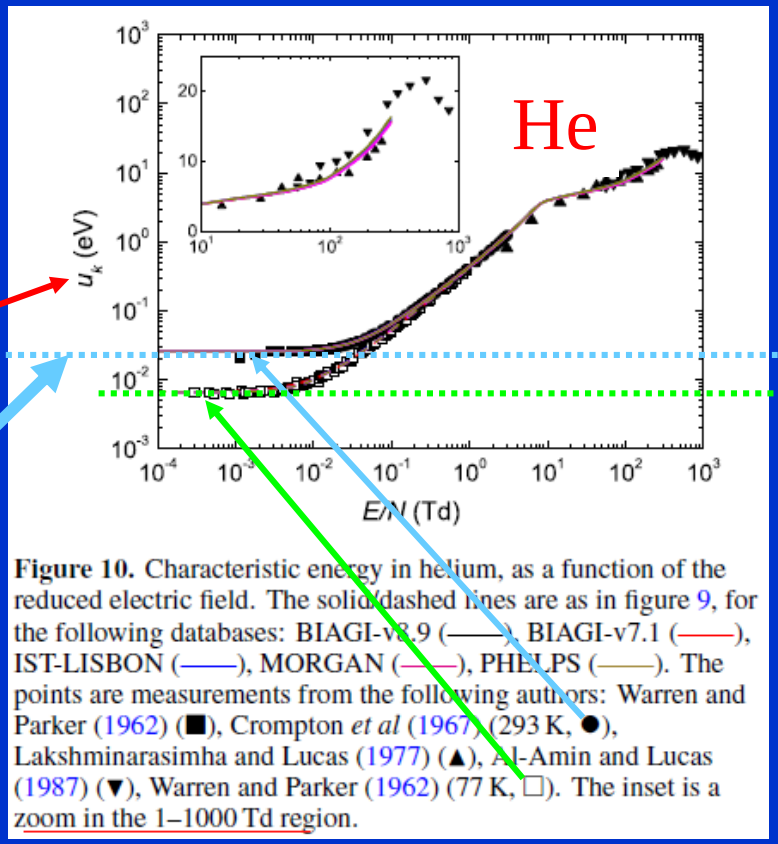

Figure 10. Characteristic energy in helium, as a function of the reduced electric field. The solid/dashed lines are as in figure 9, for the following databases: BIAGI-v8.9 (——), BIAGI-v7.1 (——), IST-LISBON (——), MORGAN (——), PHELPS (——). The points are measurements from the following authors: Warren and Parker (1962) (■), Crompton *et al* (1967) (293 K, ●), Lakshminarasimha and Lucas (1977) (▲), Al-Amin and Lucas (1987) (▼), Warren and Parker (1962) (77 K, □). The inset is a zoom in the 1–1000 Td region.

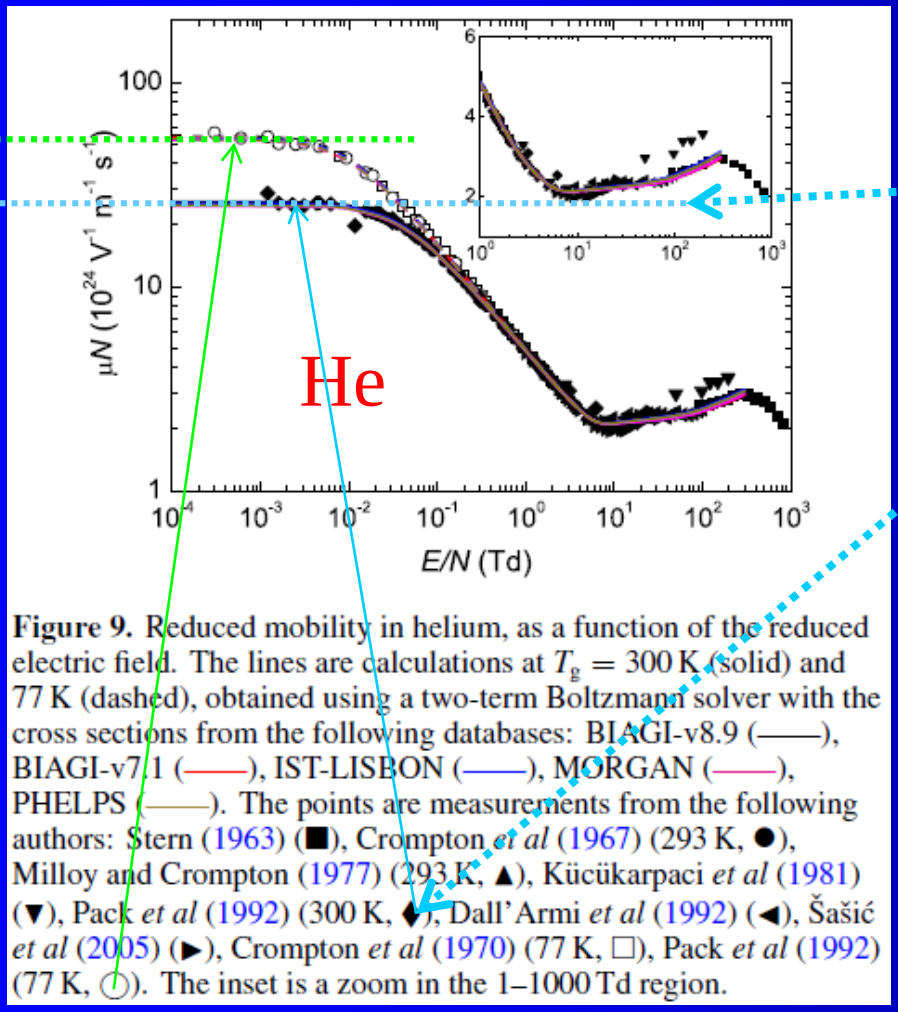

Figure 9. Reduced mobility in helium, as a function of the reduced electric field. The lines are calculations at $T_g = 300$ K (solid) and 77 K (dashed), obtained using a two-term Boltzmann solver with the cross sections from the following databases: BIAGI-v8.9 (——), BIAGI-v7.1 (——), IST-LISBON (——), MORGAN (——), PHELPS (——). The points are measurements from the following authors: Stern (1963) (■), Crompton *et al* (1967) (293 K, ●), Milloy and Crompton (1977) (293 K, ▲), Kücükarpaci *et al* (1981) (▼), Pack *et al* (1992) (300 K, ♦), Dall'Armi *et al* (1992) (◄), Šašić *et al* (2005) (►), Crompton *et al* (1970) (77 K, □), Pack *et al* (1992) (77 K, ○). The inset is a zoom in the 1–1000 Td region.

300 K

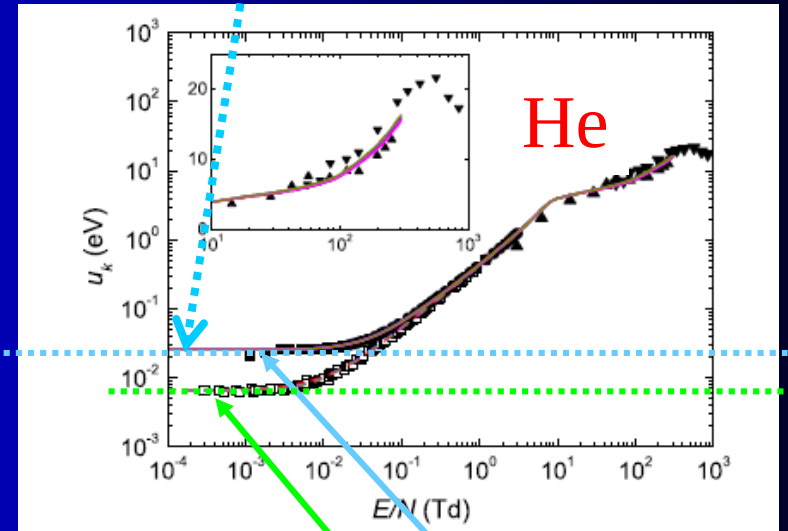

Figure 10. Characteristic energy in helium, as a function of the reduced electric field. The solid/dashed lines are as in figure 9, for the following databases: BIAGI-v8.9 (——), BIAGI-v7.1 (——), IST-LISBON (——), MORGAN (——), PHELPS (——). The points are measurements from the following authors: Warren and Parker (1962) (■), Crompton *et al* (1967) (293 K, ●), Lakshminarasimha and Lucas (1977) (▲), Al-Amin and Lucas (1987) (▼), Warren and Parker (1962) (77 K, □). The inset is a zoom in the 1–1000 Td region.

interpretace

(5.131) $$f_0 = C \exp\left\{ - \int \frac{v\,\mathrm{d}v}{\frac{kT}{m} + \frac{\mathscr{G}(v_1)}{3\gamma v_1^2}} \right\},$$

a) Nechť vnější elektrické pole je nulové, tj. $\boldsymbol{\Gamma} = 0$. Potom

(5.133) $$\mathscr{G}(v_1) = 0$$

B může byt nenulové

a pro $f_0(v)$ máme Maxwellovu rozdělovací funkci

(5.134) $$f_0 = C \exp\left(- \frac{mv^2}{2kT} \right),$$

kde

(5.135) $$C = n \left(\frac{m}{2\pi kT} \right)^{3/2}.$$

b) Nechť vnější magnetické pole je nulové, tj. $\omega_c = 0$. Potom

(5.136) $$\mathscr{G}(v_1) = \Gamma^2$$

a (5.131) můžeme upravit na tvar

(5.137) $$f_0 = C \exp\left\{ - \int \frac{m}{kT} \left(\frac{v v_1^2}{v_1^2 + \left(\frac{\Gamma^2 m}{3\gamma kT} \right)} \right) \mathrm{d}v \right\}.$$

Bude-li nyní srážková frekvence ν_1 nezávislá na rychlosti, tj.

(5.138) $$\nu_1 = \nu = \text{konst},$$

pak f_0 bude opět maxwellovské rozdělení

(5.139) $$f_0 = C \exp\left[- \frac{mv^2}{2k\left(T + \frac{\Gamma^2 m}{3\gamma k} \nu^{-2} \right)} \right] = C \exp\left(- \frac{mv^2}{2kT^*} \right)$$

ale s teplotou

(5.140) $$T^* = T + \frac{m}{3\gamma k} \left(\frac{\Gamma}{\nu} \right)^2 = T + \frac{M}{3k} \left(\frac{ZeE}{m\nu} \right)^2.$$

To ale znamená, že při $\nu_1 = \text{konst}$ je kinetická teplota lehkých nabitých částic (elektronů) vyšší ve srovnání s teplotou neutrálních částic.

Předpoklad, že srážková frekvence elektronů s neutrálními částicemi je konstantní, nezávislá na rychlosti, je příliš ostrý. V obecném případě totiž platí, že ν_1 na rychlosti elektronů závisí. Předpokládejme, že

(5.141) $$\nu_1(v) = Av^l,$$

Energia elektronů

$$1\,\mathrm{Td} = 10^{-21}\,\mathrm{V}\cdot\mathrm{m}^2 = 10^{-17}\,\mathrm{V}\cdot\mathrm{cm}^2.$$

$$D = \frac{1}{3}\left(\frac{\overline{\nu^2}}{\nu_1}\right)$$

$$\mu = \frac{e}{m\nu_1}$$

$$\frac{D}{\mu} = \frac{m}{3}\left(\frac{\overline{\nu^2}}{e}\right) = \frac{2\bar{\varepsilon}}{3e} \sim \frac{kT}{e}$$

která je to T

$$\frac{D}{\mu} = \frac{kT}{e}$$

limita

která je to T

At 300K ➔kT~.025eV

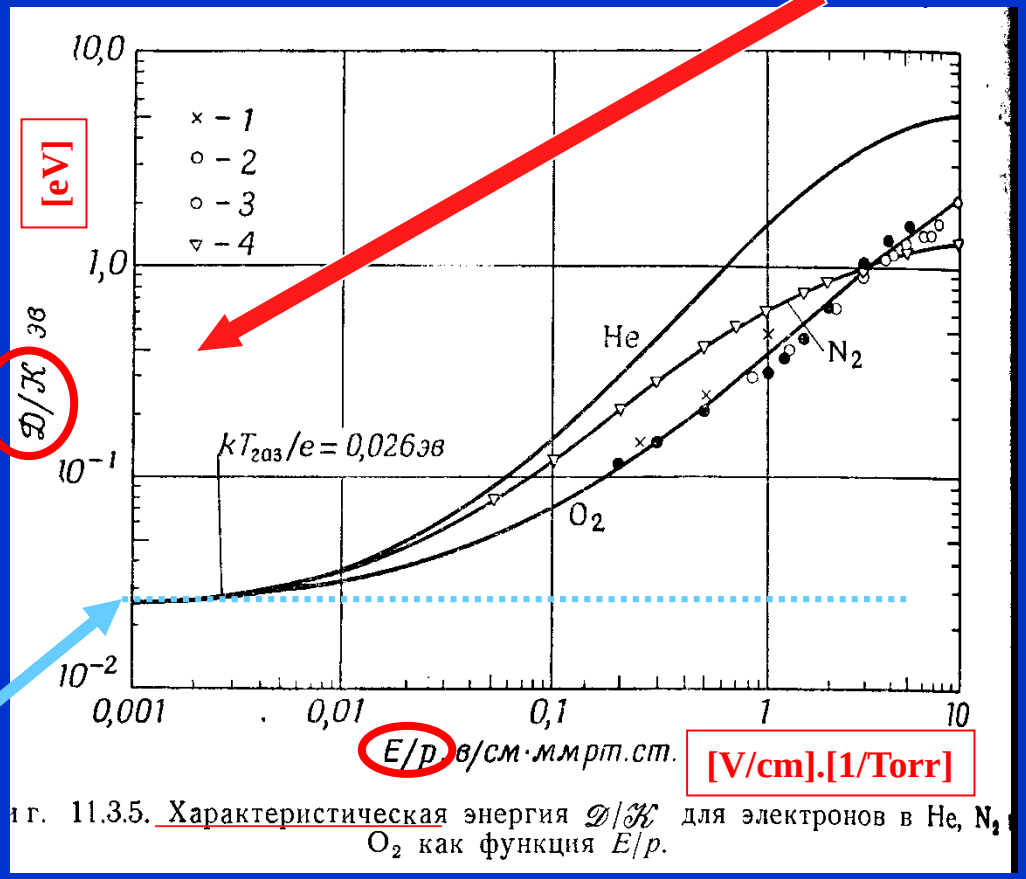

г. 11.3.5. Характеристическая энергия $\mathscr{D}/\mathscr{K}$ для электронов в He, N_2, O_2 как функция E/p.

IOP Publishing Journal of Physics D: Applied Physics
J. Phys. D: Appl. Phys. **46** (2013) 334001 (19pp) doi:10.1088/0022-3727/46/33/334001

2013

Comparisons of sets of electron–neutral scattering cross sections and swarm parameters in noble gases: I. Argon

L C Pitchford[1,2], L L Alves[3], K Bartschat[4], S F Biagi[5], M C Bordage[1,2], A V Phelps[6,10], C M Ferreira[3], G J M Hagelaar[1,2], W L Morgan[7], S Pancheshnyi[1,2], V Puech[8], A Stauffer[9] and O Zatsarinny[4]

$Ar + e^-$

IOP Publishing — Journal of Physics D: Applied Physics
J. Phys. D: Appl. Phys. **46** (2013) 334001 (19pp) doi:10.1088/0022-3727/46/33/334001

2013

Comparisons of sets of electron–neutral scattering cross sections and swarm parameters in noble gases: I. Argon

L C Pitchford[1,2], L L Alves[3], K Bartschat[4], S F Biagi[5], M C Bordage[1,2], A V Phelps[6,10], C M Ferreira[3], G J M Hagelaar[1,2], W L Morgan[7], S Pancheshnyi[1,2], V Puech[8], A Stauffer[9] and O Zatsarinny[4]

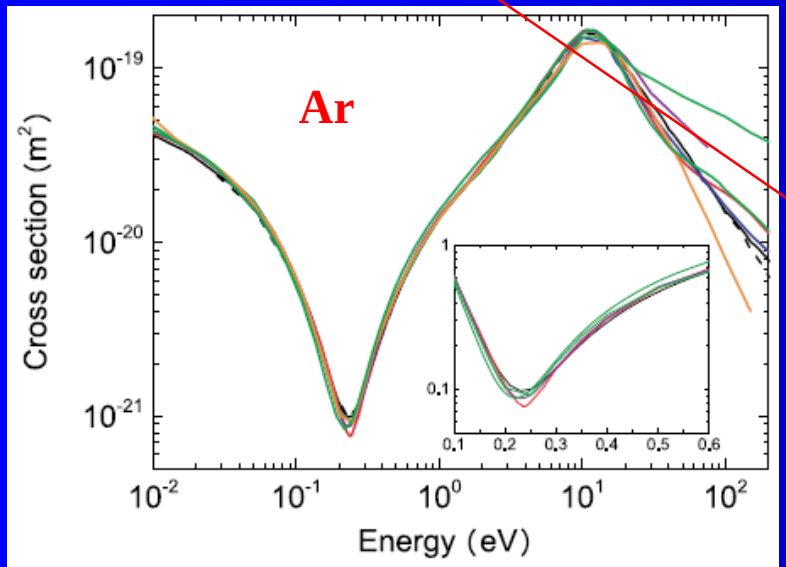

Figure 1. Comparisons of elastic momentum transfer (or effective momentum transfer from PHELPS) cross section versus electron energy in argon from the different databases. The inset is a zoom in the region of the Ramsauer minimum with cross sections in units of 10^{-20} m^2. The colour code is the same for all figures in this article: BIAGI-v8.9 (——); BIAGI-v7.1 (- - - -); BSR (——); HAYASHI (——); IST-LISBON (——); MORGAN (——); PHELPS (——); PUECH (——).

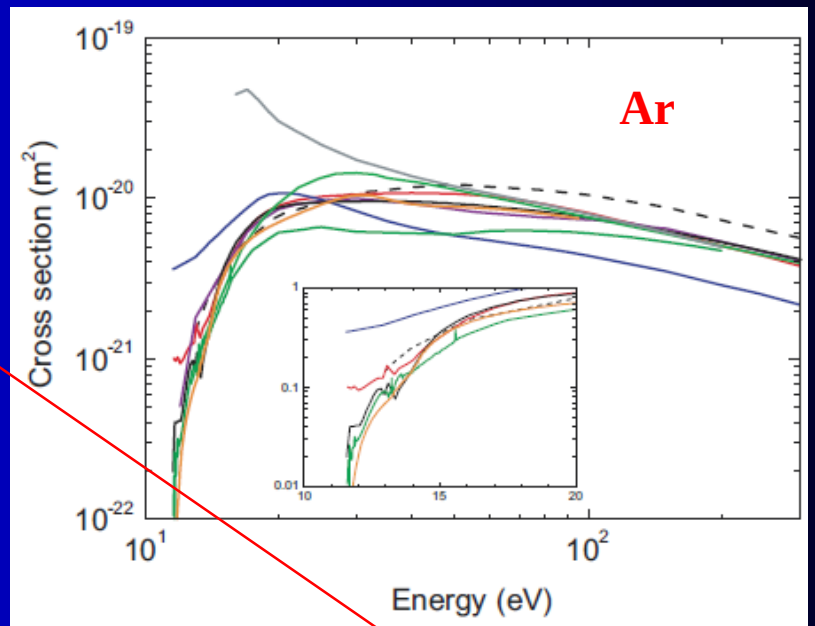

Figure 2. Total excitation cross sections versus energy in argon from the different databases. The inset is a zoom between 10 and 20 eV to show the near-threshold resonance structures, and the unit for the cross sections in the zoom is 10^{-20} m^2. The colour code is: BIAGI-v8.9 (——); BIAGI-v7.1 (- - - -); BSR (——); HAYASHI (——); IST-LISBON (——); MORGAN (——); NGFSRDW (——); PHELPS (——); PUECH (——).

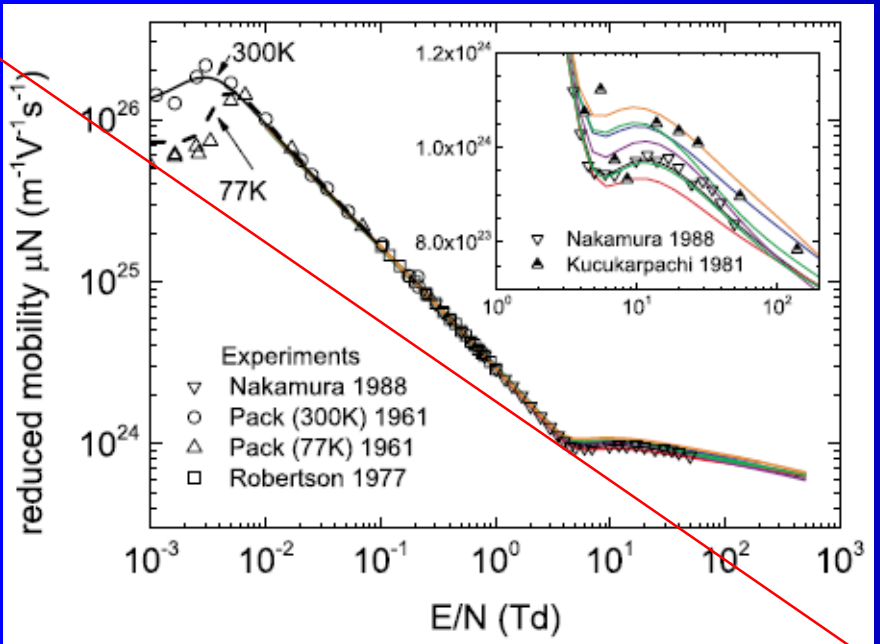

Figure 5. Reduced electron mobility versus E/N. The symbols are experimental data and the solid lines are calculations using the two-term Boltzmann solver, BOLSIG+. The inset is a zoom to illustrate the differences in the calculated results in the region of the knee at $E/N \sim 5$ Td. The colour code is BIAGI-v8.9 (——); BSR (——); HAYASHI (——); IST-LISBON (——); MORGAN (——); PHELPS (——); PUECH (——). The legend refers to the first author and year of publication of references reporting measurements shown in the figure.

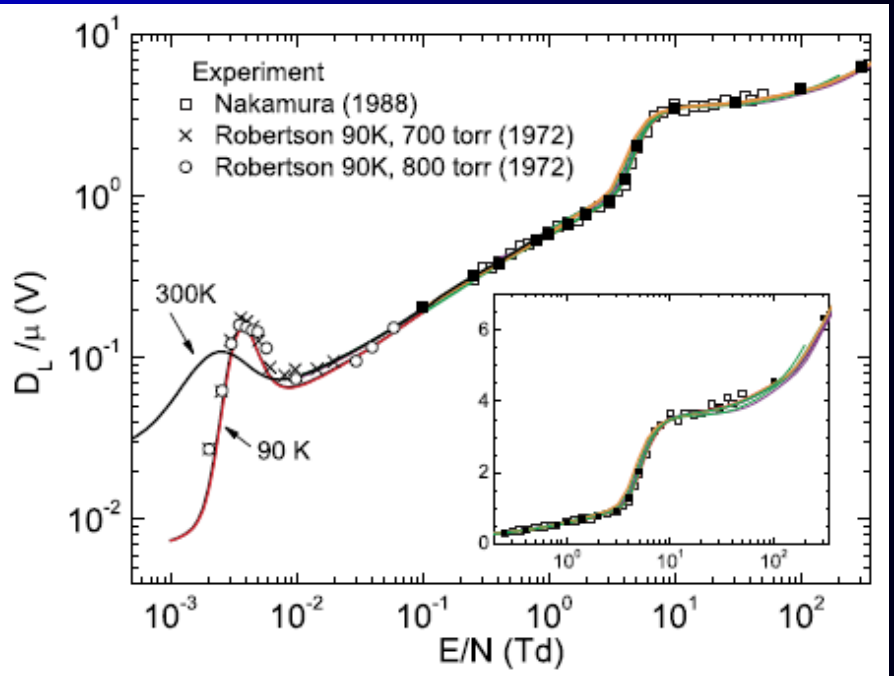

Figure 6. Comparisons of calculated and measured D_L/μ. The open symbols are measurements as indicated in the legend, the closed symbols (■) are Monte Carlo (MAGBOLTZ) results at 293 K and the lines are results of calculations using BOLSIG+. The ordinate in the inset is linear. The colour code is BIAGI-v8.9 (——); BSR (——); HAYASHI (——); IST-LISBON (——); MORGAN (——); PHELPS (——); PUECH (——). The measurements are referenced in the text.

$$\mu = \frac{e}{m\nu_1}$$

The reduced mobility μ_0 m^2 s^{-1} V^{-1} is the value at a gas number density of 2.69×10^{25} m^{-3}.

Loschmidovo číslo ~2,687x10^{19}cm^{-3}

$$\frac{D}{\mu} = \frac{kT}{e}$$

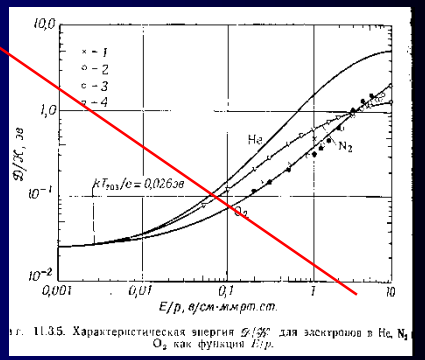

$$1\ \mathrm{Td} = 10^{-21}\ \mathrm{V \cdot m^2} = 10^{-17}\ \mathrm{V \cdot cm^2}.$$

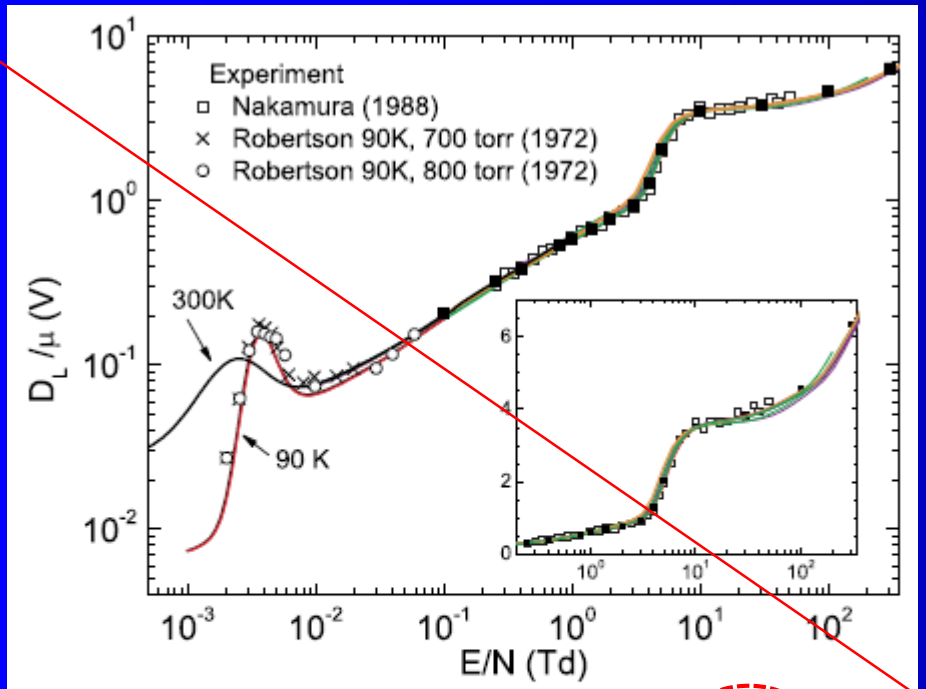

Figure 6. Comparisons of calculated and measured D_L/μ. The open symbols are measurements as indicated in the legend, the closed symbols (■) are Monte Carlo (MAGBOLTZ) results at 293 K and the lines are results of calculations using BOLSIG+. The ordinate in the inset is linear. The colour code is BIAGI-v8.9 (——); BSR (——); HAYASHI (——); IST-LISBON (——); MORGAN (——); PHELPS (——); PUECH (——). The measurements are referenced in the text.

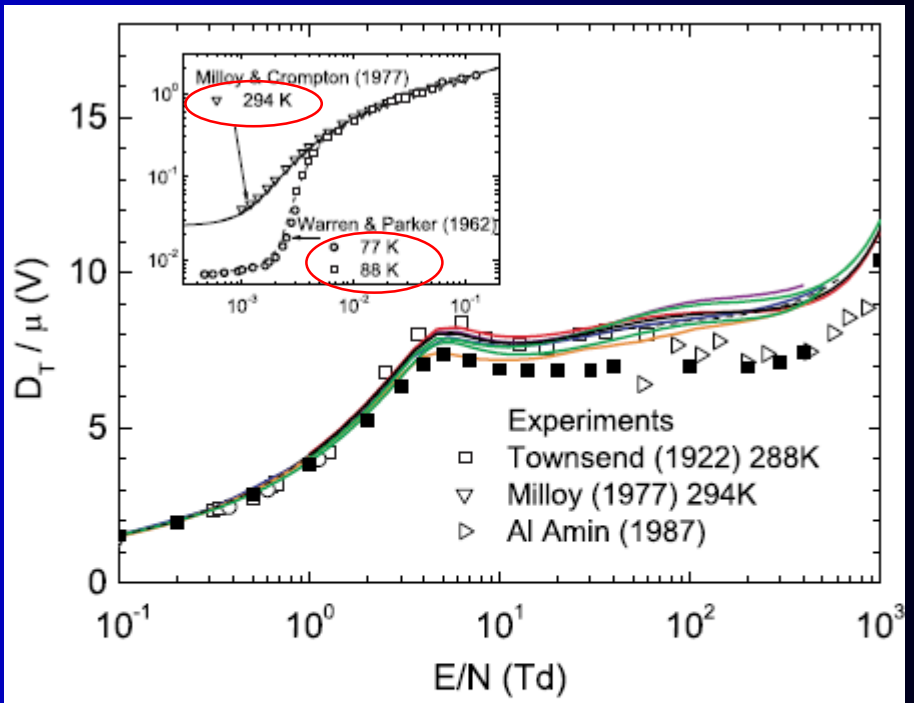

Figure 7. Measured and calculated values of D_T/μ versus E/N. The open symbols are measurements, the closed symbols (■) are Monte Carlo calculations and the lines are results from two-term Boltzmann calculations. The inset shows results at low E/N for 77, 88 and 288 K. The colour code is BIAGI-v8.9 (——); BIAGI-v7.1 (- - - -); BSR (——); HAYASHI (——); IST-LISBON (——); MORGAN (——); PHELPS (——); PUECH (——). The measurements are referenced in the text.

$$\mu = \frac{e}{m\nu_1}$$

$$\frac{D}{\mu} = \frac{kT}{e}$$

$$1\ \mathrm{Td} = 10^{-21}\ \mathrm{V \cdot m^2} = 10^{-17}\ \mathrm{V \cdot cm^2}.$$

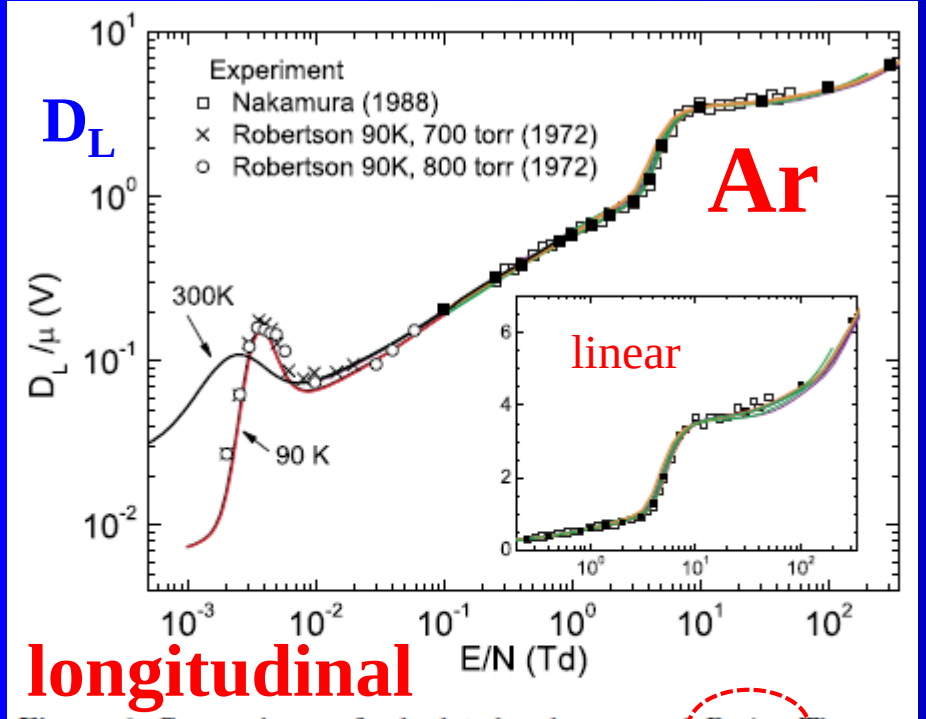

Figure 6. Comparisons of calculated and measured D_L/μ. The open symbols are measurements as indicated in the legend, the closed symbols (■) are Monte Carlo (MAGBOLTZ) results at 293 K and the lines are results of calculations using BOLSIG+. The ordinate in the inset is linear. The colour code is BIAGI-v8.9 (——); BSR (——); HAYASHI (——); IST-LISBON (——); MORGAN (——); PHELPS (——); PUECH (——). The measurements are referenced in the text.

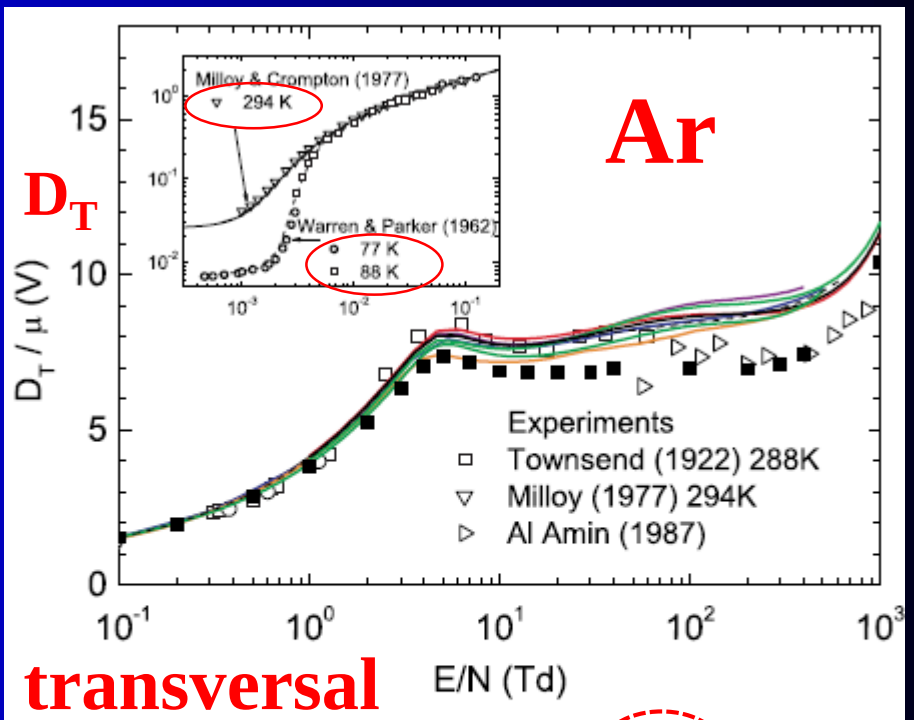

Figure 7. Measured and calculated values of D_T/μ versus E/N. The open symbols are measurements, the closed symbols (■) are Monte Carlo calculations and the lines are results from two-term Boltzmann calculations. The inset shows results at low E/N for 77, 88 and 288 K. The colour code is BIAGI-v8.9 (——); BIAGI-v7.1 (- - - -); BSR (——); HAYASHI (——); IST-LISBON (——); MORGAN (——); PHELPS (——); PUECH (——). The measurements are referenced in the text.

$$\mu = \frac{e}{m\nu_1}$$

$$\frac{D}{\mu} = \frac{kT}{e}$$

$$1\ \mathrm{Td} = 10^{-21}\ \mathrm{V}\cdot\mathrm{m}^2 = 10^{-17}\ \mathrm{V}\cdot\mathrm{cm}^2.$$

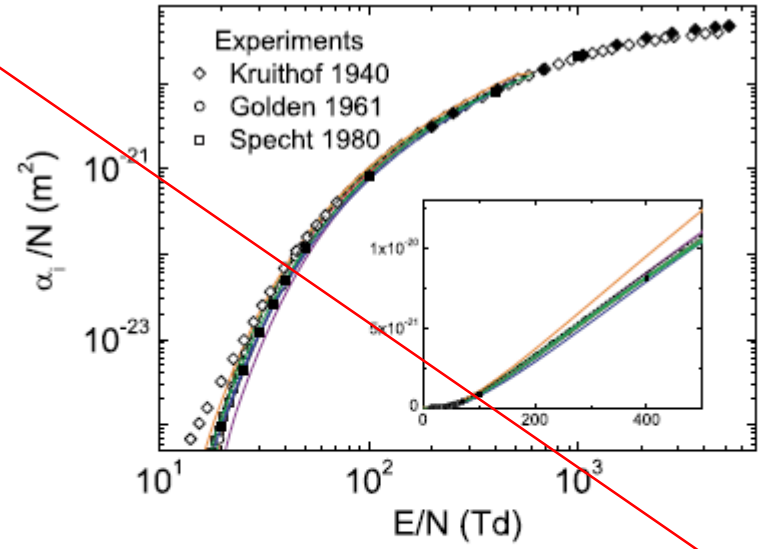

Figure 8. Measured and calculated reduced ionization coefficients. The solid lines are results from two-term Boltzmann calculations and the solid symbols (■) are from the Monte Carlo calculations using MAGBOLTZ (Biagi 2011). The colour code is BIAGI-v8.9 (——); BSR (——); HAYASHI (——); IST-LISBON (——); MORGAN (——); PHELPS (——); PUECH (——). The measurements are referenced in the text.

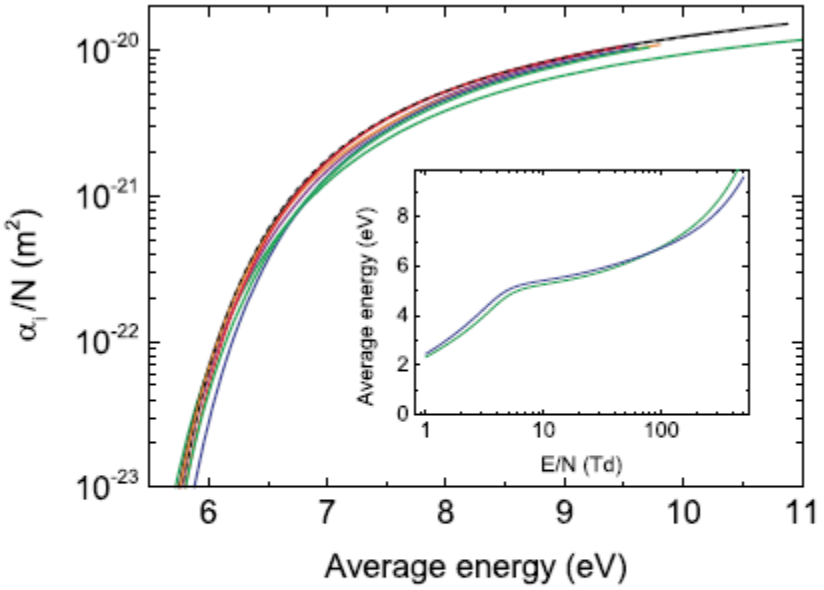

Figure 9. Reduced ionization coefficient versus average electron energy, calculated using a two-term Boltzmann solver. The inset shows the average energy versus E/N, and the colour code is BIAGI-v8.9 (——); BIAGI-v7.1 (- - - -); BSR (——); HAYASHI (——); IST-LISBON (——); MORGAN (——); PHELPS (——); PUECH (——).

IOP Publishing Journal of Physics D: Applied Physics
J. Phys. D: Appl. Phys. **46** (2013) 334002 (22pp) doi:10.1088/0022-3727/46/33/334002

2013

Comparisons of sets of electron–neutral scattering cross sections and swarm parameters in noble gases: II. Helium and neon

L L Alves[1], K Bartschat[2], S F Biagi[3], M C Bordage[4,5], L C Pitchford[4,5], C M Ferreira[1], G J M Hagelaar[4,5], W L Morgan[6], S Pancheshnyi[4,5], A V Phelps[7,9], V Puech[8] and O Zatsarinny[2]

$He + e^-$

$Ne + e^-$

IOP Publishing — Journal of Physics D: Applied Physics
J. Phys. D: Appl. Phys. **46** (2013) 334002 (22pp) doi:10.1088/0022-3727/46/33/334002

2013

Comparisons of sets of electron–neutral scattering cross sections and swarm parameters in noble gases: II. Helium and neon

L L Alves[1], K Bartschat[2], S F Biagi[3], M C Bordage[4,5], L C Pitchford[4,5], C M Ferreira[1], G J M Hagelaar[4,5], W L Morgan[6], S Pancheshnyi[4,5], A V Phelps[7,9], V Puech[8] and O Zatsarinny[2]

He +e$^-$

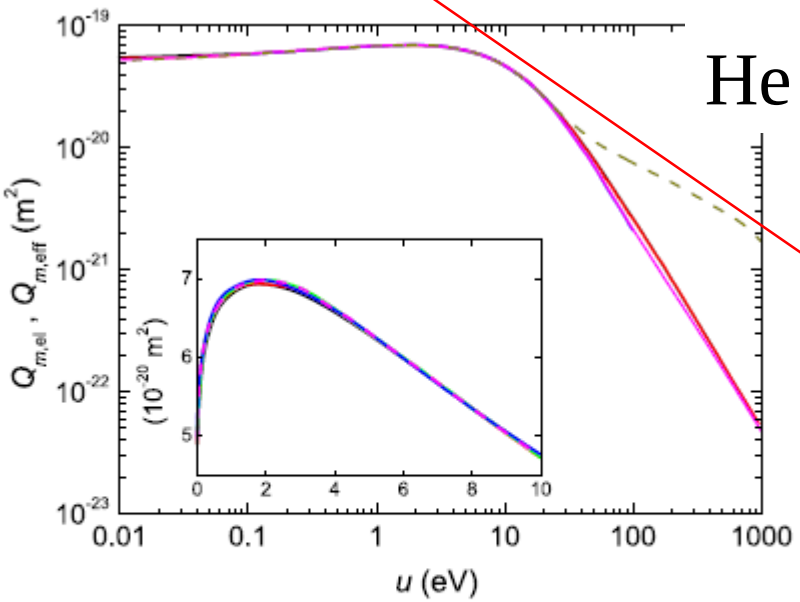

Figure 1. Elastic (solid line)/effective (dashed) momentum-transfer cross sections versus electron energy in helium, from the different databases: BIAGI-v8.9 (——), BIAGI-v7.1 (——), IST-LISBON (——), MORGAN (——), PHELPS (——). The inset is a zoom in the energy region between 0 and 10 eV.

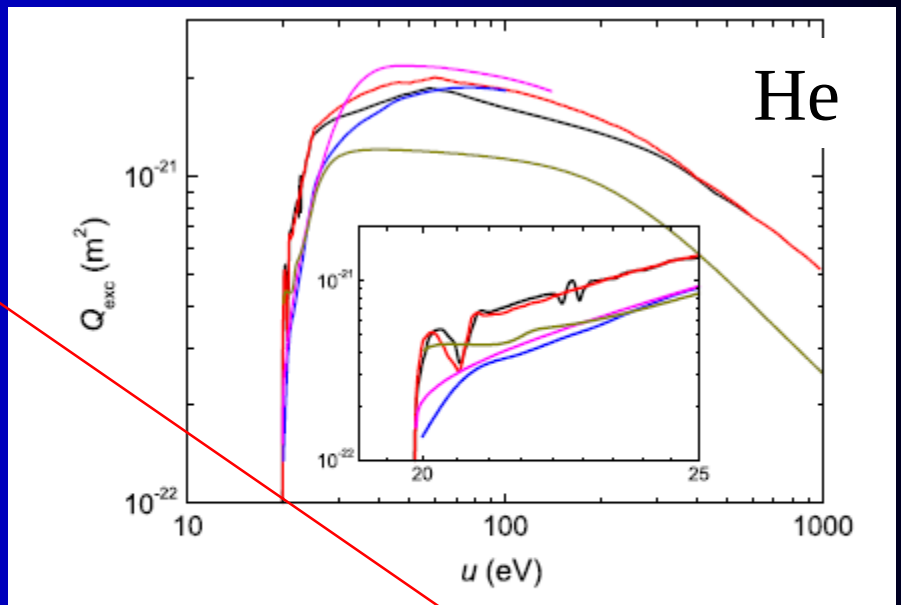

Figure 2. Total excitation cross sections versus electron energy in helium, from the different databases: BIAGI-v8.9 (——), BIAGI-v7.1 (——), IST-LISBON (——), MORGAN (——), PHELPS (——). The inset is a zoom in the near-threshold energy region.

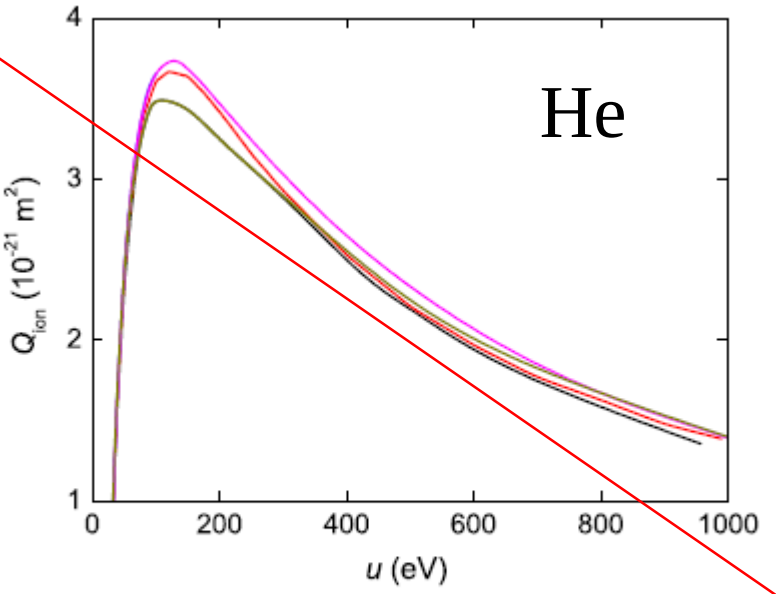

Figure 4. Ionization cross sections versus electron energy in helium, from the different databases: BIAGI-v8.9 (——), BIAGI-v7.1 (——), IST-LISBON (——), MORGAN (——), PHELPS (——).

He +e$^-$

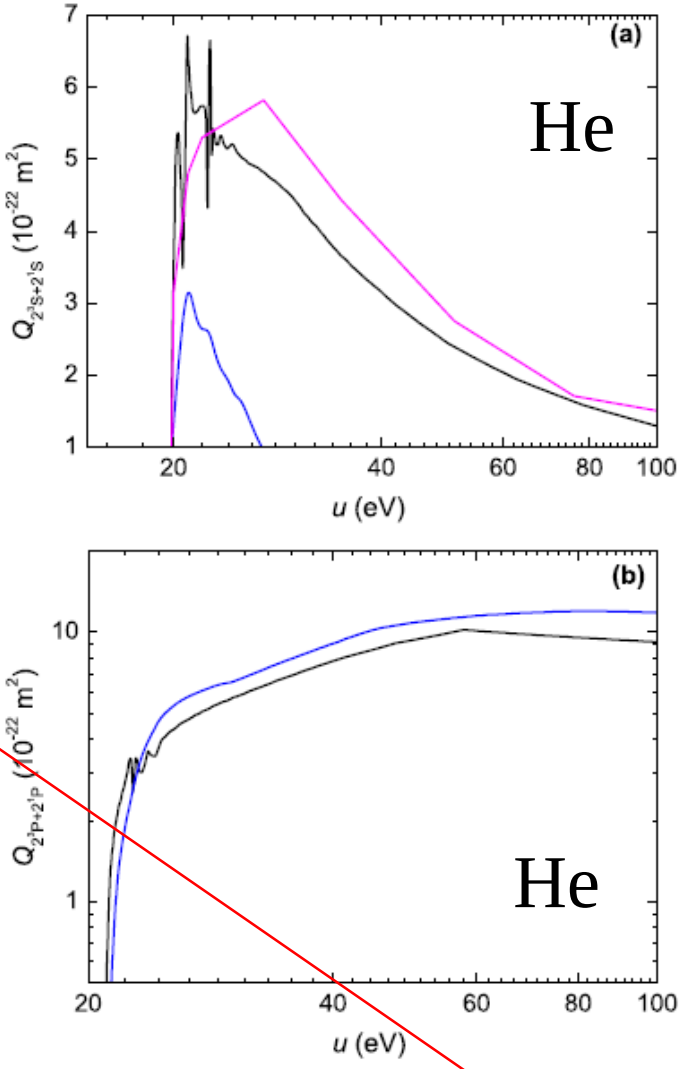

Figure 3. Excitation cross sections versus electron energy in helium for (*a*) metastable levels 2^3S+2^1S and (*b*) radiative levels 2^3P+2^1P, from the following databases: BIAGI-v8.9 (——), IST-LISBON (——), MORGAN (——).

Ne

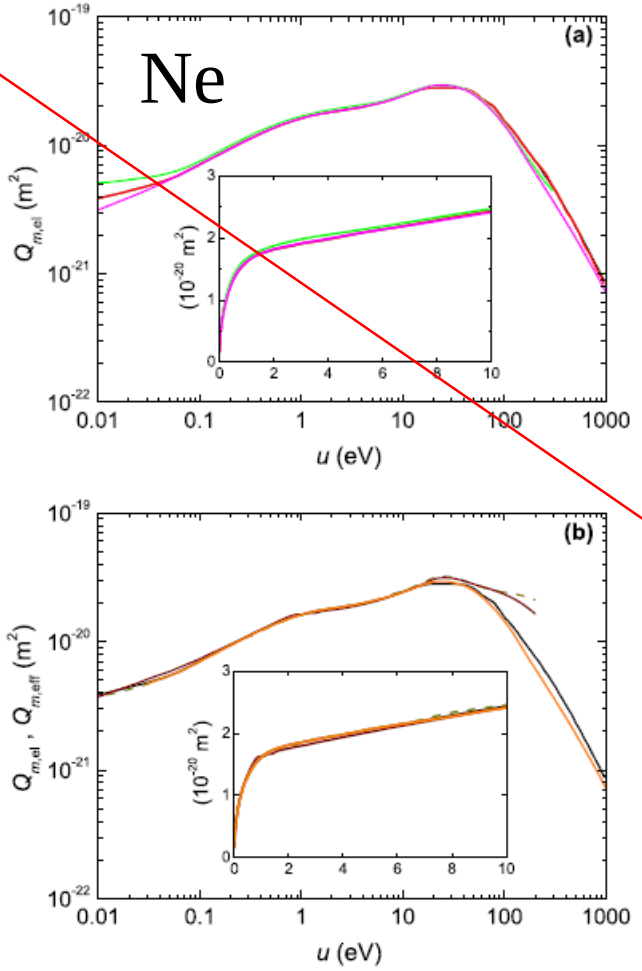

Figure 5. Elastic (solid line)/effective (dashed) momentum-transfer cross sections versus electron energy in neon, from the different databases: (*a*) BIAGI-v8.9 (——), BIAGI-v7.1 (——), BSR (——), MORGAN (——); (*b*) BIAGI-v8.9 (——), PHELPS (——), PUECH (——), SIGLO (——). The insets are zooms in the energy region between 0–10 eV. Data from BIAGI-v8.9 are repeated in (*a*) and (*b*) for comparison purposes.

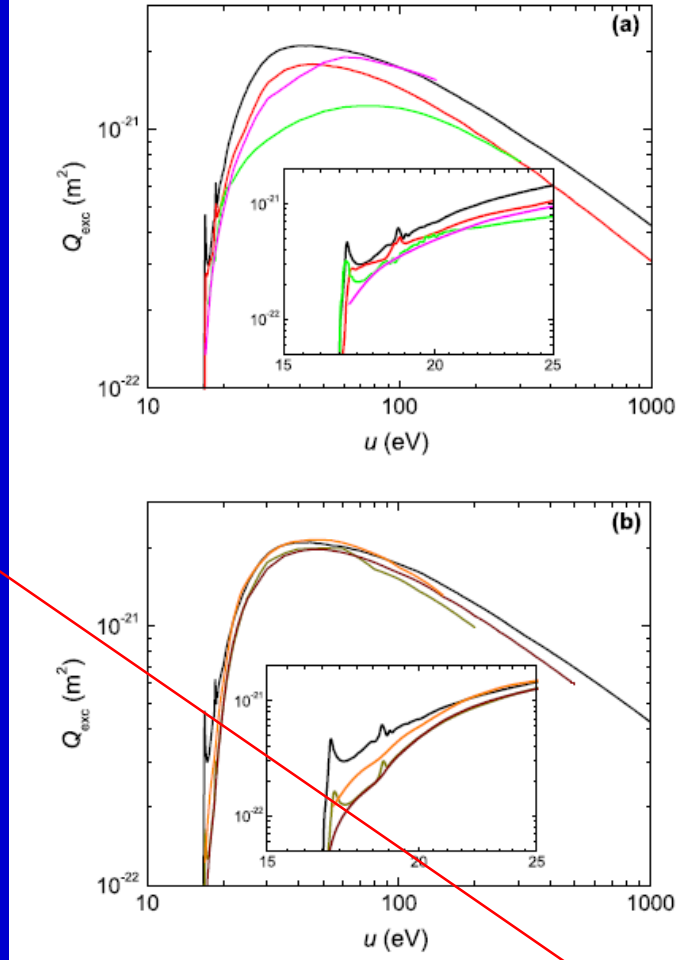

Figure 6. Total excitation cross sections versus electron energy in neon, from the different databases: (*a*) BIAGI-v8.9 (——), BIAGI-v7.1 (——), BSR (——), MORGAN (——); (*b*) BIAGI-v8.9 (——), PHELPS (——), PUECH (——), SIGLO (——). The insets are zooms in the near-threshold energy region. Data from BIAGI-v8.9 are repeated in (*a*) and (*b*) for comparison purposes.

Ne

Ne +e$^-$

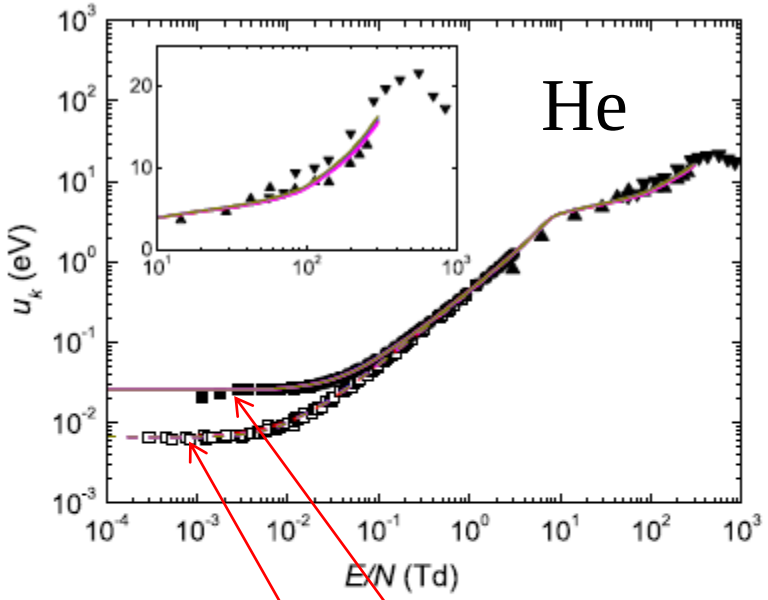

Figure 10. Characteristic energy in helium, as a function of the reduced electric field. The solid/dashed lines are as in figure 9, for the following databases: BIAGI-v8.9 (——), BIAGI-v7.1 (——), IST-LISBON (——), MORGAN (——), PHELPS (——). The points are measurements from the following authors: Warren and Parker (1962) (■), Crompton *et al* (1967) (293 K, ●), Lakshminarasimha and Lucas (1977) (▲), Al-Amin and Lucas (1987) (▼), Warren and Parker (1962) (77 K, □). The inset is a zoom in the 1–1000 Td region.

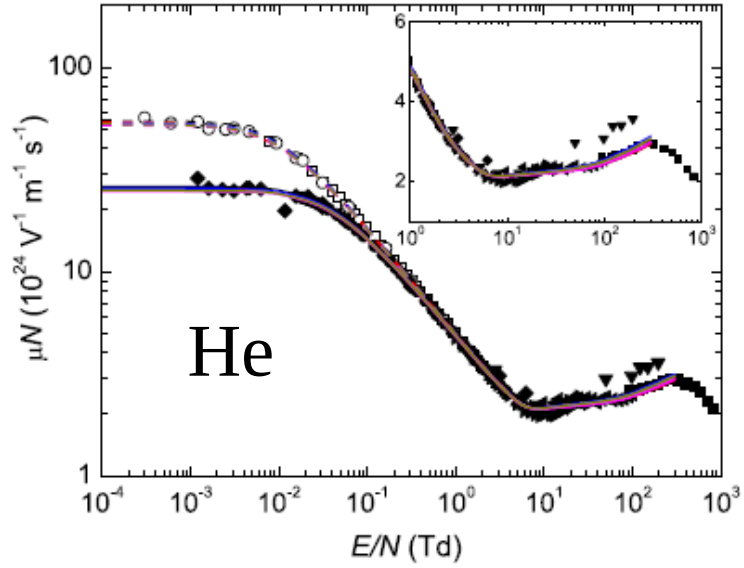

Figure 9. Reduced mobility in helium, as a function of the reduced electric field. The lines are calculations at T_g = 300 K (solid) and 77 K (dashed), obtained using a two-term Boltzmann solver with the cross sections from the following databases: BIAGI-v8.9 (——), BIAGI-v7.1 (——), IST-LISBON (——), MORGAN (——), PHELPS (——). The points are measurements from the following authors: Stern (1963) (■), Crompton *et al* (1967) (293 K, ●), Milloy and Crompton (1977) (293 K, ▲), Kücükarpaci *et al* (1981) (▼), Pack *et al* (1992) (300 K, ♦), Dall'Armi *et al* (1992) (◄), Šašić *et al* (2005) (►), Crompton *et al* (1970) (77 K, □), Pack *et al* (1992) (77 K, ◯). The inset is a zoom in the 1–1000 Td region.

$$\frac{D}{\mu} = \frac{kT}{e}$$

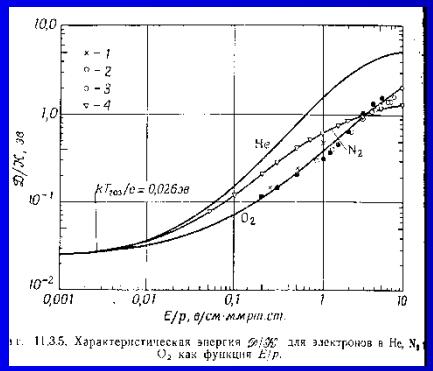

11.3.5. Характеристическая энергия $\mathscr{D}/\mathscr{K}$ для электронов в He, N_2, O_2 как функция E/p.

J. Phys. D: Appl. Phys. **46** (2013) 334003 (16pp) doi:10.1088/0022-3727/46/33/334003

2013

Comparisons of sets of electron–neutral scattering cross sections and swarm parameters in noble gases: III. Krypton and xenon

M C Bordage[1,2], S F Biagi[3], L L Alves[4], K Bartschat[5], S Chowdhury[1], L C Pitchford[1,2], G J M Hagelaar[1,2], W L Morgan[6], V Puech[7] and O Zatsarinny[5]

Kr +e^-

Xe +e^-

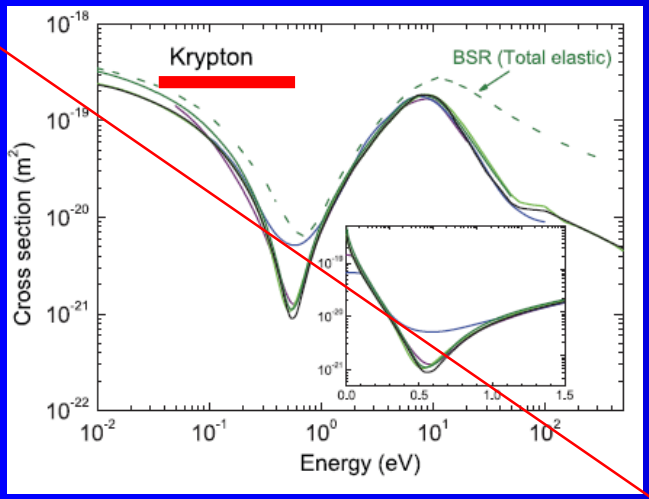

Figure 1. Comparisons of elastic momentum transfer cross section versus electron energy in krypton from the different databases. The inset is a zoom in the region of the Ramsauer minimum. The color code is the same for all figures in this paper: BIAGI-v8.9 (——); BIAGI-v7.1 (——); BSR (——); SIGLO (——); MORGAN (——).

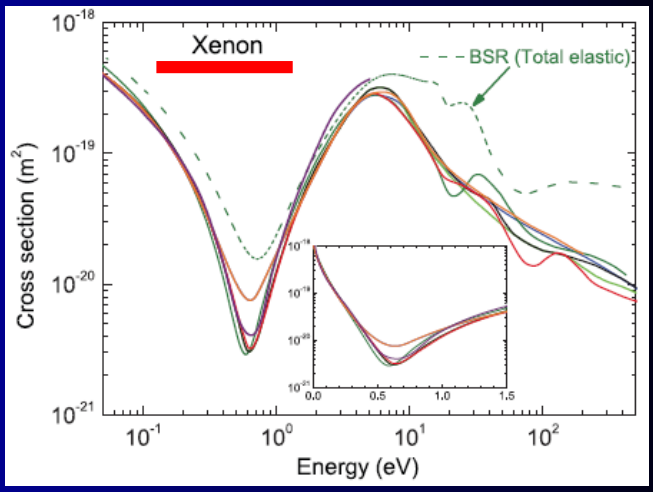

Figure 2. Comparisons of elastic momentum transfer cross section versus electron energy in xenon from the different databases. The inset is a zoom in the region of the Ramsauer minimum. The color code is the same for all figures in this paper: BIAGI-v8.9 (——); BIAGI-v7.1 (——); BSR (——); HAYASHI (——); SIGLO (——); MORGAN (——); PUECH (——).

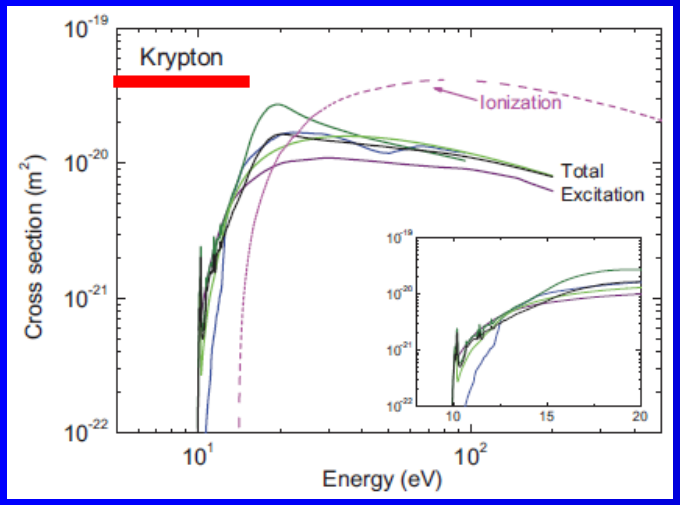

Figure 3. Total excitation and ionization cross sections versus electron energy in krypton from the different databases. The inset is a zoom between 8 and 20 eV to show the near-threshold resonance structures. The color code is: BIAGI-v8.9 (——); BIAGI-v7.1 (——); BSR (——); SIGLO (——); MORGAN (——). For ionization: Rapp and Englander-Golden (1965) (- - - -).

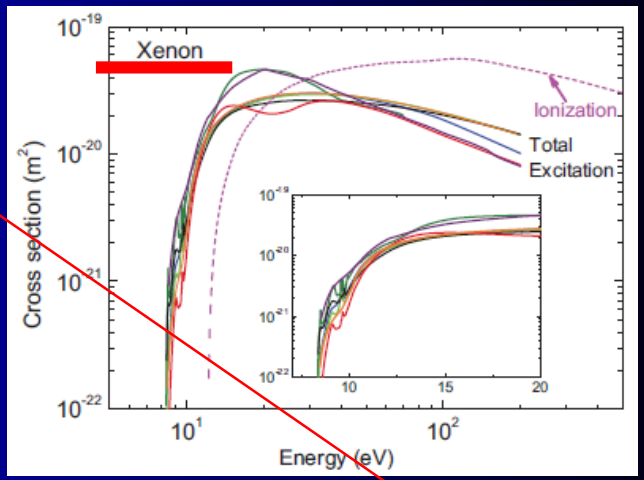

Figure 4. Total excitation and ionization cross sections versus electron energy in xenon from the different databases. The inset is a zoom between 8 and 20 eV to show the near-threshold resonance structures. The color code is: BIAGI-v8.9 (——); BIAGI-v7.1 (——); BSR (——); HAYASHI (——); SIGLO (——); MORGAN (——); PUECH (——). For ionization : Rapp and Englander-Golden (1965) (- - - -).

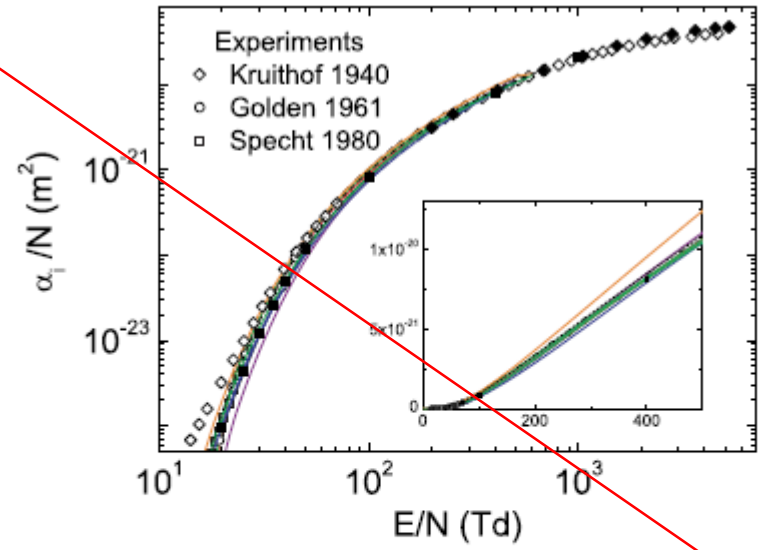

Figure 8. Measured and calculated reduced ionization coefficients. The solid lines are results from two-term Boltzmann calculations and the solid symbols (■) are from the Monte Carlo calculations using MAGBOLTZ (Biagi 2011). The colour code is BIAGI-v8.9 (——); BSR (——); HAYASHI (——); IST-LISBON (——); MORGAN (——); PHELPS (——); PUECH (——). The measurements are referenced in the text.

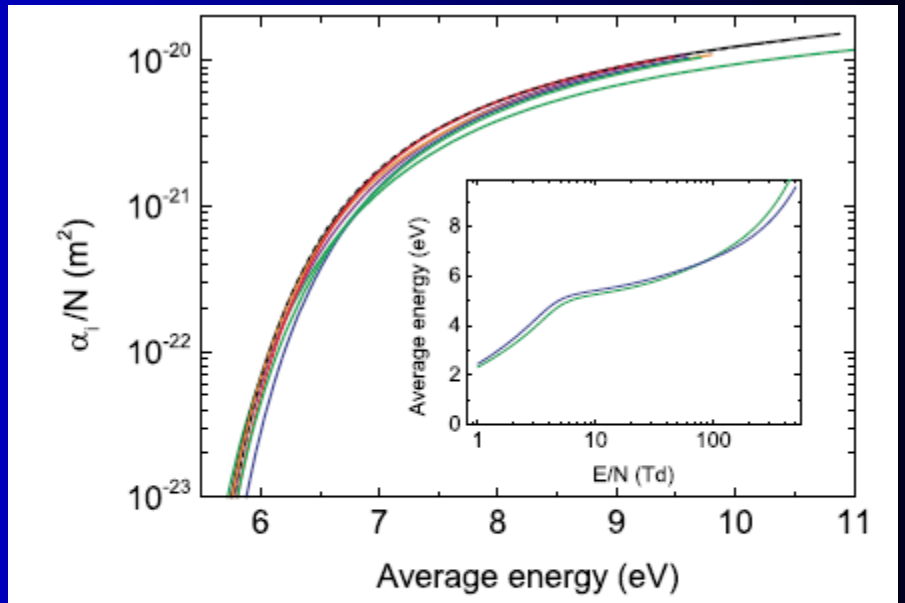

Figure 9. Reduced ionization coefficient versus average electron energy, calculated using a two-term Boltzmann solver. The inset shows the average energy versus E/N, and the colour code is BIAGI-v8.9 (——); BIAGI-v7.1 (- - - -); BSR (——); HAYASHI (——); IST-LISBON (——); MORGAN (——); PHELPS (——); PUECH (——).

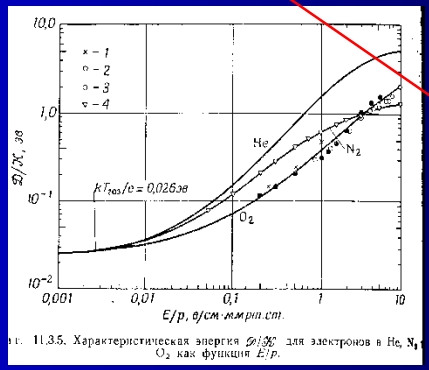

т. 11.3.5. Характеристическая энергия $\mathcal{D}/\mathcal{K}$ для электронов в He, N_2 и O_2 как функция E/p.

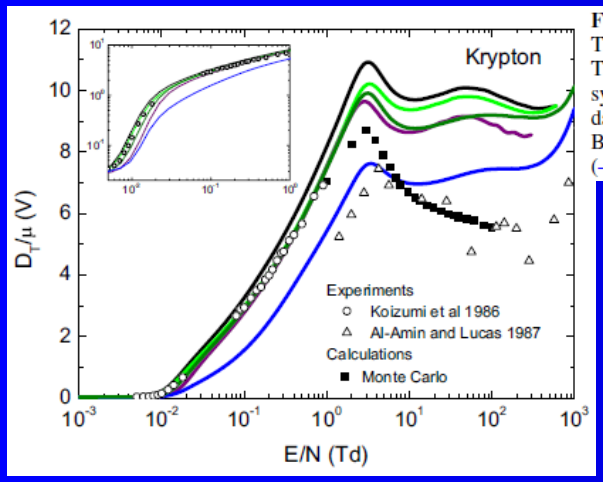

Figure 9. Measured and calculated D_T/μ versus E/N in krypton. The open symbols are experimental data referenced in the table 5. The lines are results from a two-term Boltzmann solver. The symbols (■) are for Monte Carlo calculations with BIAGI-v8.9 dataset. The inset shows results at low E/N. The color code is: BIAGI-v8.9 (——); BIAGI-v7.1 (——); BSR+ (——); SIGLO (——); MORGAN (——).

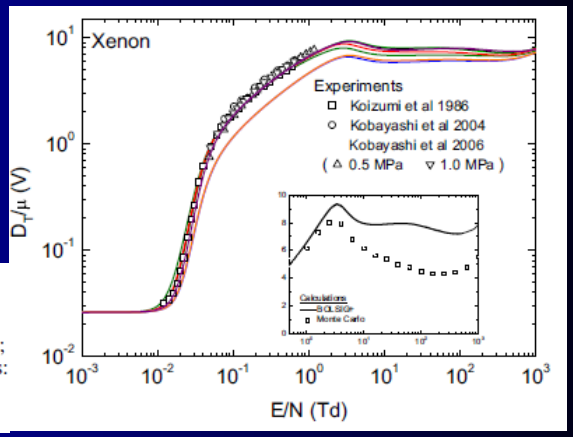

Figure 10. Measured and calculated D_T/μ versus E/N in xenon. The symbols are experimental data referenced in the table 5. The lines are results from two-term Boltzmann calculations. The inset shows comparisons between calculations using BIAGI-v8.9 dataset; the symbols (□) are for Monte Carlo calculations. The color code is: BIAGI-v8.9 (——); BIAGI-v7.1 (——); BSR+ (——); HAYASHI (——); SIGLO (——); MORGAN (——); PUECH (——).

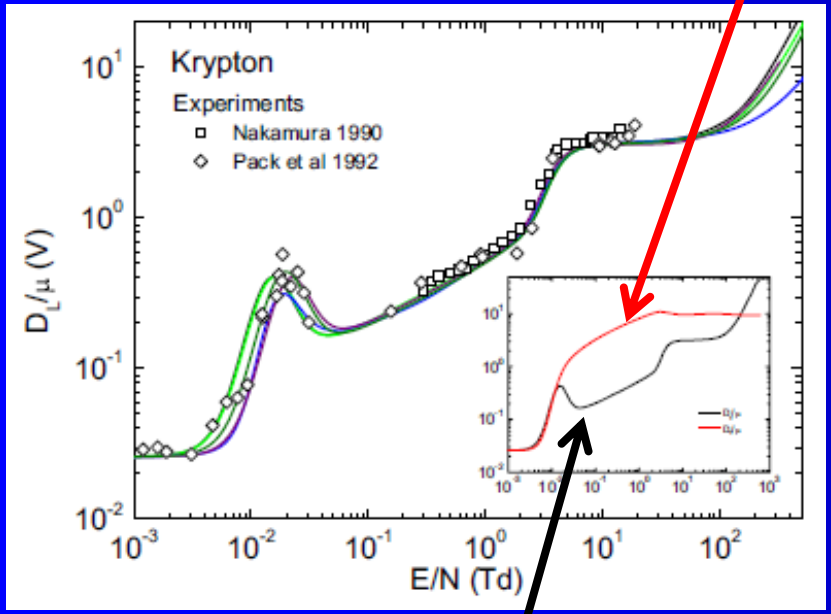

Figure 11. Calculated and measured D_L/μ versus E/N in krypton. The symbols are experimental data referenced in the table 5 and the lines are results from a two-term Boltzmann solver. The inset shows the comparison of D_T/μ and D_L/μ calculated using BIAGI-v8.9 dataset. The color code is: BIAGI-v8.9 (——); BIAGI-v7.1 (——); BSR+ (——); SIGLO (——); MORGAN (——).

$$\frac{D}{\mu} = \frac{kT}{e}$$

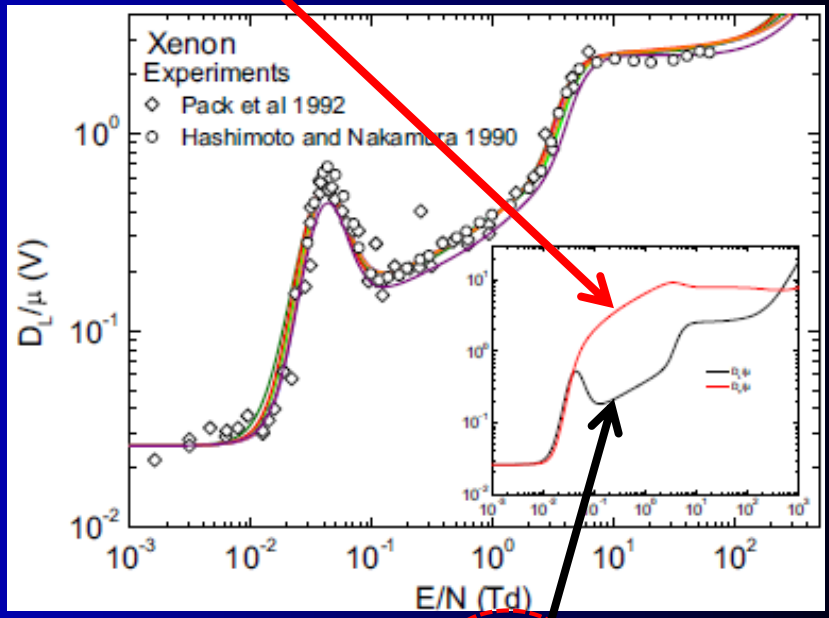

Figure 12. Calculated and measured D_L/μ versus E/N in xenon. The symbols are experimental data referenced in the table 5. The lines are results from a two-term Boltzmann solver. The inset shows the comparison of D_T/μ and D_L/μ calculated using BIAGI-v8.9 dataset. The color code is: BIAGI-v8.9 (——); BIAGI-v7.1 (——); BSR+ (——); HAYASHI (——); SIGLO (——); MORGAN (——); PUECH (——).

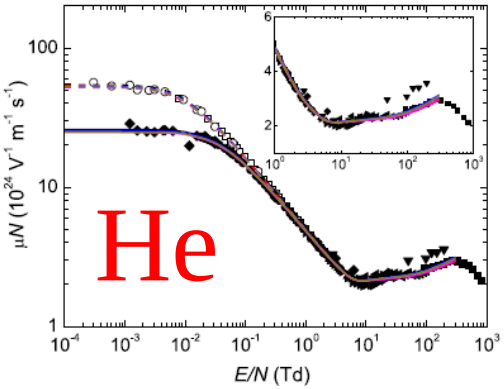

Figure 9. Reduced mobility in helium, as a function of the reduced electric field. The lines are calculations at $T_g = 300$ K (solid) and 77 K (dashed), obtained using a two-term Boltzmann solver with the cross sections from the following databases: BIAGI-v8.9 (——), BIAGI-v7.1 (——), IST-LISBON (——), MORGAN (——), PHELPS (——). The points are measurements from the following authors: Stern (1963) (■), Crompton *et al* (1967) (293 K, ●), Milloy and Crompton (1977) (293 K, ▲), Kücükarpaci *et al* (1981) (▼), Pack *et al* (1992) (300 K, ◆), Dall'Armi *et al* (1992) (◄), Šašić *et al* (2005) (►), Crompton *et al* (1970) (77 K, □), Pack *et al* (1992) (77 K, ◯). The inset is a zoom in the 1–1000 Td region.

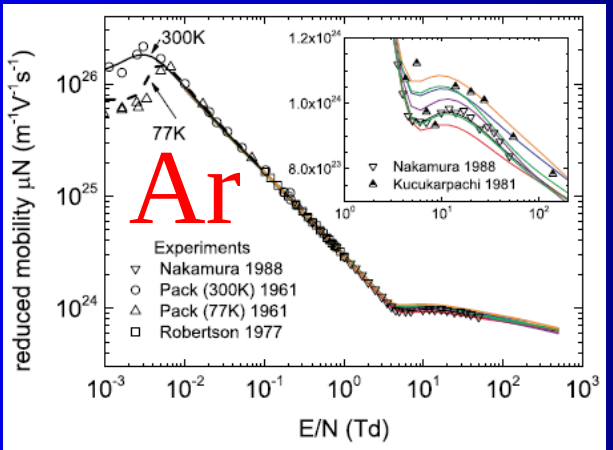

Figure 5. Reduced electron mobility versus E/N. The symbols are experimental data and the solid lines are calculations using the two-term Boltzmann solver, BOLSIG+. The inset is a zoom to illustrate the differences in the calculated results in the region of the knee at $E/N \sim 5$ Td. The colour code is BIAGI-v8.9 (——); BSR (——); HAYASHI (——); IST-LISBON (——); MORGAN (——); PHELPS (——); PUECH (——). The legend refers to the first author and year of publication of references reporting measurements shown in the figure.

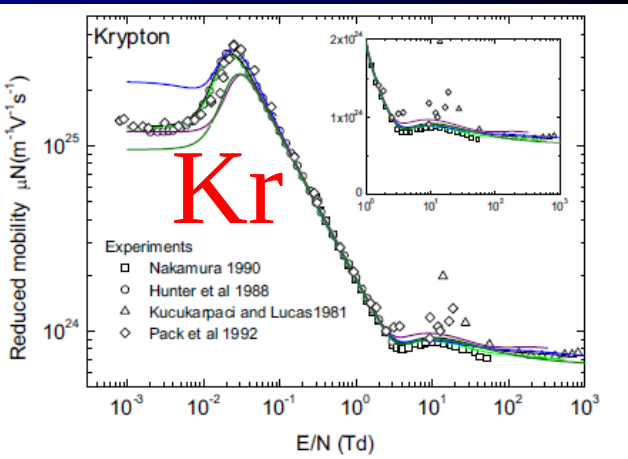

Figure 7. Measured and calculated reduced electron mobility versus E/N in krypton. The symbols are experimental data referenced in the table 5 and the solid lines are calculations using a two-term Boltzmann solver. The inset is a zoom to illustrate the differences in the results in the 1 to 1000 Td region. The color code is: BIAGI-v8.9 (——); BIAGI-v7.1 (——); BSR+ (——); SIGLO (——); MORGAN (——).

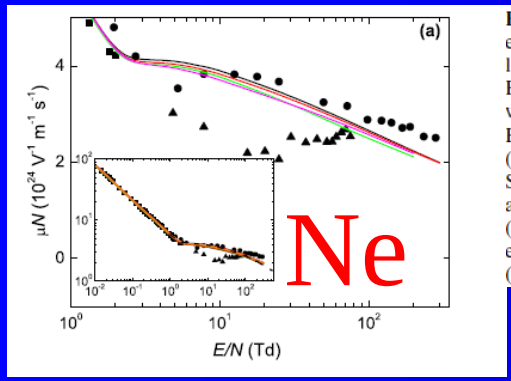

Figure 13. Reduced mobility in neon, as a function of the reduced electric field in the most relevant region of E/N = 1–500 Td. The lines are calculations at $T_g = 300$ K, obtained using a two-term Boltzmann solver (solid lines) or Monte Carlo simulations (dashed with the cross sections from the following databases: (a) BIAGI-v8.9 (——), BIAGI-v7.1 (——), BSR (——), MORGAN (——); (b) BIAGI-v8.9 (——), PHELPS (——), PUECH (——), SIGLO (——). The points are measurements from the following authors: Robertson (1972) (293 K, ■), Kücükarpaci *et al* (1981) (●), Dall'Armi *et al* (1992) (▲). The inset in (*a*) is a plot over the entire E/N region analysed here. The BIAGI-v8.9 results (Boltzmann) are repeated in (*a*) and (*b*) for comparison purposes.

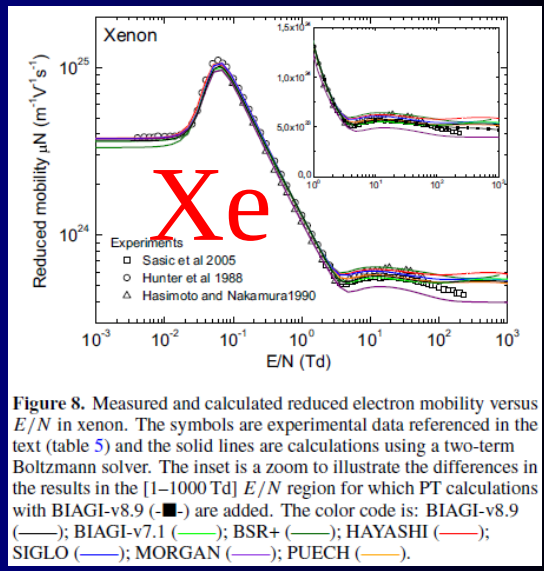

Figure 8. Measured and calculated reduced electron mobility versus E/N in xenon. The symbols are experimental data referenced in the text (table 5) and the solid lines are calculations using a two-term Boltzmann solver. The inset is a zoom to illustrate the differences in the results in the [1–1000 Td] E/N region for which PT calculations with BIAGI-v8.9 (-■-) are added. The color code is: BIAGI-v8.9 (——); BIAGI-v7.1 (——); BSR+ (——); HAYASHI (——); SIGLO (——); MORGAN (——); PUECH (——).

$$\nu_1 = 2\pi N v \int_0^{\pi} (1 - \cos\chi)\, \sigma(\chi, v) \sin\chi \, d\chi$$

$$\vec{\bar{v}} = -\frac{e}{m\nu_1}\vec{E} = \mu\vec{E}$$

$$\vec{\bar{v}} = -\frac{4\pi}{3}\frac{e}{nm}\vec{E}\int \frac{v^3}{\nu_1}\frac{\partial f_0}{\partial v}\,dv = \vec{E}\left(-\frac{4\pi}{3}\frac{e}{nm}\int \frac{v^3}{\nu_1}\frac{\partial f_0}{\partial v}\,dv\right)$$

$$\mu_1 = f\left(\frac{E}{\nu_1}\right) = f\left(\frac{E}{N}\right)$$

Drift iontů - experiment

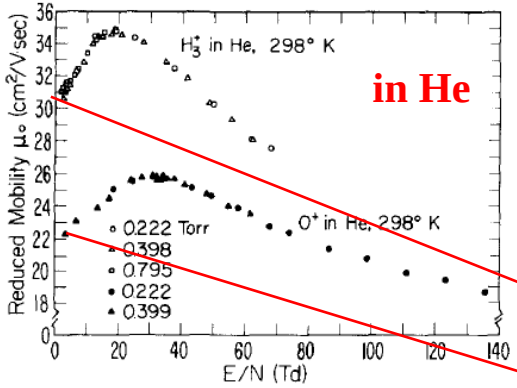

FIG. 1. Reduced mobilities of H_3^+ and O^+ in helium.

The Journal of Chemical Physics, Vol. 62, No. 9, 1 May 1975

1975

Mobilities of various mass-identified positive ions in helium and argon

W. Lindinger* and D. L. Albritton

Aeronomy Laboratory, NOAA Environmental Research Laboratories, Boulder, Colorado 80302
(Received 7 January 1975)

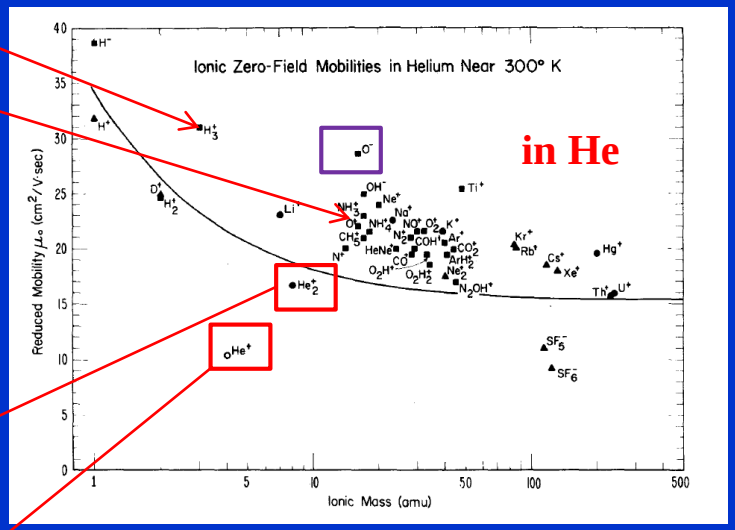

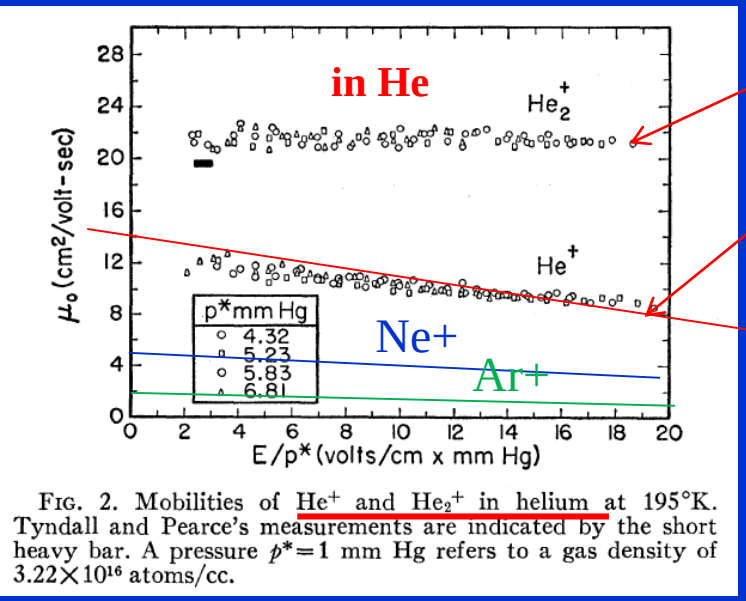

FIG. 2. Mobilities of He^+ and He_2^+ in helium at 195°K. Tyndall and Pearce's measurements are indicated by the short heavy bar. A pressure $p^*=1$ mm Hg refers to a gas density of 3.22×10^{16} atoms/cc.

TABLE II. Reduced zero-field mobilities μ_0 and free and ambipolar diffusion coefficients, D and D_a, times buffer gas pressure and number density, p and N, at 300°K, for a variety of ions in helium and in argon.

Ion	Buffer	μ_0 (cm^2/V·sec)	Dp (cm^2·Torr/sec)	DN (10^{19} cm^{-1}·sec^{-1})	D_ap (cm^2·Torr/sec)	D_aN (10^{19} cm^{-1}·sec^{-1})
H_3^+	Helium	30.5±2.4	658	2.12	1320	4.24
O^+	Helium	22.0±1.8	475	1.53	949	3.06
CO^+	Helium	19.5±1.6	421	1.35	842	2.71
COH^+	Helium	19.5±1.6	421	1.35	842	2.71
Ar^+	Helium	20.5±1.6	442	1.42	885	2.85
ArH^+	Helium	19.4±1.6	419	1.35	837	2.69
O_2^+	Helium	21.8±1.7	470	1.51	941	3.03
O_2H^+	Helium	19.5±1.6	421	1.35	842	2.71
$O_2H_2^+$	Helium	18.5±1.5	399	1.28	798	2.57
NH_3^+	Helium	23.0±1.8	496	1.60	993	3.20
NH_4^+	Helium	21.8±1.7	470	1.51	941	3.03
CH_5^+	Helium	21.0±1.7	453	1.46	906	2.92
CO_2^+	Helium	20.0±1.6	432	1.39	863	2.78
NO^+	Helium	21.5±1.7	464	1.49	928	2.99
N_2OH^+	Helium	17.2±1.4	371	1.19	742	2.39
COH^+	Argon	2.50±0.20	53.9	0.173	108	0.347
CO_2^+	Argon	2.15±0.17	46.4	0.149	92.8	0.299
N_2OH^+	Argon	2.14±0.17	46.2	0.149	92.4	0.297

Drift iontů - experiment

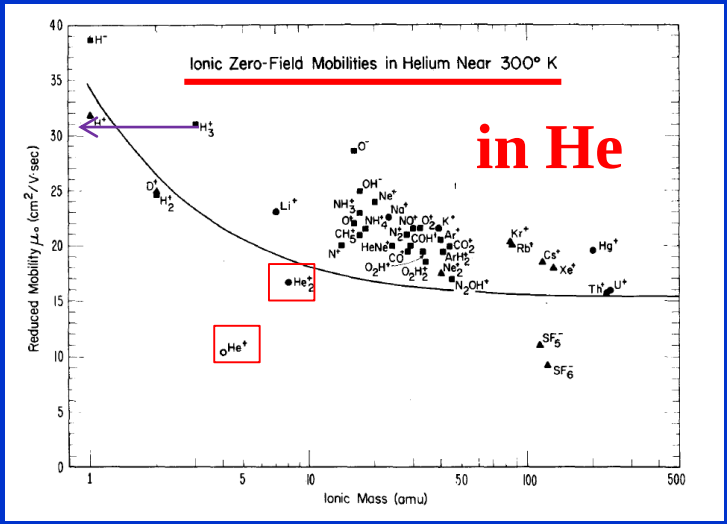

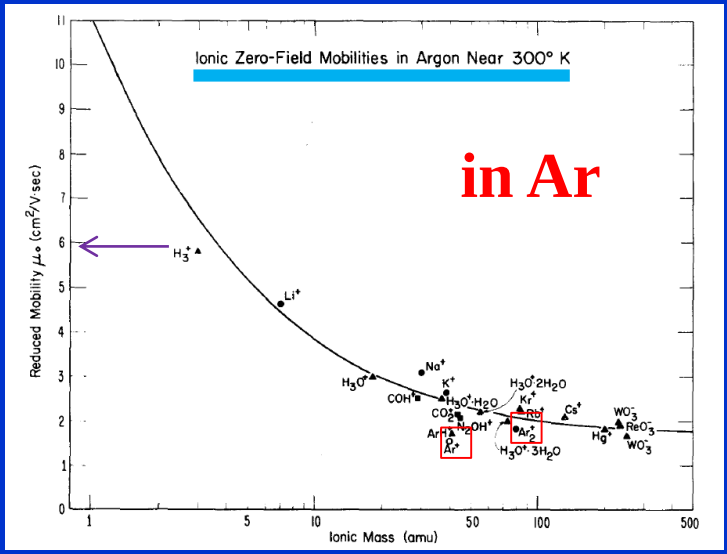

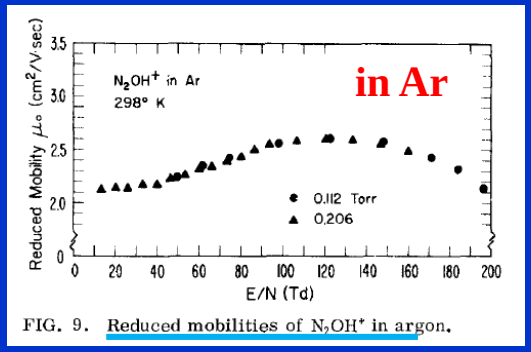

FIG. 9. Reduced mobilities of N_2OH^+ in argon.

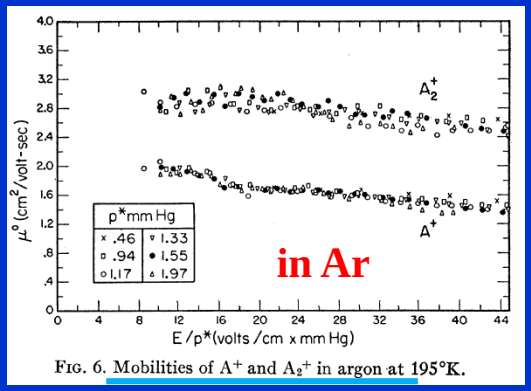

FIG. 6. Mobilities of A^+ and A_2^+ in argon at 195°K.

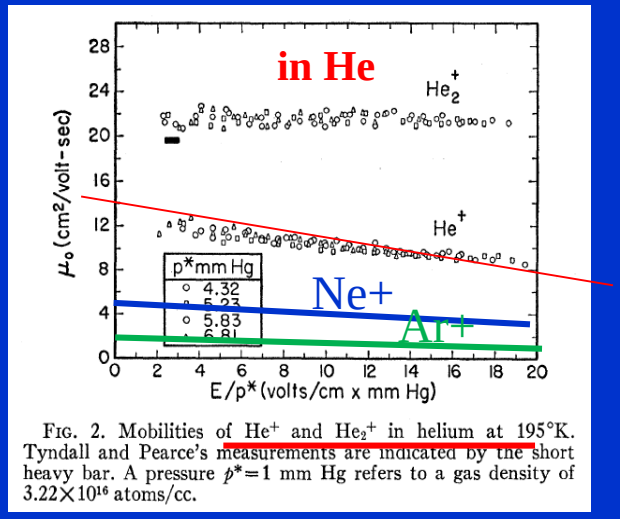

FIG. 2. Mobilities of He^+ and He_2^+ in helium at 195°K. Tyndall and Pearce's measurements are indicated by the short heavy bar. A pressure $p^*=1$ mm Hg refers to a gas density of 3.22×10^{16} atoms/cc.

For polarizable neutrals, the point-charge, induced-dipole attraction always contributes to the ion–neutral interaction. The reduced zero-field mobility for the polarization force alone is given by (Ref. 12, p. 146)

$$\mu_0(\text{Langevin}) = 13.876/(\alpha m_r)^{1/2}\ \text{cm}^2/\text{V}\cdot\text{sec}, \qquad (6)$$

where α is the polarizability in Å^3 and m_r is the reduced mass in g/mole. Since the polarization force is often the strongest long-range interaction and therefore may be the dominant contribution to the mobility at low E/N, it is instructive to test how well the polarization, i.e., Langevin, mobilities agree with the experimental zero-field values, for use when only an approximate value is needed.

Závislost na hmotě plynů a hmotě iontů

$$\mu = \frac{e}{m\nu_1}$$

$$\sigma_0 = \pi\rho_0^2 = \frac{2\pi e}{\nu_0(4\pi\varepsilon_0)}\sqrt{\frac{\alpha}{\mu}}$$

$$\sigma_{coll} = \sigma_L = const\,\frac{1}{v}\sqrt{\frac{\alpha}{\mu}} \sim \sigma_0\frac{v_0}{v}\,cm^2$$

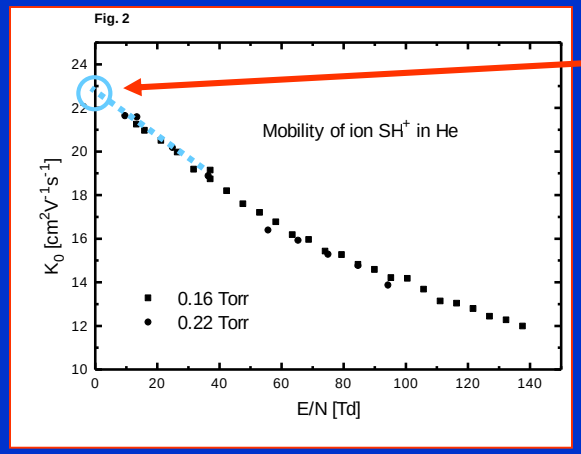

Low E region

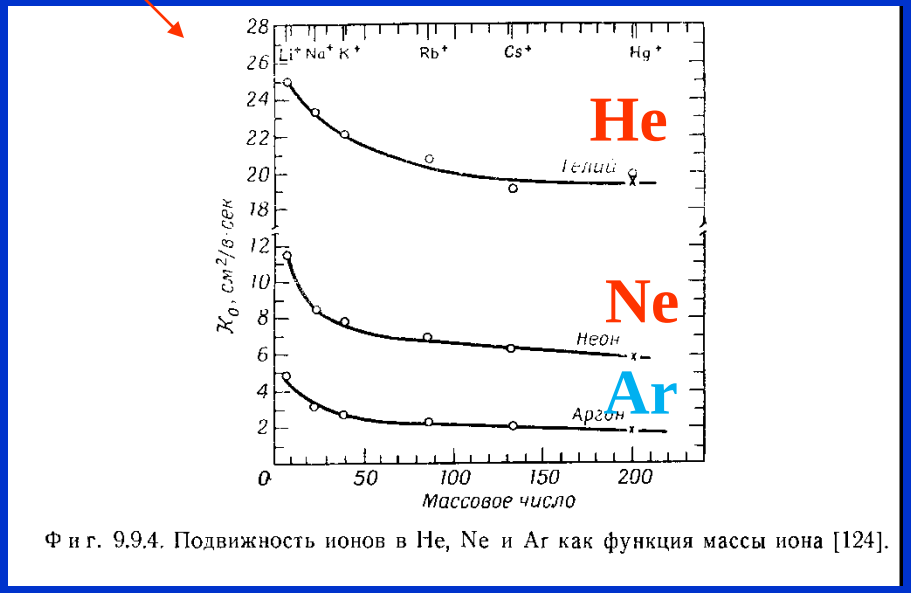

Фиг. 9.9.4. Подвижность ионов в He, Ne и Ar как функция массы иона [124].

experiments

Ion mobility spectrometry diagram

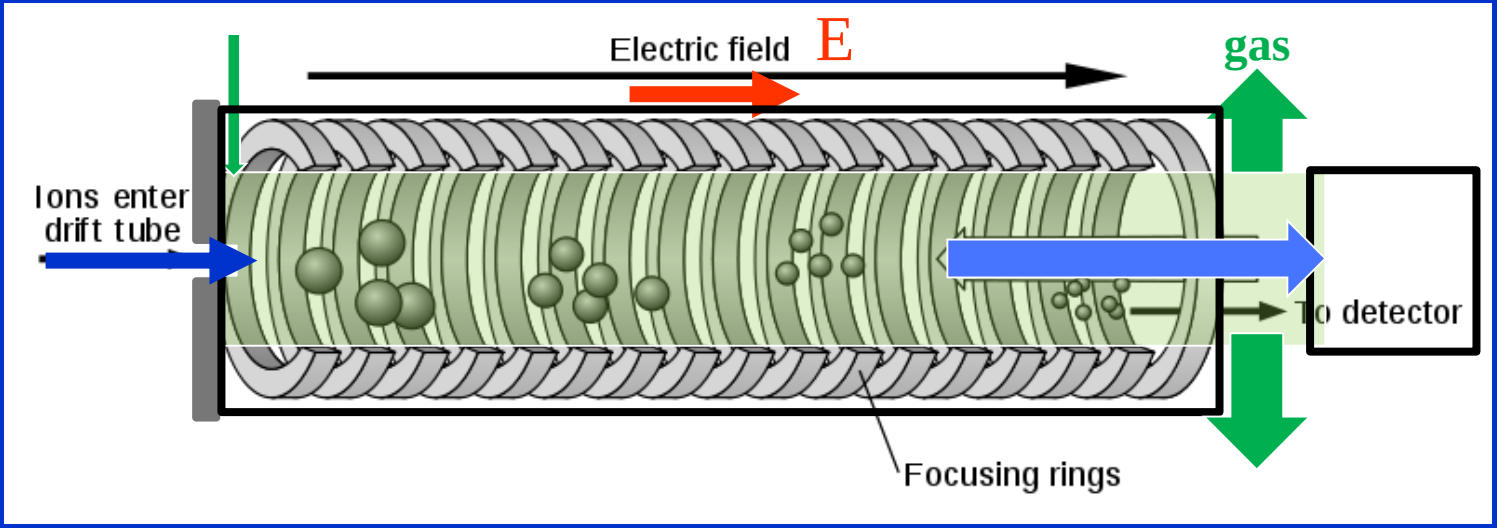

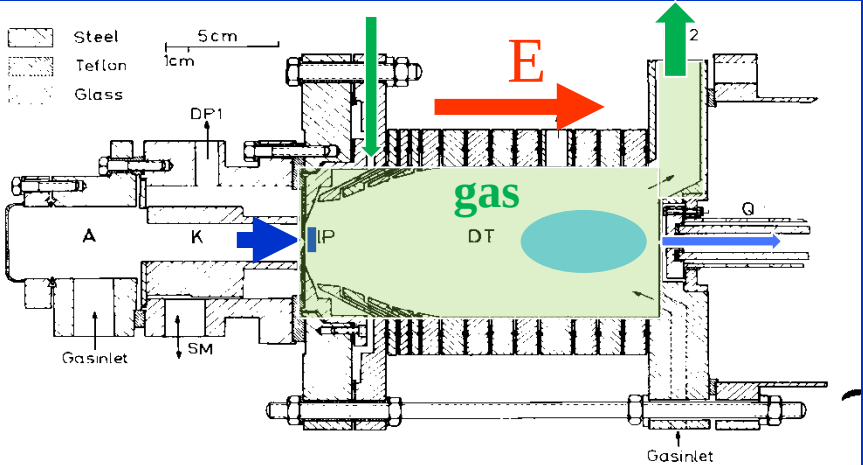

Fig. 1. Section through the main part of the apparatus. A, anode; K, cathode; DP, diffusion pump; SM, shift mechanism (not used in this work); HP, hole probe; DT, drift tube; G, pressure gauge; Q, quadrupole.

Drift tube

- Innsbruck Drift Tube

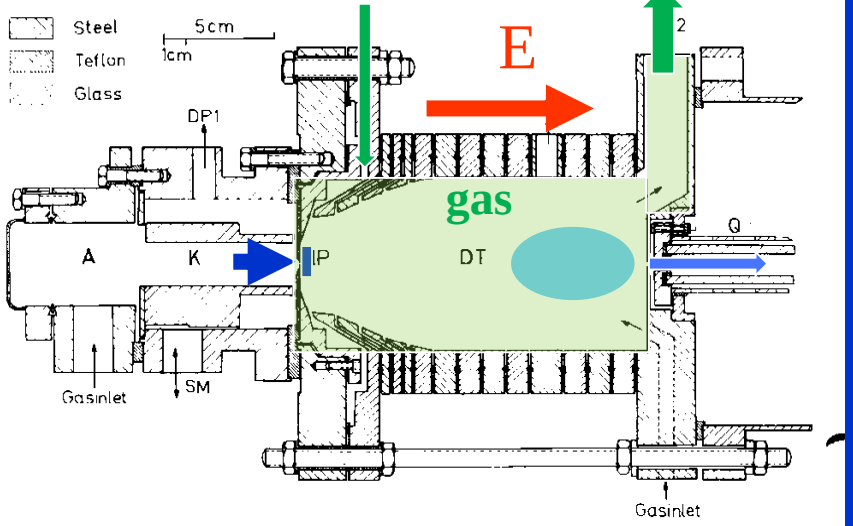

Fig. 1. Section through the main part of the apparatus. A, anode; K, cathode; DP, diffusion pump; SM, shift mechanism (not used in this work); HP, hole probe; DT, drift tube; G, pressure gauge; Q, quadrupole.

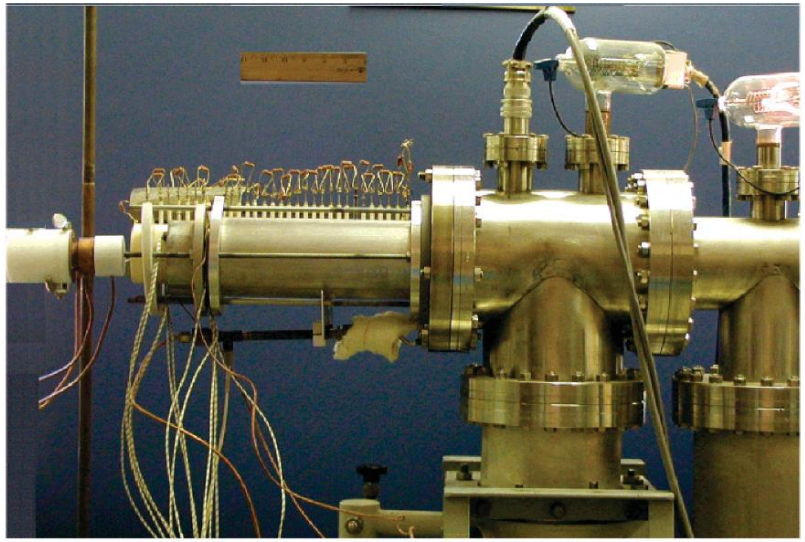

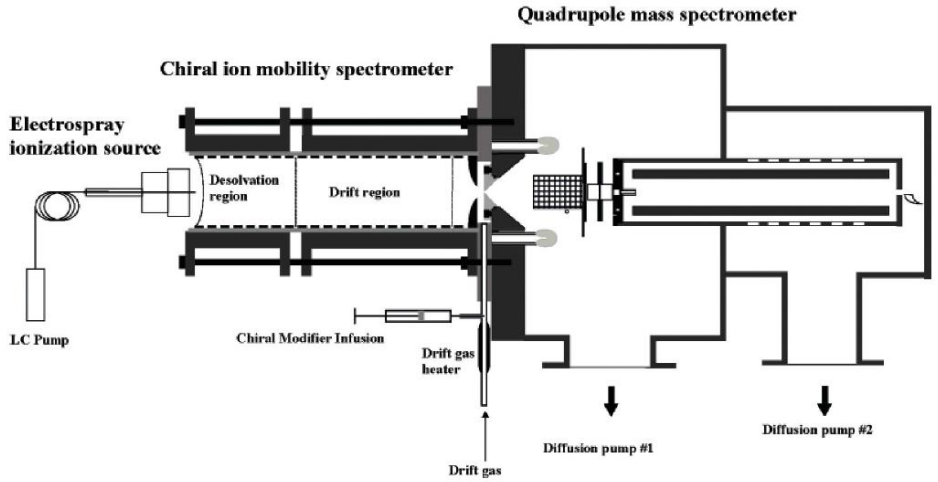

A Mass-Selective Variable-Temperature Drift Tube Ion Mobility-Mass Spectrometer for Temperature Dependent Ion Mobility Studies

Jody C May, David H Russell

Published in Journal of the America

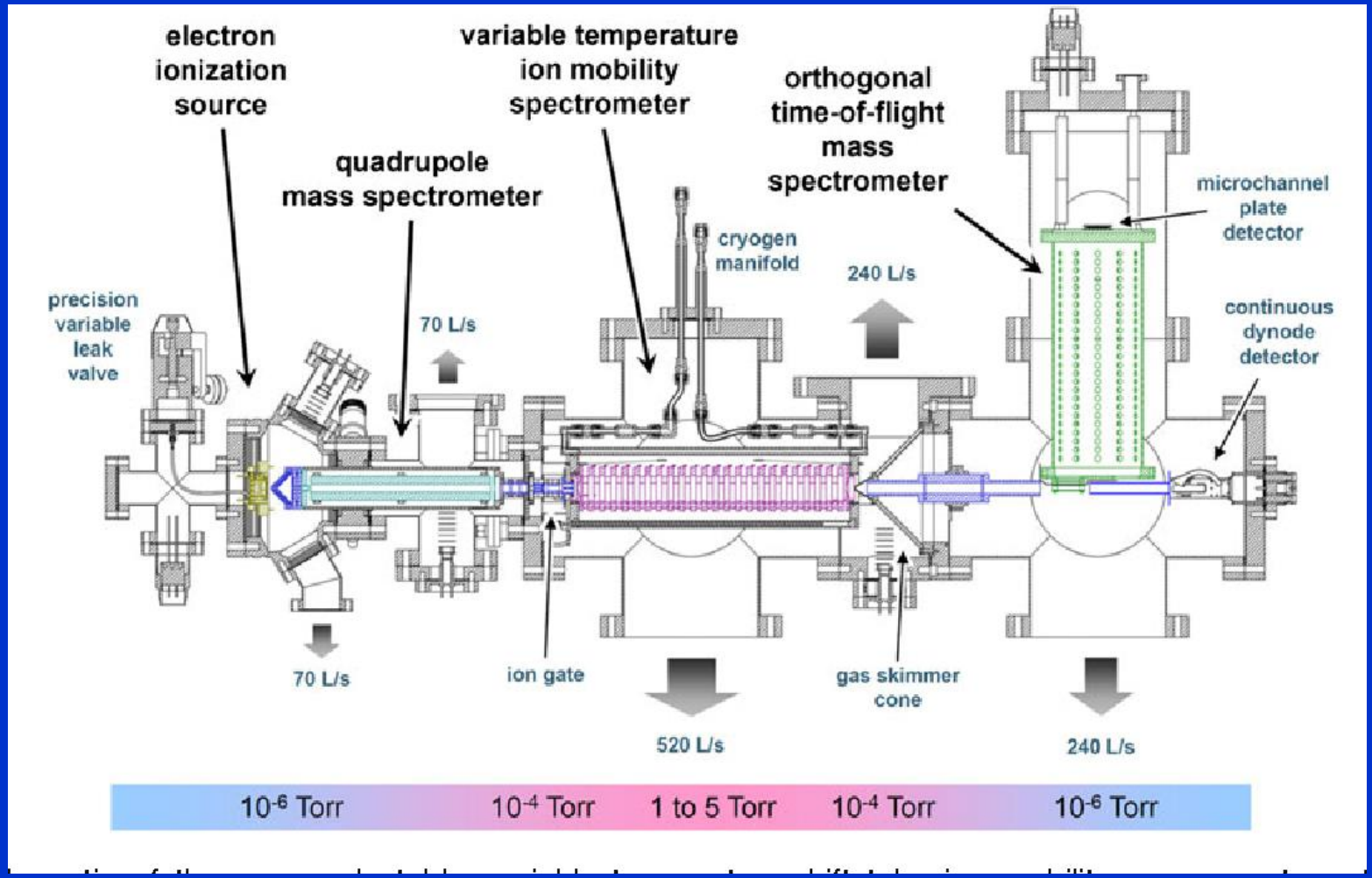

- A

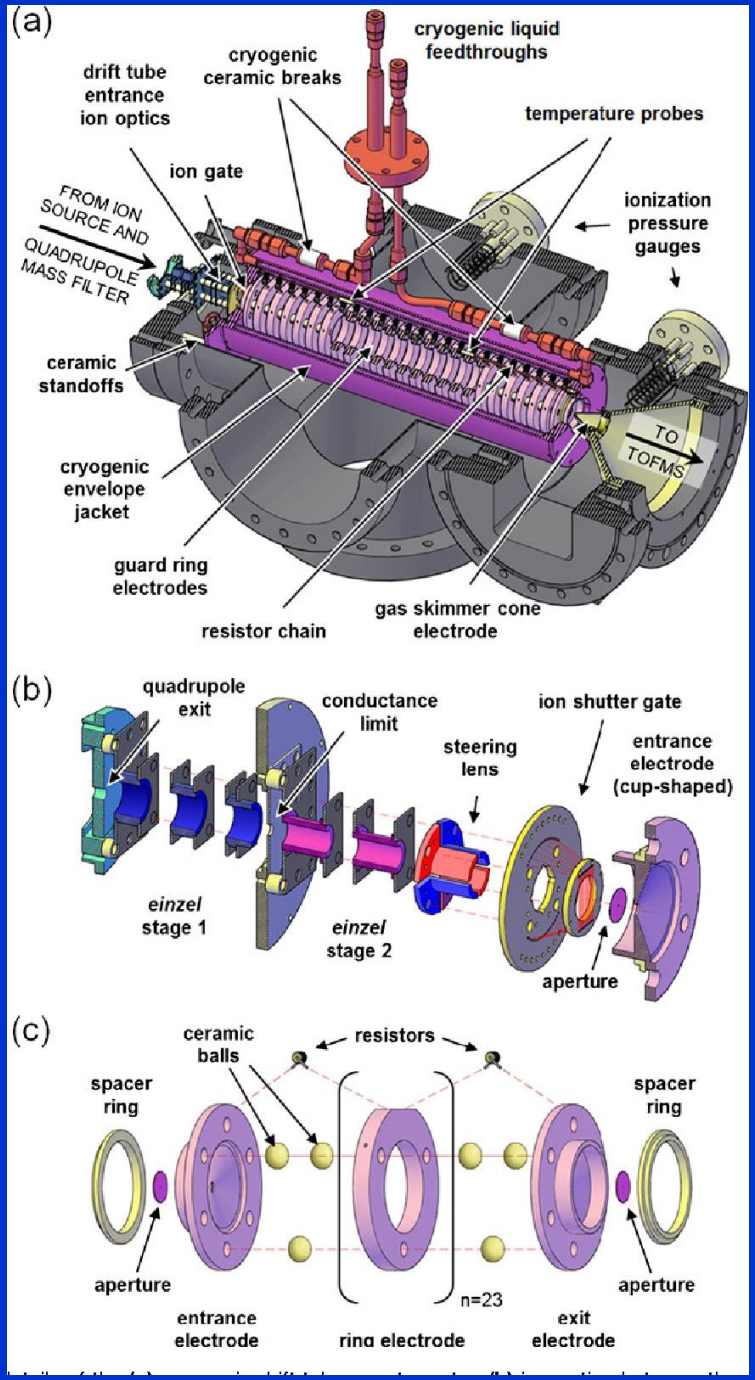
(a)
drift tube entrance ion optics
cryogenic ceramic breaks
cryogenic liquid feedthroughs
temperature probes
ion gate
FROM ION SOURCE AND QUADRUPOLE MASS FILTER
ionization pressure gauges
ceramic standoffs
TO TOFMS
cryogenic envelope jacket
guard ring electrodes
resistor chain
gas skimmer cone electrode
(b)
quadrupole exit
conductance limit
ion shutter gate
steering lens
entrance electrode (cup-shaped)
einzel stage 1
einzel stage 2
aperture
(c)
ceramic balls
resistors
spacer ring
spacer ring
aperture
aperture
n=23
entrance electrode
ring electrode
exit electrode

Ion mobility spectrometry diagram

JOURNAL OF MASS SPECTROMETRY
J. Mass Spectrom. 2008; **43**: 1–22
Published online in Wiley InterScience
(www.interscience.wiley.com) DOI: 10.1002/jms.1383

2008

SPECIAL FEATURE: PERSPECTIVE

Ion mobility–mass spectrometry

Abu B. Kanu,† Prabha Dwivedi, Maggie Tam, Laura Matz and Herbert H. Hill Jr.*

Department of Chemistry, Washington State University, Pullman, WA 99164-4630, USA

Accepted 14 December 2007

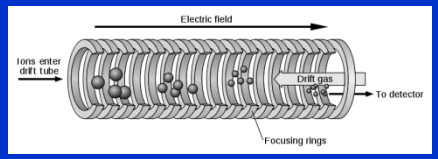

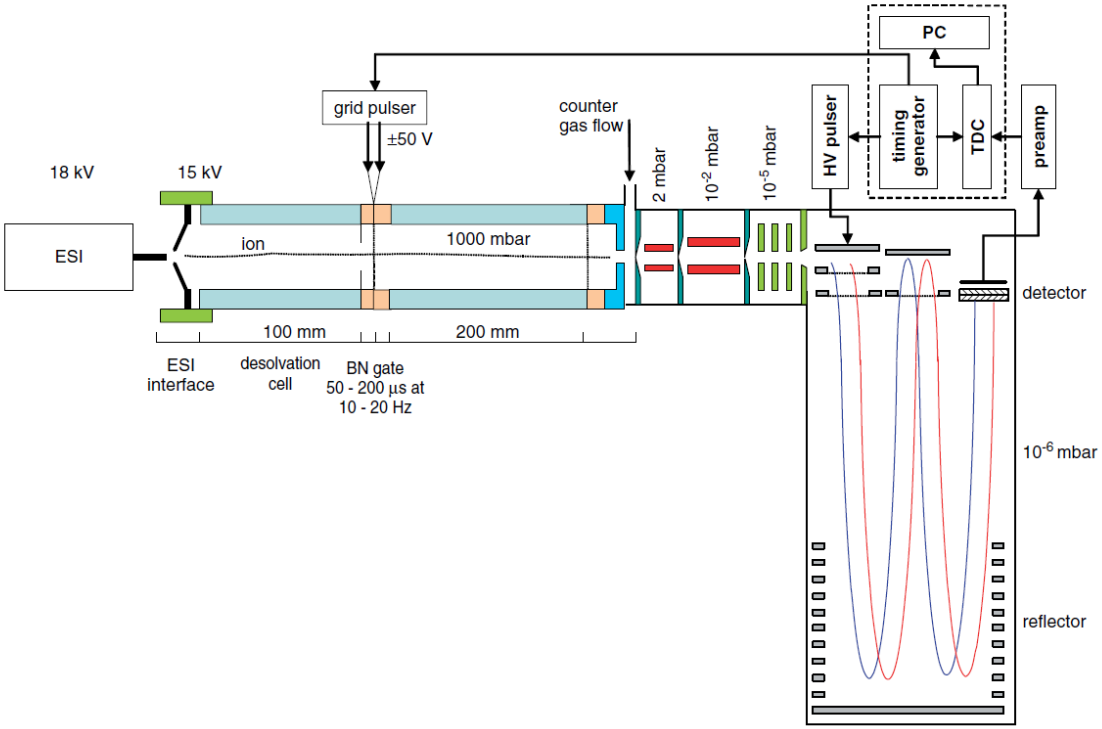

Figure 1. Schematic of an ambient-pressure IMS(tof)MS. Various components include (1) an electrospray ionization (ESI) source, (2) an ESI interface to the ion mobility spectrometer, (3) a desolvation chamber where the electrospray solvent is evaporated, (4) an ion gate which pulses packets of ions into the drift region, (5) the drift region where ions are separated according to their mobility, (6) a pinhole interface to vacuum, (7) transfer and focusing ion lenses to move the ions from high pressure to low pressure (8) a reflectron time-of-flight mass spectrometer. (Compliments of TofWerk, AG Thun, Switzerland).

EEDF from Boltzmann equation

a) Nechť vnější elektrické pole je nulové, tj. $\Gamma = 0$. Potom

(5.133) $$\mathcal{G}(v_1) = 0$$

a pro $f_0(v)$ máme Maxwellovu rozdělovací funkci

(5.134) $$f_0 = C \exp\left(-\frac{mv^2}{2kT}\right),$$

kde

(5.135) $$C = n\left(\frac{m}{2\pi kT}\right)^{3/2}.$$

b) Nechť vnější magnetické pole je nulové, tj. $\omega_c = 0$. Potom

(5.136) $$\mathcal{G}(v_1) = \Gamma^2$$

a (5.131) můžeme upravit na tvar

(5.137) $$f_0 = C \exp\left\{-\int \frac{m}{kT}\left(\frac{v v_1^2}{v_1^2 + \left(\frac{\Gamma^2 m}{3\gamma kT}\right)}\right) \mathrm{d}v\right\}.$$

Bude-li nyní srážková frekvence v_1 nezávislá na rychlosti, tj.

(5.138) $$v_1 = v = \text{konst},$$

pak f_0 bude opět maxwellovské rozdělení

(5.139) $$f_0 = C \exp\left[-\frac{mv^2}{2k\left(T + \frac{\Gamma^2 m}{3\gamma k} v^{-2}\right)}\right] = C \exp\left(-\frac{mv^2}{2kT^*}\right)$$

ale s teplotou

(5.140) $$T^* = T + \frac{m}{3\gamma k}\left(\frac{\Gamma}{v}\right)^2 = T + \frac{M}{3k}\left(\frac{ZeE}{mv}\right)^2.$$

To ale znamená, že při $v_1 = \text{konst}$ je kinetická teplota lehkých nabitých částic (elektronů) vyšší ve srovnání s teplotou neutrálních částic.

Předpoklad, že srážková frekvence elektronů s neutrálními částicemi je konstantní, nezávislá na rychlosti, je příliš ostrý. V obecném případě totiž platí, že v_1 na rychlosti elektronů závisí. Předpokládejme, že

(5.141) $$v_1(v) = Av^l,$$

kde l je libovolné číslo*) a A je konstanta (pro $l = 1$ máme

(5.141′) $$v_1 = Av$$

a tedy $A^{-1} = \lambda$, kde λ je střední volná dráha elektronů).

Rovnice pro f_0 (5.137) má nyní tvar

(5.142) $$f_0 = C \exp\left\{-\int \frac{m}{kT} \frac{v^{2l+1}}{v^{2l} + \frac{\Gamma^2 m}{3\gamma A^2 kT}} \mathrm{d}v\right\}.$$

Pro $l = 1$, tj. případ modelu dokonale pružných koulí (viz kapitolu 2), kdy

(5.143) $$v_1 = Av,$$

je integrál v (5.142) snadno spočitatelný a f_0 má tvar

(5.144′) $$f_0 = C\left[1 + \frac{3A^2}{\Gamma^2}\frac{kT}{m}v^2\right]^{(m\Gamma/AkT)^2 \cdot (1/6\gamma)} \cdot \exp\left(-\frac{mv^2}{2kT}\right).$$

Po kratších úpravách pak dostaneme

(5.144) $$f_0 = C\left[v^2 + \frac{M}{3}\left(\frac{ZeE}{mA}\right)^2 \frac{1}{kT}\right]^{(mM/6k^2T^2)\cdot(ZeE/mA)^2} \cdot \exp\left(-\frac{mv^2}{2kT}\right),$$

což je rozdělovací funkce, kterou jako první odvodil Davydov.**) Pro silné elektrické pole, kdy

(5.145) $$\frac{\Gamma^2 m}{3\gamma AkT} = \frac{M}{3kT}\left(\frac{ZeE}{mA}\right)^2 \gg v^2,$$

přechází Davydovova rozdělovací funkce na známou rozdělovací funkci Druyvesteyna (o tom je možno se přesvědčit z (5.142), kde položíme $l = 1$ a provedeme příslušné zanedbání), která má tvar

(5.146) $$f_0 = C \exp\left(-\frac{3}{4}\gamma\left(\frac{A}{\Gamma}\right)^2 v^4\right) = C \exp\left[-\frac{3}{4}\frac{m}{M}\left(\frac{mA}{ZeE}\right)^2 v^4\right].$$

---

*) Závislost (5.141) pro $l = 0$ vystihuje s dobrou přesností srážky elektronů s atomy He a H_2, pro $l = 1$ pak srážky v Ne a dále pro $l = 3$, 3.5 a 4 pak srážky pomalých elektronů v Ar, Kr a Xe; viz D. Darbiere: Phys. Rev. *84* (1951), 653; S. C. Brown: Handbuch der Physik, ed. S. Flüge, Vol. 22 (Berlin 1956), 531; G. L. Braglia: Phys. Lett. *17* (1965), 260.

**) B. Davydov, ŽETF *6* (5) (1936), 463; viz též B. Davydov, Uspěchi fiz. nauk *93* (1967), 401.

Srovnaní driftů iontů a elektronů

- Drift iontů
- Drift elektronů

$$E = 1V/cm = 100V/1m$$

$$p = 1Torr$$

CO^+ v N_2

$$v_d = \mu \cdot E = 1700cm/s = 17m/s$$

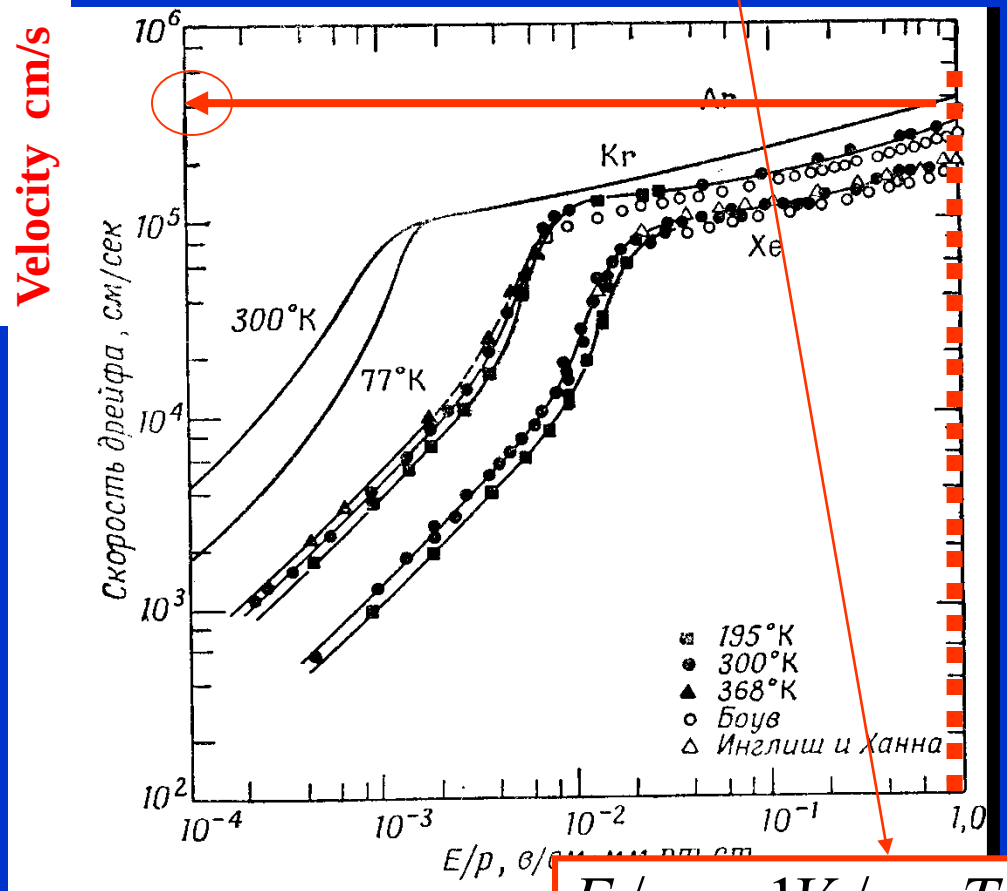

Drift elektronů

e^- v Ar

235x

$$v_{dELECTRON} = 4000m/s$$

$$\mu_e >> \mu_i$$

A co bude dělat plazma v E ??!!

$$E/p = 1V/cmTorr$$

Difúze v plazmatu

- Ambipolární difúze

$$\vec{v} = \frac{1}{nm\nu_1}(\pm ne\vec{E} - kT\nabla_r n) = \pm\frac{e}{m\nu_1}\vec{E} - \frac{kT}{m\nu_1}\frac{\nabla_r n}{n}$$

$$n_e = n_i = n_{PLAZMA} = n$$

$$\frac{\partial n}{\partial t} + \nabla \cdot \Gamma_j = 0$$

$$\Gamma_e = \Gamma_i = \Gamma$$

Potřebné elektrické pole $\boldsymbol{E}$ nalezneme z podmínky $\Gamma_i = \Gamma_e = \Gamma$

$$\Gamma = \mu_i n\boldsymbol{E} - D_i \nabla n = -\mu_e n\boldsymbol{E} - D_e \nabla n$$

$$E = \frac{D_i - D_e}{\mu_i + \mu_e}\frac{\nabla n}{n}$$

$$\Gamma = \mu_i \frac{D_i - D_e}{\mu_i + \mu_e}\nabla n - D_i \nabla n =$$

$$= \frac{\mu_i D_i - \mu_i D_e - \mu_i D_i - \mu_e D_i}{\mu_i + \mu_e}\nabla n =$$

$$= -\frac{\mu_i D_e + \mu_e D_i}{\mu_i + \mu_e}\nabla n .$$

$$D_a \equiv \frac{\mu_i D_e + \mu_e D_i}{\mu_i + \mu_e}$$

$$\partial n/\partial t = D_a \nabla^2 n$$

Ambipolární difúze

$$\partial n/\partial t = D_a \nabla^2 n$$

$$D_a \equiv \frac{\mu_i D_e + \mu_e D_i}{\mu_i + \mu_e}$$

$$\mu = \frac{e}{m\nu_1} \qquad D = \frac{kT}{m\nu_1}$$

$$\frac{\mu}{D} = \frac{e}{kT}$$

Velikost D_a můžeme odhadnout, vezmeme-li $\mu_e \gg \mu_i$. Že tomu tak je, můžeme vidět z rov. [5-7]. Poněvadž ν je úměrné tepelné rychlosti, která je zase úměrná $m^{-1/2}$, je μ úměrné $m^{-1/2}$. Rovnice [5-16] a [5-9] potom dávají

$$D_a \approx D_i + \frac{\mu_i}{\mu_e} D_e = D_i + \frac{T_e}{T_i} D_i \qquad [5\text{-}18]$$

Pro $T_e = T_i$ dostáváme

$$D_a \approx 2D_i . \qquad [5\text{-}19]$$

Pole v plazmatu, odhad

- Ambipolární difúze

$$E = \frac{D_i - D_e}{\mu_i - \mu_e}\frac{\nabla n}{n}$$

$$\frac{D}{\mu} = \frac{kT}{e}$$

$$E \sim \frac{D_e}{\mu_e}\frac{\nabla n}{n} \sim \frac{kT}{e}\frac{\nabla n}{n} \sim V^{kT}\!\!\diagup_{R} \cdot \frac{n}{n} \sim V^{kT}\!\!\diagup_{R}$$

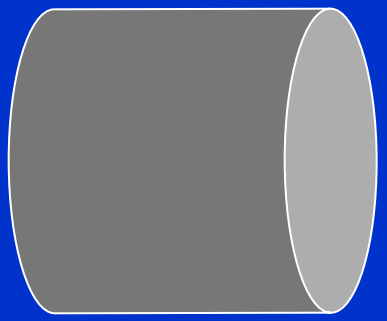

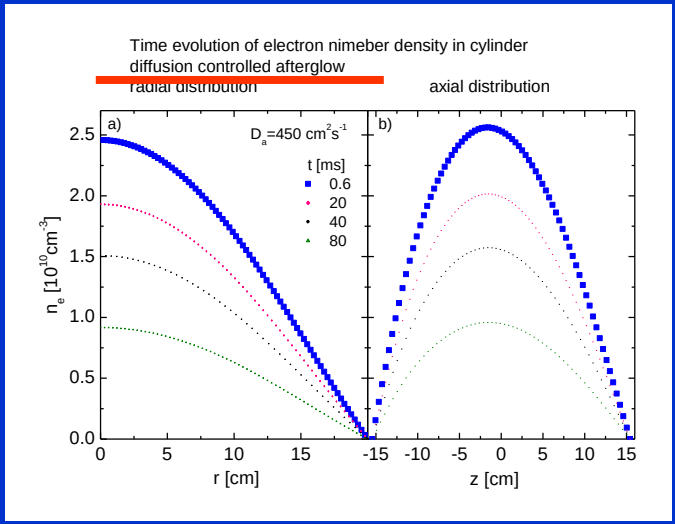

Rovnice kontinuity a difúze

- A

$$\frac{\partial n}{\partial t} + \vec{\nabla}.(n.\vec{\bar{v}}) = 0$$

$$\vec{\bar{v}} = -D\frac{\nabla_r n}{n}$$

$$\frac{\partial n}{\partial t} = -\vec{\nabla}.(n.\vec{\bar{v}}) = \vec{\nabla}.\left(nD\frac{\nabla_r n}{n}\right) = \vec{\nabla}.(D\nabla_r n) = D\vec{\nabla}.(\nabla_r n) = D\Delta n$$

Druhý Fickuv zákon

$$\frac{\partial n}{\partial t} = D\Delta n$$

Řešení rovnice

- Chen etc.
- *Collision phenomena in ionised gases*
  E.W. McDaniel

$$\frac{\partial n}{\partial t} = D\Delta n$$

$$n(\vec{r},t) = T(t).S(\vec{r})$$

$$S\frac{\partial T}{\partial t} = DT\Delta S = DT\nabla^2 S$$

$$\frac{1}{T}\frac{\partial T}{\partial t} = \frac{D}{S}\nabla^2 S$$

$$\frac{1}{T}\frac{\partial T}{\partial t} = -\frac{1}{\tau} = \frac{D}{S}\nabla^2 S \quad \rightarrow \quad \nabla^2 S = -\frac{S}{D\tau} = -\frac{S}{\lambda^2}$$

$$\frac{1}{T}\frac{\partial T}{\partial t} = -\frac{1}{\tau} \quad \rightarrow \quad T = T_0 e^{-t/\tau}$$

Difúze v rovinní geometrii

- Rovina
- Separace proměnných

$$n(\vec{r},t) = T(t).S(\vec{r})$$

$$\nabla^2 S = -\frac{S}{D\tau} = -\frac{S}{\lambda^2}$$

$$\nabla^2 S = \frac{\partial^2 S}{\partial x^2} = -\frac{S}{\lambda^2}$$

$$S = A\cos\frac{x}{\lambda} + B\sin\frac{x}{\lambda}$$

$$S = A\cos\frac{x}{\lambda} + B\sin\frac{x}{\lambda}$$

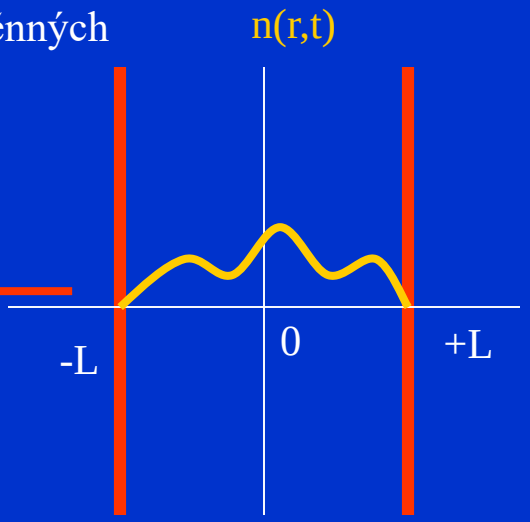

$$T = T_0 e^{-t/\tau}$$

$$n = n_0 e^{-t/\tau} \cos\frac{x}{\sqrt{D\tau}}$$

$$n(L,t) = n_0 e^{-t/\tau} \cos\frac{L}{\sqrt{D\tau}} = 0$$

$$\frac{L}{\sqrt{D\tau}} = \frac{\pi}{2} \quad \rightarrow \tau = \left(\frac{2L}{\pi}\right)^2 \frac{1}{D}$$

$$\tau = \left(\frac{2L}{\pi}\right)^2 \frac{1}{D}$$

$$\lambda^2 = \tau D = \left(\frac{2L}{\pi}\right)^2$$

$$\lambda = \left(\frac{2L}{\pi}\right)$$

$$T = T_0 e^{-t/\tau} = T_0 e^{-\left(\frac{2L}{\pi}\right)^2 Dt}$$

$$n = n_0 e^{-\frac{D}{\lambda^2}t} \cos\frac{x}{\lambda}$$

Charakteristická difúzní délka

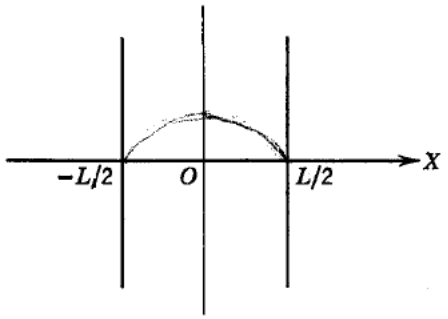

FIG. 10-8-1. A one-dimensional cavity with plane parallel walls.

independent of position in order that $\mathscr{D}$ may be constant. The extrapolation distance is neglected, and N_0 is required to vanish at the geometrical boundaries of the containers.

A. INFINITE PARALLEL PLATES. As the first example of the solution of the time-independent diffusion equation, consider the case of a one-dimensional cavity whose walls are the infinite plane parallel plates shown in Fig. 10-8-1. In this simple case the diffusion equation (10-6-6) becomes

$$\frac{d^2N_0(x)}{dx^2} + \frac{N_0(x)}{\mathscr{D}\tau} = 0 \tag{10-8-1}$$

Since $\mathscr{D}\tau$ is positive, the solution of (10-8-1) is

$$N_0(x) = A\cos\frac{x}{\sqrt{\mathscr{D}\tau}} + B\sin\frac{x}{\sqrt{\mathscr{D}\tau}} \tag{10-8-2}$$

where A and B are constants of integration which must be determined from the boundary conditions and from the requirement that we shall impose for symmetry about the midplane. If the width of the cavity is L and the origin of the coordinate system is located at the midplane, the boundary conditions are $N_0(x) = 0$ when $x = \pm L/2$.

The symmetry requirement makes $B = 0$, and the boundary conditions force τ to assume one of the infinite number of values τ_k $(k = 1, 2, 3, \ldots)$ which satisfy the equation

$$\cos\frac{L}{2\sqrt{\mathscr{D}\tau_k}} = 0 \quad \text{or} \quad \frac{L}{2\sqrt{\mathscr{D}\tau_k}} = (2k-1)\frac{\pi}{2} \tag{10-8-3}$$

Now define a quantity Λ_k which represents the *characteristic diffusion length for the* kth *mode of diffusion*:

$$\Lambda_k^2 = \mathscr{D}\tau_k = \left(\frac{1}{2k-1}\frac{L}{\pi}\right)^2 \tag{10-8-4}$$

The diffusion length is useful in describing the shape of a cavity in the diffusion process. The solution for the kth mode can then be written

$$N_0(x)_k = A_k\cos\frac{x}{\Lambda_k} \tag{10-8-5}$$

The function $\cos x/\Lambda_k$ assumes negative values in certain regions within the cavity for all modes of diffusion except the lowest, or fundamental, mode corresponding to $k = 1$. Therefore, if we consider each solution singly, we must discard all but the fundamental mode on physical grounds, since the particle number density can never be negative. However, since the diffusion equation is linear, the total solution of the diffusion problem consists of an infinite number of modes, many of which may be excited simultaneously. Any sum of these modes is then a possible solution, provided the constants A_k have values which prevent the number density from becoming negative. The use of an ionization source that provides uniform ionization throughout the cavity will ensure that the fundamental mode predominates.

After the ionization source is abruptly turned off at $t = 0$ each diffusion mode decays out with its own characteristic time constant τ_k. The total solution of the time-dependent diffusion problem is thus given by

$$N(x, t) = \sum_{k=1}^{\infty} A_k\cos\frac{x}{\Lambda_k}e^{-t/\tau_k} \tag{10-8-6}$$

- In slab geometry,

$$\frac{d^2S}{dx^2} = -\frac{1}{D_\alpha \tau} S$$

$$S = A\cos\frac{x}{(D_\alpha\tau)^{1/2}} + B\sin\frac{x}{(D_\alpha\tau)^{1/2}}$$

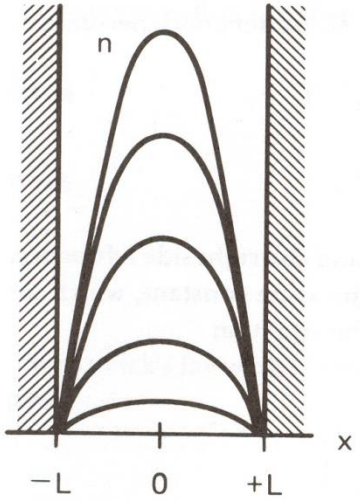

FIGURE 5-3 Density of a plasma at various times as it decays by diffusion to the walls.

- Boundary conditions S=0 at $x = \pm L$

$$\tau = \left(\frac{2L}{\pi}\right)^2 \cancel{D_\alpha}\ \frac{1}{D}$$

$$\tau = \left(\frac{2L}{\pi}\right)^2 \frac{1}{D}$$

$$n = n_0 e^{-t/\tau} \cos\frac{\pi x}{2L}$$

In general,

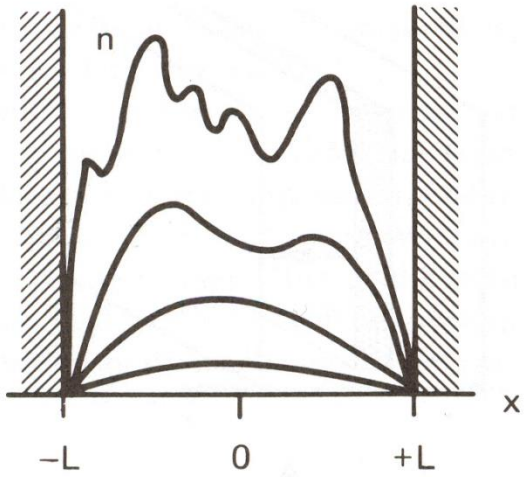

Decay of an initially nonuniform plasma, showing the rapid disappearance of the higher-order diffusion modes.

$$\tau_l = \left(\frac{L}{(l+1/2)\pi} \right)^2 \frac{1}{D_\alpha}$$

$$n = n_0 \left(\sum_l a_l e^{-t/\tau_l} \cos \frac{(l+1/2)\pi x}{L} + \sum_m b_m e^{-t/\tau_m} \sin \frac{m\pi x}{L} \right)$$

Difúze ve válci

- Válec

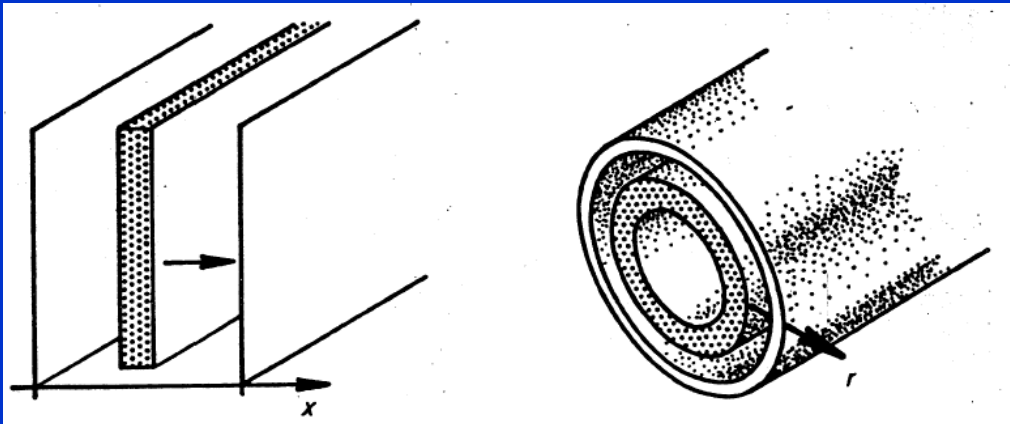

Pohyb plazmatické vrstvy při rovinné a cylindrické konfiguraci. Obrázek slouží k ilustraci rozdílu mezi kosinem a Besselovou funkcí.

$$\frac{1}{T}\frac{\partial T}{\partial t} = \frac{D}{S}\nabla^2 S$$

$$\frac{1}{T}\frac{\partial T}{\partial t} = -\frac{1}{\tau} = \frac{D}{S}\nabla^2 S$$

$$\frac{d^2S}{dr^2} + \frac{1}{r}\frac{dS}{dr} + \frac{1}{D\tau}S = 0$$

$$\frac{\partial N_0}{\partial r^2} + \frac{1}{r}\frac{\partial N_0}{\partial r} + \frac{\partial^2 N_0}{\partial z^2} + \frac{N_0}{D\tau} = 0$$

$$N_0(r,z) = R(r)Z(z)$$

$$\frac{1}{R}\left(\frac{d^2R}{dr^2} + \frac{1}{r}\frac{dR}{r}\right) + \frac{1}{Z}\frac{d^2Z}{dz^2} + \frac{1}{D\tau} = 0$$

$$R(r) = AJ_0(u) = AJ_0(\alpha r)$$

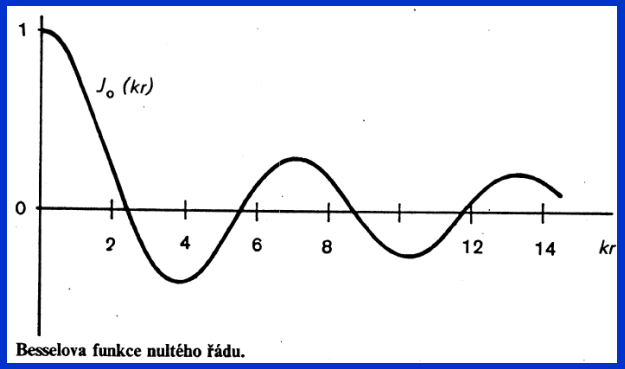

Besselova funkce nultého řádu.

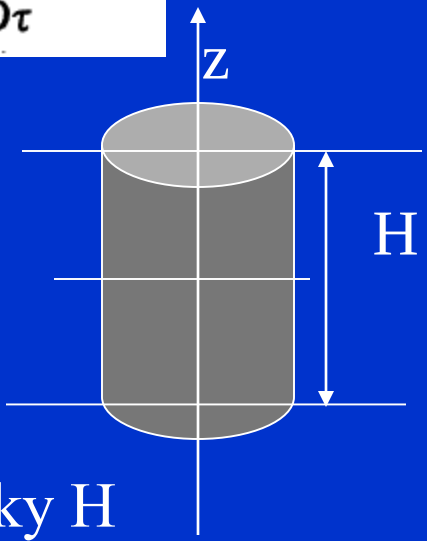

Konečný válec délky H

Okrajové podmínky

$$R(r) = AJ_0\left(\frac{2{,}405r}{r_0}\right)$$

$$\frac{1}{\Lambda_D^{\,2}} = \frac{1}{D\tau_D} = \left(\frac{2.405}{r_0}\right)^2 + \left(\frac{\pi}{H}\right)^2$$

$$N(r,z,t) = G_{11}J_0\left(\frac{2{,}405r}{r_0}\right)\cos\frac{\pi z}{H}e^{-t/\tau_{11}}$$

positive. The solution of the z equation is then

$$Z(z) = C \cos \beta z \tag{10-8-40}$$

The boundary conditions that N_0 must vanish at $z = \pm H/2$ require that $\beta_1 = \pi/H$ for the fundamental mode.

The time-dependent solution for the lowest mode of diffusion can now be written

$$N(r, z, t) = G_{11} J_0\left(\frac{2.405r}{r_0}\right) \cos \frac{\pi z}{H} e^{-t/\tau_{11}} \tag{10-8-41}$$

where

$$\frac{1}{\Lambda_{11}^2} = \frac{1}{\mathscr{D}\tau_{11}} = \left(\frac{2.405}{r_0}\right)^2 + \left(\frac{\pi}{H}\right)^2 \tag{10-8-42}$$

The total solution, containing the radial higher modes as well as the fundamental, is

$$N(r, z, t) = \sum_{i=1}^{\infty} \sum_{j=1}^{\infty} G_{ij} J_0(\alpha_i r) \cos \frac{(2j-1)\pi z}{H} e^{-t/\tau_{ij}} \tag{10-8-43}$$

The diffusion length is given by

$$\frac{1}{\Lambda_{ij}^2} = \frac{1}{\mathscr{D}\tau_{ij}} = \alpha_i^2 + \left[\frac{(2j-1)\pi}{H}\right]^2 \tag{10-8-44}$$

where $\alpha_i r_0$ is the ith root of J_0.

If we assume that $\mathscr{K}^- \gg \mathscr{K}^+$ and $T^- \gg T^+$ and use the relationship

$$\frac{\mathscr{D}}{\mathscr{K}} = \frac{kT}{e} \tag{10-3-2}$$

we find that

$$\mathscr{D}_a \approx \mathscr{D}^- \frac{\mathscr{K}^+}{\mathscr{K}^-} = \frac{kT^-}{e}\mathscr{K}^+ \tag{10-10-5}$$

When $T^+ = T^- = T$, on the other hand,

$$\mathscr{D}_a \approx 2\mathscr{D}^+ = \frac{2kT}{e}\mathscr{K}^+ \tag{10-10-6}$$

B. EXPERIMENTAL RESULTS. The time-dependent diffusion equation for the ambipolar case is

$$\frac{\partial N}{\partial t} = \nabla \cdot (\mathscr{D}_a \nabla N) \tag{10-10-7}$$

If $\mathscr{D}_a$ is taken to be constant and the particle number density is assumed to decay as $e^{-t/\tau}$, the time-independent ambipolar diffusion equation is obtained:

$$\nabla^2 N_0 + \frac{N_0}{\mathscr{D}_a \tau} = 0 \tag{10-10-8}$$

This equation is solved for specific problems by the methods of Section 10-8. $\mathscr{D}_a$ is given in terms of the decay constant τ, and the appropriate diffusion length Λ, by the equation

$$\mathscr{D}_a = \frac{\Lambda^2}{\tau} \tag{10-10-9}$$

Hence $\mathscr{D}_a$ may be evaluated from a determination of the rate of decay of the charged particle density in a cavity after the ionization source has been turned off.

Gas in a cavity may be broken down to form a plasma by the application of microwaves, and the electron density may be determined by measuring the shift in the frequency of resonance[16] (see also Section 12-7). The experimental values of N are then plotted as a function of t on a semilogarithmic scale. If the plot is linear, indicating that the decay is exponential as assumed, the diffusion coefficient may be obtained from the slope. Since the sensitivity of the microwave method is not great enough to allow determination of electron densities below about $10^7/\text{cm}^3$, the diffusion coefficient measured is $\mathscr{D}_a$. Here we assumed that the effects of electron attachment and recombination are negligible, as is frequently the case in practice. The techniques of analyzing diffusion data when attachment and recombination must be considered are discussed by Brown in Chapters 6 and 8 of his book and in Section 12-8 of this book.

Sometimes the plots are not linear on a semilogarithmic scale even though diffusion is the controlling mechanism. Nonlinearity, in this case, indicates the simultaneous presence of more than one mode of diffusion. (The higher modes may be excited by breaking down the gas in an asymmetric discharge.) The discussion in Section 10-8 shows that the higher modes decay faster than the fundamental mode, and regardless of its initial complexity

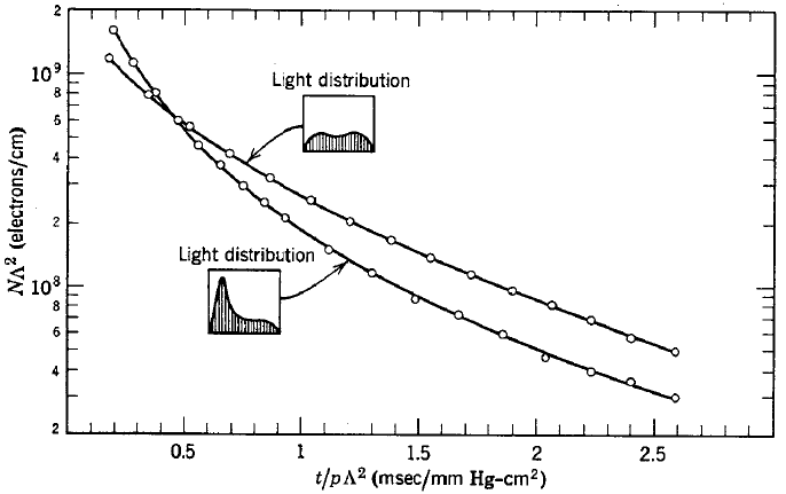

FIG. 10-10-1. The influence of the initial spatial distribution on the decay of electron density. K. B. Persson and S. C. Brown, *Phys. Rev.* **100,** 729 (1955).

the plot will approach linearity for large values of t. Two plots corresponding to different discharge conditions and different combinations of modes are shown in Fig. 10-10-1.[17] Note that the curves become straight and parallel to one another at large t, each having the slope corresponding to the lowest mode of diffusion. The "light distributions" shown in the figure are qualitative measures of the initial spatial electron density at the start of the decay period. They were obtained by scanning the discharge with a photomultiplier and slit system and displaying the signal on an oscilloscope.

Theory predicts that $\mathscr{D}_a$ will vary inversely with the pressure if the electrons and ions are in thermal equilibrium with the gas at a temperature that is held constant as the gas pressure is varied. A verification of this prediction taken from a paper on ambipolar diffusion in helium by Biondi and Brown,[18] is presented in Fig. 10-10-2. (The identity of the ions to which these data refer is uncertain. The $\mathscr{D}_a p$ products for He^+ and He_2^+ ions in helium are given in Table 10-10-1.) Figure 10-10-3, taken from the same

- A

Vývoj plazmatu řízený difúzi

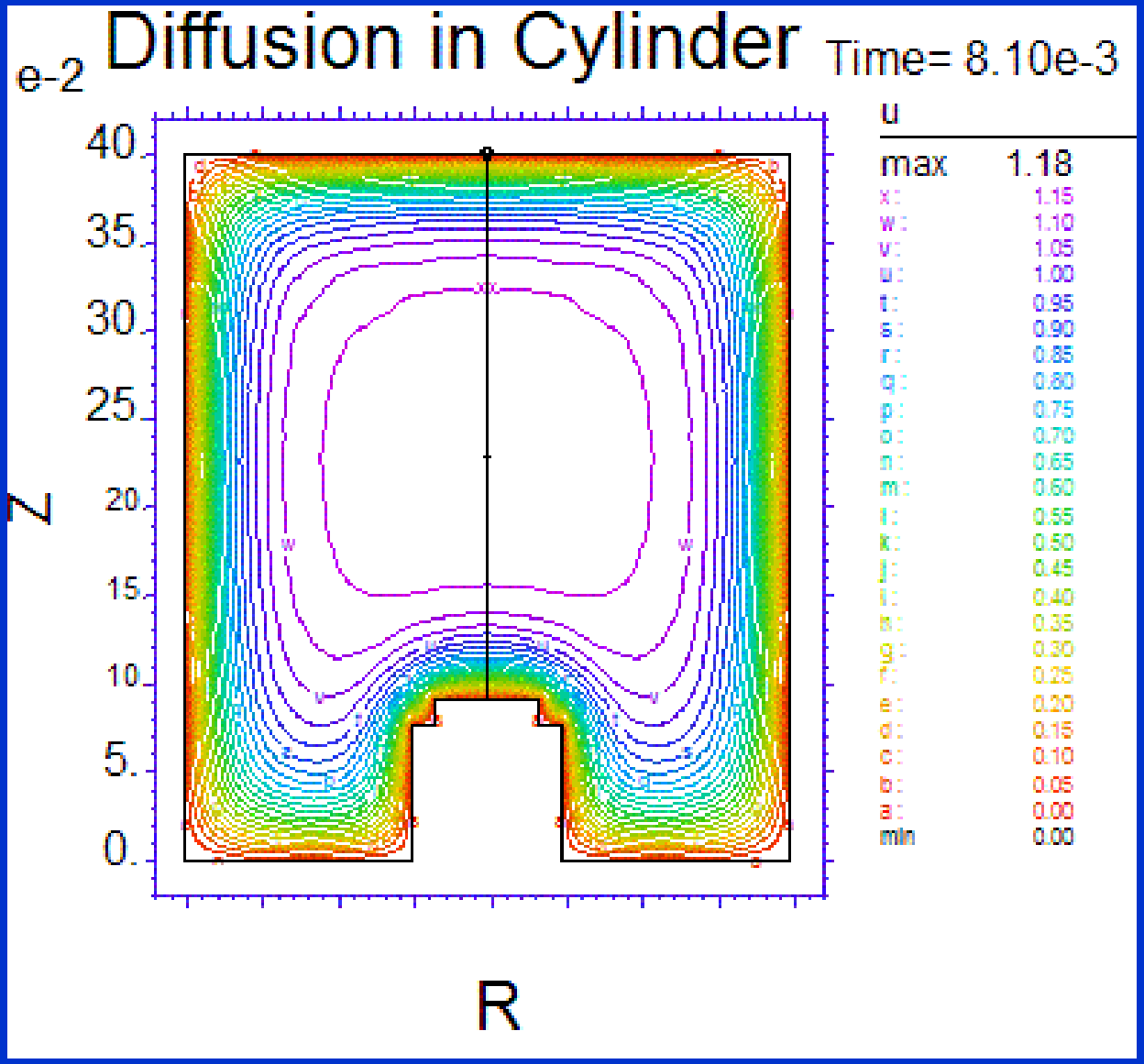

Radiální a axiální rozložení elektronů a iontů

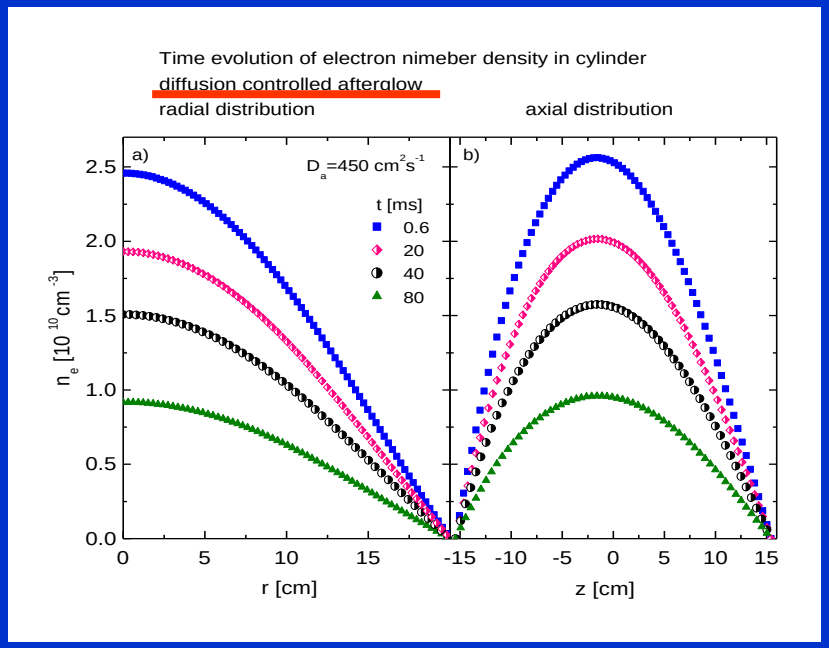

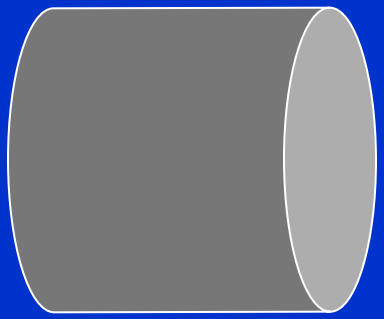

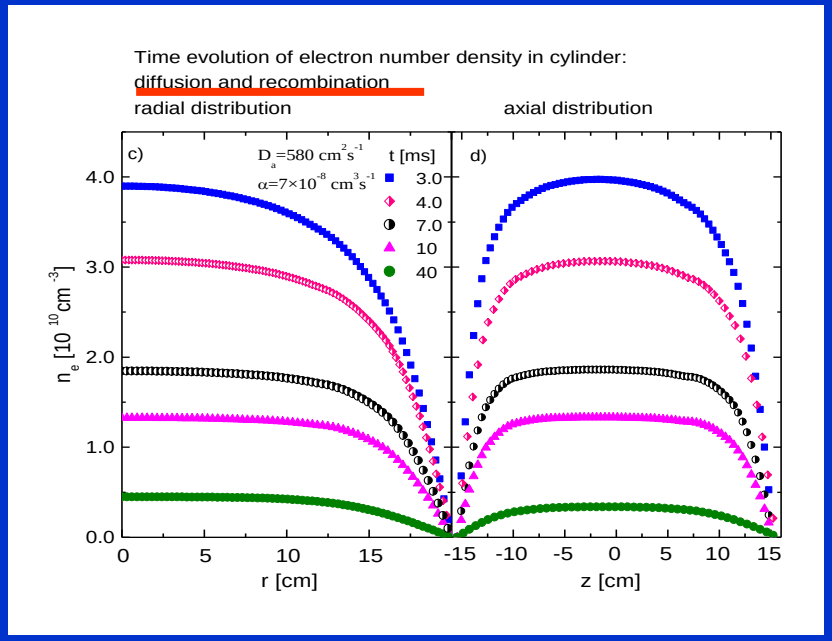

CALCULATION OF PLASMA DECAY IN CYLINDER

DIFFUSION AND RECOMBINATION

τ_D=60 ms, α=1x10^{-7}cm^{3}s^{-1} and α=5x10^{-9}cm^{3}s^{-1}

$$\tau = \left(\frac{2L}{\pi}\right)^2 \frac{1}{D}$$

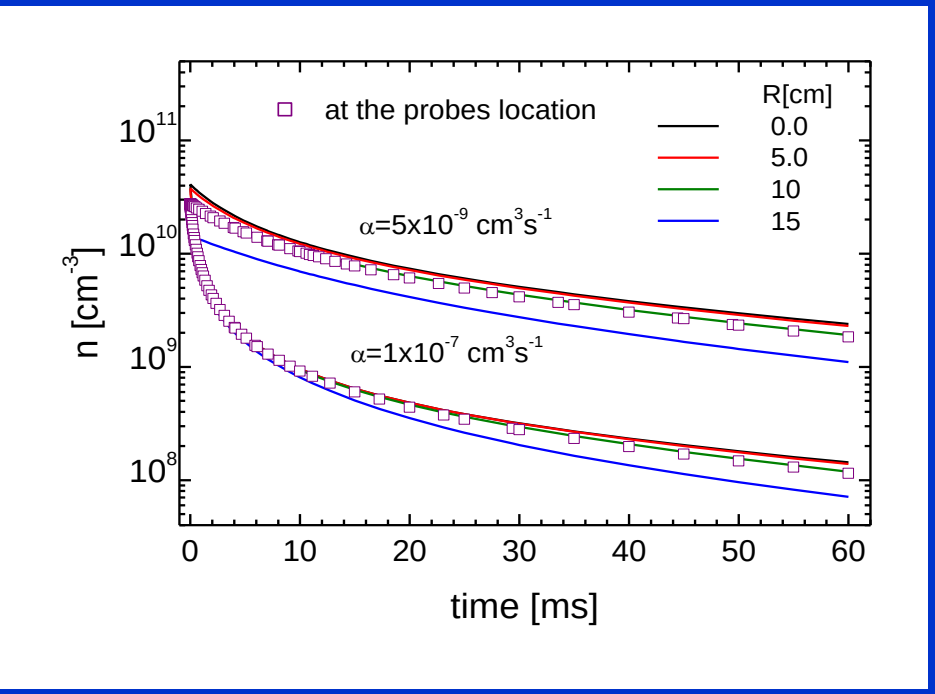

Time evolution

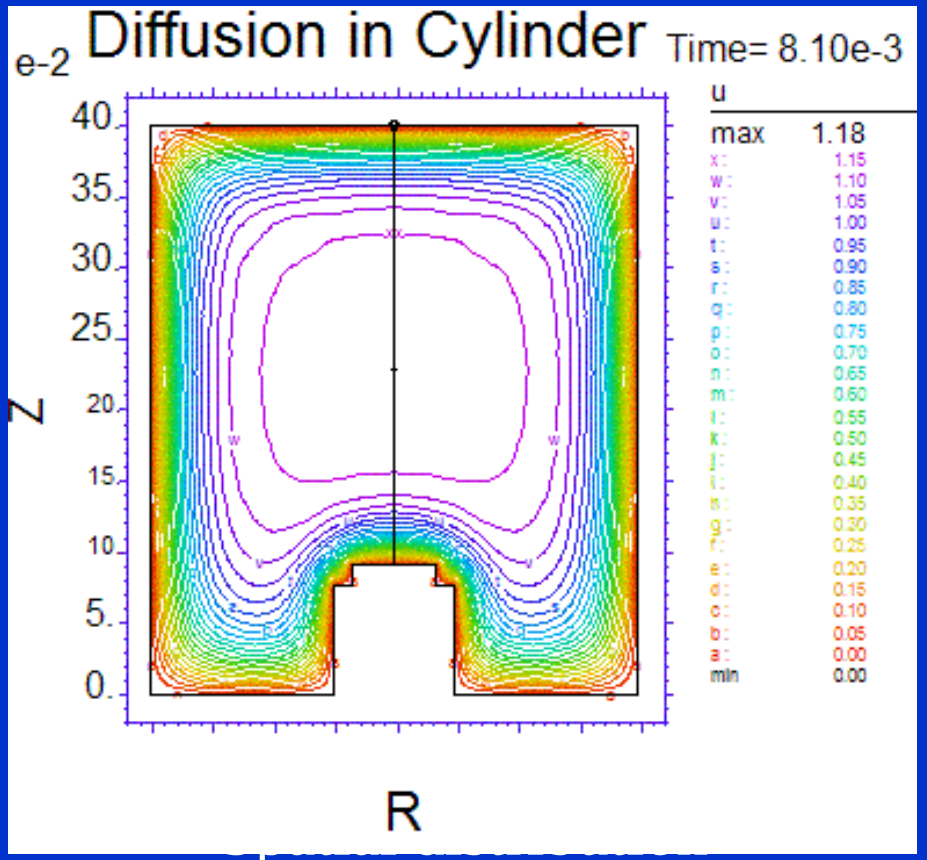

after 8 ms

Decay in diffusion and recombination governed plasma

$$\frac{dn_e}{dt} = -\alpha\, n_e^2 + D_a \nabla^2 n_e$$

$$\frac{dn_e}{dt} = -\alpha\, n_e^2 - \frac{D_a}{\Lambda^2} n_e$$

n_0

$$\frac{1}{n_e} - \frac{1}{n_0} = \alpha (t_e - t_0)$$

$$n_e = n_0 \exp(-\nu t)\ ; \nu = D_a / \Lambda^2$$

$$\frac{1}{n_e} = \alpha\ \frac{\exp(\nu t) - 1}{\nu} + \frac{1}{n_0} \exp(\nu t)$$

Diffusion and recombination

$$\frac{dn_e}{dt} = -\alpha\, n_e^2 - \frac{D_a}{\Lambda^2} n_e$$

$$\frac{1}{n_e} = \alpha\, \frac{\exp(\nu t) - 1}{\nu} + \frac{1}{n_0} \exp(\nu t)$$

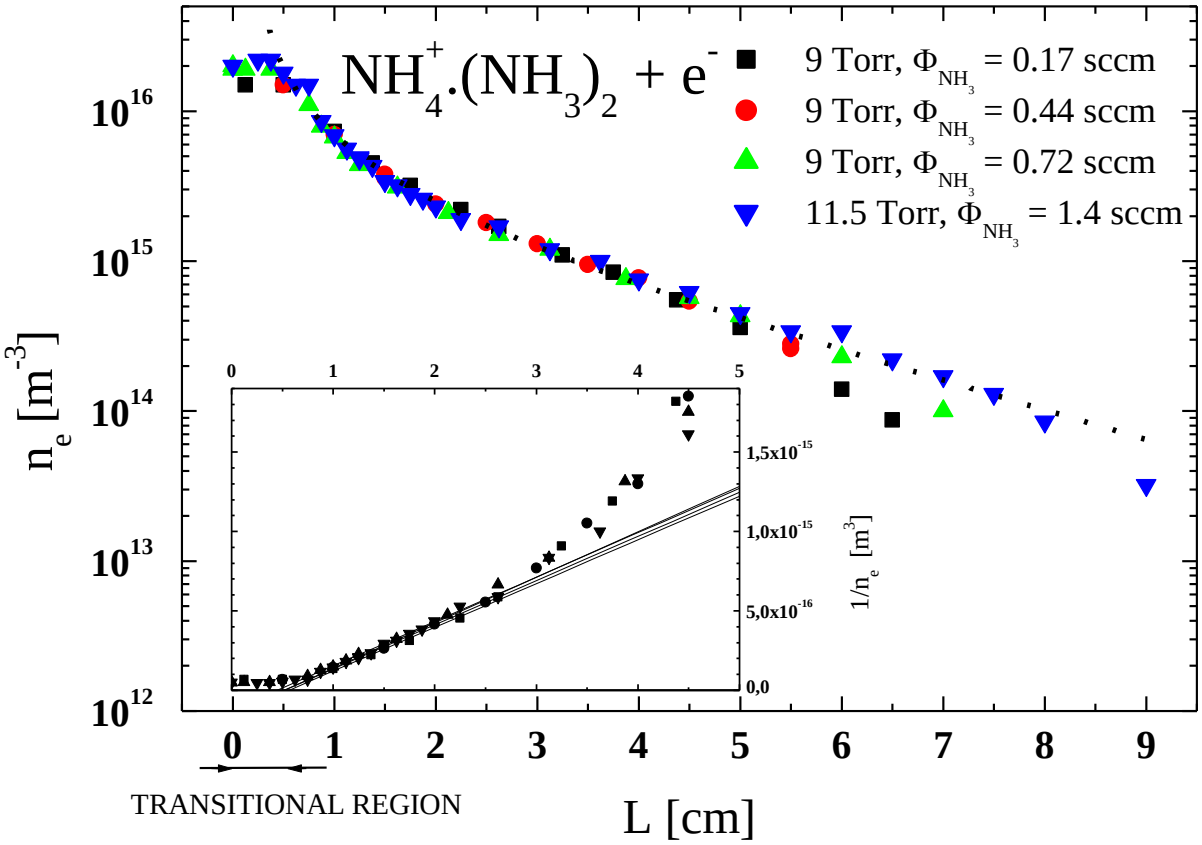

AISA vypočtené difúzní ztráty

- Difúze a rekombinace

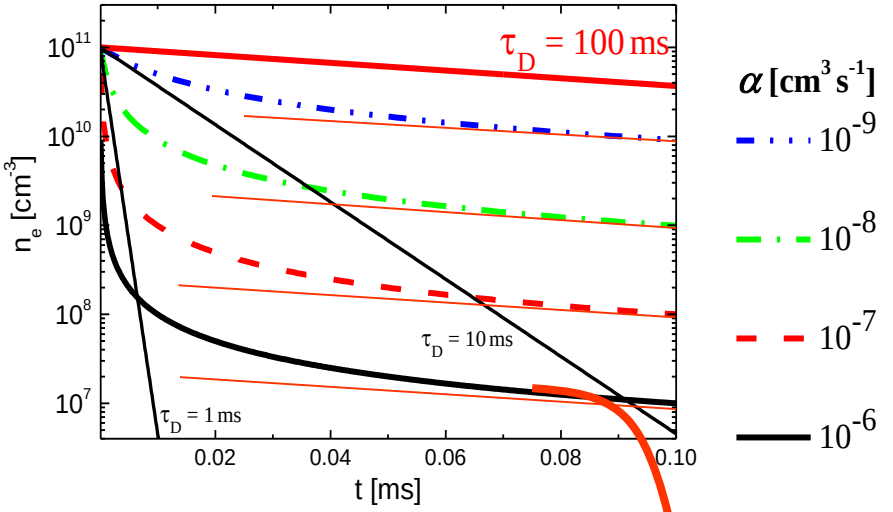

Free diffusion

Experimentální data

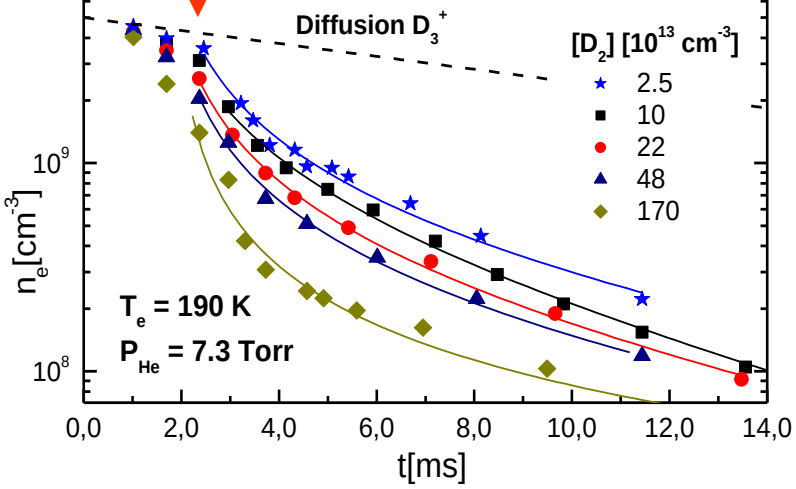

Difúze v plazmatu

- Ambipolární difúze

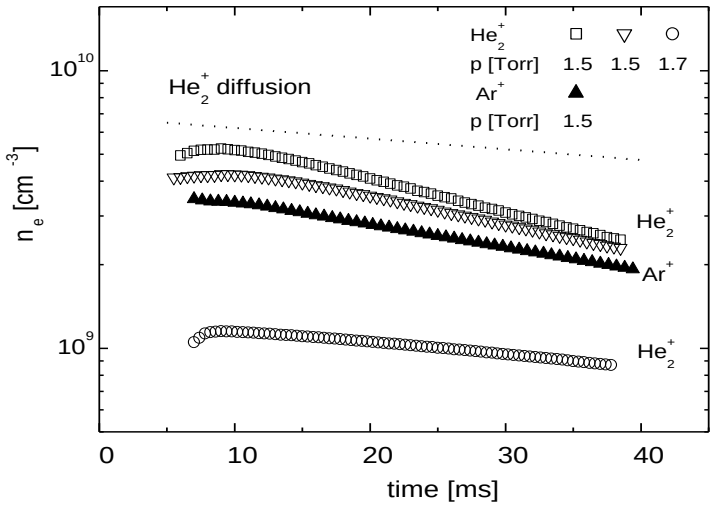

$$T = T_0 e^{-t/\tau} = T_0 e^{-\left(\frac{2L}{\pi}\right)^2 Dt}$$

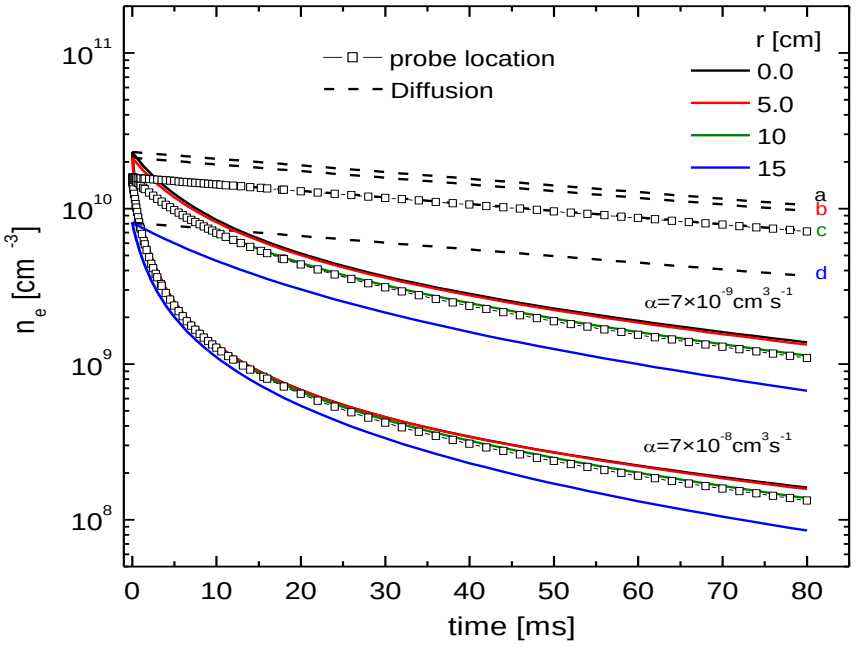

Recombination of $H_3^+(v=0)$ in He/Ar/H_2 Stationary afterglow

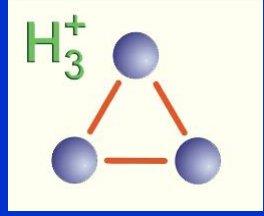

PULSE REGIME

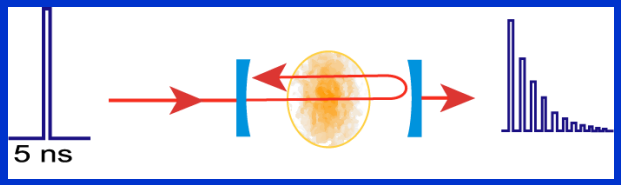

TEST TUBE

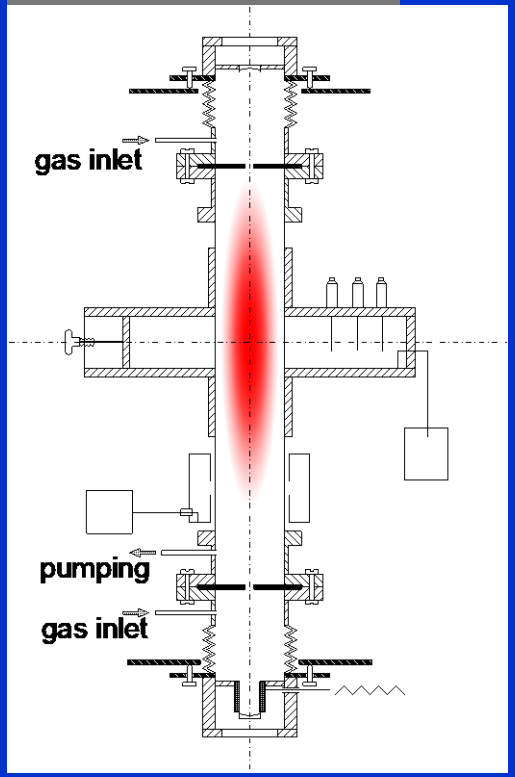

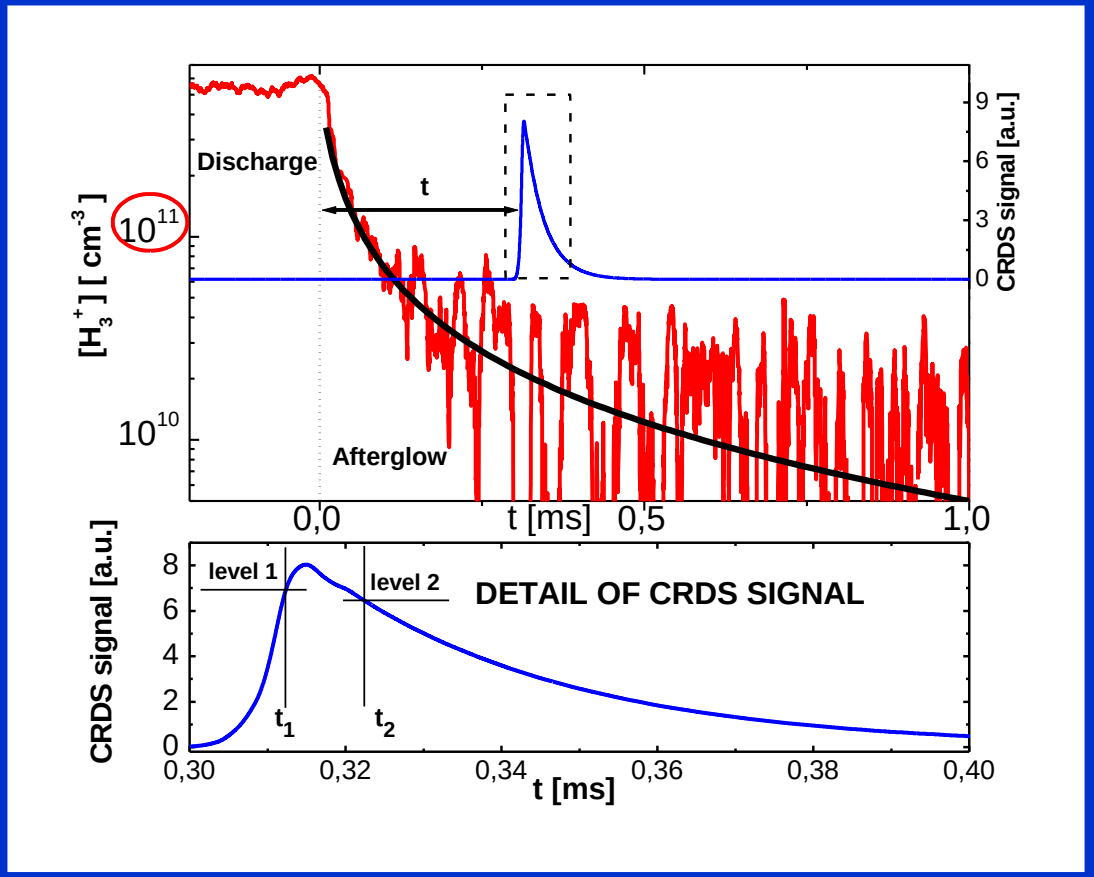

EEDF Argon plasma

- Ricard

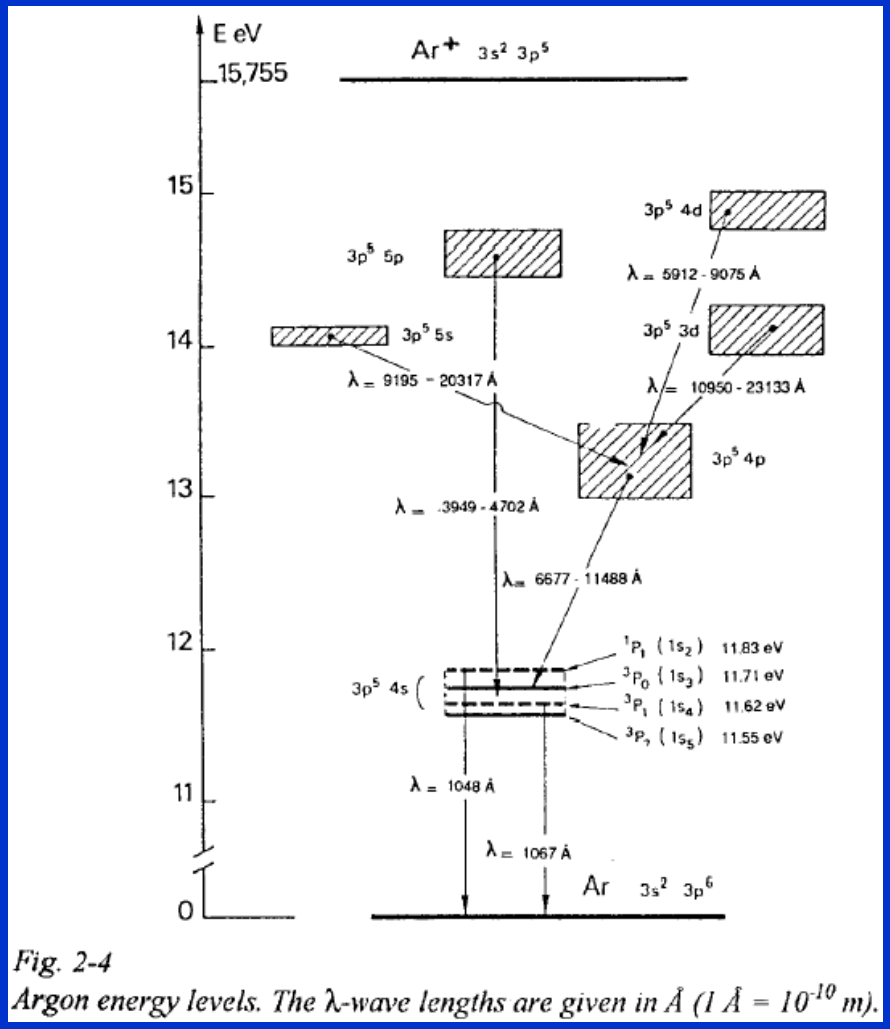

Fig. 2-4
Argon energy levels. The λ-wave lengths are given in Å (1 Å = 10^{-10} m).

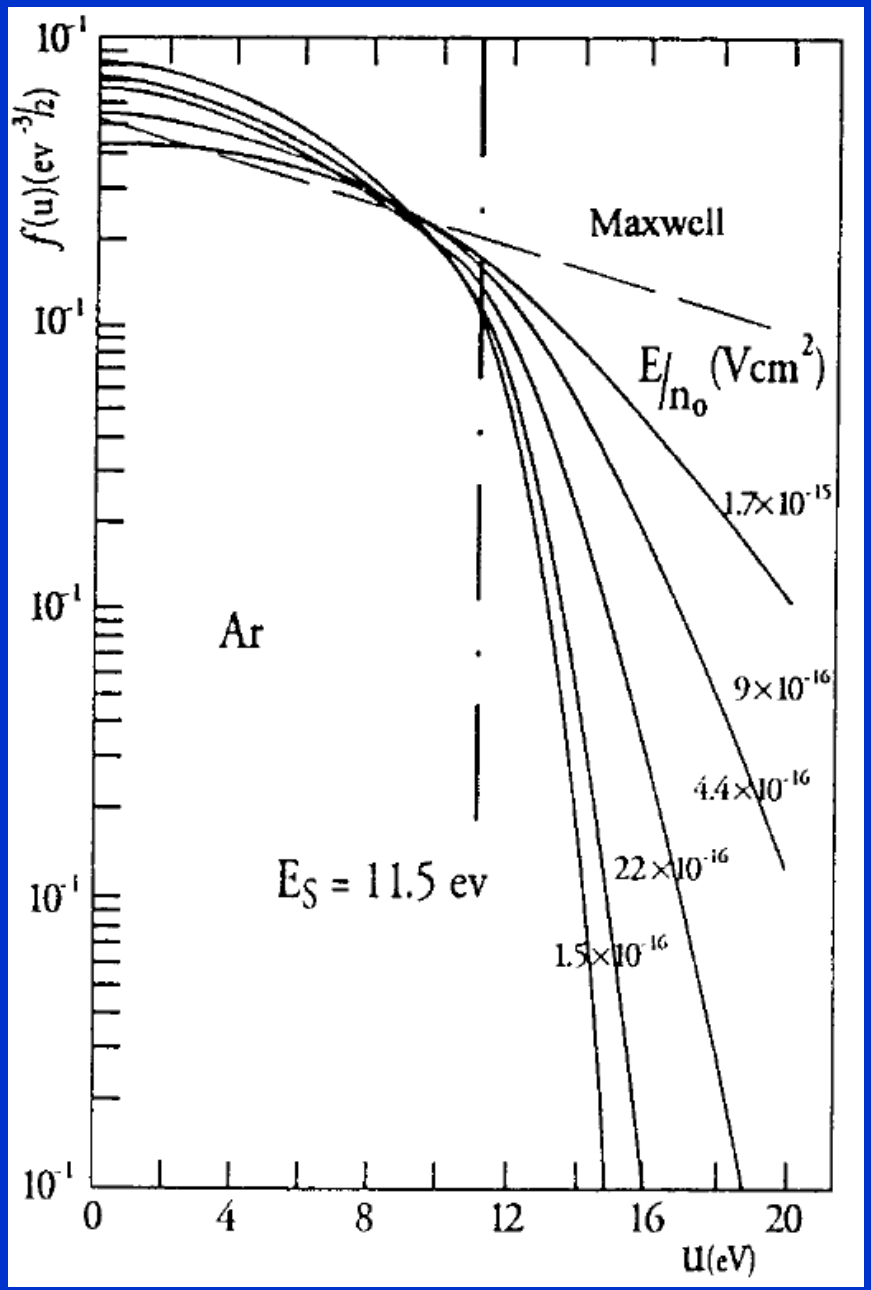

PTMS

Mass Fragmentation:

Electron impact
about. 70eV

Charge transfer
with Xe+

Soft and efficient ionization:

PTR-MS

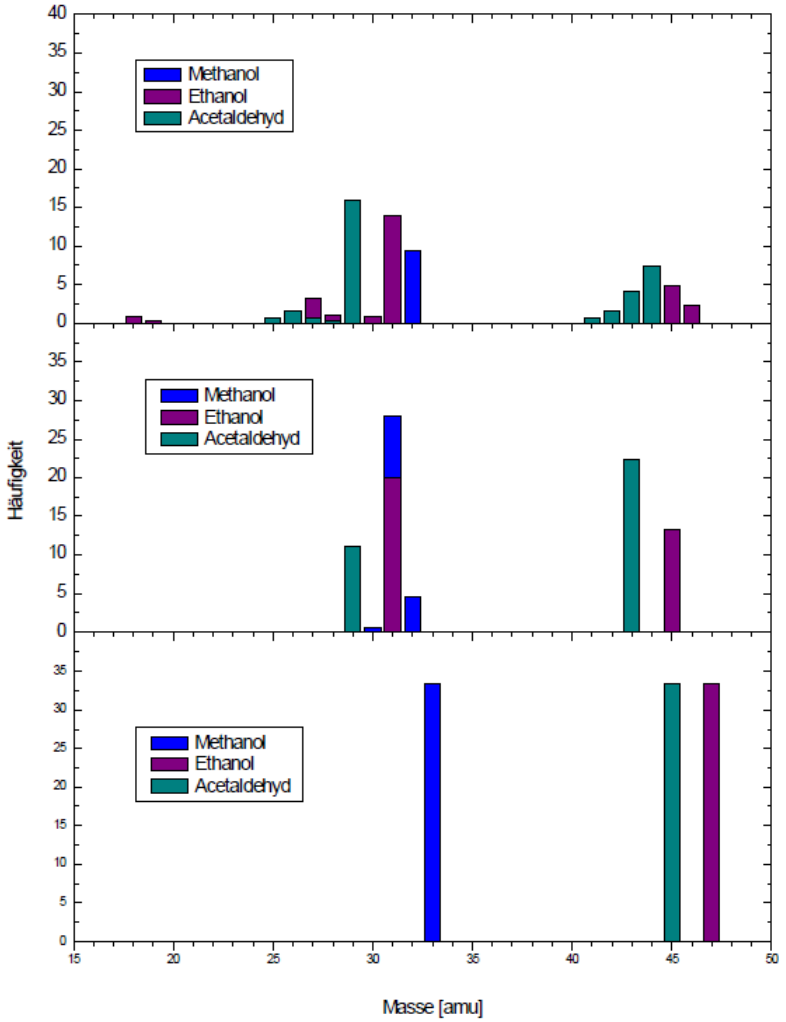

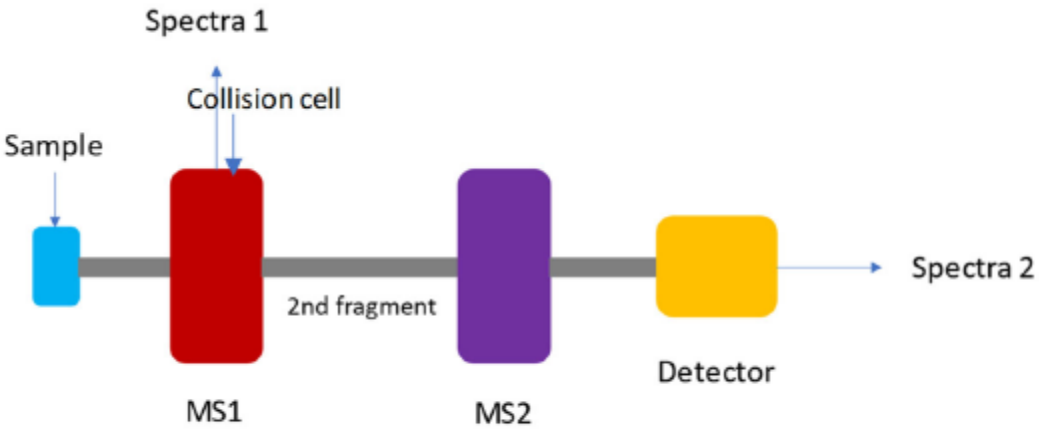

Figure 1. A simple schematic of a tandem mass spectrometry.

PA ladder

$H_3^+ + X \rightarrow XH^+ + H_2$

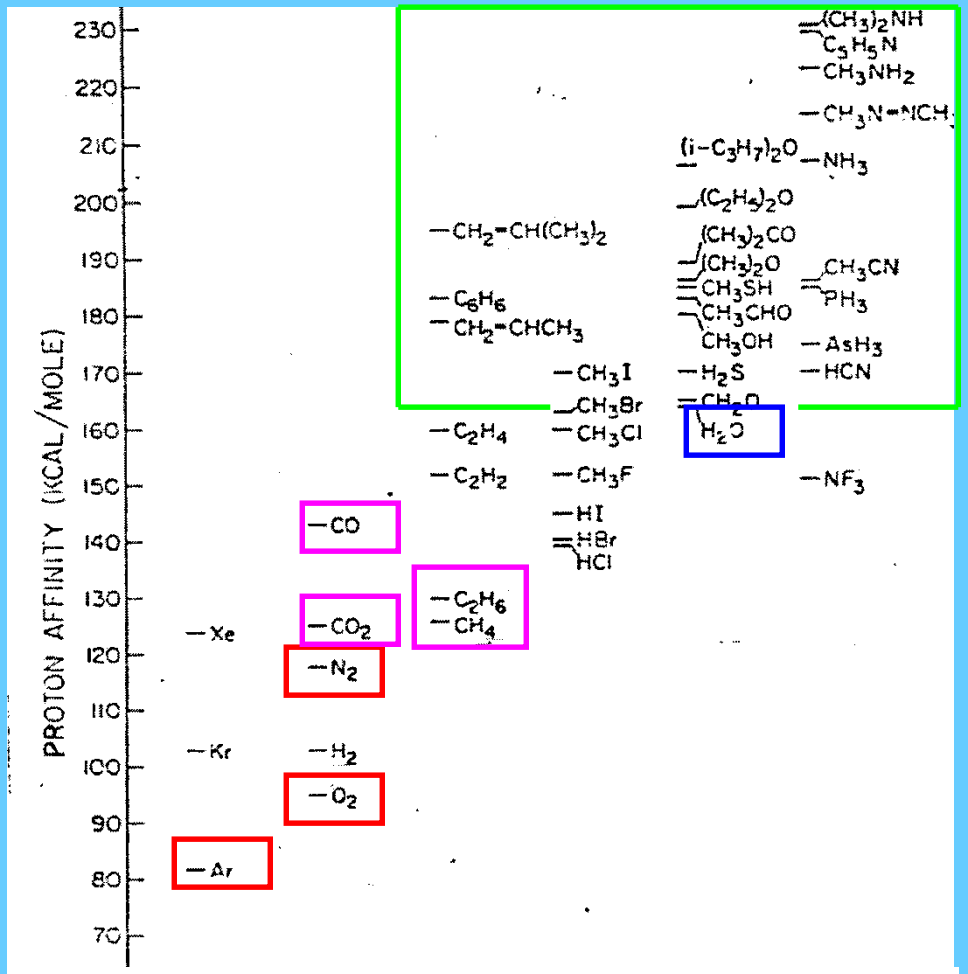

PTR-MS is sensitive to most **hydrocarbons** and **hydrocarbon derivatives** and **some inorganic species**.

$H_3O^+ + X \rightarrow XH^+ + H_2O$

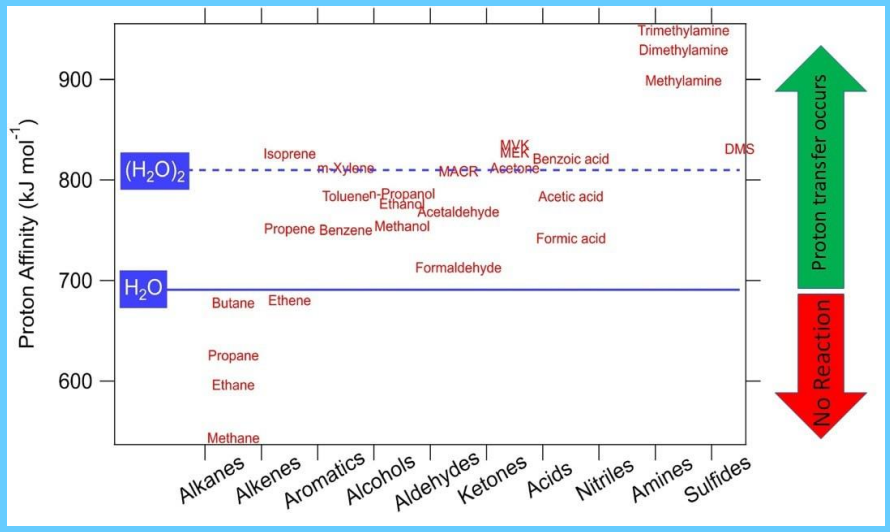

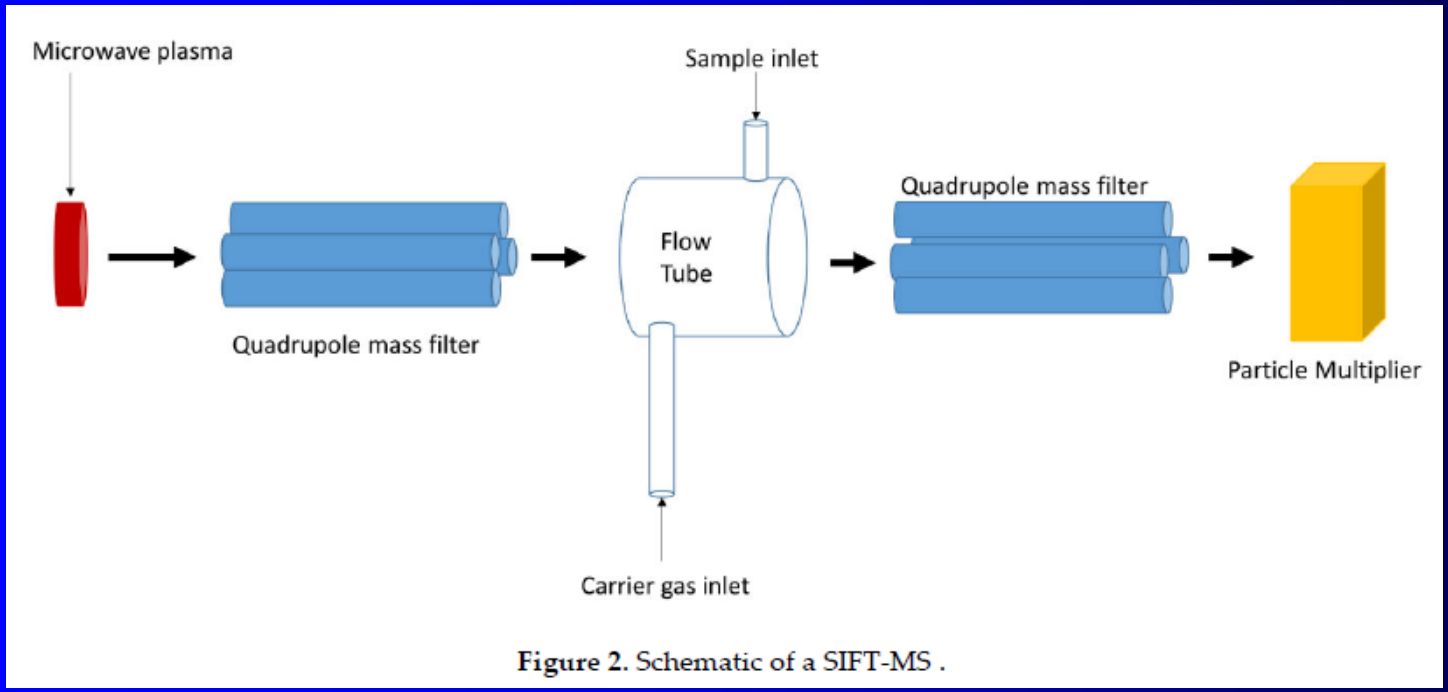

Figure 2. Schematic of a SIFT-MS .

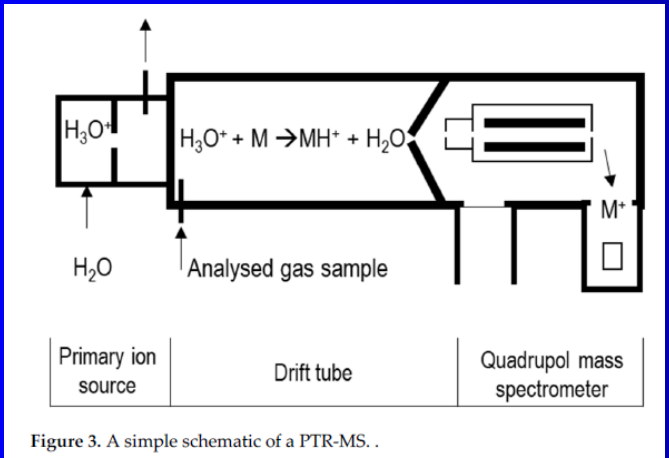

Figure 3. A simple schematic of a PTR-MS. .

The Technology

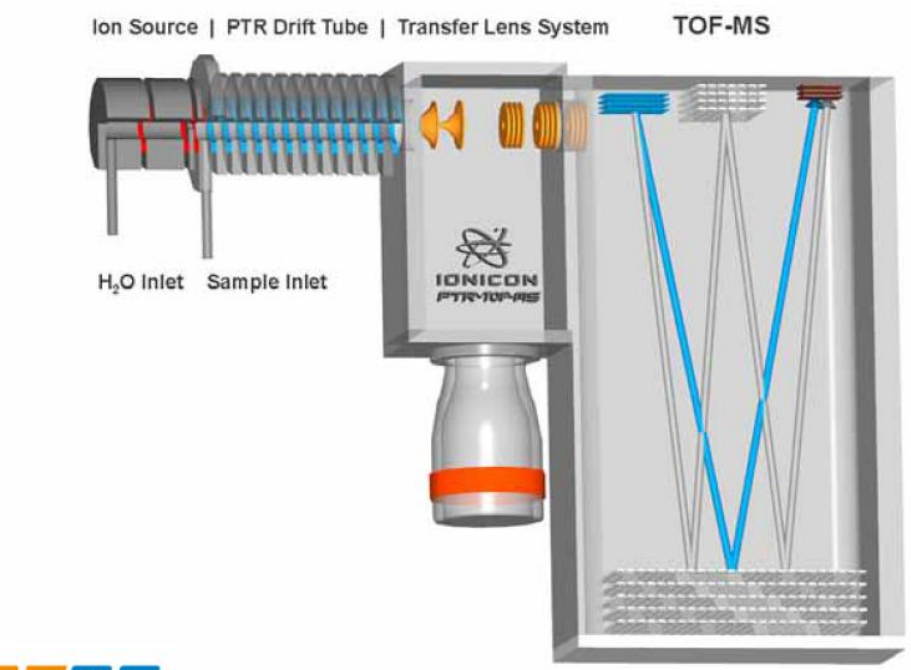

PTR-TOFMS

PTMS

The Technology

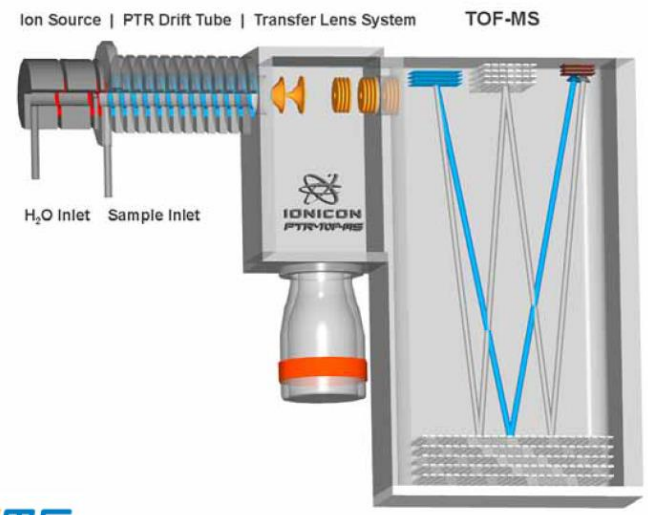

PTR-TOFMS

Mass Fragmentation:

Electron impact
about. 70eV

Charge transfer
with Xe+

Soft and efficient ionization:

PTR-MS

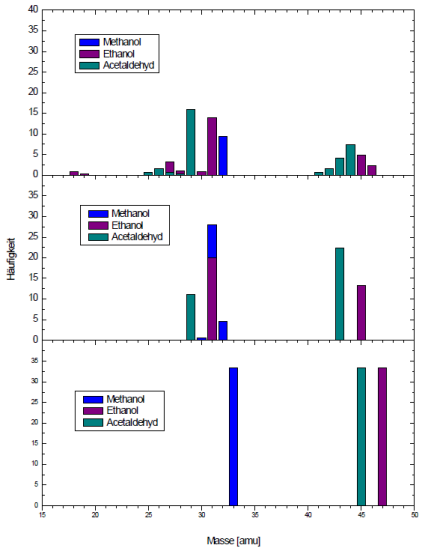

The drift tube (H_3O^+-mode):

- Sample gas collides with H_3O^+ ions
- Proton (H^+) switches to (and ionizes) sample gas, if proton affinity is higher than the one of water.

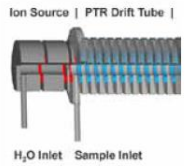

endothermic collisions

$H_2O{\cdot}H^+$ + N_2 → / + O_2 → / + Ar → / + CO_2 → / + CH_4 → **no reaction**

$H_2O{\cdot}H^+$

exothermic collisions

+ C_3H_6 → $C_3H_6{\cdot}H^+$
+ C_6H_6 → $C_6H_6{\cdot}H^+$
+ CH_3OH → $CH_3OH{\cdot}H^+$ + H_2O
+ CH_3CN → $CH_3CN{\cdot}H^+$
+ CH_3SH → $CH_3SH{\cdot}H^+$

In-situ measurements of environmental trace gases by PTR-MS

Armin Wisthaler

Institut für Ionenphysik
Leopold-Franzens-Universität Innsbruck
AUSTRIA

PTR-MS → SIFT → SIFDT

The Innsbruck Selected Ion Flow Drift Tube (SIFDT) converted to Proton Transfer MS

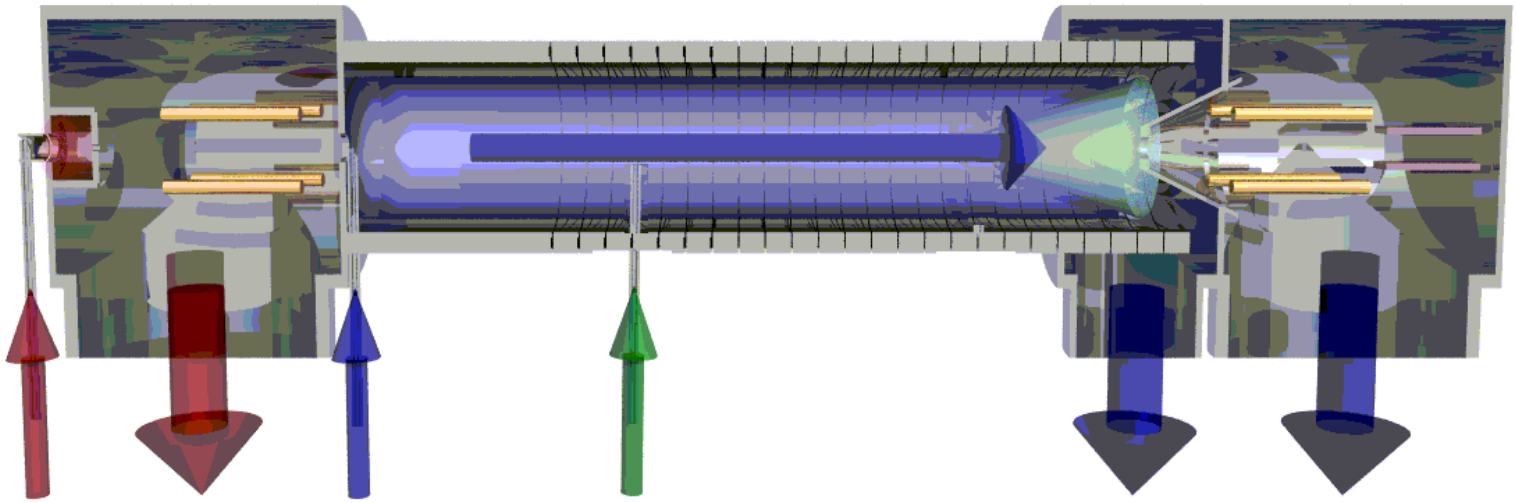

H_2O He Reactant

$H_3O^+ + X \rightarrow XH^+ + H_2O$

Cluster formation in SIFT

$H_3O^+(H_2O)_{n\ (n=0,1,2)}$ + HONO: product study

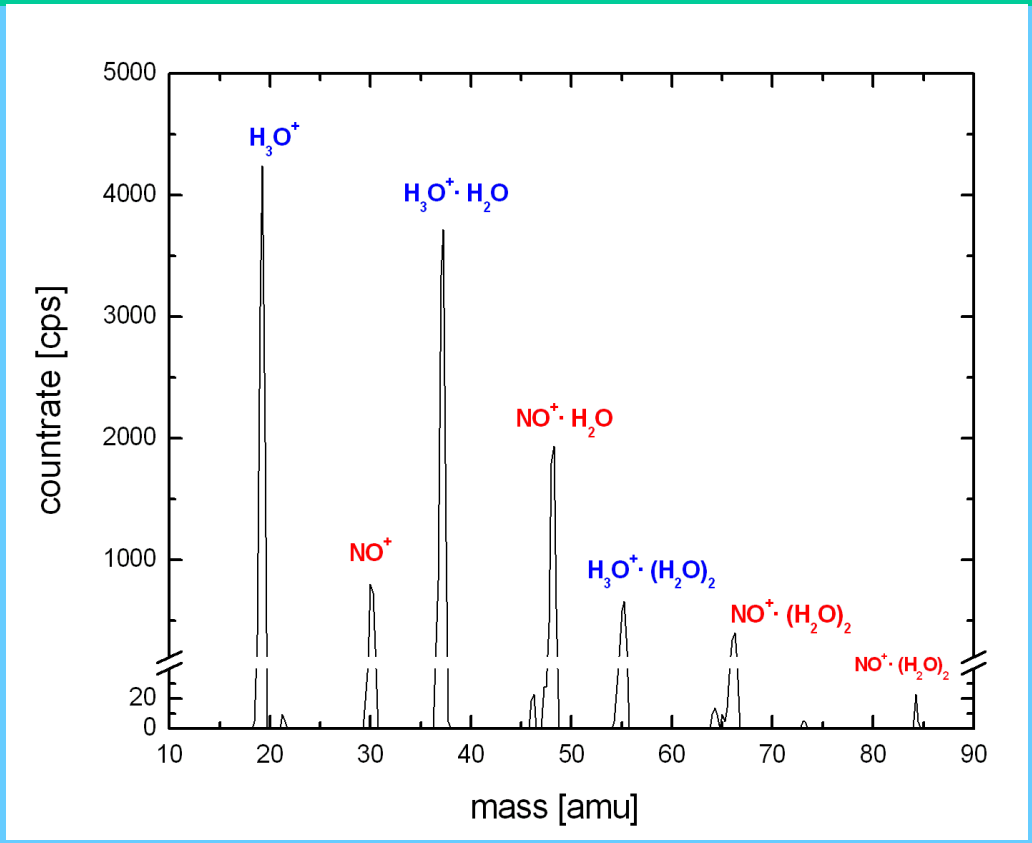

$H_2NO_2^+$: $NO^+ \bullet H_2O$

De Petris, G. et. al., *J. Phys. Chem.*, 76, 5183, 1982

PTR-MS

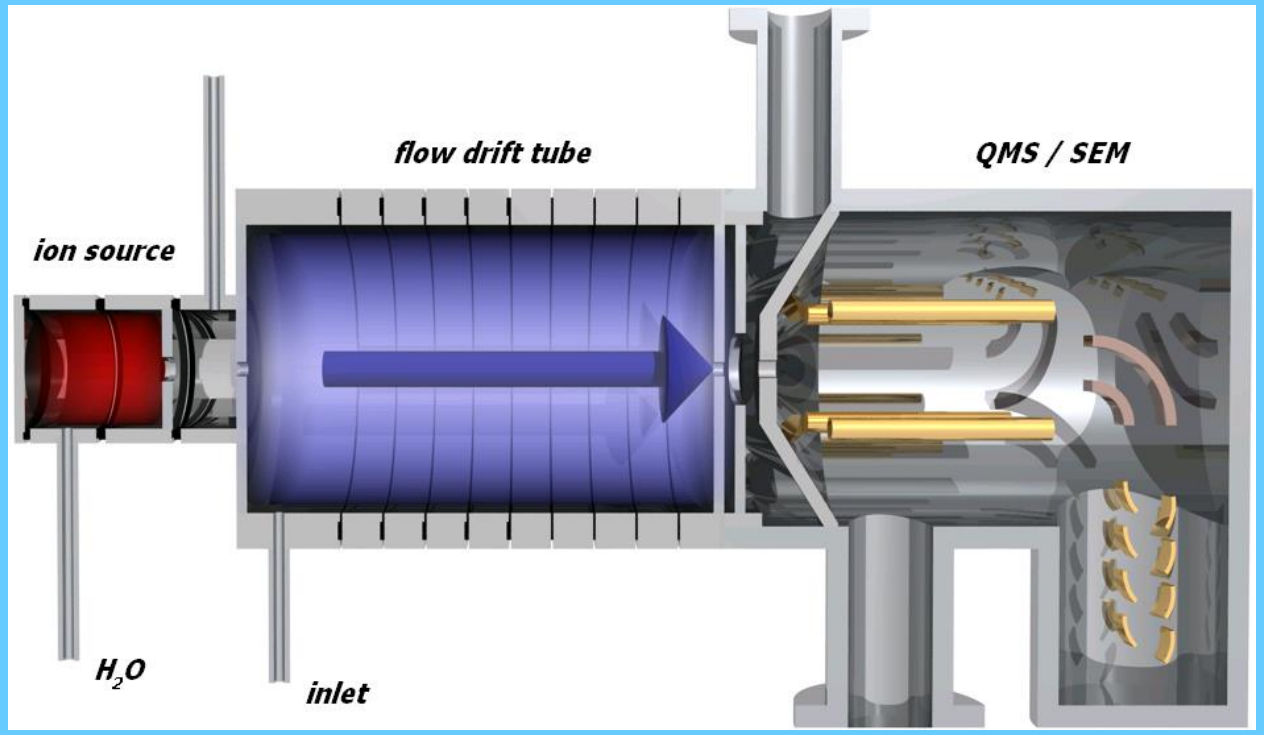

H_3O^+

Non-dissociative PT reaction

$H_3O^+ + A \rightarrow AH^+ + H_2O$

$PA(A) > PA(H_20)$

AH^+

H_3O^+

Kinetics

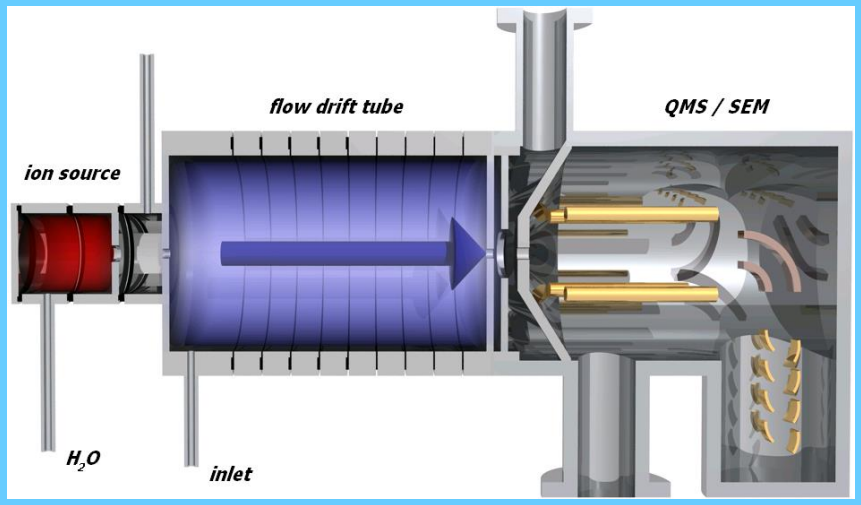

$H_3O^+ + A \xrightarrow{k} AH^+ + H_2O$ **obeys pseudo first-order kinetics**

$$[A] = \frac{i(AH^+)}{i(H_3O^+)} \frac{1}{kt}$$

The reaction rate coefficients for exothermic PT reactions is close (± 30%) to the collisional value predicted by ion-molecule capture theories.

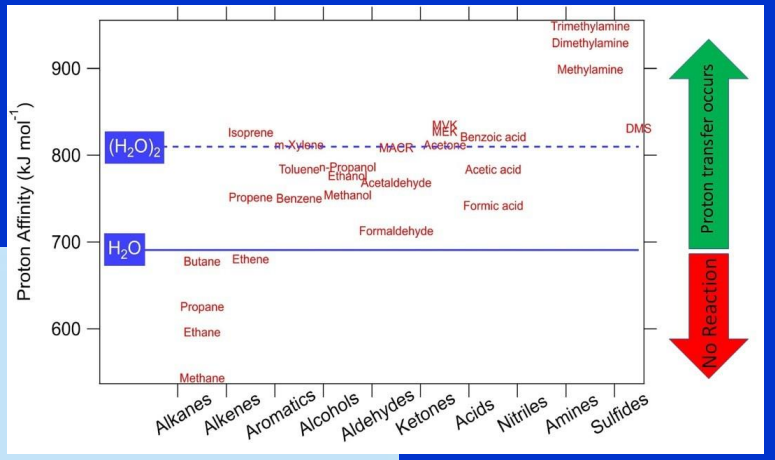
Proton Affinity (kJ mol^{-1})
900
800
700
600
$(H_2O)_2$
H_2O
Trimethylamine
Dimethylamine
Methylamine
DMS
Benzoic acid
Acetic acid
Formic acid
Formaldehyde
Isoprene
m-Xylene
MVK
MEK
MACR
Acetone
Toluene
n-Propanol
Ethanol
Acetaldehyde
Propene
Benzene
Methanol
Butane
Ethene
Propane
Ethane
Methane
Alkanes
Alkenes
Aromatics
Alcohols
Aldehydes
Ketones
Acids
Nitriles
Amines
Sulfides
Proton transfer occurs
No Reaction

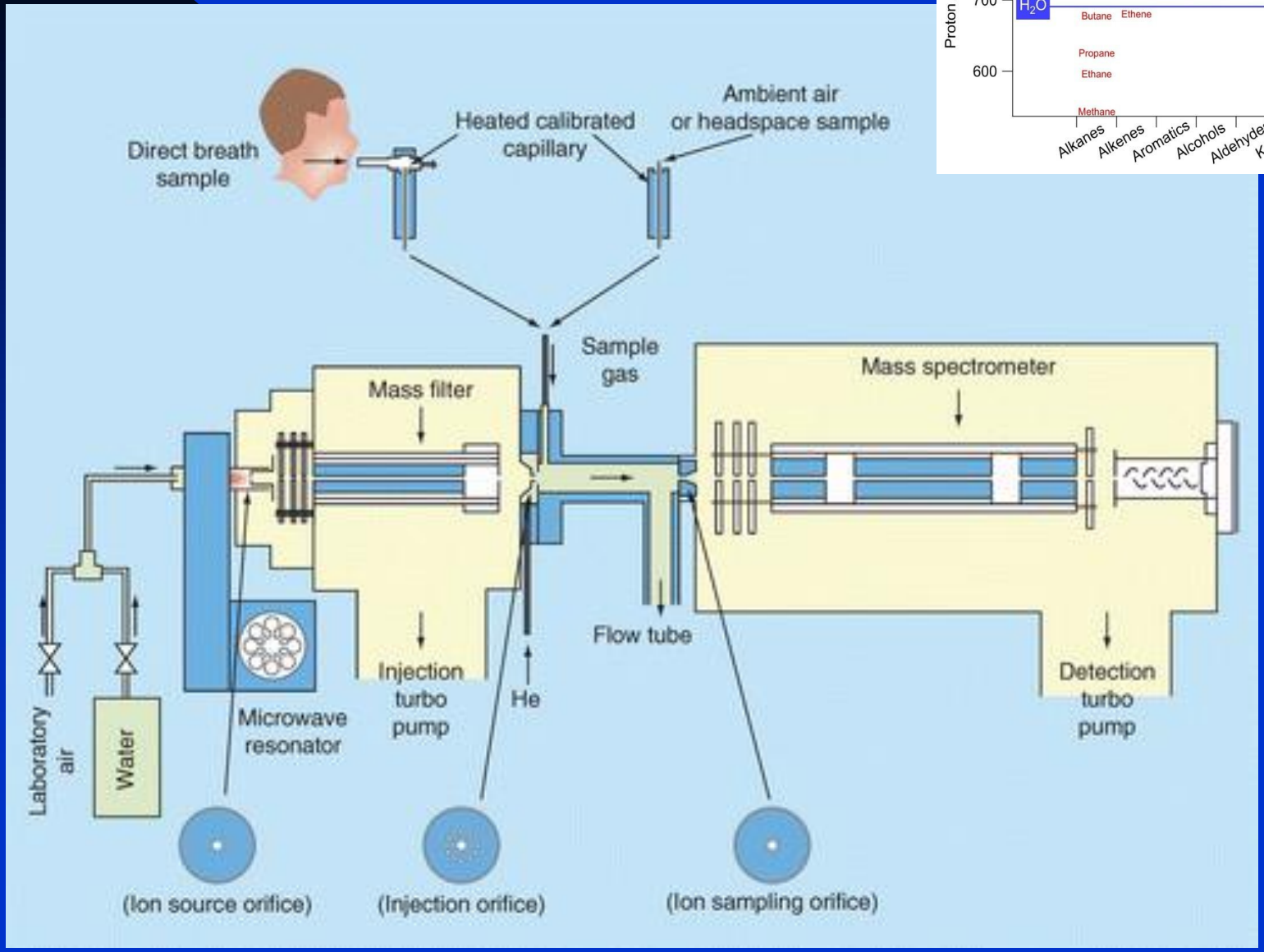
Direct breath sample
Heated calibrated capillary
Ambient air or headspace sample
Sample gas
Mass filter
Mass spectrometer
Flow tube
Injection turbo pump
He
Detection turbo pump
Microwave resonator
Laboratory air
Water
(Ion source orifice)
(Injection orifice)
(Ion sampling orifice)

Clinical Mass Spectrometry 16 (2020) 18–24

Contents lists available at ScienceDirect

Clinical Mass Spectrometry

journal homepage: www.elsevier.com/locate/clinms

Viewpoint

Quantification of volatile metabolites in exhaled breath by selected ion flow tube mass spectrometry, SIFT-MS

Patrik Španěl *, David Smith

J. Heyrovský Institute of Physical Chemistry, Academy of Sciences of the Czech Republic, Dolejškova 3, 182 23 Prague 8, Czech Republic

H_3O^+, NO^+ and O_2^+

ranging from sub-*ppbv*

20 *ppbv*

2. SIFT-MS analytical method

Detailed overviews of the SIFT-MS technique have been given previously in several reviews [5–7]. Briefly, it is based on the chemical ionization by selected reagent ions, H_3O^+, NO^+ and O_2^+., that ionise gaseous analytes present in air/breath samples in trace amounts. The range of neutral analytes accessible using the SIFT-MS technique has been extended recently by the exploitation of five additional negative reagent ions (O^-, OH^-, O_2^-, NO_2^-, and NO_3^-) [8]. Reactions occur between the selected reagent ion and the neutral analyte molecules present in sample that continuously

Details of interaction of electron with molecules

Details of interaction of electron with H_2

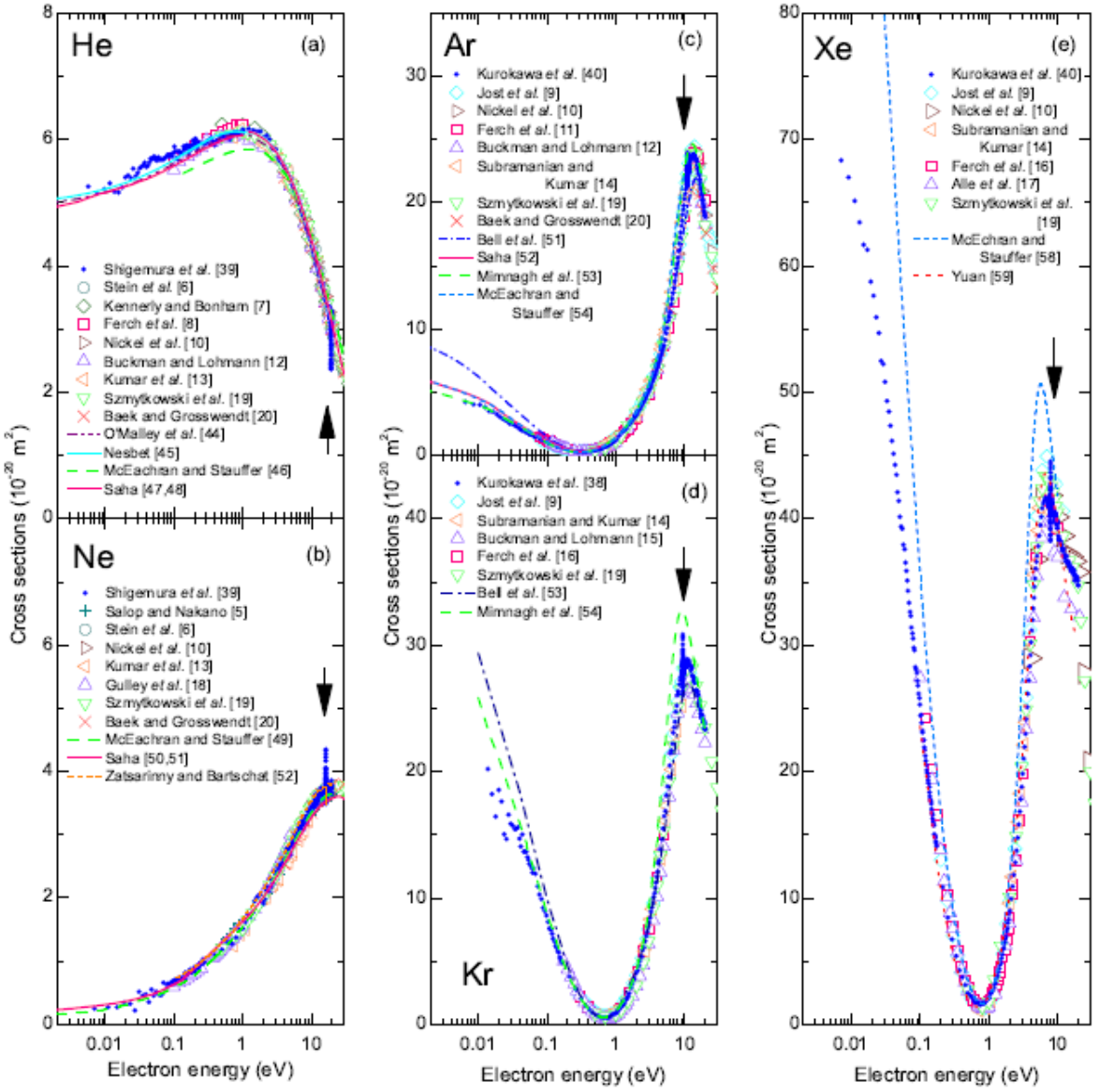

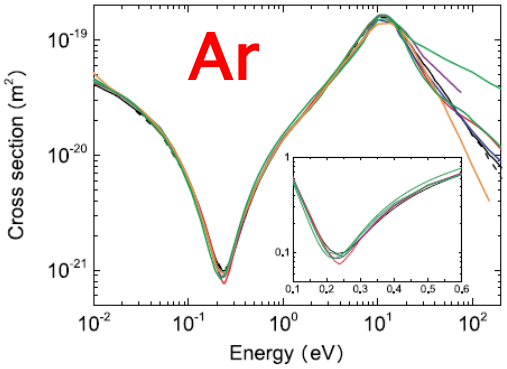

Figure 1. Comparisons of elastic momentum transfer (or effective momentum transfer from PHELPS) cross section versus electron energy in argon from the different databases. The inset is a zoom in the region of the Ramsauer minimum with cross sections in units of 10^{-20} m^2. The colour code is the same for all figures in this article: BIAGI-v8.9 (——); BIAGI-v7.1 (- - - -); BSR (——); HAYASHI (——); IST-LISBON (——); MORGAN (——); PHELPS (——); PUECH (——).

Figure 2. Comparison of the total cross sections for electron scattering from He, Ne, Ar, Kr and Xe. Arrows in each figure indicate the positions of the Feshbach resonances for each target atoms.

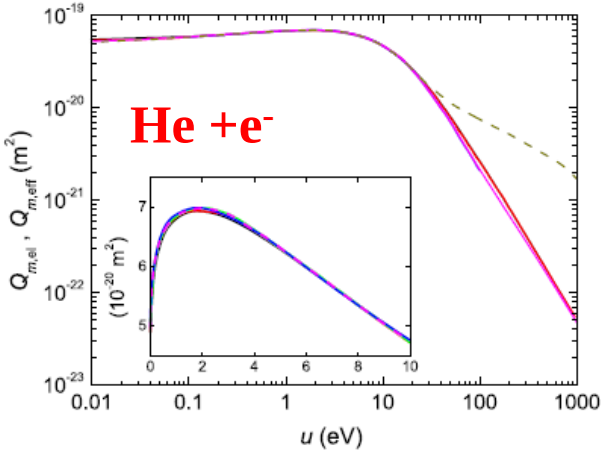

Figure 1. Elastic (solid line)/effective (dashed) momentum-transfer cross sections versus electron energy in helium, from the different databases: BIAGI-v8.9 (——), BIAGI-v7.1 (——), IST-LISBON (——), MORGAN (——), PHELPS (——). The inset is a zoom in the energy region between 0 and 10 eV.

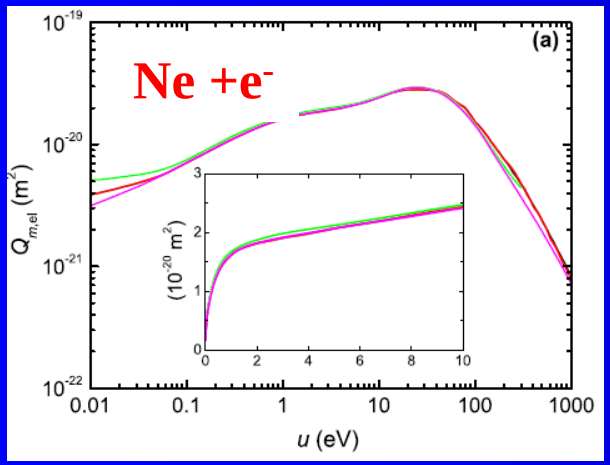

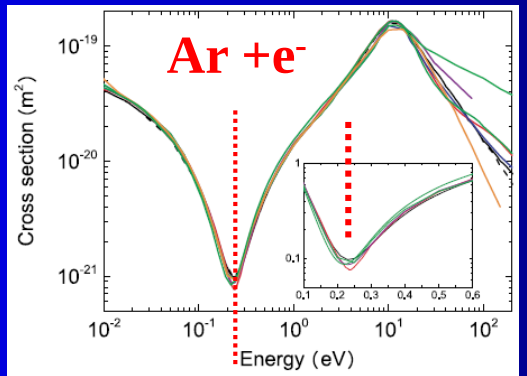

Figure 1. Comparisons of elastic momentum transfer (or effective momentum transfer from PHELPS) cross section versus electron energy in argon from the different databases. The inset is a zoom in the region of the Ramsauer minimum with cross sections in units of 10^{-20} m^2. The colour code is the same for all figures in this article: BIAGI-v8.9 (——); BIAGI-v7.1 (- - - -); BSR (——); HAYASHI (——); IST-LISBON (——); MORGAN (——); PHELPS (——); PUECH (——).

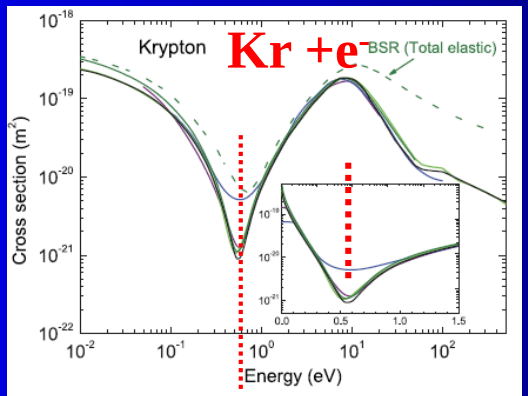

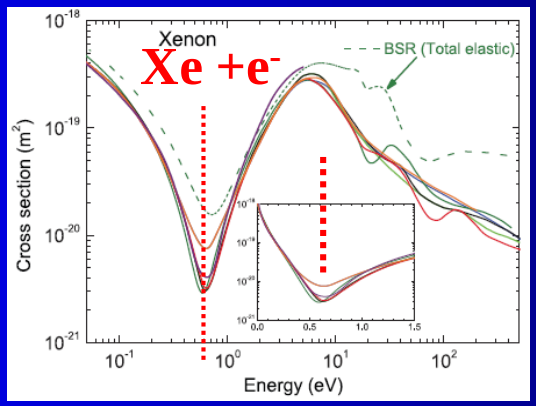

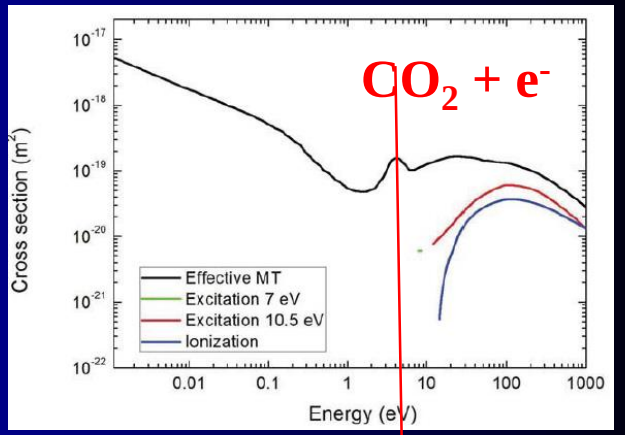

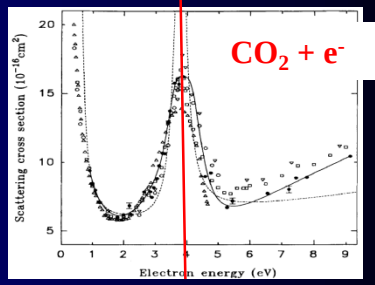

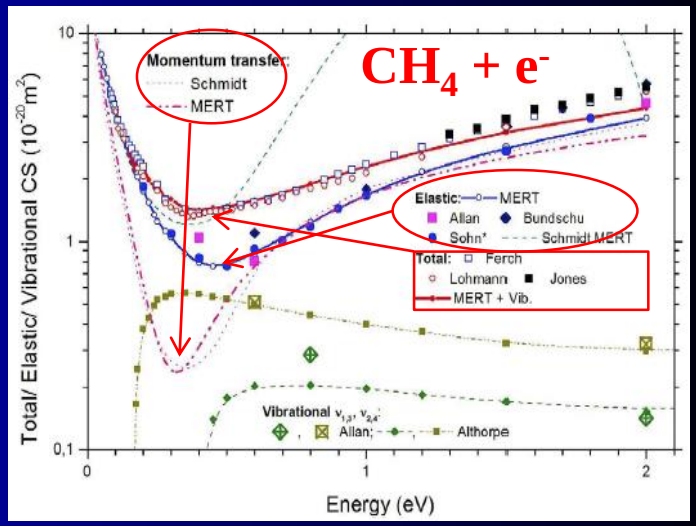

IMR ….
Atom molecule reactions….

Temperature dependence of reaction rate coefficients …k(T).

Arhenius dependence …..